

Rotational stiffness of timber-to-timber connections with inclined screws

P.C.B. Zeelenberg



Rotational stiffness of timber-to-timber connections with inclined screws

by

P.C.B. Zeelenberg

Student number:	4697936	
Project duration:	April-November 2024	
Thesis committee:	Prof. dr. ir. J.W.G. van de Kuilen	Delft University of Technology
	ir. P.A. de Vries	Delft University of Technology
	PD. Dr.-ing. M. Frese	Karlsruhe Institute of Technology
	S. Egner MSc.	Karlsruhe Institute of Technology
Cover:	Laboratory tests of FaNaBu truss in the KIT Research Centre for Steel, Timber and Masonry, Karlsruhe, Germany Image from personal correspondence with Sebastian Egner.	

Abstract

In timber connections, screws have a benefit over dowels or nails, as due to their withdrawal capacity they can transfer loads both perpendicular and parallel to the screw axis. Screws display their largest stiffness and load-bearing capacity in the direction parallel to the screw axis. These properties can be taken advantage of in case timber elements are connected with screws inserted under an angle with respect to the shear plane. Although a calculation method for the translational stiffness of connections with inclined screws is currently not included in Eurocode 5, multiple methods are discussed in the literature. This work focuses on the rotational stiffness of connections with inclined screws, which remains a considerable knowledge gap to date.

An extensive literature study is carried out, in which methods for the calculation of translational stiffness of inclined screws as well as methods for the calculation of rotational stiffness of dowel-type fasteners are studied. Combinations of these methods are used to put forward fourteen calculation methods for the rotational stiffness of inclined screw connections. Rotational stiffness tests of connections with inclined screws have been carried out prior to the start of this thesis project. The calculated rotational stiffness values of each of the fourteen methods are compared to the experimentally obtained values. Two prototypes of a novel truss concept developed at Karlsruhe Institute of Technology, in which inclined screws are implemented in the chord-diagonal connections, are modelled in Rhinoceros Grasshopper. The influence of the rotational stiffness of the chord-diagonal connections on the serviceability and ultimate limit state behaviour is studied.

A correction for friction occurring between the timber members as a result of the specific sequence of the application of the loads in a subset of the rotational stiffness experiments is proposed. After this correction, the best method shows good similarity with experimental results, yielding a coefficient of determination of 0.79 for a total of 91 tests. With regard to the truss model, it is concluded that the rotational stiffness has no influence on the deflections of the truss, however, the moments in the connections increase for higher rotational stiffness values. Individual screws in the connections are found to receive an additional load of 5-10 % in their main loading direction as a result of the moments in the connections in the large-scale truss prototype. The model can be used in the preliminary design of these trusses to quantify moments in the connections and the forces per screw as a result of these moments.

Preface

The subject of this thesis is timber connections and the influence they have on structures they are applied in. Timber structures have been a personal interest since I started my education at Delft University of Technology. The demand for a more sustainable construction industry has pushed exciting recent innovations in the field of timber engineering, enabling a revival of the material in the last decades. The objective of this thesis is to contribute to the understanding of timber connections and structures.

This thesis was written at the Research centre for Steel, Timber and Masonry of Karlsruhe Institute of Technology. I would like to thank Carmen Sandhaas and Geert Ravenshorst for enabling me to write my thesis in Karlsruhe. I would also like to express my gratitude towards my graduation committee; Jan-Willem van de Kuilen and Peter de Vries, and Sebastian Egner and Matthias Frese of Karlsruhe Institute of Technology. A special thanks to Sebastian, whose door was always open for questions.

On a personal note, I would like to thank my family and friends for their unlimited support during this period. I could not imagine having undergone this adventure without you.

*P.C.B. Zeelenberg
Delft, November 2024*

Contents

1	Introduction	1
1.1	Research Context	1
1.2	Research Problem	1
1.3	Research objectives	3
1.4	Scope	3
1.5	Research questions	3
1.6	Structure of the thesis	3
2	Timber trusses	5
2.1	Introduction	5
2.2	Connections	5
2.3	Brief history	6
2.4	Structural behaviour	7
2.5	Bending moments in connections	8
3	Connection properties	10
3.1	Introduction	10
3.2	Dowel type fasteners	10
3.2.1	Load-bearing capacity	10
3.2.2	Connection stiffness	17
3.3	Axially loaded screws	19
4	Inclined screw connections	20
4.1	Introduction	20
4.2	Geometry	20
4.3	Current Standard: EN-1995-1-1	21
4.4	Bejtka Blass approach	21
4.5	Kevarinmäki approach	24
4.6	Tomasi, Crosatta and Piazza approach	26
4.7	Jockwer, Steiger and Frangi approach	29
4.8	Girhammar, Jacquier and Kälsner approach	30
4.9	Blass Steige approach	34
4.10	De Santis & Fragiaco approach	35
4.11	Comparison of methods by Kullander and Sandström	37
4.12	Eurocode 5: EN-1995-1-1 draft (2023)	37
4.13	Conclusion	39
5	Moment capacity and rotational stiffness of dowel type groups	40
5.1	Introduction	40
5.2	Connection capacity	40
5.2.1	Individual dowel capacity	40
5.2.2	Capacity of reduced cross section	43
5.2.3	Shear force	44
5.3	Rotational stiffness	44
5.3.1	Screw forces	46
5.3.2	Eurocode 5: EN-1995-1-1 draft (2023)	48
5.3.3	Noguchi & Komatsu	48
5.3.4	Centre of rotation displacement	49
5.4	Conclusion	50

6	Timber-to-timber friction	51
6.1	Introduction	51
6.2	Parameters influencing friction.	51
6.3	Friction beech LVL and coniferous wood	53
6.4	Conclusion	53
7	Experimental investigations	54
7.1	Introduction	54
7.2	Test setup.	54
7.3	Test specimens	54
7.3.1	Test series 1	54
7.3.2	Test series 2	55
7.4	Testing procedure	58
7.4.1	Test series 1	58
7.4.2	Test series 2	59
7.5	Measuring technique and data processing	60
7.5.1	Test series 1	60
7.5.2	Test series 2	61
7.5.3	Test results	61
8	Calculation model	64
8.1	Introduction	64
8.2	Testing of methods	64
8.3	Pre-load theory	64
8.4	Spring model	66
8.5	Screws under compression	67
8.6	Conclusion	68
9	Truss model	71
9.1	Introduction	71
9.2	Grasshopper model	71
9.3	Small-scale prototype	73
9.3.1	Serviceability limit state	74
9.3.2	Ultimate limit state	75
9.4	Large-scale prototype	77
9.4.1	Serviceability limit state	78
9.4.2	Ultimate limit state	78
9.5	Screw forces as a result of moment in the connections	80
9.6	Conclusion	81
10	Connection details	82
10.1	Diagonal-chord connection in trusses	82
10.2	Chord connection.	83
10.3	Beam-column joint	85
11	Conclusion and discussion	87
11.1	Conclusion	87
11.1.1	Main research question	87
11.1.2	Sub-questions	87
11.2	Discussion	89
11.2.1	Calculation method for rotational stiffness	89
11.2.2	Structural model	90
12	Recommendations	91
12.1	Recommendations for connection design	91
12.2	Recommendations for future research	91

A	Method plots	97
B	Details of performed tests found in literature	102
C	Compression screws	104
D	Python code plot Noguchi & Komatsu	106
E	Python code methods	108
F	Embedment capacity truss prototypes	122
G	Rotational stiffness values tests	124

Introduction

1.1. Research Context

The buildings and construction sector is a big contributor to global energy-related carbon emissions and is responsible for 37 % of the global carbon dioxide emissions in 2021 [59, p. 1]. These emissions consist of operational emissions, and emissions associated with the construction and deconstruction of buildings, also referred to as embodied emissions. Embodied emissions from steel, concrete, and aluminium make up at least 6 % of the total energy-related carbon dioxide emissions [59, p. 1]. The utilisation of bio-based materials in the construction industry has the potential to limit the carbon footprint of the industry dramatically. While large amounts of carbon dioxide are emitted during steel and concrete production, wood captures carbon dioxide from the atmosphere in the process of production. Also, the material properties of timber are beneficial for large-span structures. In relation to the material's density, timber shows high deflection and buckling efficiency, and is very efficient in taking up compressive, tensile, and bending loads [19].

1.2. Research Problem

A current research project at Karlsruhe Institute of Technology aims to develop a standardized timber truss concept to span large distances, which is given the name FaNaBu (Fachwerkträger aus Nadel- und Buchenholz, or trusses made of coniferous wood and beech in English). The current concept of the project combines the material properties of softwood glued laminated timber and hardwood laminated veneer lumber (LVL) to optimise high load-bearing capacity and simple assembly for large-span timber structures. Figure 1.1 shows a prototype of the FaNaBu truss.



Figure 1.1: FaNaBu truss concept with composite upper and lower chords and LVL tensile diagonals connected using inclined screws [25, p. 63].

It is common knowledge that in timber structures, connections are usually a limiting factor for the load-carrying capacity of the entire structure. Connections of elements often result in geometrical and structural challenges during the structural design phase of timber structures. Steel connecting agents are often used to realise these connection details. The complex interplay of stress buildups around fasteners, differences in material properties, multi-axial stress states, and the anisotropic and brittle behaviour of wood makes for the fact that design codes often do not reflect the full complexity of these connection details.

For large-span timber structures, the stiffness of the connections has a direct effect on the deformations in the structure. An often-used upper limit for the vertical deformation at the mid-span of a structure is 1/250 of the spanned distance [52]. The deformations of structures are addressed in the serviceability limit state (SLS), which ensures acceptable human comfort, guaranteed functionality, and an acceptable visual appearance of structures [13, p. 520]. Deformations of a structure can also have an impact on its load-bearing capacity, addressed in the ultimate limit state (ULS), for instance in case deformations cause additional stress buildups.

In the FaNaBu concept, inclined screws are used for the connections between the tensile diagonals and chords. Screws as a connecting agent have a benefit over dowels or nails, as due to their withdrawal capacity they can transfer loads both perpendicular to the screw axis and parallel to the screw axis. Screws display their largest stiffness and capacity in the axial direction. This makes a compelling case for placing screws under an angle in connections in which small deformations and high capacity are desirable. Additionally, the timber elements are pressed against each other in this geometrical configuration, so that friction effects add to their stiffness and strength. Under such applications, screws experience a combination of both axial and shear force, depending on the angle of inclination.

To date, research has mainly focussed on the axial properties of connections with inclined screws. Different methods to calculate stiffness and capacity have been proposed in the literature. There are cases in which the application of this type of connection is preferred due to the aforementioned benefits regarding axial stiffness and strength, but the exposure of the connection to bending moments cannot be ruled out. This is also the case in the application of inclined screws in the FaNaBu truss concept, as shown in figure 1.2. Deformations of the truss theoretically cause relative rotations $\Delta\phi$ between the diagonals and chords. In case the connections are perfect rotational hinges, the connections would only be loaded axially, but because these connections are presumed to have a certain rotational stiffness k_r , moments develop in the connections according to the simple relation $M = k_r \cdot \Delta\phi$. Prediction of the magnitude of these moments depends on a reliable method to quantify the rotational stiffness of connections with inclined screws. Such methods exist for connections consisting of perpendicularly inserted dowel-type fasteners, but the case of inclined screws forms a clear research gap.

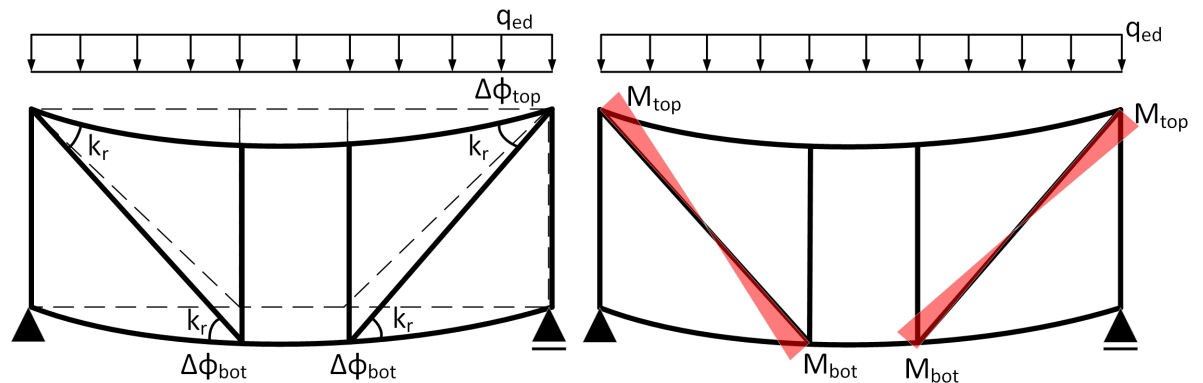


Figure 1.2: Representation of the moments that develop in the connections due to relative rotations $\Delta\phi$ and rotational stiffness k_r of the chord-diagonal connections in the FaNaBu truss. Source: own image.

1.3. Research objectives

The first research objective of this thesis is to develop a calculation method to accurately assess the rotational stiffness of timber-to-timber connections utilising inclined screws. A second objective is to assess the influence of the rotational and translational stiffness of the chord-diagonal connections in the FaNaBu truss on both its SLS and ULS behaviour and quantify the forces each screw receives as a result of the moments that develop in the connections. A final objective is to develop concepts for inclined screw connections other than the chord-diagonal connection in the FaNaBu truss.

1.4. Scope

Although many connection methods exist, this research is focused on timber-to-timber connections with inclined screws. The research is further limited to the tests that have been conducted prior to the start of this MSc thesis project with respect to the angle of inclination, screw type, timber species, angles to the grain and loading conditions. The main focus of the thesis is on the FaNaBu truss concept, but possible other connection types are briefly discussed.

1.5. Research questions

The main research question this thesis aims to answer is:

How can the rotational stiffness of timber-to-timber connections with inclined screws be quantified?

And the following sub-questions:

- What are current calculation methods for the stiffness and capacity of connections with inclined screws, and how do these compare?
- What are current calculation methods for the rotational stiffness and moment capacity of connections with dowel-type fasteners and how do these compare?
- Which parameters are of influence for the rotational stiffness of connections with inclined screws?
- What is the influence of the rotational stiffness of connections on the serviceability and ultimate limit state behaviour of the trusses in which the connections are applied?
- What could be other possible applications of connections with inclined screws, and is the developed method for rotational stiffness applicable to these connections?

1.6. Structure of the thesis

The thesis consists of 4 different parts, which are briefly discussed below.

Literature

An extensive literature study is carried out. The literature study aims to first provide background information of timber trusses and connection properties. Different methods to quantify the stiffness of inclined screws identified in the literature are discussed and analysed, as well as methods for rotational stiffness and moment capacity of connections with dowel-type fasteners.

Analytical works

In this part, the experimental rotational stiffness tests carried out as part of the FaNaBu research project are discussed. Methods for the stiffness of individual inclined screws and rotational stiffness are combined in order to collect a number of possible calculation methods for the rotational stiffness of connections with inclined screws. These methods are compared to the experimental test data in order to find a method that yields good results.

Structural modelling

A structural model of the FaNaBu truss is built in a structural analysis software tool, and the influence of the rotational stiffness of the chord-diagonal connections on the serviceability limit state and ultimate limit state is analysed.

Connection details

Considerations concerning the connections in the FaNaBu truss are discussed, as well as possibilities for the use of inclined screws in other connection types.

2

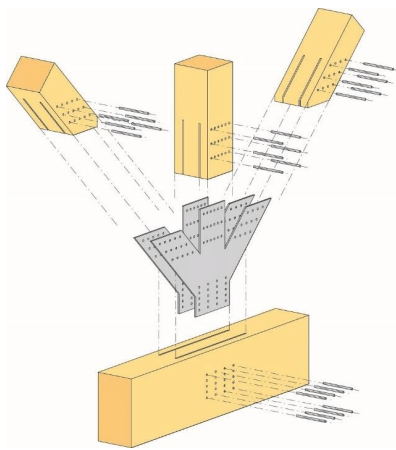
Timber trusses

2.1. Introduction

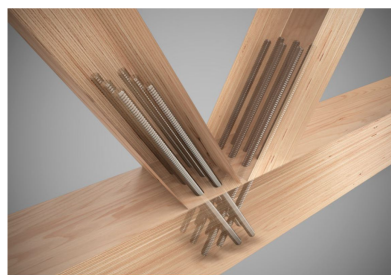
Timber trusses are an often-used method to span large distances. The connections are of large importance for the load-bearing capacity and serviceability limit state behaviour of timber trusses. In this chapter, literature on timber trusses, their connections, and the influence of rotational stiffness of their connections is discussed.

2.2. Connections

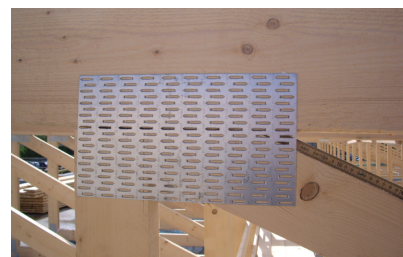
Trusses are an efficient way to span large distances with timber as no material is used in places without considerable stresses [25, p. 1]. Additionally, the members are loaded almost exclusively along their axis, which is the optimal loading situation for timber [64, p. 14]. Connections usually are a limiting factor in timber trusses, and therefore often dictate the design of the entire structure. Not rarely this phenomenon results in oversized truss members, thereby posing economical and technical limits on a viable use of timber structures [45, p. 105].



(a) Dowel connection with slotted-in steel plates [19]



(b) Glued-in rod connection [17]



(c) Nail plate connection [35, fig. 1]

Figure 2.1

The most common types of connections used in timber trusses at present are steel dowels in combination with slotted-in steel plates, glued-in rods, and nail plates [64, p. 12]. Examples of these connections are shown in figure 2.1. Recent developments of timber truss connections include combinations of glued- or screwed-in rods for tension members and enhanced step joints for compression members by Blass & Meyer [50] and by Blass & Enders-Comberg [12] respectively (see figure 2.2a). Another innovation in the connections of timber trusses is the use of inclined screws by Egner & Frese [25] (see figure 2.2b).

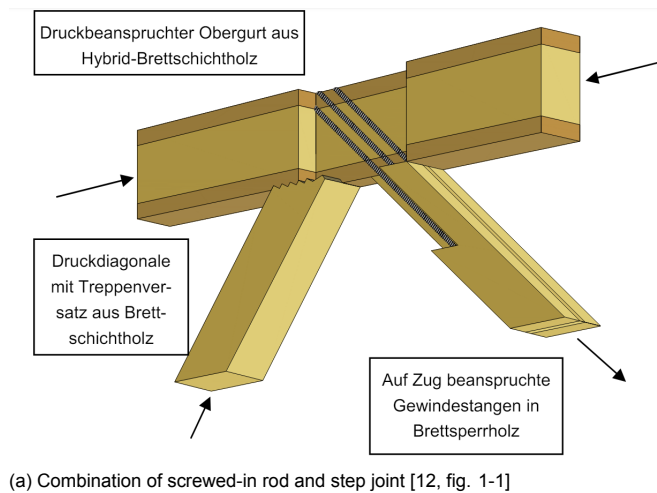


Figure 2.2



2.3. Brief history

Large-scale production of timber trusses began in the 19th century, when trusses with parallel chords made of squared timber sections connected with step joints and split ring dowels were developed [64, p. 15]. An interesting development in this period is the HOWE truss, which was used in the USA since 1840, and consisted of crossed timber diagonals that were loaded in compression by prestressed vertical tension bars, as illustrated in figure 2.3a [64, p. 16]. Figure 2.3b shows the König-Ludwig-Brücke in Kempten, which is built according to the Howe truss principle.

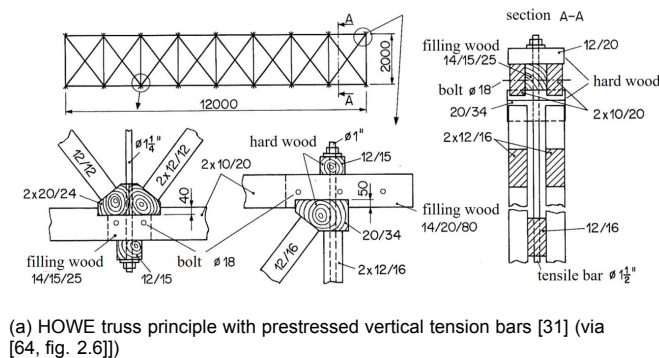


Figure 2.3



Since 1850 steel bolts have been used for the connections in trusses [32], and later pin-shaped nails made of oak inserted in tight-fitting pre-drilled holes became more widespread [64, p. 16]. Around the turn of the century, these wooden nails and pin-shaped connectors were replaced by steel variants, which came under patents as "Meltzer-" and "Ambistifte". These typically came in the range of 8-12 [mm] and had tensile strengths of 800-900 [MPa] [32]. With the emergence of new connection types such as dowel connections, split ring dowel connections, and nailed connections in the 1930s in Europe, the bolted connections fell into oblivion [32]. This preference was not due to the mechanical superiority of nailed connections over bolted connections, but rather an overestimation of nailed connections in design codes at the time due to too favourable testing conditions [32]. From the 1940s

until the 1960s, first nailed connections and later glued connections were used more often. Trusses with parallel chords became increasingly common in more simple structures, which resulted in highly variable ratios of truss height over truss length [64, p. 17].

2.4. Structural behaviour

The different ratios of truss height over truss length resulted in the realisation that for trusses with small height compared to their length, the stiffness of the beams and connections had to be taken into account. This meant that the ideal truss model, described by Culmann (1866) [20] could no longer be used (i.e. connections are modelled as friction-free hinges without translational slip, chords are not continuous, and external loads are introduced in the connections so that only normal forces occur in the truss members). Schilling (2022) [64, p. 17] states that Scheer & Golze (1981) [63] therefore investigated the design of timber trusses taking into account the continuity of the chords making use of the finite element method and that their calculations showed only 1-2 % less normal forces and deflections than the ideal truss model, although considerable bending moments occurred in the chords in the continuous model (see figure 2.4).

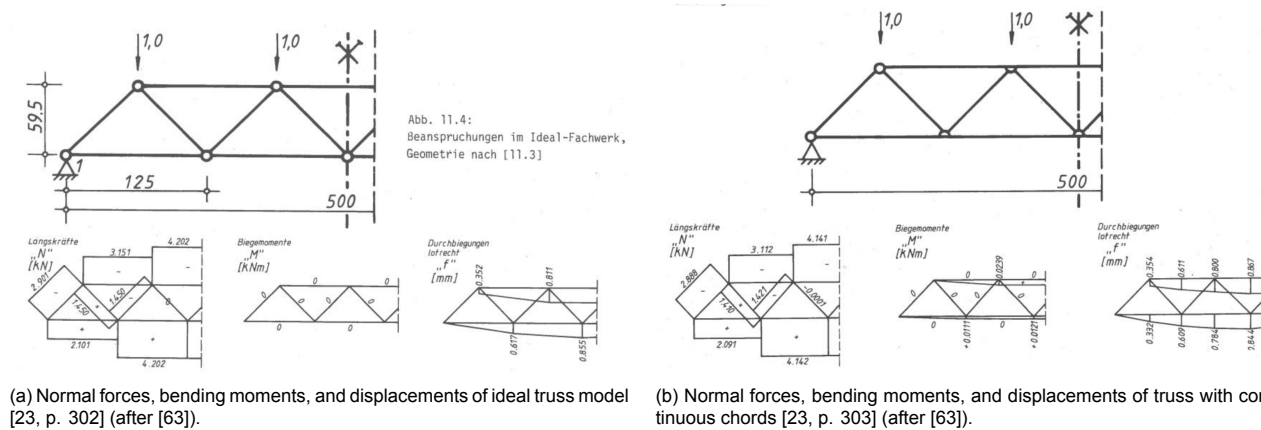


Figure 2.4: Comparison of normal forces, bending moments, and displacements in different truss models.

Dubas et al. [23, p. 304] describe tests performed by Möhler (1966) [51] that compare the stiffness of trusses with glued and nailed connections. It was observed that trusses with glued connections exhibited a 15 % reduction in overall stiffness, while those with nailed connections showed a 25 % reduction in overall stiffness when compared to the rigid model. The lower stiffnesses lead to larger deflections, and therefore also to larger bending moments in the continuous chords. The corresponding truss model including continuous chords and these translational stiffnesses is given in figure 2.5a. It was concluded by Dubas et al. (1981) [23, p. 304] that also the rotational stiffness of the connections should be taken into account, leading to the model as given in figure 2.5b. However, it was not possible to accurately quantify the rotational stiffness values of connections yet. Tests are described by Dubas et al. [23, p. 305] with trusses with slotted-in steel plates and dowels as connections. It was concluded that for the load level of serviceability limit state, the assumption of rigid connections was a valid assumption. Also, Dubas et al. (1981) [23, p. 308] conclude that for trusses with parallel chords, in contrast to triangular-shaped trusses, the diagonals have a primary function, and therefore the influence of the connection stiffness on the system's behaviour is also more pronounced. The slenderness (=truss height/truss span) of parallel chord trusses also influences the magnitude of section forces: trusses with smaller slenderness experience more deflection, and therefore larger bending moments in the chords occur. Also, in case the cross sections of the chords of the truss are larger, the chords have more bending stiffness and hence, attract more bending moment [23, p. 308].

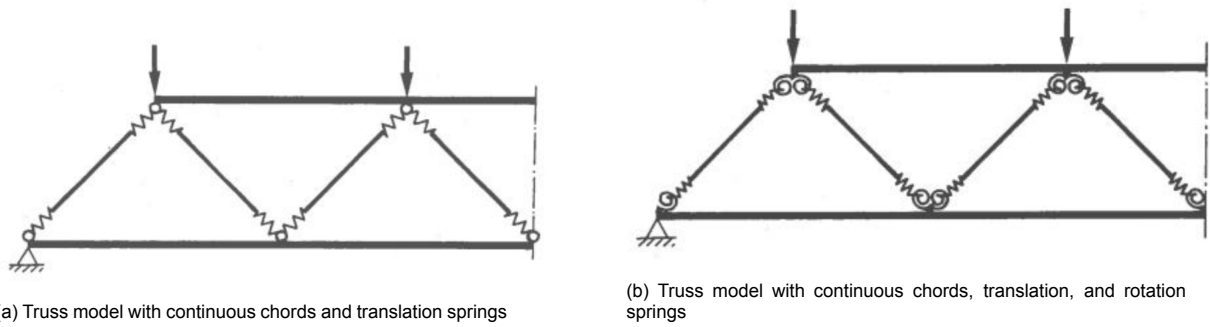
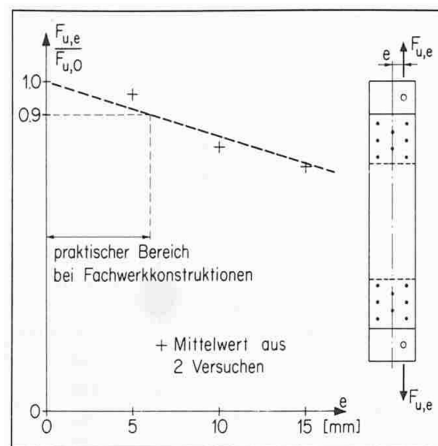


Figure 2.5: [23, fig. 11.6 & 11.8]

2.5. Bending moments in connections

The phenomenon of additional bending moments in timber trusses as a result of connection stiffness was first studied by Gehri [32]. In this study, the influence of an external couple on the axial load-carrying capacity of the connection F_u was explored by loading specimens eccentrically, as shown in figure 2.6. The connections consisted of two parallel slotted-in steel plates in combination with steel dowels. It is suggested that for trusses without direct loading of members, a reduction of the maximum allowable tensile load of 10 % should be taken into account [32, p. 1342].

Figure 2.6: Influence of external couple on axial load-carrying capacity F_u [32, Fig. 14]

Similar research was done by Schilling et al. [65]. The authors propose a reduction factor for connections that are subjected to complex loading of normal force and bending moment. To this end, multiple tests from the literature were compared, including the tests conducted by Gehri [32], in which truss members are subjected to load cases of both tensile normal force and bending moment.

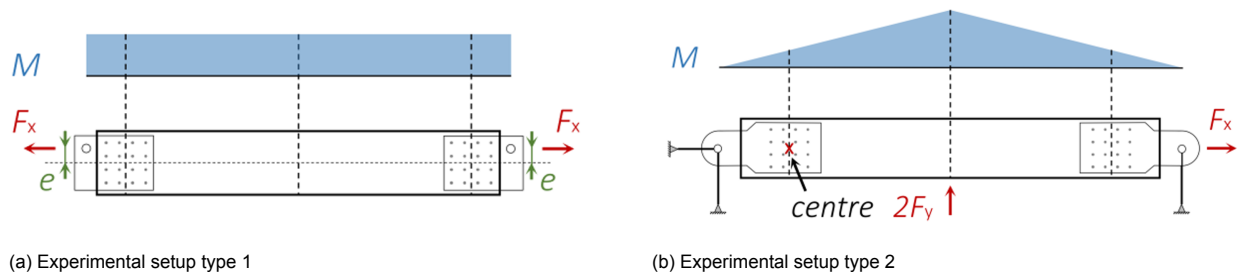


Figure 2.7: Experimental test setups from the literature used by Schilling [65, p. 11]

The tests used in the analysis either applied an eccentric tensile normal force on a specimen (type 1,

see figure 2.7a) or combined the tensile normal force with a point load in the center point of the specimen (type 2, see figure 2.7a). The bending moment values for type 2 were adjusted and expressed in the normal force acting at a certain eccentricity, so that type 1 and type 2 could be compared. The results are shown in figure 2.8b. Non-linear regression was applied to the results of all tests, to come to the proposed reduction factor which is to be calculated according to equation 2.1.

$$k_e = \frac{F_{u,e}}{F_{u,0}} = 1 - 1.56 \left(\frac{e}{h_{conn}} \right)^{1.25} \quad R^2 = 0.88 \quad (2.1)$$

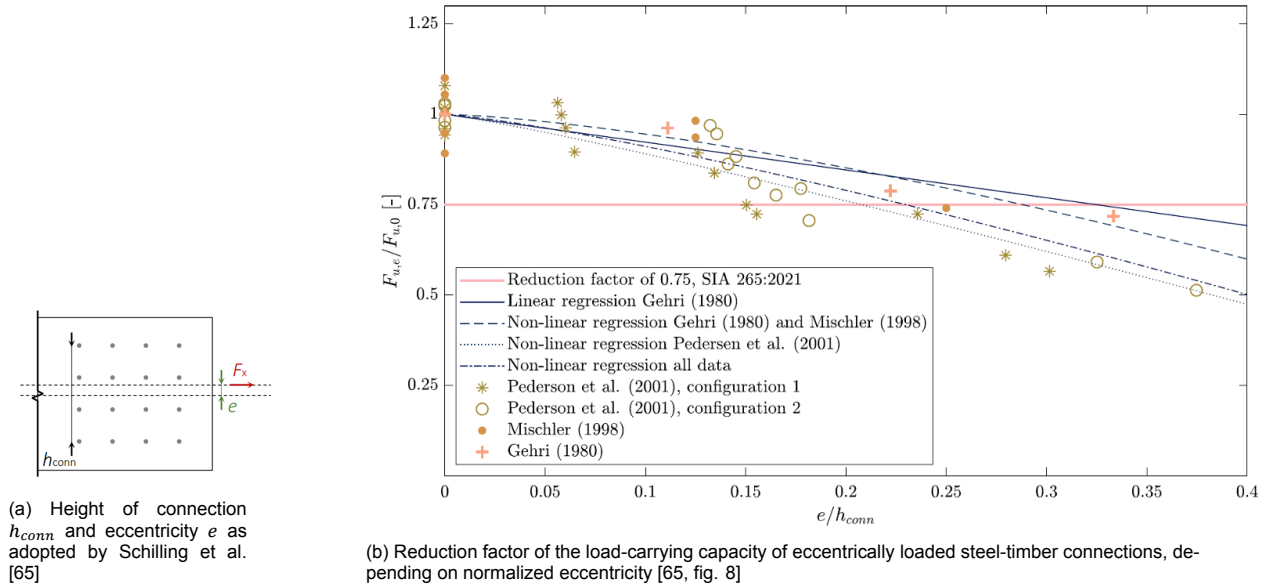


Figure 2.8

It is concluded that rotational stiffness of the connections in timber trusses negatively impacts the load-bearing capacity of dowel connections with slotted-in steel plates. The studies by Gehri [32] and Schilling [65] underline the importance of quantification of rotational stiffness and subsequent reduction of capacity of these connections.

Connection properties

3.1. Introduction

Connections with inclined screws are a special type of connection, as the screws are loaded both in shear and in withdrawal. In this chapter, both the shearing behaviour and axial behaviour of inclined screw connections are discussed. Dowels are an often used connecting agent to connect timber members by transferring shear forces. Dowel-type fasteners are all fasteners that exhibit dowel-type behaviour and include laterally loaded screws, bolts, nails, and dowels. In the final part of this chapter, screws loaded in withdrawal are discussed, also referred to as axially loaded screws.

3.2. Dowel type fasteners

Dowel-type fasteners are well reflected in both standards and literature. This section discusses both the load-bearing capacity and stiffness of dowel-type fasteners.

3.2.1. Load-bearing capacity

The load-bearing capacity of dowel-type connections is governed by three main parameters. These are the embedment strength of the wood f_h , the strength of the dowel, expressed in the yield moment of the dowel M_y , and finally the dowel's capacity for load uptake in tension, also referred to as the anchorage capacity F_{ax} [54, p. 89].

Brittle failure modes and group effects

Connections often need multiple dowel-type fasteners in order to carry their load. The fasteners in connections are often placed close to one another, as otherwise, the dimensions of the connections have to be enlarged resulting in over-dimensioned, uneconomical structures [54]. On the other hand, if fasteners are placed too closely together, the risk of splitting and other brittle failure mechanisms occurring before timber embedment or dowel yielding increases. The brittle failure mechanisms that may occur in timber connections with multiple dowel-type fasteners are given in figure 3.1. In order to prevent brittle failure mechanisms in connections, sufficient screw spacings and end/edge distances must be applied. These distances are specified in standards, for instance, EN-1995-1-5 [55]. For connections with inclined screws, EN-1995-1-1 prescribes the minimum screw spacings and end/edge distances as given in table 3.1 and figure 3.2. Besides these minimum values for spacings and end/edge distances, EN-1995-1-1 provides verification formulas for connections per failure mechanism.

Ductility of dowel-type connections can be improved by further endeavours to prevent brittle failure mechanisms. This can be achieved by applying reinforcements of connections with screws as described by Betjka [7], or by using engineered wood such as LVL with cross layers as described by Kobel et al. [45], who found satisfactory results for a cross-layer percentage of 14 % to prevent immature splitting.

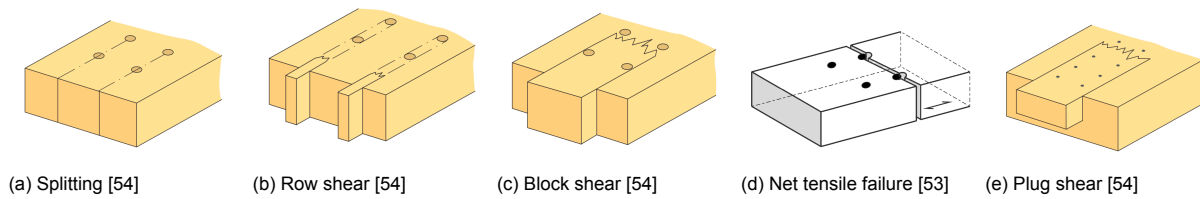


Figure 3.1: Brittle failure modes in timber joints.

Individual fasteners in a fastener group are typically not loaded equally, even in case the load perfectly aligns with the geometrical centre of gravity of the individual fasteners [13, p. 342]. Reasons for this phenomenon are local variations in hole sizes, timber strength, hole misalignment, and unintentional uneven load transfer between connected timber members [54, p. 104]. In case multiple fasteners in a row are loaded, typically the first and last fastener experience the highest load and therefore are most inclined to fail first, as first described by Lantos [47] and Cramer [18], according to information in the handbook of Swedish Wood [54, p. 104]. Standards typically solve this by specifying an effective number of fasteners lower than the amount of fasteners present. The effective number of fasteners is then used to check the capacity of a row of fasteners (see equation 3.1).

$$F_{v,Rk} = n_{ef} F_{v,Rk} \quad (3.1)$$

In which:

- $F_{v,Rk}$: effective characteristic load carrying capacity of a single row of fasteners parallel to the grain
- n_{ef} : effective number of fasteners in line parallel to the grain, depending on fastener spacing, number of fasteners, fastener diameter, and pre-drilling

[55, p. 56]

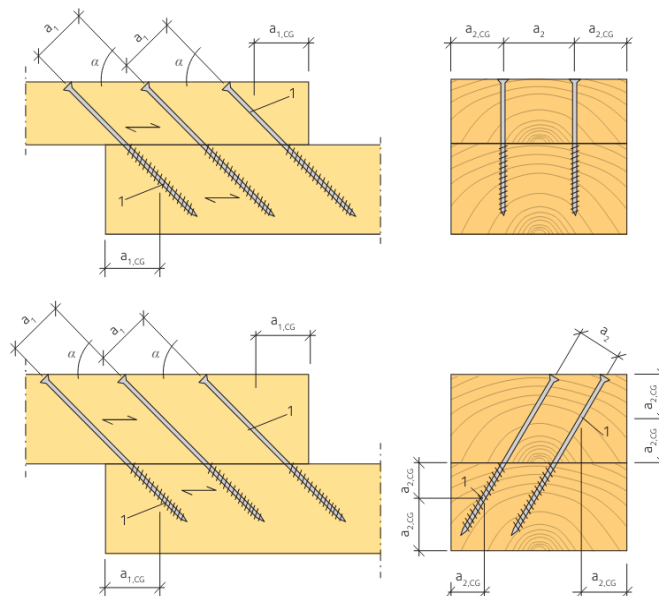


Figure 3.2: Minimum edge and end distances for connections with inclined screws [56, p. 48].

Embedment strength

The embedment strength is the stress that can be sustained by the timber around a dowel, and depends on several parameters:

Minimum screw spacing in a plane parallel to the grain	Minimum screw spacing perpendicular to a plane parallel to the grain	Minimum end distance of the centre of gravity of the threaded part of the screw in the member	Minimum edge distance of the centre of gravity of the threaded part of the screw in the member
a_1	a_2	$a_{1,CG}$	$a_{2,CG}$
7d	5d	10d	4d

Table 3.1: The minimum values for end and edge distances as given in EN-1995-1-1 for connections with inclined screws [55].

- Density of timber: higher densities yield higher embedment strengths.
- Diameter of the fastener: small dowel diameters yield higher embedment strengths.
- Angle between grain and load direction: compression parallel to the grain yields the highest embedment strengths. Conversely, compression perpendicular to the grain yields the lowest embedment strengths.
- Friction that occurs between the timber and fastener: dowels with a rougher surface and thus higher values of friction between timber and dowel yield higher embedment strengths.
- Moisture content of the timber: higher moisture content of the wood leads to lower embedment strengths.
- Reinforcement perpendicular to the grain, if present: embedment failure is initiated by a crack propagating along the grain of the wood. Therefore, any reinforcement in this direction yields higher embedment strengths.
- Pre-drilling of the hole: in case the hole is pre-drilled, the vast majority of the load parallel to the grain is resisted by compression of the timber fibres parallel to the grain. In case the hole is not pre-drilled, a relatively larger portion of the load is resisted via compression perpendicular to the grain, yielding lower embedment strengths (see figure 3.3).

[54, p. 90]

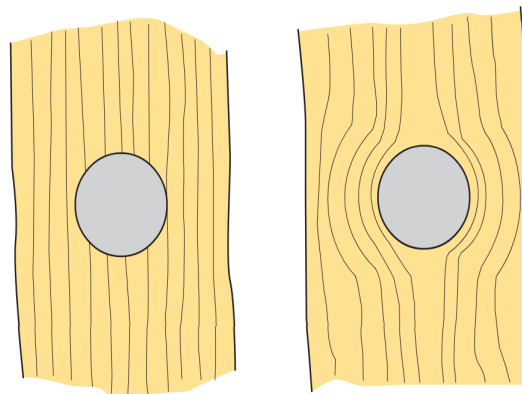


Figure 3.3: Difference in timber structure around a dowel-type fastener between a case with a pre-drilled hole (left) and without a pre-drilled hole (right). The timber fibres are cut in the first case, while they are bent in the latter [54, p. 90].

Because timber is an orthotropic material, the compressive strength depends on the angle at which compressive force is applied. This relation was first experimentally determined by Hankinson [34], who proposed equation 3.2, relating the angle between the line of force α to the compressive timber strength parallel to the grain $f_{c,0}$ and perpendicular to the grain $f_{c,90}$. The formula is found to be applicable in

tension as well [54, p. 36]. A formula for the embedment strength based on the Hankinson equation is adopted in EN 1995-1-1 [55] (see equation 3.6).

$$f_{c,\alpha} = \frac{f_{c,0}f_{c,90}}{f_{c,0} \sin^2(\alpha) + f_{c,90} \cos^2(\alpha)} \quad (3.2)$$

The embedment strength can be found from an embedment test, and is a property related to the total system rather than to a material [13, p. 348]. It is usually tested in an embedment test as given in figure 3.4a and described in further detail in EN383 [28]. The embedment strength is defined as the maximum stress that is obtained before or at a displacement of 5 [mm], divided by the projected area of the dowel-type fastener, according to formula 3.3.

$$f_h = \frac{F_{max}}{d \cdot t} \quad (3.3)$$

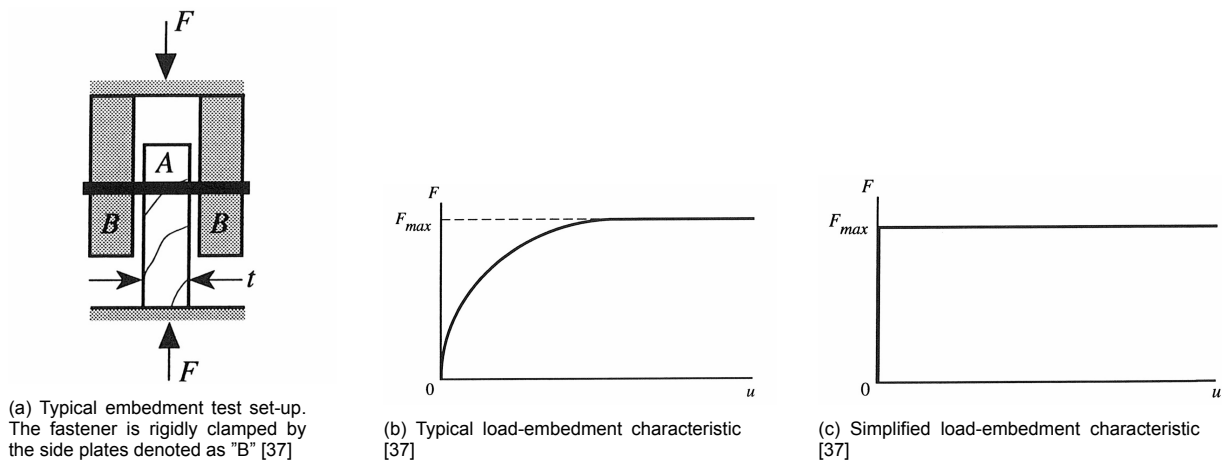


Figure 3.4

Tests have been performed by Ehlbeck & Werner [26], in which multiple timber species were subjected to embedment tests under different angles to the grain. Ehlbeck and Werner [26] proposed equation 3.4 for smooth round fasteners in pre-drilled holes in softwood loaded parallel to the grain. The equation is adopted in EN-1995-1-1 [55] for bolts and dowels with diameters up to 30 [mm], with the slight difference that the characteristic values are used for embedment strength and density, as given in equation 3.5. Embedment strengths for different angles to the grain can be obtained by making use of equation 3.6 given in EN-1995-1-1, which is based on the equation proposed by Hankinson. A typical load-embedment characteristic for steel dowels in timber is given in figure 3.4b. For the capacity of timber connections with dowel-type connections, an ideal rigid-plastic material behaviour is usually assumed, so that the simplified load-embedment characteristic as given in figure 3.4c can be adopted. This approximation significantly simplifies the calculation procedure and has little influence on its result [37].

$$f_{h,0} = 0.082 \cdot (1 - 0.01d) \cdot \rho_{mean} \quad (3.4)$$

$$f_{h,0,k} = 0.082 \cdot (1 - 0.01d) \cdot \rho_k \quad (3.5)$$

$$f_{h,\alpha,k} = \frac{f_{h,0,k}}{k_{90} \sin^2(\alpha) + \cos^2(\alpha)} \quad (3.6)$$

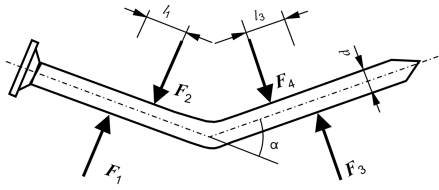
In which:

- α : the angle between the grain direction and load vector

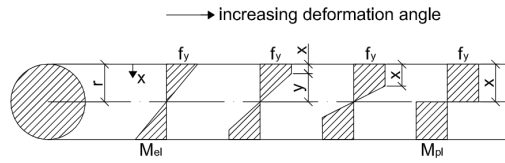
- $k_{90} = \begin{cases} 1.35 + 0.015d, & \text{for softwoods} \\ 1.30 + 0.015d, & \text{for LVL} \\ 0.90 + 0.015d, & \text{for hardwoods} \end{cases}$
- $f_{h,0,k}$: embedment strength of the timber parallel to the grain

Yield moment

The strength of the dowel or dowel-type fastener is represented by its yield moment. The procedure to determine this property is described in EN 409 [29] and consists of a four-point bending test of the dowel-type fastener. The loading is increased until angle α reaches a value of 45° for nails and staples, or $(110/d)^\circ$ for screws, dowels, or bolts.



(a) Test set-up to determine the yield moment of dowel-type fasteners [29]



(b) Plastic and elastic bending moment for increasing rotation angle [61, p. 154]

$$M_{el} = \frac{\pi}{32} f_y d^3$$

$$M_{pl} = \frac{1}{6} f_y d^3$$

Figure 3.5

One method to determine a first estimate of the yield moment would be to use the plastic bending moment as derived in equation 3.7. However, there is ambiguity between EN 409 [29] which requires dowels to reach a certain rotation angle in order to reach their yield moment, and EN 26891 [27] that states that connections should be tested up to either a deformation of 15 [mm] or ultimate load. It is stated by Sandhaas [61, p. 152] that thicker dowels therefore do not reach their plastic limit before a deformation of 15 [mm], while on the contrary thinner dowels will reach full plasticity in the hinge before a deformation of 15 [mm]. Therefore, equation 3.7 can only be used for high-strength steel dowels and very high-strength steel dowels, which already show relatively high levels of plasticity for small rotation angles [61, p. 152]

$$M_{pl} = \frac{\pi r^2}{2} \frac{4r}{3\pi} 2f_y = \frac{8r^3}{6} f_y = \frac{1}{6} d^3 f_y \quad (3.7)$$

The phenomenon described above had also been noted by Blass et al. [8] after a large number of tests had been performed measuring load and bending angles of dowels [42], [43]. Blass et al. proposed equation 3.10 as an improvement of the old version of eurocode [30] which used two formulas for the yield moment, given in equations 3.8 and 3.9. Equation 3.10 was indeed adopted in a slightly rearranged form in the current version of EN-1995-1-1 [55], given by equation 3.11.

$$M_{y,k} = 0.8 f_{u,k} \frac{d^3}{6} \quad (\text{for round steel bolts, with } f_{u,k} \text{ the char. tensile strength}) \quad (3.8)$$

$$M_{y,k} = 180 d^{2.6} \quad \text{for round steel nails with minimum tensile strength of } 600 \text{ [N/mm}^2\text{]} \quad (3.9)$$

$$M_{y,k} = 0.24 f_{u,k} d^{2.7} \quad (3.10)$$

$$M_{y,Rk} = 0.3 f_{u,k} d^{2.6} \quad (3.11)$$

Johansen yield theory

The failure behaviour of timber-to-timber connections making use of dowels was first described by Johansen in 1949 [41]. Johansen studied connections both with single and double shear planes. The research found that not only the embedment behaviour of the timber was of importance for the capacity, but also the yield moment of the dowel itself. For this, ideal rigid-plastic material behaviour is assumed of the timber in embedding. The same holds for the steel of the dowel in bending. Three distinct failure modes shown in figure 3.6 were proposed by Johansen [41]:

- failure mode 1: failure with no plastic hinges in the dowel
- failure mode 2: failure with one plastic hinge in the dowel
- failure mode 3: failure with two plastic hinges in the dowel

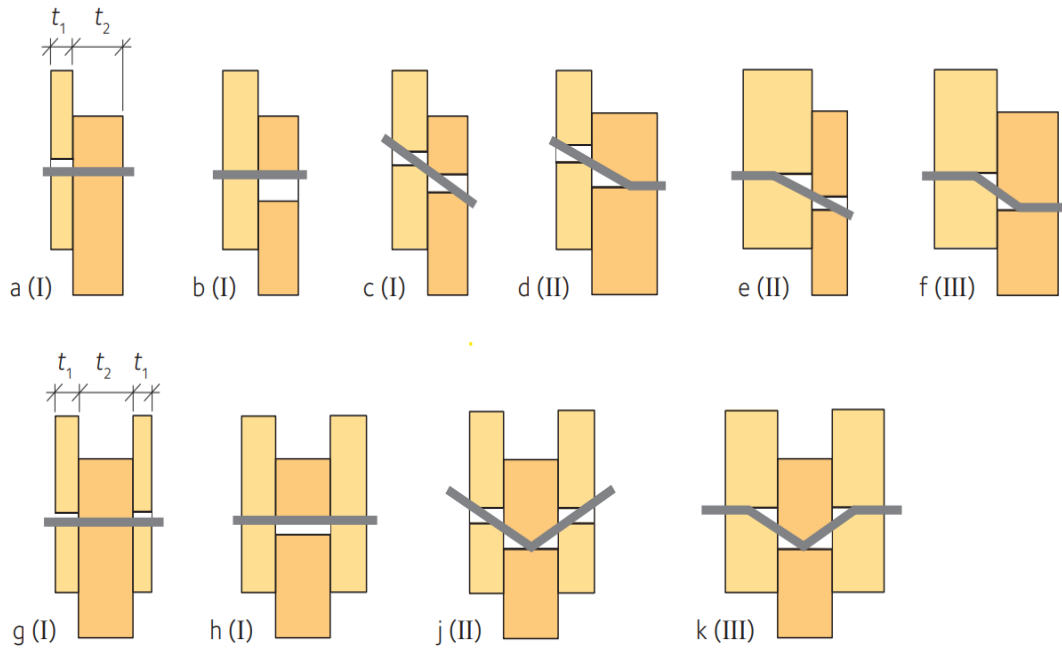


Figure 3.6: Timber-to-timber failure modes with dowel connection, [54, p. 92]

By setting up the moment equilibrium of the dowel, different formulas for the failure modes with single shear planes can be derived. In case the two timber elements consist of different species, the fraction of their embedment strengths is expressed utilising the factor β , which is determined via equation 3.12.

$$\beta = \frac{f_{h,2,k}}{f_{h,1,k}} \quad (3.12)$$

The basic formulae for the resistance based on moment equilibrium are expressed as:

- $F_{v,Rk} = f_{h,1,k} t_1 d$ for modes a(I) and b(I) in figure 3.6
- $F_{v,Rk} = \frac{f_{h,1,k} d t_1}{1+\beta} \left(\sqrt{\beta + 2\beta^2 \left(1 + \frac{t_2}{t_1} + \left(\frac{t_2}{t_1} \right)^2 \right) + \beta^3 \left(\frac{t_2}{t_1} \right)^2} - \beta \left(1 + \frac{t_2}{t_1} \right) \right)$ for mode c(I) in figure 3.6
- $F_{v,Rk} = \frac{f_{h,1,k} d t_1}{2+\beta} \left(\sqrt{2\beta(1+\beta) + \frac{4\beta(2+\beta)M_{y,Rk}}{f_{h,1,k} d t_1^2}} - \beta \right)$ for modes d(II) and e(II) in figure 3.6
- $F_{v,Rk} = \sqrt{\frac{2\beta}{1+\beta}} \sqrt{2M_{y,Rk} f_{h,1,k} d}$ for mode f(III) in figure 3.6

European Yield Model

The equations given in section 3.2.1 form the basis for the verification method referred to as the European Yield Model (EYM) used in Eurocode 5 [55, p. 58]. These formulas typically consist of four parts, being:

- Partial safety factor
- Ratio between embedment strengths of the two timber parts
- Johansen part
- Part taking into account the rope effect

Correction factors are used to correct for material factors of the timber, steel, and the k_{mod} factor for short-term loading. Instead of applying these factors separately before inputting them in the verification formula, these different factors are combined into a single factor the verification formula can be multiplied with. Correction factors only have to be used in failure modes in which the dowels are deformed, because in these formulas $M_{y,Rk}$ and $f_{h,1,k}$ are modified by a square root. Originally Johansen [41] published his paper taking into account only cases in which the two connected timber parts have equal characteristic embedment strengths $f_{h,k}$. The European Yield Model also takes into account the possibility of timber parts with different embedment strengths, conveniently expressed in the term β , the ratio of the two embedment strengths as specified by equation 3.12.

The part of the formula that was analytically derived by Johansen [41] is usually referred to as the "Johansen part" of the equations of the EYM. A final addition to the equations is the so-called rope effect. In case the dowel-type fastener is bent or inclined as a result of the shear force between the timber elements, a considerable amount of resistance can result from the tension that is taken up by the dowel-type fastener. This tension force can be the result of the surface friction between the dowel-type fastener and the timber, or of washers or nuts attached to the dowel-type fastener. This effect is taken into account by means of adding a factor of magnitude $\frac{F_{ax,Rk}}{4}$ to the shear resistance. This addition makes the verification method not only suited for dowels, but also for screws, bolts, or nails. The maximum contribution from the rope effect depends on the kind of fastener that is used. The maximum contribution from the rope effect as a percentage of the shear capacity is given in table 3.2 for different types of dowel-type fasteners.

The four distinct parts of the EYM are most clearly seen in the verification equation for failure mode f(III), which is given in equation 3.13. In this equation the safety factor is written in red, the embedment ratio in grey, the Johansen part in blue, and the contribution from the rope effect in black. The equations for the failure modes of the EYM in single shear are given by equation 3.14.

$$F_{v,Rk} = 1,15 \sqrt{\frac{2\beta}{1+\beta}} \sqrt{2M_{y,Rk}f_{h,1,k}d} + \frac{F_{ax,Rk}}{4} \quad (3.13)$$

Round nails	15 %
Square and grooved nails	25 %
Other nails	50 %
Screws	100 %
Bolts	25 %
Dowels	0 %

Table 3.2: Maximum contribution from the rope-effect as a percentage of the shear capacity [55]

$$F_{v,Rk} = \min \left\{ \begin{array}{l} f_{h,1,k} t_1 d \\ f_{h,2,k} t_2 d \\ \frac{f_{h,1,k} t_1 d}{1+\beta} \left[\sqrt{\beta + 2\beta^2 \left[1 + \frac{t_2}{t_1} + \left(\frac{t_2}{t_1} \right)^2 \right] + \beta^3 \left(\frac{t_2}{t_1} \right)^2} - \beta \left(1 + \frac{t_2}{t_1} \right) \right] + \frac{F_{ax,Rk}}{4} \\ 1,05 \frac{f_{h,1,k} t_1 d}{2+\beta} \left[\sqrt{2\beta(1+\beta) + \frac{4\beta(2+\beta)M_{y,Rk}}{f_{h,1,k} d t_1^2}} - \beta \right] + \frac{F_{ax,Rk}}{4} \\ 1,05 \frac{f_{h,1,k} t_2 d}{1+2\beta} \left[\sqrt{2\beta^2(1+\beta) + \frac{4\beta(1+2\beta)M_{y,Rk}}{f_{h,1,k} d t_2^2}} - \beta \right] + \frac{F_{ax,Rk}}{4} \\ 1,15 \sqrt{\frac{2\beta}{1+\beta}} \sqrt{2M_{y,Rk} f_{h,1,k} d} + \frac{F_{ax,Rk}}{4} \end{array} \right. \quad (3.14)$$

3.2.2. Connection stiffness

For the determination of the stiffness of timber connections the testing procedure as given in EN 26891 is most often used in Europe. The loading procedure and corresponding idealized load-deformation curve are given in figure 3.7. In the test procedure, the applied load is always related to the value of the estimated maximum load F_{est} of the connection, which may be determined based on experience, calculations, or preliminary tests [27]. A reloading cycle is included in the procedure in order to find the elastic stiffness thereby excluding the influence of initial slip, a term defined as the deformation at load levels of little or no load [39]. Testing may be stopped in case the ultimate load is reached i.e. failure has occurred, or in case joint slip has reached a value of 15 [mm] [27]. In timber connections typically 40 % of the ultimate load is regarded as the serviceability limit state (SLS). From the testing procedure, different stiffness values can be calculated. These stiffnesses are calculated according to equations 3.15, 3.16 and 3.17. The visualizations of these stiffnesses in the load-deformation curve of EN 26891 [27] are illustrated in figure 3.8.

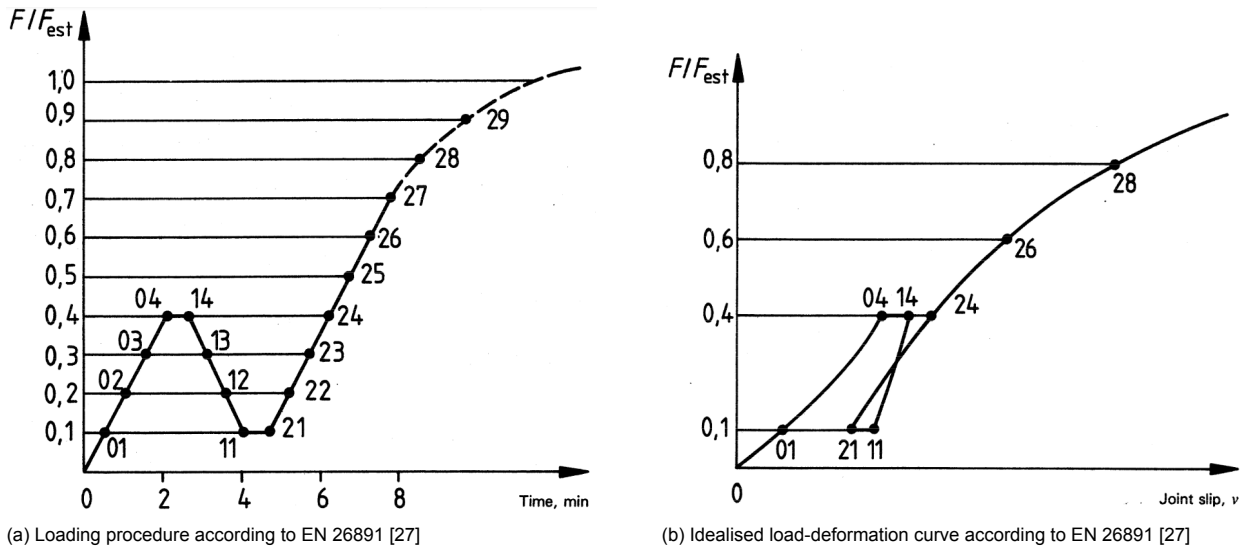


Figure 3.7

1. Initial stiffness k_i , defined as the secant stiffness at 40 % of the estimated maximum load F_{est} , making use of the initial deformation v_i :

$$k_i = \frac{0.4 \cdot F_{est}}{v_i} \quad \text{with} \quad v_i = v_{04} \quad (3.15)$$

2. Stiffness k_s , making use of a modified initial deformation $v_{i,mod}$:

$$k_s = \frac{0.4 \cdot F_{est}}{v_{i,mod}} \quad \text{with} \quad v_{i,mod} = \frac{4}{3} \cdot (v_{04} - v_{01}) \quad (3.16)$$

3. Elastic stiffness k_e , making use of the elastic deformation v_e :

$$k_e = \frac{0.4 \cdot F_{est}}{v_e} \quad \text{with} \quad v_e = \frac{2}{3} \cdot (v_{14} + v_{24} - v_{11} - v_{21}) \quad (3.17)$$

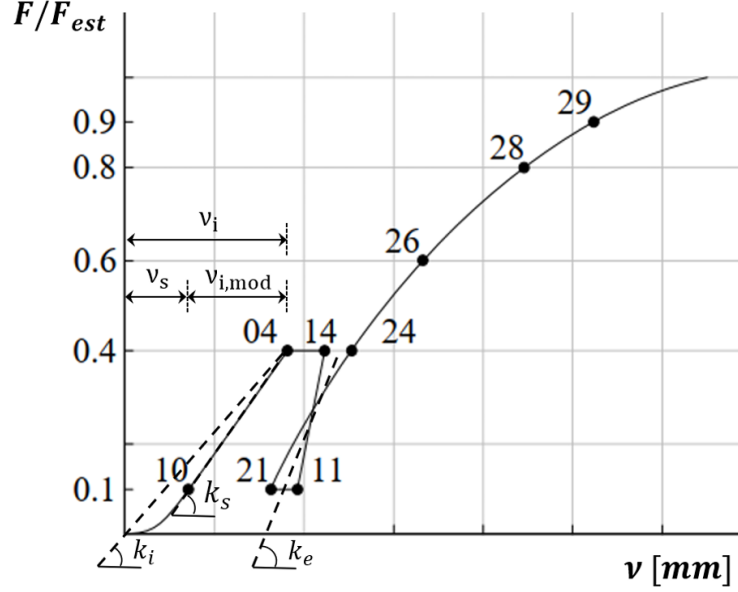


Figure 3.8: Stiffness parameters visualised in the load-deformation curve [49, p. 14]

Lateral connection stiffness of connections with dowel-type fasteners is calculated in EN 1995-1-1 [55] with slip modulus K_{ser} , given in equation 3.18.

$$K_{ser} = \frac{\rho_m^{1.5} d}{23} \quad (3.18)$$

In which:

- ρ_m : mean density of timber [kg/m^3], if two timber elements are connected, $\rho_m = \sqrt{\rho_{m,1} \cdot \rho_{m,2}}$
- d : outer diameter of screw [mm]

The background of this equation is based on the assumption of initial stiffness as given by equation 3.15, i.e. the secant modulus in the region up until 40 % of the maximum load on the load-deformation curve. The instantaneous deformation around 40 % of the maximum load-carrying capacity has been estimated from multiple tests and is given by equation 3.19 [39]. The derivation of slip modulus K_{ser} is given by equation 3.20, and is based on the resistance given by Johansen's failure mode 3, i.e. with two plastic hinges, the yield moment from the old Eurocode [30] given by equation 3.9 and the embedment strength as given by equation 3.5. The penultimate step in the derivation is somewhat vague. It is stated that for diameters between 2 and 8 [mm], the root may be dropped and the fraction simplified to one-twentieth [39]. However, it has been stated that this is only the case for a value of $d = 15.31$ [mm] [49, p. 110]. It is suggested that based on further research or for the sake of applicability, the fraction of one twentieth was chosen [49, p. 110]. It is noted that the slip modulus K_{ser} is derived based on the assumption of embedment strength parallel to the grain. Furthermore, plastic deformation of the fastener is assumed, owing to the assumption of Johansen's yield theory.

$$u_{inst} = 40 \frac{d^{0.8}}{\rho_k} \quad (3.19)$$

$$\left. \begin{aligned}
 K_{ser} &= \frac{0.4R}{u_{inst}} \\
 u_{inst} &= 40 \frac{d^{0.8}}{\rho_k} \\
 R &= \sqrt{\frac{2\beta}{1+\beta}} \sqrt{2M_y f_h d} \\
 \beta &= 1 \\
 f_{h,k} &= 0.082(1 - 0.01d)\rho_k \\
 M_{y,k} &= 180d^{2.6}
 \end{aligned} \right\} \Rightarrow K_{ser} = \frac{0.543}{100} \sqrt{(100-d)} \rho_k^{1.5} d \Rightarrow \left. \begin{aligned}
 K_{ser} &\approx \frac{\rho_k^{1.5} d}{20} \\
 \rho_k &= \frac{\rho_m}{1.1}
 \end{aligned} \right\} \Rightarrow K_{ser} = \frac{\rho_m^{1.5} d}{23}$$

(3.20)

3.3. Axially loaded screws

Screws that experience only a tensile load parallel to their axis are defined as axially loaded screws. To determine the capacity of axially loaded screws, the minimum of the following three failure modes should be considered:

- withdrawal failure of the threaded part of the screw
- pull-through failure of the screw head
- tensile failure of the screw head

Different equations and values are used for these failure modes, for instance by EN-1995-1-1 or European technical assessment documents (ETA) that are available for individual screw types. The stiffness of axially loaded screws is not defined in EN-1995-1-1 so equations from specific ETA documents should be used. An alternative is to use equations from the literature, which is described in more detail in chapter 4.

Inclined screw connections

4.1. Introduction

The stiffness of connections with inclined screws is complex, and a calculation approach is not included in the current version of EN-1995-1-1 [55]. This section briefly discusses capacity calculation methods for connections with inclined screws, although the main focus is on the identification of stiffness calculation methods for connections with inclined screws.

4.2. Geometry

Connections with inclined screws have a more complex geometry than connections consisting of laterally loaded dowels or axially loaded screws. The parameters of importance in this thesis are the angle between the screw axis and shear plane α_s , screw stiffness in the inclination direction of the screw k_{SLs} , and screw stiffness perpendicular to the inclination direction $k_{SLs,v}$. It is assumed that the grain direction of both timber members 1 and 2 are always parallel to the shear plane in section view. The angles between the grain direction of the timber and screw axis in top view are defined as ϕ_1 and ϕ_2 . An overview is given in figure 4.1.

The literature that is discussed in this chapter forms an exception to this rule. It is decided to use the parameters as they are introduced in a specific piece of literature in their descriptions so that no confusion arises between equations and figures.

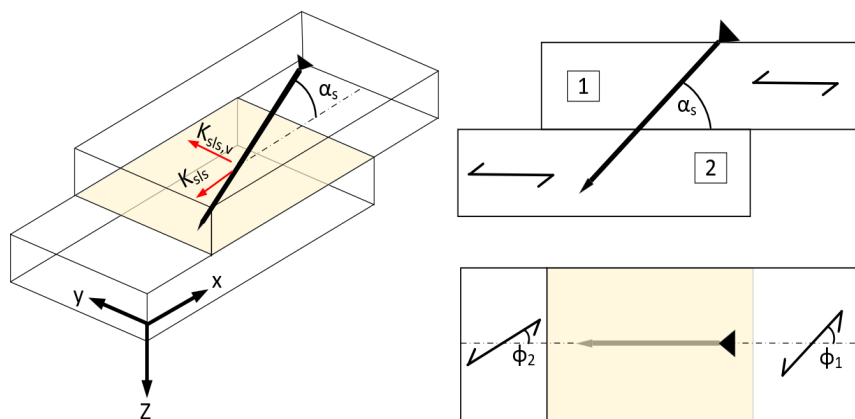


Figure 4.1: Definitions of stiffness directions and angles used throughout the thesis. The shaded plane is the shear plane between timber elements 1 and 2. Source: own image.

4.3. Current Standard: EN-1995-1-1

In the current version of EN-1995-1-1, the load-bearing capacity of screws under a combination of axial and lateral load is calculated as a combination of the axial and lateral behaviour of the screw, as given by equation 4.1.

$$\left(\frac{F_{ax,Ed}}{F_{ax,Rd}}\right)^2 + \left(\frac{F_{v,Ed}}{F_{v,Rd}}\right)^2 \leq 1 \quad (4.1)$$

In which:

- $F_{ax,Ed}$: design axial force per fastener
- $F_{ax,Rd}$: design value for axial capacity of the fastener
- $F_{v,Ed}$: design shear force per fastener
- $F_{v,Rd}$: design value for shear capacity of fastener

The design axial withdrawal capacity $F_{ax,Rd}$ is calculated from the characteristic value $F_{ax,Rk}$ making use of the partial factor for material properties γ_M and modification factor k_{mod} taking into account moisture content and load duration. The characteristic axial withdrawal capacity is given in section 8.7.2 in EN-1995-1-1 [55]. Individual screws should be checked for the withdrawal capacity of the threaded part, screw head pull-through, and tensile failure of the screw shaft. The characteristic shear strength per fastener is calculated according to the European yield model, which is given in equation 8.6 in EN-1995-1-1 [55].

In table 7.1 of EN-1995-1-1 [55], the slip modulus of dowel-type fasteners is given, among which dowels, screws, nails, and bolts. In the document, only slip moduli of fasteners loaded in shear are provided, so that values for the specific case of inclined screws subjected to both axial and lateral load remain undefined. Therefore, according to EN-1995-1-1, the slip modulus of inclined screws is to be determined with the same equation as for laterally loaded screws, as given by equation 3.18.

4.4. Bejtka Blass approach

Based on the European Yield Model (EYM), Bejtka and Blass [11] proposed a calculation model to describe the capacity of joints with inclined screws based on failure mode f(III) of the EYM. In their model, Bejtka and Blass define angle α as the angle between the screw axis and the plane perpendicular to the shear plane, so that $\alpha_s = 90^\circ - \alpha$ (see figure 4.2b). Bejtka and Blass [11] present the results of experimental tests, in which two timber parts loaded parallel to the grain are connected with screws in shear tension with angles α varying between 45° to 90° , as shown in figure 4.2a.

To gain insight into the role of friction in the connection type, tests were also performed with a piece of foil in between the timber specimens. As shown in figure 4.3a it was found that maximum values for load carrying capacity were obtained for an angle of 60° , yielding values that are approximately 53% higher than for screws inserted perpendicularly. The connection stiffness was found to increase for decreasing angles, where connections with screws inserted under 45° showed approximately 12 times higher stiffness values than perpendicularly inserted screws, as given in figure 4.3b. The proposed formula for the load-carrying capacity for connections with inclined screws under shear tension is given by equation 4.2, adjusting failure mode f(III) of the EYM for the inclination of the screw α . The roping effect is taken into account by making use of the withdrawal parameter f_1 of the screw under its inclination α .

$$R = f_1 \cdot d \cdot s_{min} \cdot \tan(\alpha) + \sqrt{\frac{2 \cdot \beta}{1 + \beta}} \cdot \sqrt{2 \cdot M_y \cdot d \cdot f_{h,1} \cdot \cos(\alpha)} \quad (4.2)$$

In which:

- s_i : penetration depth of the screw in timber part i , see figure 4.2b.

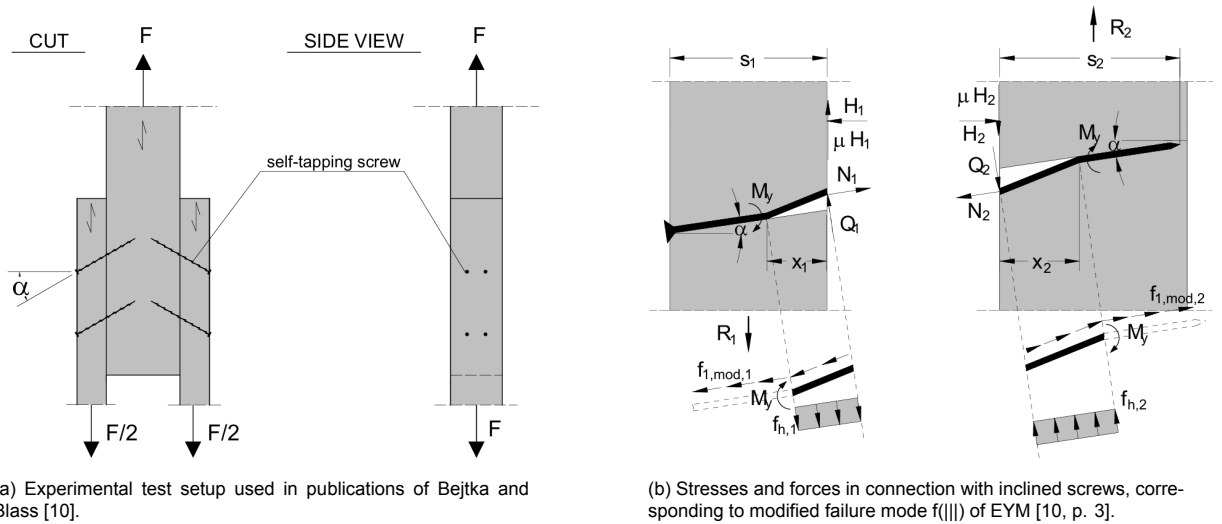


Figure 4.2

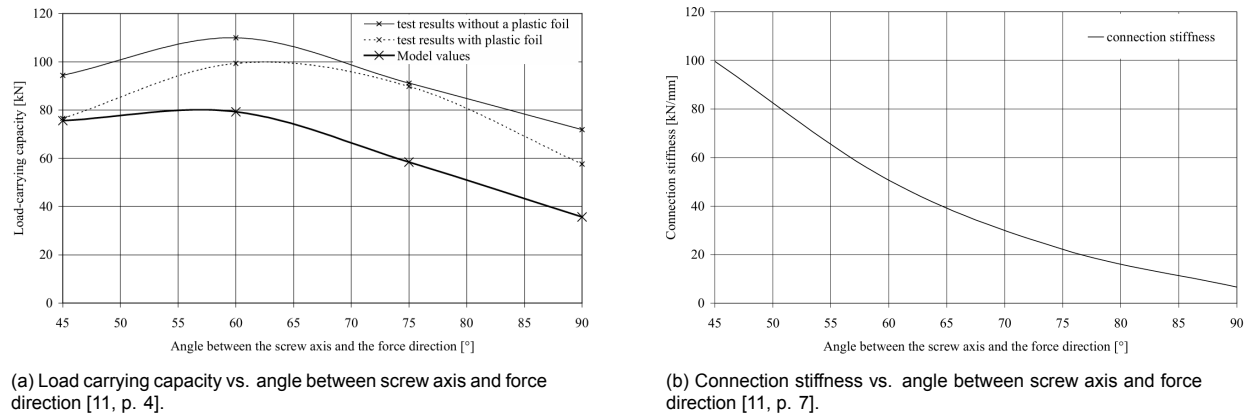


Figure 4.3

$$\bullet s_{\min} = \min \left\{ \begin{matrix} s_1 \\ s_2 \end{matrix} \right\}$$

- f_1 : axial withdrawal parameter for screws, as defined in E DIN 1052 [15].
- α : angle between screw axis and the line perpendicular to the shear plane (so that $\alpha_s = 90^\circ - \alpha$).

A second paper was published by Bejtka and Blass [10], in which they propose modified equations for all failure modes with a single shear plane of the EYM, as given in equation 4.3. The equations of the EYM are modified so that the influence of friction, screw insertion angle, and withdrawal capacity of the individual screws are taken into account.

Bejtka and Blass [10] found that the timber opens up as a result of the assumed rigid plastic behaviour of the screw and the timber, as shown in figure 4.2b and figure 4.4b. Because the screw is in this case not enclosed by the timber over its full circumference, a reduced withdrawal capacity is proposed. The total screw displacement along the deformed screw axis Δ_{tot} is related to the original inclination of the screw α for a fixed connection deformation δ_{tot} of 15 [mm] (as defined by ISO 6891, [27, p. 2]) via a geometric model, given in figure 4.4b. Modified withdrawal tests are performed, in which screws are given a certain lateral displacement before the withdrawal load is applied, to simulate the opening-up effect of the timber. Combining the results of these tests and the aforementioned relation between total screw displacement and inclination angle, modified withdrawal parameters are proposed,

by taking the average value of $f_{1,mod,i,j}$ over the screw insertion length s_i (see figure 4.4a). Because it was found that screws with large diameters ($d > 8$ [mm]) do not reach their withdrawal capacity for small angles between the screw axis and shear plane ($\alpha < 15^\circ$) before a connection displacement δ_{tot} of 15 [mm], these configurations have significantly smaller modified withdrawal capacities. In order to simplify the design procedure, Bejtka and Blass [10] propose a value for the modified withdrawal capacity $f_{1,mod,i,j} = 0.7 \cdot f_{1,i}$, in which $f_{1,i}$ is defined as the ultimate withdrawal capacity parameter obtained from an axial withdrawal test performed on member i .

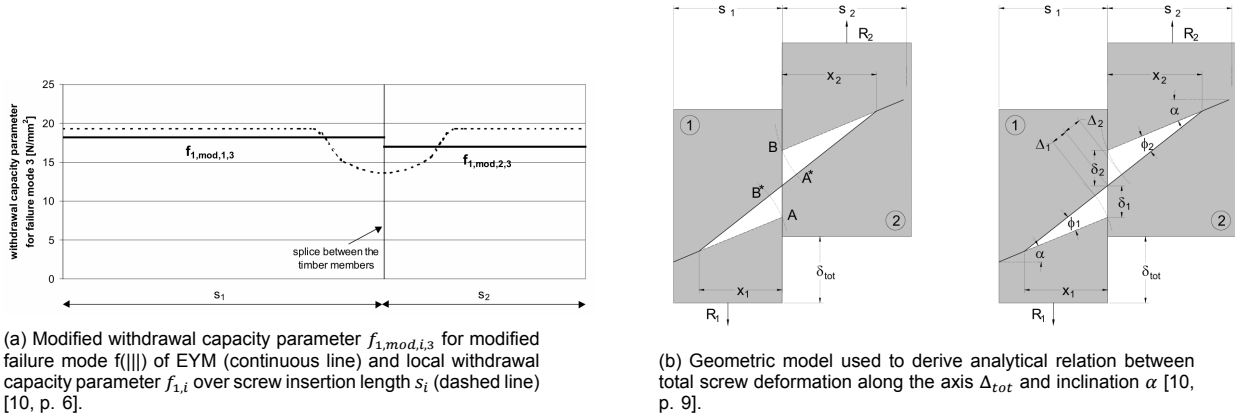


Figure 4.4

$$R_{VM1a,l} = R_{ax,1a,l} \cdot \sin \alpha + f_{h,1} \cdot d \cdot s_1 \cdot \cos \alpha$$

$$R_{VM1a,r} = R_{ax,1a,r} \cdot \sin \alpha + f_{h,2} \cdot d \cdot s_2 \cdot \cos \alpha$$

$$R_{VM1b} = R_{ax,1b} \cdot (\mu \cdot \cos \alpha + \sin \alpha)$$

$$+ \frac{f_{h,1} \cdot d \cdot s_1}{1 + \beta} \cdot (1 - \mu \cdot \tan \alpha) \cdot \left[\sqrt{\beta + 2 \cdot \beta^2 \cdot \left[1 + \frac{s_2}{s_1} + \left(\frac{s_2}{s_1} \right)^2 \right] + \beta^3 \cdot \left(\frac{s_2}{s_1} \right)^2} - \beta \cdot \left(1 + \frac{s_2}{s_1} \right) \right]$$

$$R_{VM2a} = R_{ax,2a} \cdot (\mu \cdot \cos \alpha + \sin \alpha)$$

$$+ (1 - \mu \cdot \tan \alpha) \cdot \frac{f_{h,1} \cdot s_1 \cdot d}{2 + \beta} \cdot \left[\sqrt{2 \cdot \beta \cdot (1 + \beta) + \frac{4 \cdot \beta \cdot (2 + \beta) \cdot M_y \cdot \cos^2 \alpha}{f_{h,1} \cdot d \cdot s_1^2}} - \beta \right] \quad (4.3)$$

$$R_{VM2b} = R_{ax,2b} \cdot (\mu \cdot \cos \alpha + \sin \alpha)$$

$$+ (1 - \mu \cdot \tan \alpha) \cdot \frac{f_{h,1} \cdot s_2 \cdot d}{1 + 2 \cdot \beta} \cdot \left[\sqrt{2 \cdot \beta^2 \cdot (1 + \beta) + \frac{4 \cdot \beta \cdot (2 \cdot \beta + 1) \cdot M_y \cdot \cos^2 \alpha}{f_{h,1} \cdot d \cdot s_2^2}} - \beta \right]$$

$$R = \min \left\{ \begin{array}{l} R_{VM1a,l} \\ R_{VM1a,r} \\ R_{VM1b} \\ R_{VM2a} \\ R_{VM2b} \\ R_{VM3} \end{array} \right\} \quad (4.4)$$

$$R_{ax,j} = \min \left\{ \begin{array}{l} f_{1,mod,1,j} \cdot d \cdot \frac{s_1}{\cos \alpha} \\ f_{1,mod,2,j} \cdot d \cdot \frac{s_2}{\cos \alpha} \end{array} \right\} \quad (4.5)$$

In which:

- $f_{1,mod,i,j}$: modified withdrawal capacity parameter of the screw for timber member i and failure mode j

- μ : coefficient of friction between timber members

In a publication that was released a few years later than the ones discussed above, Blass, Bejtka and Uibel [9, eq. 32] present a method to calculate the connection stiffness of timber-to-timber connections per screw and per shear plane, as given by equation 4.6.

$$K_G = \frac{1 + \mu \cdot \tan(\alpha)}{\frac{1}{K_{ax,1}} + \frac{1}{K_{ax,2}}} \quad (4.6)$$

In which:

- K_G : connection stiffness [N/mm]
- α : angle between screw axis and load [°], so that $\alpha = \alpha_s$ in case the load is applied parallel to the grain direction.
- $K_{ax,i}$: axial withdrawal stiffness of screw in timber element i [N/mm]
- d : screw diameter [mm]
- l_s : threaded length in timber element i [mm]

The validity of this formula seems questionable, as the stiffness K_G increases for larger values of angle α , so that connections with inclined screws would be less stiff than connections with perpendicularly inserted screws. Also, the definition of the tangent does not allow angles α of 90°. The authors have only performed tests with angles α of 45°, so a possible explanation could be that the definition of α should be the angle between the screw axis and line perpendicular to the grain/load [33, P. 580], as is the case in the earlier work by Bejtka and Blass.

4.5. Kevarinmäki approach

Following the research of Bejtka and Blass [11], Kevarinmäki [44] performed individual screw tests and connection tests for screws both in shear tension configuration and crossed configuration. Kevarinmäki defines the angle between the screw axis and shear plane α , so that α is equal to the definition α_s defined in section 4.2. Only tests under an angle α_s of 45° were performed. In the developed model, Kevarinmäki [44] only takes friction between the timber elements into account for the calculation of connection strength, and not for the calculation of connection stiffness. The equations for the stiffness are given by equations 4.7 - 4.10.

$$K_s = \frac{1}{\frac{1}{k_1} + \frac{1}{k_2}} \quad (4.7)$$

$$k_1 = K_{1,ser} \cdot \pi \cdot d \cdot l_1 \quad (4.8)$$

$$k_2 = K_{2,ser} \cdot \pi \cdot d \cdot (l_2 - d) \quad (4.9)$$

$$K_{i,ser} = K_{ser} \cdot \left(\frac{8 \cdot d}{l_i} \right)^{0.3} \quad (4.10)$$

In which:

- K_s : slip modulus for an axially loaded screw [N/mm]
- k_i : slip modulus for an axially loaded screw in timber part i [N/mm]
- d : outer diameter of the screw [mm]
- l_i : length of the threaded screw part in member i [mm]

- K_{ser} : mean withdrawal slip modulus per unit area of the individual screw, under an angle of 45° between screw axis-grain direction, and a penetration length $l_2 = 8d$ [N/mm³]

(Parameter l_i is referred to as s_i by Kevärinmäki, definitions are identical)

The stiffness model proposed by Kevärinmäki [44] is intended for both tension screws (screws loaded in shear tension) and crossed screw joints. A separate expression for the initial slip of the joint is given, defined by equation 4.11. The red part of the equation should only be added in case of tension (shear tension) joints and takes into account the instantaneous slip due to possible shrinkage as a result of drying of the timber members. The size of the gap δ should be obtained by calculating the shrinkage in the direction perpendicular to the shear plane. To clarify the contribution of shrinkage to the instantaneous slip, figure 4.5 is added. Kevärinmäki [44] states that connections making use of inclined screws loaded in shear tension should not be used in cases where wood drying could cause a gap δ larger than $0.2d$.

$$u_{inst} = \frac{F}{n \cdot K_s} + \frac{\delta}{\tan(\alpha_s)} \quad (4.11)$$

In which:

- u_{inst} : instantaneous slip due to shrinkage [mm]
- F : external force [N]
- n : the total number of individual screws in the connection [-]
- δ : gap width as a result of timber shrinkage [mm]
- α_s : angle between screw and grain/force [°]

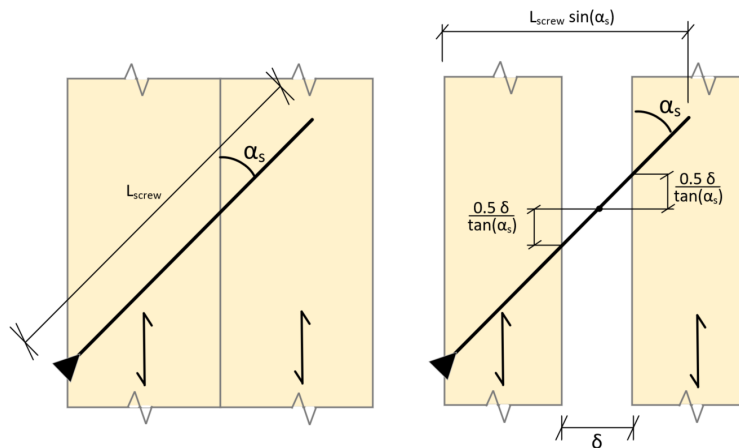


Figure 4.5: Instantaneous slip as a result of timber shrinkage, original state (left), and shrunk state (right). Source: own image.

Important to note is that the stiffness calculation proposed by Kevärinmäki [44] is an empirical formula. The stiffness value for an individual screw is determined by employing experimental tests as defined by expression 4.12, after which it is converted to a stiffness per unit area according to equation 4.13. This stiffness value per unit area K_{ser} is then inserted in equation 4.10 and ultimately in the double stiffness model as given by equation 4.7. No geometrical decomposition for the inclination of the screws is made for the stiffness equation.

$$k_s = \frac{0.5 \cdot F_{max}}{\frac{5}{3} \cdot (\delta_{05} - \delta_{02})} \quad (4.12)$$

$$K_{ser} = \frac{k_s}{\pi \cdot d \cdot l_{ef}} \quad (4.13)$$

In which:

- δ_{05} and δ_{02} : measured mean slip values for load values of $0.5F_{max}$ and $0.2F_{max}$, respectively [mm]
- F_{max} : mean value of failure load of tested series [N]
- l_{ef} : effective penetration length, defined as penetration depth (l_p) minus d (nominal screw diameter) for 4.5x70, 6x90 and 7.5x152 screws, and $l_p - 2d$ for bore bit screws 8x140 [mm]

The calculated stiffness values correspond well with experimental connection stiffness tests. Tests were performed both for connections consisting of solid C24-sawn timber specimens and for Kerto-LVL. The ratio of the experimental slip modulus and calculated slip modulus $k_{s,test}/n \cdot K_s$ was found to be equal to 1.01 for solid C24 timber, and 1.21 for Kerto-LVL, in the case of tension screw joints. For the crossed connections, ratios of 0.96 and 1.01 were found for solid C24 timber and Kerto-LVL, respectively [44, p. 7]. A typical load-slip relation from the experimental tests is presented in 4.6. Figure 4.7 shows the experimental test setup.

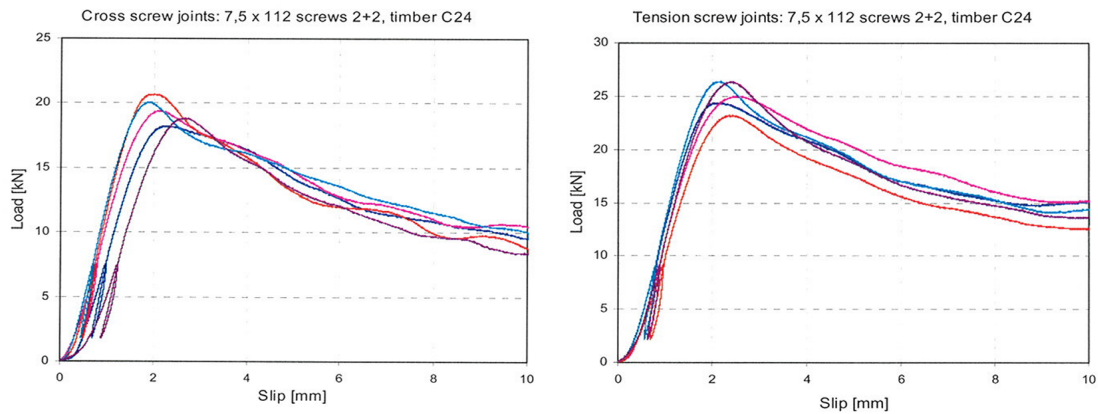


Figure 4.6: Load-slip behaviour as typically found in the tests performed of joints with inclined screws [44, p. 133].

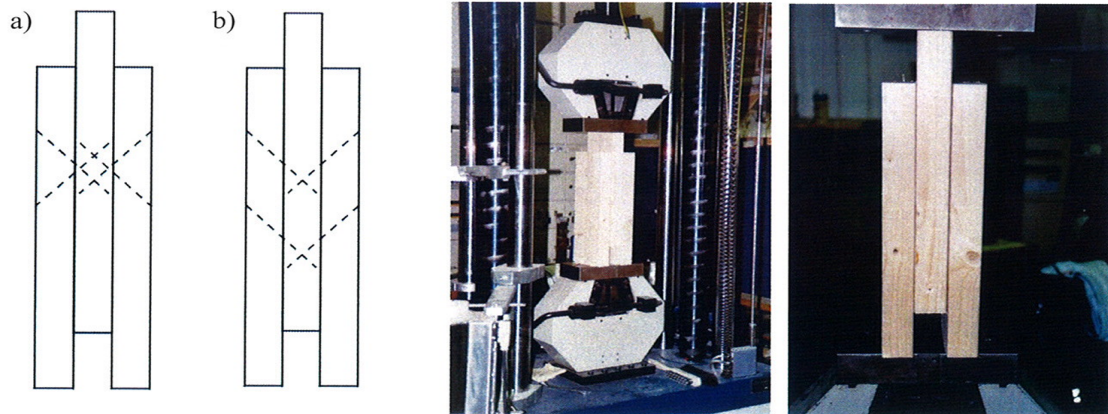


Figure 4.7: Left: schematic representation of test specimens for crossed configuration (a) and tension configuration (b). Right: experimental test setup of push-out tests [44, p. 133].

4.6. Tomasi, Crosatta and Piazza approach

Tomasi et al. [67] propose a method to assess the connection stiffness of inclined screw connections, taking into account friction and slip both perpendicular and parallel to the screw axis. The geometrical decomposition of the stiffness along the shear plane is given by figure 4.8. Equation 4.14 is proposed for the stiffness parallel to the shear plane. Tomasi et al. [67] define angle α as the angle between the

screw axis and the plane perpendicular to the shear plane, so that $\alpha_s = 90^\circ - \alpha$.

$$K_{ser} = K_{\perp} \cdot \cos(\alpha) \cdot (\cos(\alpha) - \mu \cdot \sin(\alpha)) + K_{\parallel} \cdot \sin(\alpha) \cdot (\sin(\alpha) + \mu \cdot \cos(\alpha)) \quad (4.14)$$

In which:

- K_{ser} : instantaneous slip modulus per screw [N/mm]
- K_{\perp} : connector stiffness for lateral loading of the screw [N/mm]
- K_{\parallel} : connector stiffness for withdrawal load of the screw [N/mm]
- μ : coefficient of friction between the timber elements [-]
- α : angle between screw axis and plane perp. to the shear plane (so $\alpha_s = 90^\circ - \alpha$) [°]
- d : outer screw diameter [mm]

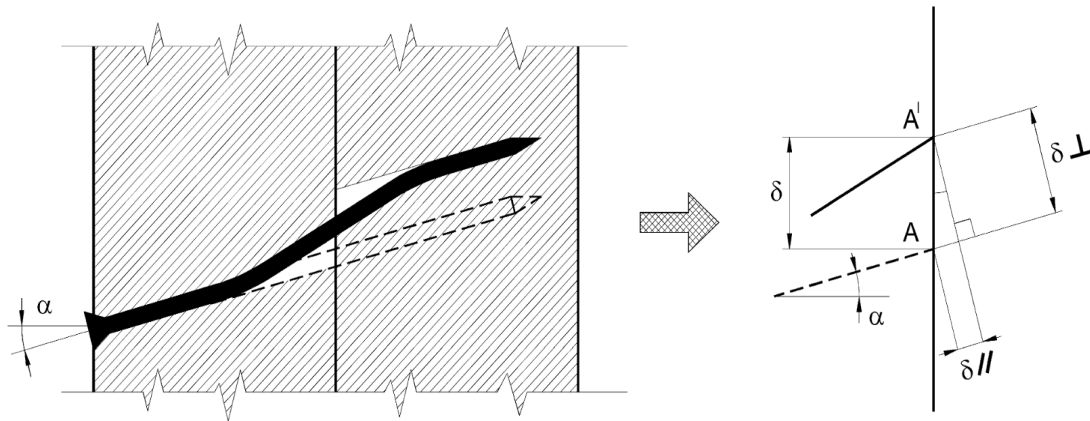


Figure 4.8: Geometrical decomposition of displacement on the shear plane [67, p. 1562].

$$K_{\parallel} = \frac{1}{\frac{1}{K_{ser,ax,1}} + \frac{1}{K_{ser,ax,2}}} \quad (4.15)$$

$$K_{\perp} = \rho_m^{1.5} \cdot d \cdot \frac{1}{23} \quad \text{see eq. 3.18 [55]} \quad (4.16)$$

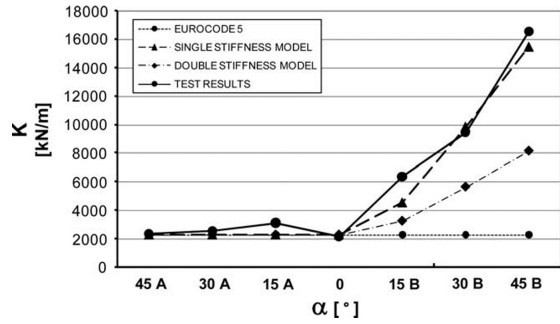
$$K_{ser,ax,i} = 30 \cdot L_{ef} \cdot d \quad [22] \quad (4.17)$$

$$K_{\parallel} = K_{ser,ax,i} \quad (4.18)$$

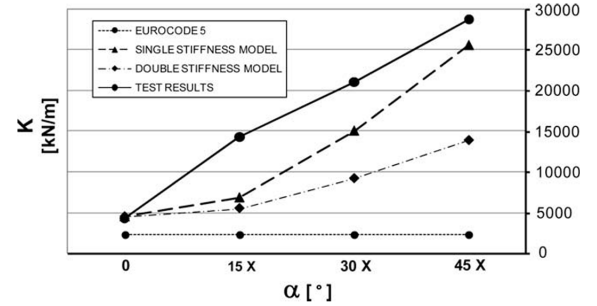
Tomasi et al. [67] note that the value for K_{\perp} can be taken equal to the Eurocode 5 stiffness equation, as given by equation 4.16. The value for perpendicular stiffness K_{\parallel} is more complex, and the axial withdrawal stiffness $K_{ser,ax}$ must be considered, as given by equation 4.15. This relation takes the withdrawal stiffnesses of the screw in both timber specimens and assumes the threaded parts of the screw are pulled out of the two specimens at the same instance, a phenomenon Tomasi et al. [67] refer to as "double stiffness model". Tomasi et al. [22] state that in case the screw is only pulled out of one of the two timber parts, equation 4.18, referred to as the "single stiffness model" should be used, instead of equation 4.15. Since the value for $K_{ser,ax,i}$ is not given by design standards, Tomasi et al. [67] propose it is determined by means of experimental tests. However, in case screws come with a homologation certificate in which axial stiffness is given, the formulations stated therein can be used. In their study, Tomasi et al. [67] use equation 4.17 from the general homologation certificate from the

German Institute for Building Technology [22]. Tomasi et al. [67] reason that in the case of crossed screw configurations, the friction part is not effective anymore, because the timber specimens are not compressed. Therefore, in case crossed screw configurations are used, equation 4.19 is proposed instead of equation 4.14.

$$K_{\text{ser}} = K_{\perp} \cdot \cos(\alpha)^2 + K_{\parallel} \cdot \sin(\alpha)^2 \quad (4.19)$$



(a) Comparison between mean experimental results and calculated stiffness values for screws loaded in shear tension under different inclination angles [67, p. 1569].



(b) Comparison between mean experimental results and calculated stiffness values for crossed screws under different inclination angles [67, p. 1570].

Figure 4.9

The experimental tests that were conducted to verify the calculation methods consisted of 64 push-out tests in total. The test setup is schematically shown in figure 4.10. Screws were loaded under shear compression, shear tension, and crossed configurations under angles α of 0° , 15° , 30° and 45° . Tomasi et al. [67] note that the so-called double stiffness model given by equation 4.15 is not in all cases the best approximation of the test results. After opening the test specimens after collapse, it was found that the heads of the screws had in some cases penetrated the timber by up to 4 cm, while the screw tips remained at their original position. Figure 4.9a shows that the single stiffness model resembles the experimental test results more closely for screws loaded in shear tension than the double stiffness model.

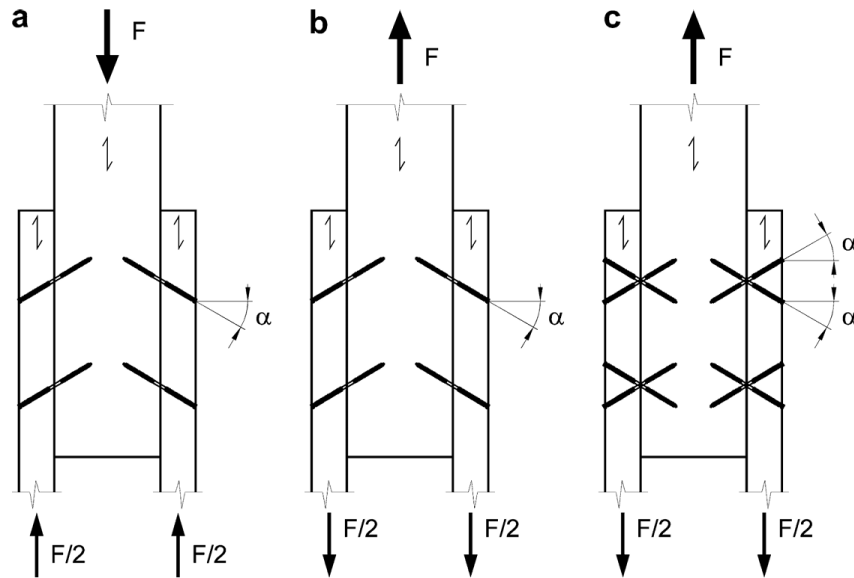


Figure 4.10: Connection details and test setup used by Tomasi et al. [67, p. 1565].

It was found that for the configurations subjected to shear compression (figure 4.10a), stiffness values show approximately the same values for angles of 45°, 30°, 15° and 0°, and thus the Eurocode 5 equation for stiffness (see equation 4.16) can be used. For screws loaded in shear tension and for crossed configurations (figures 4.10b and 4.10c), equations 4.14 respectively 4.19 should be used according to Tomasi et al. [67]. For screws loaded in shear tension and crossed configurations, stiffness values were found to increase with larger values of α . The largest stiffness value of all tests was found for the crossed configuration under an angle of 45°, as given in figure 4.9b.

4.7. Jockwer, Steiger and Frangi approach

Instead of only examining one loading direction, Jockwer et al. [38] present a calculation method for both loading parallel and perpendicular to the shear plane, as shown in figure 4.11. The stiffness for the load case in which the timber parts are loaded perpendicular to the shear plane (pulling) is given in equation 4.20. Jockwer et al. [38] define γ as the angle between the screw axis and the grain direction. As the grain direction is parallel to the shear plane in the described tests, γ is equal to α_s .

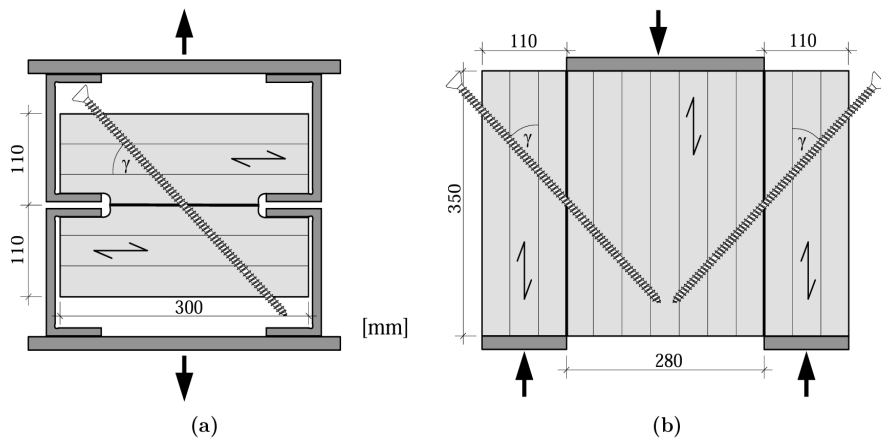


Figure 4.11: Experimental tests performed by Jockwer et al. [38]: pulling test (a), and shearing test (b) [38, p. 5].

$$\frac{1}{K_{90}} = \frac{1}{K_{v,pulling}} + \frac{1}{K_{ax,pulling}} \quad (4.20)$$

$$K_{v,pulling} = \frac{3 \cdot E_{steel} \cdot \pi \cdot d_1^4}{64 \cdot x_1^3} \quad (4.21)$$

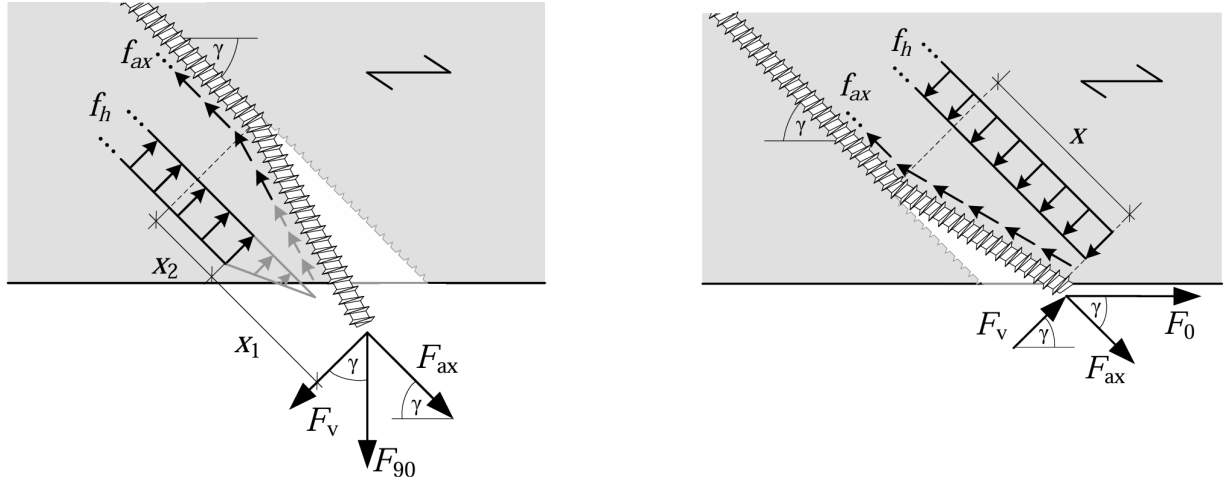
$$x_1 = \frac{f_h \cdot d_{ef}}{2 \cdot \tan(\gamma) \cdot f_{v,roll}} \quad (4.22)$$

In which:

- K_{90} : stiffness for load case perpendicular to the grain [N/mm]
- $K_{v,pulling}$: screw stiffness perpendicular to the screw axis [N/mm], see equation 4.21
- $K_{ax,pulling}$: screw stiffness in direction parallel to the screw axis [N/mm]
- E_{steel} : Youngs modulus of steel grade of the screw [N/mm²]
- d_1 : inner diameter of the screw [mm]
- x_1 : length of the screw along which reduced embedment capacity is available [mm], see equation 4.22
- f_h : embedment strength of the timber [N/mm²]
- $f_{v,roll}$: rolling shear strength [N/mm²]

- γ : angle between screws axis and grain direction ($=\alpha_s$) [°]

For the analytical derivation of the pulling case, two assumptions are made. First, it is assumed that for a certain length x_1 along the screw axis, the timber thickness and therefore the embedment capacity is severely reduced (see figure 4.12a). Therefore, the embedment strength f_h is simply omitted for this part. The second assumption is that the screw's stiffness against the load perpendicular to the screw axis (F_v) is equal to that of a cantilever beam, resulting in equation 4.21.



(a) Stresses working on screw for joint loaded perpendicular to the shear plane (pulling) [38, p. 3].

(b) Stresses working on the screw for joint loaded parallel to the shear plane (shearing) [38, p. 8].

Figure 4.12

For the stiffness in the shearing load case, Jockwer et al. [38] use the equations as suggested by Tomasi et al. [67] using the double stiffness proposal. The equation is modified for the different angle definitions. Another difference is that another formula for the axial stiffness $K_{ax,shear}$ is used, as given in equation 4.23. The reason for this probably lies in the fact that between the publication of Tomasi et al. [67] and Jockwer et al. [38], the formula from the Deutsches Institut für Bautechnik [21] was updated. The expression Jockwer et al. [38] use for axial stiffness in the shearing case $K_{ax,shear}$ is different from the expression $K_{ax,pulling}$ Jockwer et al. [38] propose for the pulling case.

$$K_{ax,shear} = 25 \cdot l_{ef} \cdot d \quad [21] \quad (4.23)$$

$$K_{ax,pull} = 40 \cdot l_{ef} \cdot d \quad (4.24)$$

4.8. Girhammar, Jacquier and Kälšner approach

In their design model, Girhammar et al. [33] introduce a method to calculate the stiffness of connections with inclined screws allowing for different properties of the two timber elements, in contrast to the previously introduced models. Another important difference is that the model proposed by Girhammar et al. [33] assumes a rotation of the screw in the timber elements as a result of the applied load, and therefore triangular embedment stress distributions are used instead of rectangular, as shown in figure 4.13. Finally, the model takes into account the possibility of an angle between the grain direction and the shear plane when observed in cross-section. Girhammar et al. [33] define angle α as the angle between the screw axis and the plane perpendicular to the shear plane, so that $\alpha_s = 90^\circ - \alpha$.

Analytical derivations lead to the expression given in equation 4.25. In case the connected timber elements have the same properties, so that ($\beta_h = 1$; $\beta_{ax} = 1$; $l_2/l_1 = l_{thr,2}/l_{thr,1} = 1$; $x_1 = 2s_1/3$; $x_2/x_1 = 1$) are satisfied, the equation simplifies to equation 4.26. The equation consists of a sum of two parts, where the first part takes into account the effect of the shearing behaviour of the screw. The second part concerns the withdrawal behaviour of the screw.

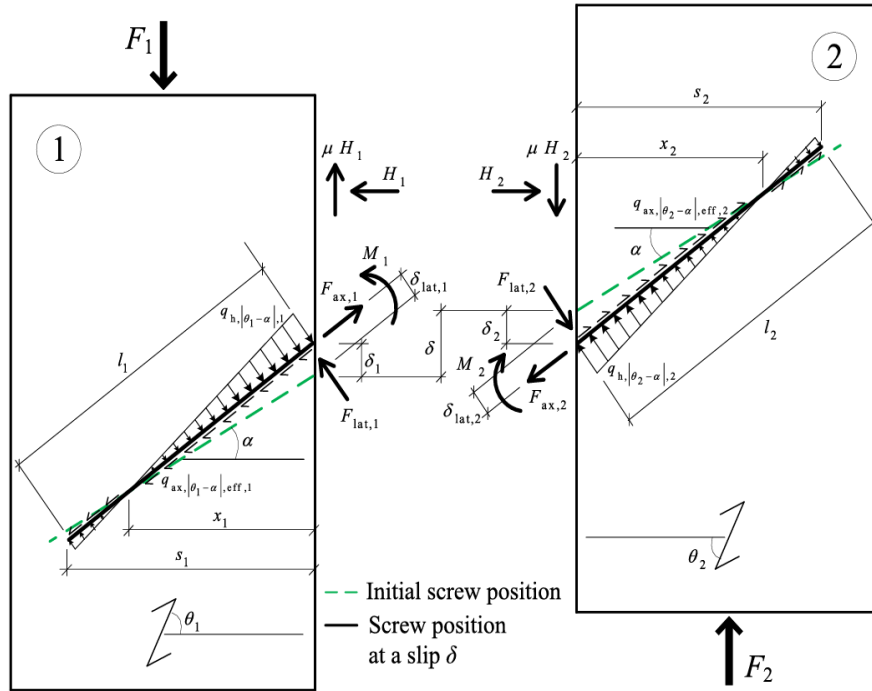


Figure 4.13: Forces and bending moments in the model proposed by Girhammar et al., [33, p. 581].

$$k = \frac{1}{2} K_{h,|\theta_1-\alpha|,1} d_h l_1 \frac{2 - s_1/x_1}{1 + x_2/x_1} \cos(\alpha) (\cos(\alpha) - \mu \sin(\alpha)) + \frac{1}{1 + (1/\beta_{ax})(l_{thr,1}/l_{thr,2})} K_{ax,|\theta_1-\alpha|,eff,1} \pi d_{ax} l_{thr,1} \sin(\alpha) (\sin(\alpha) + \mu \cos(\alpha)) \quad (4.25)$$

$$k_{ident} = \frac{1}{8} K_{h,|\theta_1-\alpha|,1} d_h l_1 (\cos(\alpha) - \mu \sin(\alpha)) + \frac{1}{2} K_{ax,|\theta_1-\alpha|,eff,1} \pi d_{ax} l_{thr,1} \sin(\alpha) (\sin(\alpha) + \mu \cos(\alpha)) \quad (4.26)$$

In which:

- k : connection stiffness [N/mm]
- k_{ident} : connection stiffness for identical conditions for the timber members [N/mm]
- $K_{h,|\theta_i-\alpha|,i}$: embedment stiffness per unit area of timber element i [N/mm³], see equation 4.30
- d_h : embedment diameter of screw [mm]
- l_i : length of screw in timber element i [mm]
- s_i : length of screw in timber element i perp. to shear plane [mm]; $s_i = l_i \cos(\alpha)$
- x_i : perp. distance from the shear plane to the rotation point of the screw in timber element i [mm], see equation 4.27
- α : angle between screw axis and line perpendicular to shear plane [°]
- μ : coefficient of friction between timber members [-]
- $K_{ax,|\theta_i-\alpha|,eff,i}$: effective axial withdrawal stiffness of screw in element i per unit area [N/mm³]
- d_{ax} : withdrawal diameter of screw [mm]

- $l_{thr,i}$: length of threaded part of screw i [mm]
- β_{ax} : ratio of effective axial withdrawal stiffnesses of the screw in the two elements [-], see equation 4.28
- β_h : ratio of embedment stiffnesses of the screw in the two elements [-], see equation 4.29

$$\frac{x_1}{l_1} = \frac{(4 + 3l_2/l_1) + \beta_h(l_2/l_1)^3}{6(1 + l_2/l_1)} \cos(\alpha) \quad (4.27a)$$

$$\frac{x_2}{l_1} = \frac{1 + \beta_h(l_2/l_1)^2(3 + 4l_2/l_1)}{6\beta_h(l_2/l_1)(1 + l_2/l_1)} \cos(\alpha) \quad (4.27b)$$

$$\beta_{ax} = \frac{K_{ax,|\theta_2-\alpha|,eff,2}}{K_{ax,|\theta_1-\alpha|,eff,1}} \quad (4.28)$$

$$\beta_h = \frac{K_{h,|\theta_2-\alpha|,2}}{K_{h,|\theta_1-\alpha|,1}} = \frac{k_{h,|\theta_2-\alpha|,2}}{k_{h,|\theta_1-\alpha|,1}} \quad (4.29)$$

$$K_{h,|\theta_i-\alpha|,i} = \frac{K_{h,0^\circ,i}K_{h,90^\circ,i}}{K_{h,0^\circ,i} \sin^2(|\theta_i - \alpha|) + K_{h,90^\circ,i} \cos^2(|\theta_i - \alpha|)} \quad (\text{Hankinson}) \quad (4.30)$$

In which:

- $K_{h,0^\circ,i}$: embedment strength of timber element i when $\alpha = 0^\circ$ and $\theta_i = 0^\circ$
- $K_{h,90^\circ,i}$: embedment strength of timber element i when $\alpha = 0^\circ$ and $\theta_i = 90^\circ$

For the axial withdrawal stiffness, effective values are proposed by Girhammar et al. [33]. This is done to compensate for the previously mentioned difference in withdrawal behaviour between screws loaded in standard withdrawal and screws loaded simultaneously in the axial and lateral direction by Bejtka and Blass [10]. Girhammar et al. [33] suggest these values can be found experimentally. The method includes two extensions of the model, which are the flexibility and extensibility of the screw. These effects are taken into account by making use of a beam on elastic foundation model and an extensible rod in elastic foundation model, given by equations 4.31 and 4.32, respectively.

$$K_{h,|\theta_i-\alpha|,i}^{Eq} = K_{h,|\theta_i-\alpha|} \frac{2 \sinh^2(\lambda l_i) - \sin^2(\lambda l_i)}{\lambda l_i (\sinh(\lambda l_i) \cosh(\lambda l_i) - \sin(\lambda l_i) \cos(\lambda l_i))} \quad (4.31)$$

$$\approx K_{h,|\theta_i-\alpha|} \frac{2}{\lambda l_i} \quad \text{for } \lambda l_i \leq 2.5$$

In which:

$$\lambda l_i = 2 \sqrt{\frac{K_{h,|\theta_i-\alpha|,i}^{Eq} d_h}{\pi E_s}} \frac{l_i}{d_h} \quad [-]$$

- E_s : the modulus of elasticity of steel [N/mm²]

$$K_{ax,|\theta_i-\alpha|,eff,i}^{Eq} = K_{ax,|\theta_i-\alpha|,eff,i} \frac{\tanh(\omega l_i)}{\omega l_i} \quad (4.32)$$

In which:

$$\omega l_i = 2 \sqrt{\frac{K_{ax,|\theta_i-\alpha|,eff,i} d_{ax}}{E_s}} \frac{l_{thr,i}}{d_{ax}} \quad [-]$$

- E_s : the modulus of elasticity of steel [N/mm²]

Girhammar et al. [33] state that their model is capable of predicting the connection stiffness in the serviceability limit state and that its validity is limited to the point at which a plastic hinge forms in the screw. The connection slip at which this happens is given by equation 4.33.

$$\delta_y \leq \left(\frac{f_{ax,1}}{N_y} + \frac{m_{s,1,max}}{M_y} \right)^{-1} \quad (4.33)$$

In which:

- $f_{ax,1}$: axial force in screw in timber element 1 divided by joint slip δ [N], see equation 4.34
- $m_{s,1,max}$: max. screw moment in timber element 1 divided by joint slip δ [Nmm], see equation 4.35
- N_y : plastic normal force capacity of screw [N]
- M_y : plastic moment capacity of screw [Nmm]

$$f_{ax,1} = K_{ax,|\theta_1-\alpha|,eff,1} \pi d_{ax} l_{thr,1} \frac{\sin(\alpha)}{1 + (1/\beta_{ax})(l_{thr,2}/l_{thr,1})} \quad (4.34)$$

$$m_{s,1,max} = \frac{2}{3} K_{h,|\theta_1-\alpha|,1} d_h l_1^2 \cos(\alpha) \cdot \frac{s_1}{x_1} \frac{(1 - x_1/s_1)^3}{1 + x_2/x_1} \quad (4.35)$$

No experimental tests were performed by Girhammar et al. [33], but the model was compared to the tests conducted by Tomasi et al. [67]. The result found by Tomasi et al. [67] that the single stiffness model corresponded with their results better than the double stiffness model was confirmed by the model of Girhammar et al. [33], who found good correspondence between the test results and their model (see figure 4.14) using a value for β_{ax} of 2 to (partially) take into account the single stiffness model. The reason given for this phenomenon by Girhammar et al. [33] is that the head part is penetrated twice by the screw, which could damage the timber around the screw in this part and cause a lower local stiffness.

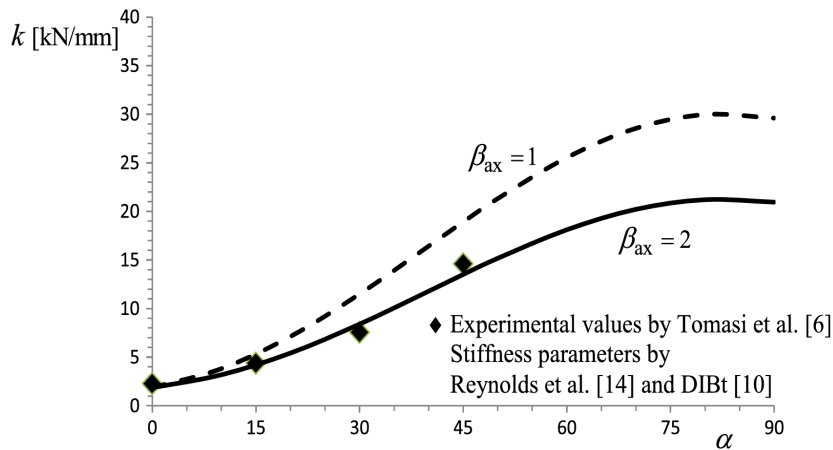


Figure 4.14: Experimental results found by Tomasi et al. [67] compared to theoretical stiffness values for various inclination angles α . Grain direction is parallel to the load, i.e. $\theta_{1,2} = 90^\circ$, [33, p. 586].

However, the authors state: "If we assume, as did Tomasi et al. [67], that the withdrawal stiffness in the head part of the screw is reduced to 50% of that of the tip part, then the β_{ax} -value changes from $\beta_{ax} = 1$ to $\beta_{ax} = 2$ " [33, p. 587]. This statement is ambiguous because in case Tomasi et al. [67] assumed a stiffness value of the head part of the screw that amounts to 50% of the tip part, this would yield $K_{//} = \frac{2}{3} k_{head}$ instead of $K_{//} = k_{head}$ which is proposed by Girhammar et al. [67]. Rather, the

single stiffness model proposed by Tomasi et al. [67] should be understood as $k_{tip} \gg k_{head}$. This derivation is given in equation 4.36.

$$\begin{aligned} k_{head} &= 0.5 \cdot k_{tip} \\ \Rightarrow k_{tip} &= 2 \cdot k_{head} \end{aligned} \quad (4.36a)$$

$$K_{//} = \frac{1}{\frac{1}{k_{tip}} + \frac{1}{k_{head}}} = \frac{1}{\frac{1}{2 \cdot k_{head}} + \frac{1}{k_{head}}} = \frac{2}{3} k_{head} \neq k_{head} \quad (4.36b)$$

4.9. Blass Steige approach

The method proposed by Blass & Steige [14] consists of an analytical expression for the stiffness of fully threaded inclined screw connections, given by equation 4.37. The expression takes into account the influence of friction, but versions of the expression omitting the friction component are also found in the literature (for example Egner & Frese [24]). The expression for the axial screw stiffness $k_{ax,i}$ is obtained via non-linear regression of test results. Blass & Steige define angle α as the angle between the screw axis and the grain direction of the timber so that in case the grain direction is parallel to the shear plane, α_s is equal to α .

$$k = \frac{\cos^2(\alpha) \cdot (1 + \mu \cdot \tan(\alpha))}{\frac{1}{k_{ax,1}} + \frac{1}{k_{ax,2}}} \quad (4.37)$$

$$k_{ax,i} = 0.48 \cdot d^{0.4} \cdot l_{ef,i}^{0.4} \cdot \rho_m^{0.3} \quad (4.38)$$

In which:

- k : connection stiffness [kN/mm]
- α : Angle between screw axis and grain direction in timber elements [°]
- μ : coefficient of friction in grain direction [-]
- $k_{ax,i}$: withdrawal stiffness of screw in timber member i [kN/mm]
- d : outer screw diameter [mm]
- $l_{ef,i}$: effective length of screw in timber member i [mm]
- $\rho_{m,i}$: mean timber density of timber element i [kg/m³]

Three types of tests have been performed in the study, i.e. parallel shear tests, diagonal shear tests, and screw withdrawal tests. The parallel and diagonal shear tests have been performed for both crossed and shear tension geometries. In the parallel tests, additional horizontal supports had to be introduced to guarantee moment equilibrium. To minimize friction generated by the reaction force of these supports, Teflon elements were applied at the interface between the test specimens and support of the test setup [14, p. 16] (see figure 4.15a). A horizontal reaction force results from the horizontal supports, resulting in additional friction between the timber elements. This force was taken into account in the calculation of the total force [14, p. 16].

For the diagonal shear tests, additional supports were not necessary, as the line of force intersected the centre of gravity of the test specimens, see figure 4.15b. However, in these tests, the influence of the compression forces under a slight angle β had to be taken into account, including the extra friction generated by the perpendicular force component [14, p. 24]. Stiffness results had to be corrected for these effects. Finally, in order to assess the withdrawal stiffness of individual screws in formula 4.37 directly, withdrawal tests were performed under different angles to the grain [14, p. 25].

In order to find the value for axial stiffness k_{ax} needed in equation 4.37, the axial stiffness was back-calculated from the crossed screw and shear tension experiments. Non-linear regression was performed on the results for k_{ax} of all 290 tests, taking into account the following parameters [14, p. 69]:

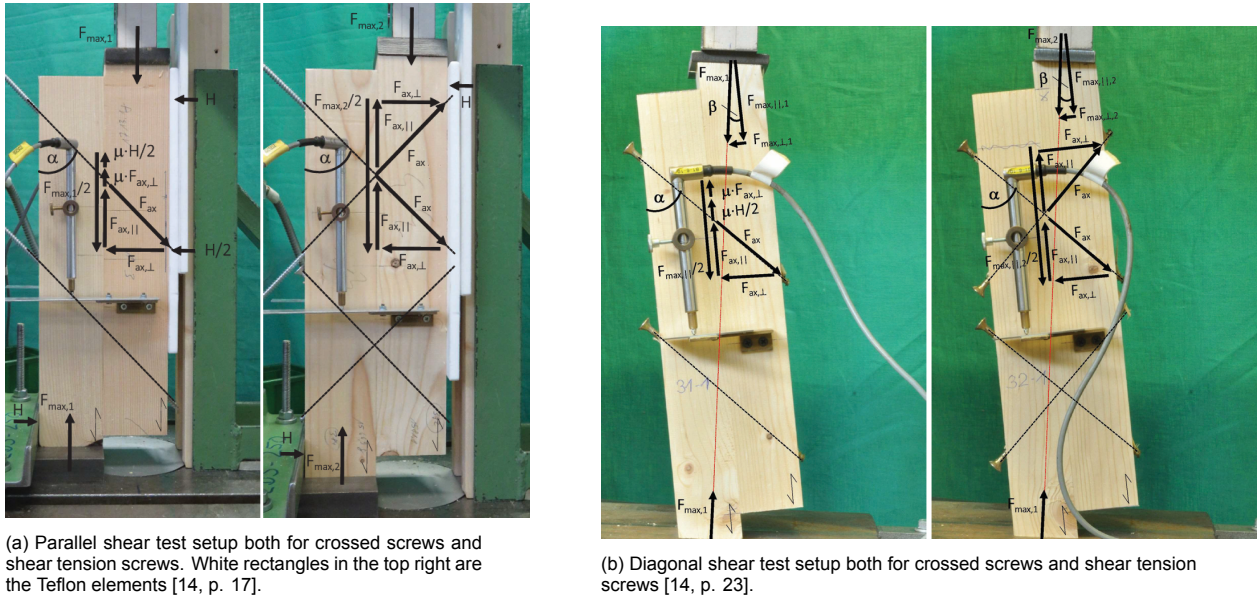


Figure 4.15

- Embedment length l_{eff}
- Outer thread diameter d
- Screw inclination angle α
- Timber moisture content
- Pre-drilling

It was found that the value for axial stiffness k_{ax} to be used in equation 4.37 could best be determined from the shear tests with crossed screw geometries [14, p. 82], resulting in equation 4.38.

4.10. De Santis & Fragiaco approach

An inclined beam on elastic foundation model is proposed by De Santis & Fragiaco [62], as given in figure 4.16. De Santis & Fragiaco [62] first describe an analytical model, in which equation 4.39 is used to find the theoretical stiffness of the joint. Making use of 12 boundary and interface conditions an analytical solution for the stiffness can be found. Since the main objective of the study was to find simplified equations, interpolation equations are proposed, given by equation 4.40a and 4.40b. It should be noted that De Santis & Fragiaco [62] do not include the influence of friction in their calculation approach. Also, there is no distinction made for the threaded length of the screw, so that only the penetration length of the screw is used. De Santis & Fragiaco [62] define angle θ as the angle between the screw axis and the plane perpendicular to the shear plane, so that $\alpha_s = 90^\circ - \theta$.

$$k_{ser,An} = \frac{E \cdot A \cdot u'_1(l_1) \cdot \sin(\theta)}{\delta} + \frac{E \cdot I \cdot v_1'''(l_1) \cdot \cos(\theta)}{\delta} \quad (4.39)$$

$$k_{ser,int} = dd \cdot (\rho_1^{aa} \cdot l_1^{bb} + \rho_2^{aa} \cdot l_2^{bb}) \cdot \phi^{cc} \quad \theta < 30^\circ \quad (4.40a)$$

$$k_{ser,int} = \frac{dd \cdot \phi^{cc}}{\frac{1}{\rho_1^{aa} \cdot l_1^{bb}} + \frac{1}{\rho_2^{aa} \cdot l_2^{bb}}} \quad \theta \geq 30^\circ \quad (4.40b)$$

In which:

- $k_{ser,int}$: connection stiffness [N/mm]

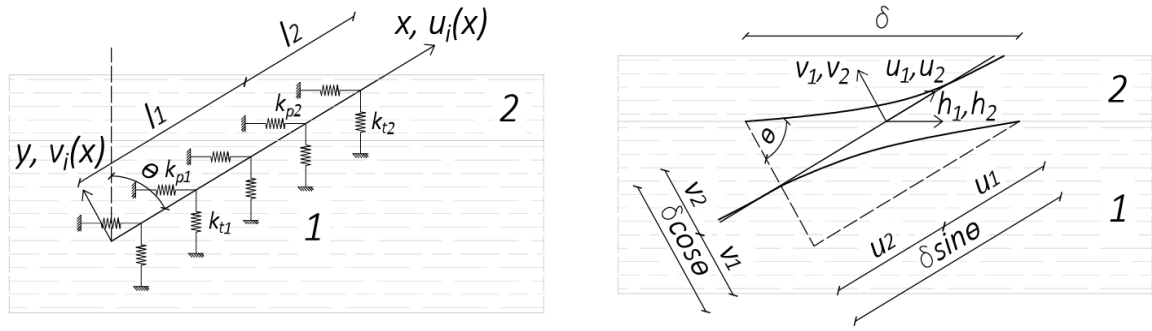


Figure 4.16: Inclined beam on elastic foundation model as proposed by De Santis & Fragiaco (left) and original and deformed geometry of the screw (right) [62, p. 3].

- ϕ : outer diameter of the screw [mm]
- ρ_i : mean density of timber element i [kg/m³]
- l_i : the penetration length of the screw in timber element i [mm], see figure 4.16
- aa, bb, cc, dd : interpolation coefficients, given in table 4.18
- θ : Angle between screw axis and plane perp. to shear plane [°]

The proposed interpolation equations were tested for different random combinations of parameters, with densities ρ_m in the range of 400 - 750 [kg/m³] and screw lengths l_i in the range of 50-200 [mm] for equation 4.40a, and 60-150 [mm] for equation 4.40b. Screw diameters ϕ were in the range of 6-18 [mm]. The percentage differences between the exact analytical and interpolated solutions are given by the box plots in figure 4.17.

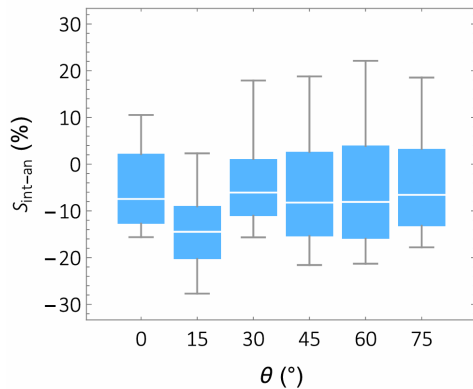


Figure 4.17: Maximum, 95th percentiles, median, 5th percentiles, and minimum values of percentage differences between analytical and interpolated solutions [62, p. 6].

$\theta(^{\circ})$	aa	bb	cc	dd
0	1.04	0.056	1.11	0.18
15	1.04	0.056	1.11	0.18
30	1.07	0.51	0.76	0.31
45	1.07	0.68	0.65	0.29
60	1.09	0.77	0.58	0.23
75	1.14	0.86	0.47	0.095

Figure 4.18: The interpolation coefficients needed for equations 4.40. For $\theta = 15^{\circ}$ the same values as for $\theta = 0^{\circ}$ were used [62, p. 6].

No new experiments were performed by De Santis & Fragiaco [62], but experimental test results carried out in earlier studies from other authors were used to compare experimental and predicted stiffness values of different calculation methods. The methods that are compared are the analytical method (see equation 4.39), the proposed formulas (see equation 4.40), Eurocode 5: EN-1995-1-1 draft (2021), Eurocode 5: EN-1995-1-1 (2004), Girhammar et al. [33] and Tomasi et al. [67]. The results of the predicted stiffness values and the experimental stiffness values are given in figures 4.19a and 4.19b. The coefficients of determination found for the methods are given in table 4.1. De Santis & Fragiaco mention the omission of friction in the proposed formulas as a possible cause for its slight underestimation of the test results.

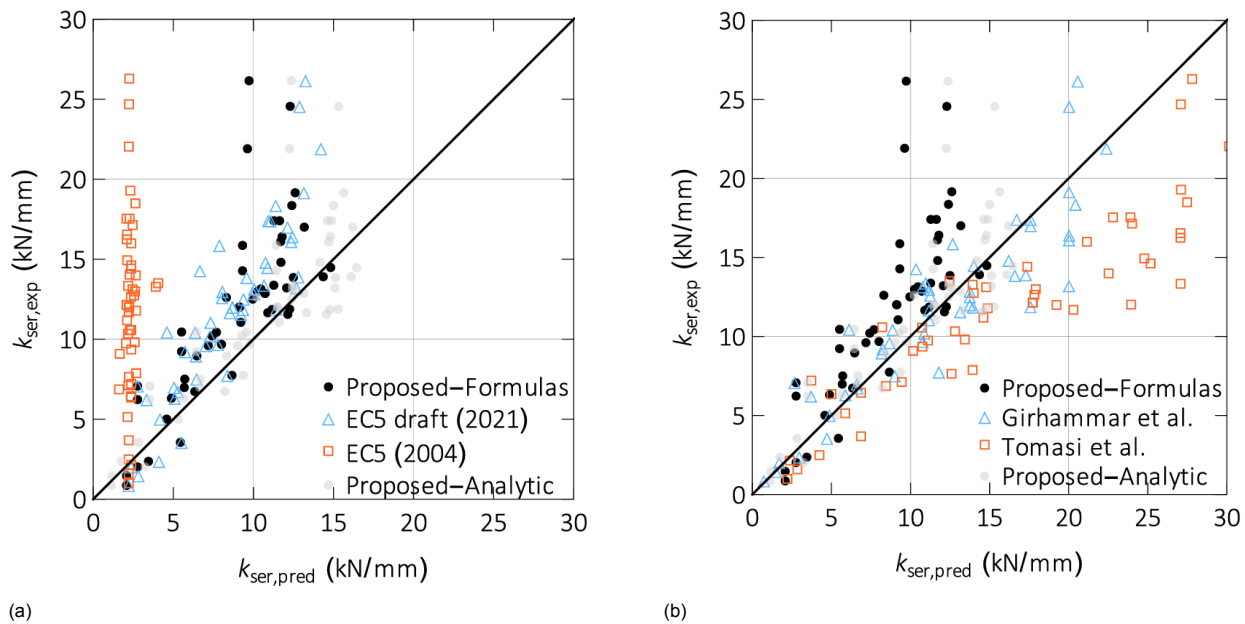


Figure 4.19: Predicted and experimental stiffness values according to different calculation methods [62].

Model	Proposed Analytic	Proposed Formula	EC 5 draft (2021)	EC 5 (2004)	Girhammar et al.	Tomasi et al.
r^2	0.62	0.28	0.28	-3.03	0.79	-0.29

Table 4.1: Coefficients of determination of analysed methods [62].

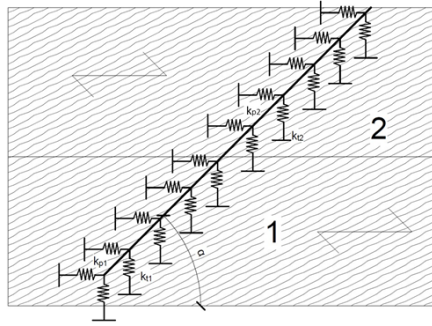
De Santis & Fragiaco have subjected the models to sensitivity analyses in which the screw diameter, the ratio between tip and head stiffness, and the ratio between the densities of the timber elements were altered. De Santis & Fragiaco conclude that the reliability of the proposed analytical model given in equation 4.39 is comparable to the model proposed by Girhammar et al. [33], but both models are not suitable for inclusion in design codes due to their complexity. The proposed interpolated equations given in equation 4.40 are found to be more accurate than both the approach given in prEN-1995-1-1 (see section 4.12) and the method proposed by Tomasi et al. [67]. Finally, the proposed model does not require withdrawal tests and accurately predicts the joint stiffness in case external screw diameter, material densities, insertion angle, and screw length are known.

4.11. Comparison of methods by Kullander and Sandström

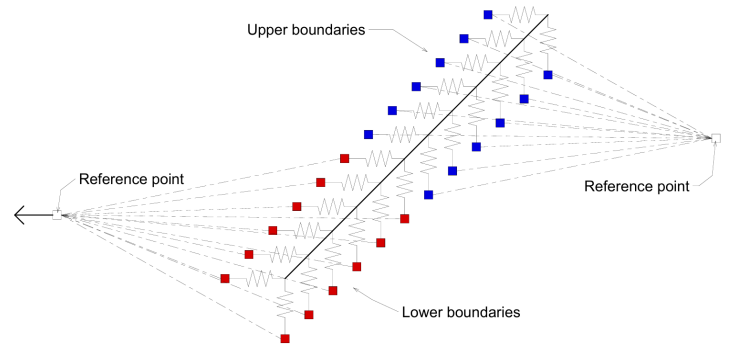
Kullander and Sandström [46] wrote a master's thesis under the supervision of Robert Jockwer in 2023. In this thesis, an inclined beam on foundation model was built in the FE software package ABAQUS to find the stiffness and capacity of inclined screw connections. This model was then calibrated making use of the test results of Jockwer et al. [38]. The calculation methods for connection stiffness as proposed by Tomasi et al. [67], Jockwer et al. [38] and second generation of EN-1995-1-1 [53] were compared. It was concluded that the method proposed by Tomasi et al. [67] in combination with the equation for lateral stiffness given by the new generation of EN-1995-1-1 [53] (see equation 4.42) gave the best results compared to the FE model and the test results by Jockwer et al. [38]. An important remark for this result is that the double stiffness model was used, which can be found by back-calculating the results that are presented in the thesis.

4.12. Eurocode 5: EN-1995-1-1 draft (2023)

In contrast to EN-1995-1-1 [55], the pre-norm version of Eurocode 5, prEN1995-1-1 [53] gives a method for the stiffness calculation specifically for inclined screws. Equation 4.41 is proposed for connections



(a) Schematic overview of the model [46, p. 46].



(b) Schematic overview of the model as built in ABAQUS [46, p. 48].

Figure 4.20: Beam-on-foundation model as presented by Kullander and Sandström [46].

with inclined screws loaded in shear tension. In case the connection consists of multiple screws, the stiffness values of individual screws may be summed. Angle ϵ is defined as the angle between the screw axis and the grain direction so that α_s is equal to ϵ in case the grain direction is parallel to the shear plane.

$$K_{SLS} = K_{SLS,v} \sin(\epsilon)(\sin(\epsilon) - \mu \cos(\epsilon)) + \frac{1}{2} K_{SLS,ax} \cos(\epsilon)(\cos(\epsilon) + \mu \sin(\epsilon)) \quad (4.41)$$

$$K_{SLS,v} = \frac{\rho_m^{1.5} d}{23} \quad (4.42)$$

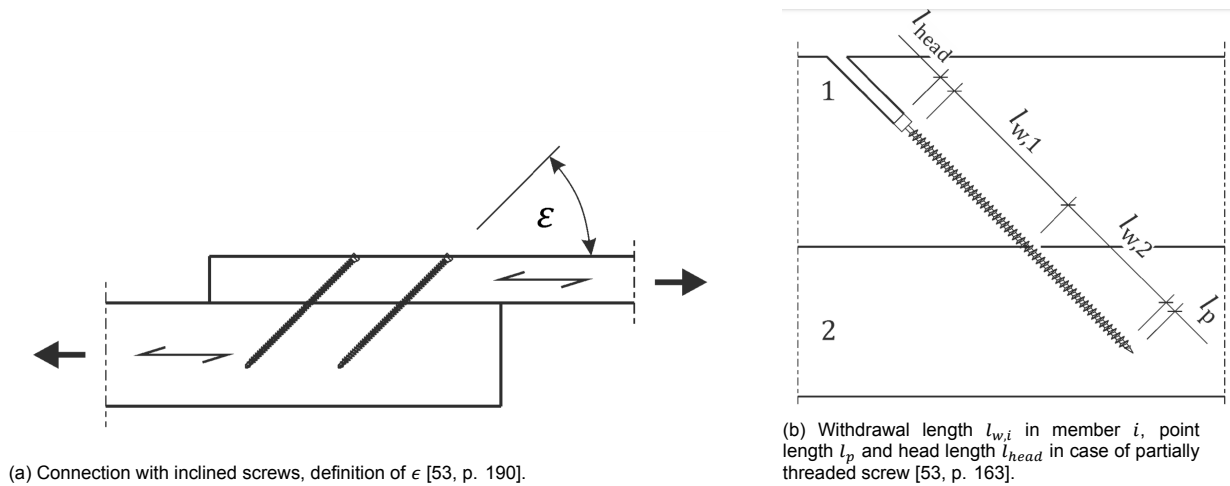
$$K_{SLS,ax} = 160 \left(\frac{\rho_{mean}}{420} \right)^{0.85} d^{0.9} l_w^{0.6} \quad (4.43)$$

In which:

- K_{SLS} : mean slip modulus per shear plane per fastener [N/mm]
- $K_{SLS,v}$: mean slip modulus per shear plane per fastener in lateral direction [N/mm]
- $K_{SLS,ax}$: mean slip modulus per fastener per connected member in axial direction [N/mm]
- ϵ : angle between screw axis and grain direction, see figure 4.21a
- μ : coefficient of friction between timber members [-]
- d : outer thread diameter of the screw [mm]
- $l_{w,i}$: withdrawal length of screw in timber member i [mm]

The method proposed is unclear concerning the mean slip modulus in axial direction $K_{SLS,ax}$ in case two timber elements are connected with different properties (for example different withdrawal length l_w or mean densities). It is assumed that the equation consists of the method proposed by Tomasi, making use of a double stiffness model and assuming $K_{SLS,ax}$ is always equal for both timber elements, as shown in equation 4.44.

$$\left. \begin{aligned} K_{SLS,ax} &= \frac{1}{\frac{1}{K_{SLS,ax,1}} + \frac{1}{K_{SLS,ax,2}}} \\ K_{SLS,ax,1} &= K_{SLS,ax,2} \end{aligned} \right\} \Rightarrow K_{SLS,ax} = \frac{1}{2} K_{SLS,ax,1} = \frac{1}{2} K_{SLS,ax,2} \quad (4.44)$$



(a) Connection with inclined screws, definition of ϵ [53, p. 190].

(b) Withdrawal length $l_{w,i}$ in member i , point length l_p and head length l_{head} in case of partially threaded screw [53, p. 163].

Figure 4.21

4.13. Conclusion

Of the methods discussed in this chapter, some are not suited for further analysis. The method proposed by Kevarinmäki [44] for instance relies on the value F_{max} , which is defined as the mean failure load of the connections tested. Because of its dependence on this experimentally determined parameter, the Kevarinmäki model [44] is discarded. The method proposed by Girhammar et al. [33] is discarded as well. It preferably relies on experimentally determined values for axial and embedment stiffness. Also, the method does not propose a value to be used for the parameter β_{ax} , and finally, the model is considered computationally too exhaustive.

The methods proposed by Tomasi et al. [67], Jockwer et al. [38] and the method described in prEN1995-1-1 [53] are considered very similar, although different formulas for embedment and axial stiffness are proposed. The method given by prEN-1995-1-1 is not suitable for connections of two timber elements with different properties. The methods given by Tomasi et al. [67] and Jockwer et al. [38] use withdrawal stiffnesses suitable only for screws that are covered by the homologation certificates given by the Deutsches Institut für Bautechnik (see [22] and [21] respectively). It is decided to use the method proposed by Tomasi et al. [67] in combination with the axial stiffness formula 4.43 of prEN-1995-1-1 [53] and the axial stiffness formula postulated by Blass and Steige [14] as given by equation 4.38. Both the single and double stiffness model are selected for further analysis. Finally, the Blass and Steige [14] method as described by equation 4.37 is used for further analysis. In literature, this method is encountered both without a friction term taken into account and with a friction term taken into account. Both methods are used for further analysis, labeled "Blass Steige" and "Blass Steige friction", respectively. An overview of the methods selected for further analysis is given in table 4.2.

Method ID	Method name
1	Blass Steige
2	Blass Steige friction
3	Tomasi et al. (EC) single stiffness model
4	Tomasi et al. (Blass Steige) single stiffness model
5	Tomasi et al. (EC) double stiffness model
6	Tomasi et al. (Blass Steige) double stiffness model
7	De Santis Fragiaco

Table 4.2: Stiffness calculation methods for inclined screws selected for further analysis.

Moment capacity and rotational stiffness of dowel type groups

5.1. Introduction

Currently, no calculation approach is given for the rotational stiffness nor the moment capacity of dowel-type group connections in codes or standards [40, p. 3]. However, analytical methods for both have been developed and are presented in the literature, incorporating stiffness and capacity values given in EN-1995-1-1 [55]. This chapter first discusses the capacity calculation, and then several methods for rotational stiffness are discussed.

5.2. Connection capacity

Moment-resisting beam-column connections are often used in hall structures and are of vital importance for their overall structural behaviour and capacity [40, p. 2]. They are often seen in three hinged frames, in which case they often consist of two column elements and a single beam element, and are connected employing steel dowels. To verify whether these connections have sufficient capacity, the following must be checked:

- The capacity of the individual dowels, which can be done based on the European Yield Model (see section 3.2.1). For the embedding strength, the angle between the vector resultant of the force each dowel exerts on the timber elements and the grain direction of these elements must be taken into account.
- The capacity of the reduced cross sections of the connected timber elements for bending moment, normal force, and shear force that occur at the location of the connection.
- The capacity of the reduced cross-section for increased shear force. The value of the shear force at the location of the connection will be significantly larger due to the individual contributions of the dowels. The reduced cross-section must be checked for this increased shear force.

[68, p. 73]

Multiple connection geometries are possible. In literature [60], [36], [68], connections consisting of a single circle of dowels, a double circle of dowels and rectangular patterns are discussed.

5.2.1. Individual dowel capacity

The load-bearing capacity of beam-column connections was described by Heimeshoff in 1977 [36]. The assumption is made that an individual dowel experiences load both from the moment contribution and from the normal and shear force acting on the connection. The individual force as a result of the moment exerted on each dowel is given in equation 5.2, and the contributions of normal force and shear force on column and beam are given in equations 5.1a to 5.1d. The contributions of normal and shear force are combined by Heimeshoff to the term $|D_{NQ}|$ and calculated according to equation 5.3.

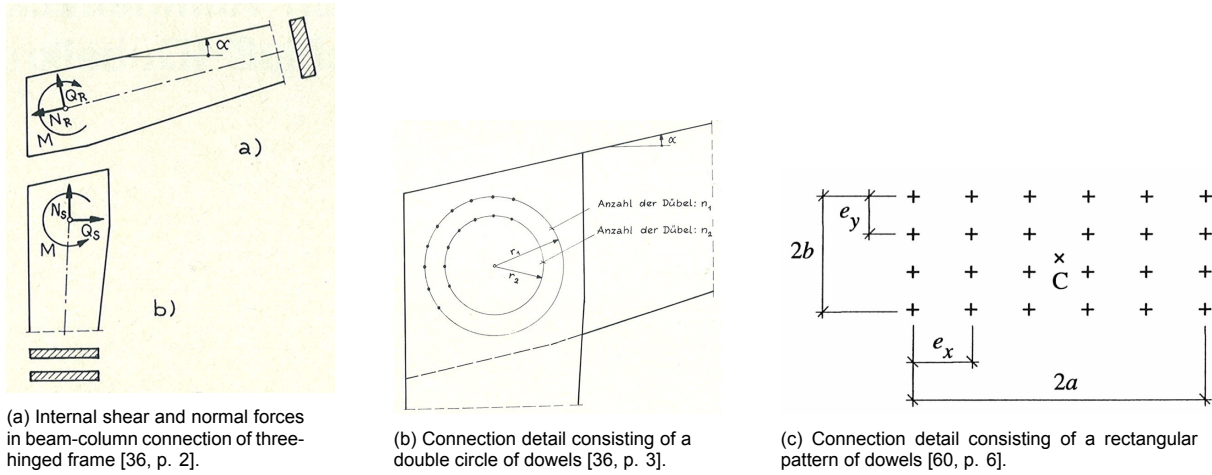


Figure 5.1

$$|D_{NR}| = \frac{|N_R|}{n_{tot}} \quad (\text{dowel normal force on beam}) \quad (5.1a)$$

$$|D_{NS}| = \frac{|N_S|}{n_{tot}} \quad (\text{dowel normal force on column}) \quad (5.1b)$$

$$|D_{QR}| = \frac{|Q_R|}{n_{tot}} \quad (\text{dowel shear force on beam}) \quad (5.1c)$$

$$|D_{QS}| = \frac{|Q_S|}{n_{tot}} \quad (\text{dowel shear force on column}) \quad (5.1d)$$

$$|D_M| = |M| \frac{r_1}{n_1 r_1^2 + n_2 r_2^2} \quad (\text{dowel force as result of moment } M) \quad (5.2)$$

$$|D_{NQ}| = \sqrt{D_{NR}^2 + D_{QR}^2} = \sqrt{D_{NS}^2 + D_{QS}^2} \quad (\text{dowel force as result of shear and normal force}) \quad (5.3)$$

In which:

- N_R : normal force in beam
- N_S : normal force in column
- Q_R : shear force in beam
- Q_S : shear force in column
- r_i distance dowel i to the centre of the dowel circle(s)
- n_i number of dowels in dowel circle i

The largest vector resultant of D_M and D_{NQ} occurs for the dowel for which the direction of both components align, e.g. the bottom right dowel in figure 5.2. This is not necessarily the most critical dowel, as the maximum allowable embedment strength of the timber is a function of the angle between the grain and the load as described by equation 3.2. Figure 5.3 shows the maximum allowable load exerted by the dowels on the timber as a dashed line. It is clear that this value, denoted in this case by "zul D" is largest for dowels that load the timber parallel to the grain and smallest for dowels that load the timber perpendicular to the grain. Heimeshoff [36] states that the dowel that applies the largest load perpendicular to the grain is calculated according to equation 5.4. It is stated by Heimeshoff [36] that in case $|D_{NR}|$ and $|D_{NS}|$ are both smaller than approximately 20% of $|D_M|$ (which is stated to be the case

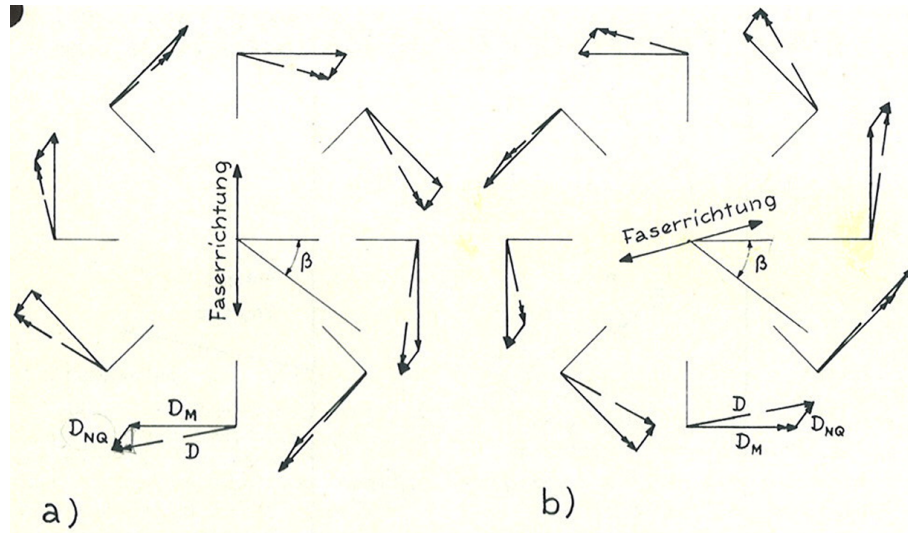
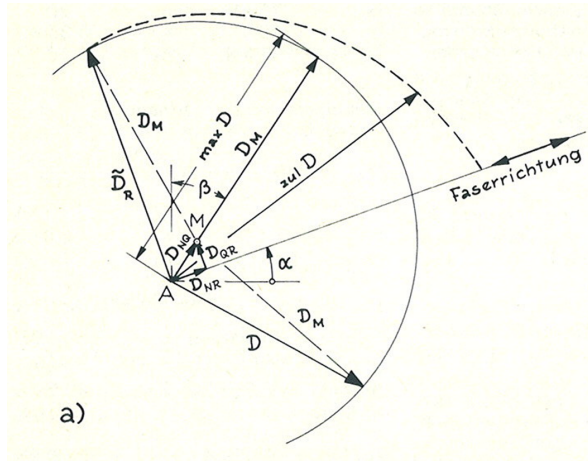


Figure 5.2: Load exerted by the dowels on the column (a) and on the beam (b) as result of moment contribution D_M and shear/normal force contribution D_{NQ} .

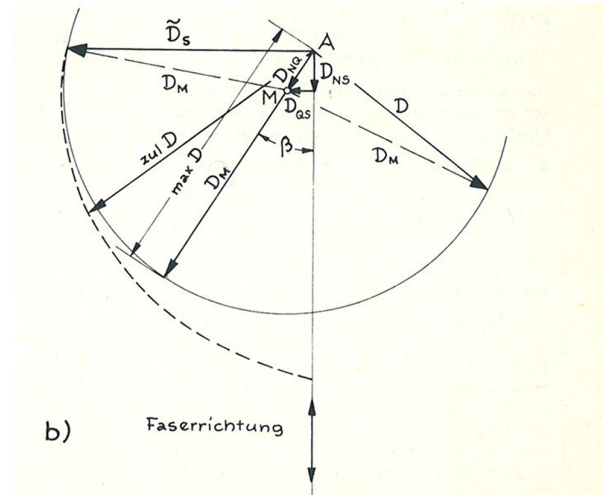
for frame corners), the dowel that loads the timber perpendicular to the grain in either column or beam indeed is the critical dowel concerning the timber embedment capacity.

$$\tilde{D}_R = D_{QR} + \sqrt{D_M^2 - D_{NR}^2} \approx D_{QR} + D_M \quad (5.4a)$$

$$\tilde{D}_S = D_{QS} + \sqrt{D_M^2 - D_{NS}^2} \approx D_{QS} + D_M \quad (5.4b)$$



(a) Load components acting on a single dowel and maximum allowable load on timber (dashed line) for beam element [36, p. 3].



(b) Load components acting on a single dowel and maximum allowable load on timber (dashed line) for column element [36, p. 3].

Figure 5.3

Racher [60] describes a method that is also suited for rectangular or trapezoidal dowel patterns, for which the force on an individual dowel as a result of the moment is described by equation 5.5. Racher [60] proposes equation 5.6, for the individual dowel force as a result of normal force, shear force, and force as a result of moment. The capacity should be checked under an angle to the grain α_1 , given by equation 5.7. For rectangular or trapezoidal geometries, an additional check for the furthest dowel should be performed according to equation 5.8 [60], with an angle to the grain given by α_2 (see equation 5.9).

$$F_M = |M| \frac{\sqrt{a^2 + b^2}}{\mu_x e_x^2 + \mu_y e_y^2} \quad (\text{for rectangular geometries, [60]}) \quad (5.5)$$

With:

- $\mu_x = 4 \cdot m_y \sum_{i=1}^{m_x} (i - 0.5)^2$
- $\mu_y = 4 \cdot m_x \sum_{j=1}^{m_y} (j - 0.5)^2$
- $m_x = \text{mod} \left[\frac{n_x + 1}{2} \right]$ with n_x the number of screws in hor. row, see fig. 5.1c
- $m_y = \text{mod} \left[\frac{n_y + 1}{2} \right]$ with n_y the number of screws in vert. row, see fig. 5.1c

$$F_{1,d} = \sqrt{(F_M + F_V)^2 + F_N^2} \quad (5.6)$$

$$\alpha_1 = \tan^{-1} \left[\frac{F_M + F_V}{F_N} \right] \quad (\text{see figure 5.4}) \quad (5.7)$$

$$F_{2,d} = \sqrt{\left(F_V + \frac{a}{\sqrt{a^2 + b^2}} F_M \right)^2 + \left(F_V + \frac{a}{\sqrt{a^2 + b^2}} F_M \right)^2} \quad (5.8)$$

$$\alpha_2 = \tan^{-1} \left[\frac{a F_M + \sqrt{a^2 + b^2} F_V}{b F_M + \sqrt{a^2 + b^2} F_N} \right] \quad (5.9)$$

In which:

- F_M : dowel force as a result of moment, see equation 5.2 or 5.5
- F_V : dowel force as a result of shear force
- F_N : dowel force as a result of normal force
- a, b : half width and half height of rectangular dowel connection, see 5.1c

The geometrical differences between the approaches of Heimeshoff [36] and Rancher [60] for circular patterns are shown in figure 5.4. Next to timber embedment failure, a dowel can form one or several plastic hinges, and should therefore also be checked according to the European Yield Model, in this case for double shear plane connections. For testing a complete connection, at least the capacity of the most heavily loaded dowel (the dowel at which alignment of $|D_M|$ and $|D_{NQ}|$ occurs and thus has the largest risk of forming a plastic hinge) and the two most heavily loaded dowels located at or near the centre lines of both connected members (highest risk of timber embedment failure i.e. splitting) must be checked according to the European Yield Model [68, p. 77].

5.2.2. Capacity of reduced cross section

The capacity check for the reduced cross-section is assumed to be trivial and is not discussed in this thesis. A calculation example can be found in literature, for instance [68, p.71].

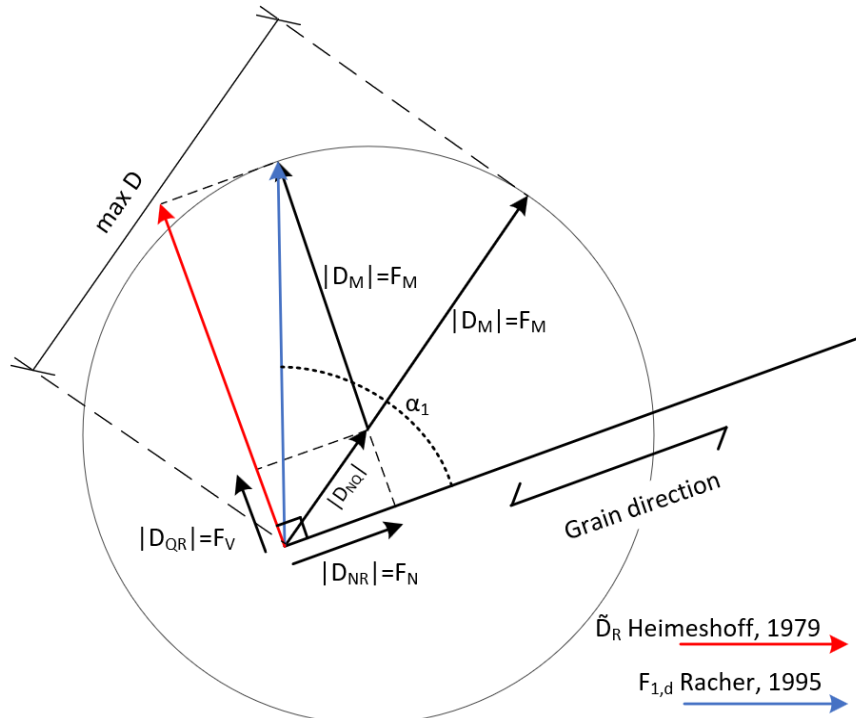


Figure 5.4: Critical load according to Heimeshoff [36] and Racher [60]. Source: own image.

5.2.3. Shear force

The shear force at the centre lines of both connected elements is critical, as extra shear force is introduced by the summation of the perpendicular decomposition of the moment contributions of the individual dowels. Both the individual shear force transferred by the dowels and the decomposition of the moment should be taken into account, as given in equation 5.10. This value can then be checked according to the standard check for shear force given in EN-1995-1-1 [55].

$$F_{V,d} = V_M - \frac{V_{u,d}}{2} \quad (5.10)$$

In which:

- $V_{u,d}$: Shear force on the column.
- V_M : Shear force contribution from moment, given as:

$$V_M = \begin{cases} \frac{M}{\pi \cdot r}, & \text{for dowel patterns consisting of a single circle} \\ \frac{M}{\pi} \cdot \frac{n_1 r_1 + n_2 r_2}{n_1 r_1^2 + n_2 r_2^2}, & \text{for dowel patterns consisting of a double circle} \\ M \cdot \frac{2\mu_y e_x}{\mu_x e_x^2 + \mu_y e_y^2} \sum_{i=1}^{\mu_y} \left(i - \frac{1}{2}\right), & \text{for rectangular dowel patterns} \end{cases}$$

In which:

- e_x : horizontal distance between dowels, see figure 5.1c
- e_y : vertical distance between dowels, see figure 5.1c

[60, p. 8]

5.3. Rotational stiffness

The rotational stiffness can be calculated based on a spring model and is given by equation 5.11. This equation is valid in the serviceability limit state (SLS). The analytical derivation is given in equation

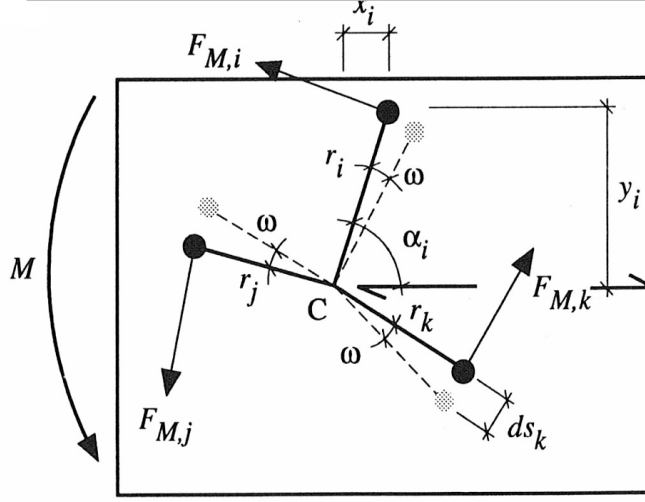


Figure 5.5: Geometrical definitions of individual dowels according to Racher [60].

5.13, based on the parameters given in figure 5.5, with $F_{M,i}$ the force as a result of the moment per dowel, ω the connection rotation, r_i the distance between the dowel i and the centre of rotation and α_i the angle between the grain direction and r_i .

$$k_r = K_{ser} \sum_{i=1}^n r_i^2 = K_{ser}(n_1 r_1^2 + n_2 r_2^2) \quad (\text{for circular patterns, in this case two rings}) \quad (5.11)$$

$$= K_{ser}(\mu_x e_x^2 + \mu_y e_y^2) \quad (\text{for rectangular or trapezoidal patterns}) \quad (5.12)$$

$$\left. \begin{aligned} ds_i &= \frac{F_{M,i}}{K_{\alpha_i}} \\ \omega &= \frac{ds_i}{r_i} = \frac{F_{M,i}}{K_{\alpha_i} r_i} \\ M &= \sum_{i=1}^n F_{M,i} r_i \end{aligned} \right\} \Rightarrow k_r = \frac{M}{\omega} = \frac{\sum_{i=1}^n F_{M,i} r_i}{\frac{F_{M,i}}{K_{\alpha_i} r_i}} = \sum_{i=1}^n K_{\alpha_i} r_i^2 \quad (5.13)$$

Equation 5.13 depends on the parameter $K_{\alpha,i}$, which is defined as the stiffness of dowel at position i , as a function of the angle α_i between the grain direction and the moment arm of screw i , indicating a dependence of the stiffness of a dowel type fastener on the direction of the load application. Equation 5.13 for the rotational stiffness can be split in the stiffness parallel to the grain k_{SLS} and perpendicular to the grain $k_{SLS,v}$. The proof that equations 5.14 and 5.15 are indeed equal is given below.

$$k_r = \sum_{i=1}^n k_i r_i^2 = \sum_{i=1}^n k_{SLS,combined}(x_i^2 + y_i^2) \quad (5.14)$$

$$k_r = \sum_{i=1}^n k_{SLS} y_i^2 + k_{SLS,v} x_i^2 \quad (5.15)$$

$$\cos(\alpha) = \frac{y_i}{\sqrt{x_i^2 + y_i^2}}, \quad \sin(\alpha) = \frac{x_i}{\sqrt{x_i^2 + y_i^2}} \quad (5.16)$$

$$u_1 = \cos(\alpha) u_{tot}, \quad u_2 = \sin(\alpha) u_{tot} \quad (5.17)$$

$$F_1 = k_{SLs}u_1 = k_{SLs}\cos(\alpha)u_{tot}, \quad F_2 = k_{SLs,v}u_2 = k_{SLs,v}\sin(\alpha)u_{tot} \quad (5.18)$$

$$F_{1,decomp} = k_{SLs}u_1 = k_{SLs}\cos(\alpha)^2u_{tot}, \quad F_{2,decomp} = k_{SLs}u_2 = k_{SLs}\sin(\alpha)^2u_{tot} \quad (5.19)$$

$$\begin{aligned} k_{SLs,combined} &= \frac{F_{1,decomp} + F_{2,decomp}}{u_{tot}} \\ &= \frac{k_{SLs}\cos(\alpha)^2u_{tot} + k_{SLs,v}\sin(\alpha)^2u_{tot}}{u_{tot}} \\ &= k_{SLs}\cos(\alpha)^2 + k_{SLs,v}\sin(\alpha)^2 \end{aligned} \quad (5.20)$$

$$\begin{aligned} k_r &= \sum_{i=1}^n k_{SLs,combined}(x_i^2 + y_i^2) \\ &= \sum_{i=1}^n (k_{SLs}\cos(\alpha)^2 + k_{SLs,v}\sin(\alpha)^2)(x_i^2 + y_i^2) \\ &= \sum_{i=1}^n (k_{SLs}\cos(\alpha)^2x_i^2 + k_{SLs}\cos(\alpha)^2y_i^2 + k_{SLs,v}\sin(\alpha)^2x_i^2 + k_{SLs,v}\sin(\alpha)^2y_i^2) \\ &= \sum_{i=1}^n \left[k_{SLs} \left(\left(\frac{y_i}{\sqrt{x_i^2 + y_i^2}} \right)^2 x_i^2 + \left(\frac{y_i}{\sqrt{x_i^2 + y_i^2}} \right)^2 y_i^2 \right) + k_{SLs,v} \left(\left(\frac{x_i}{\sqrt{x_i^2 + y_i^2}} \right)^2 x_i^2 + \left(\frac{x_i}{\sqrt{x_i^2 + y_i^2}} \right)^2 y_i^2 \right) \right] \\ &= \sum_{i=1}^n k_{SLs}y_i^2 + k_{SLs,v}x_i^2 \end{aligned} \quad (5.21)$$

5.3.1. Screw forces

Making use of the derivation given in equations 5.14 to 5.21, it is possible to calculate the theoretical forces parallel and perpendicular to the inclination direction of the screw in case the relative rotation of two connected timber elements is known. Figure 5.7 shows the chord-diagonal connection of the FaNaBu truss. The relative rotation between the diagonal and the chord is drawn in white.

$$\left. \begin{aligned} F_{screw,par,i} &= F_1 = k_{SLs} \cdot \cos(\theta_i) \cdot u_{tot,i} \\ F_{screw,perp,i} &= F_2 = k_{SLs,v} \cdot \sin(\theta_i) \cdot u_{tot,i} \\ u_{tot} &= \phi_{diag-chord} \cdot r_i \end{aligned} \right\} \Rightarrow \begin{aligned} F_{screw,par,i} &= k_{SLs} \cdot \cos(\theta_i) \cdot \phi_{diag-chord} \cdot r_i \\ F_{screw,perp,i} &= k_{SLs,v} \cdot \sin(\theta_i) \cdot \phi_{diag-chord} \cdot r_i \end{aligned} \quad (5.22)$$

In which:

- $F_{screw,par,i}$: force parallel to the inclination direction of screw i
- $F_{screw,perp,i}$: force perpendicular to the inclination direction of screw i
- r_i : distance between screw i and centre of rotation
- θ_i : angle between line r_i and the line perpendicular to the inclination direction of the screw
- $\phi_{diag-chord}$: relative rotation between the timber elements
- $u_{tot,i}$: displacement of screw i as a result of $\phi_{diag-chord}$

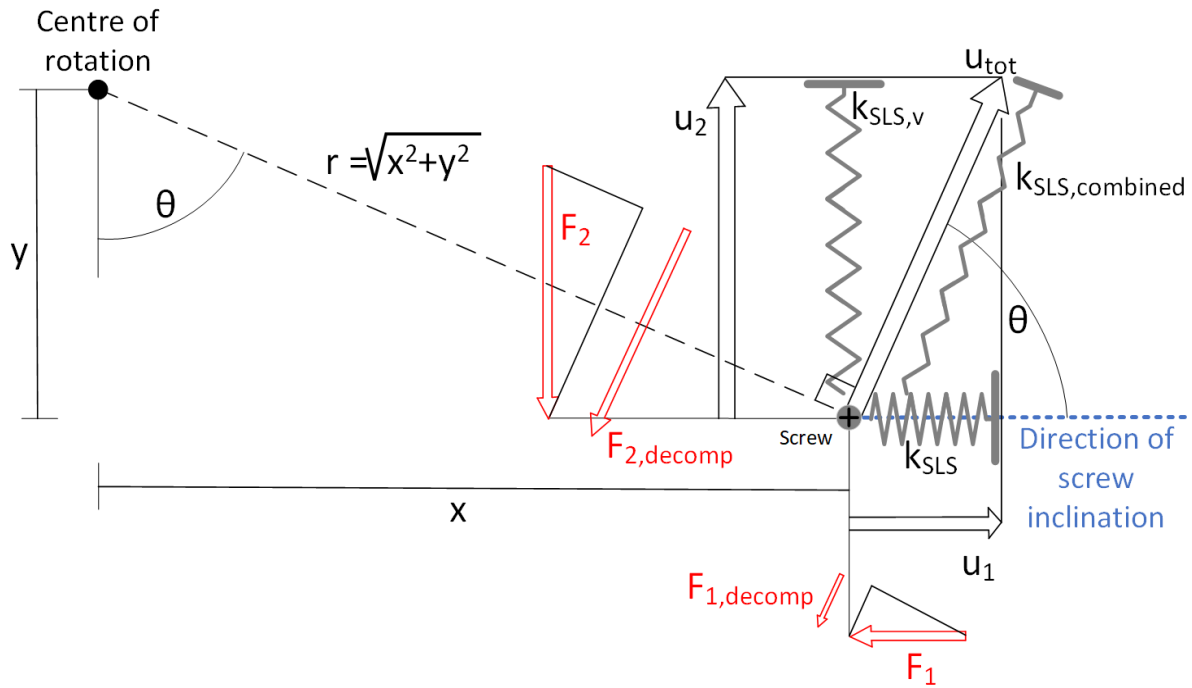


Figure 5.6: Schematic representation of screw subject to rotation around centre of rotation, with stiffness parallel to grain k_{SLS} and stiffness perpendicular to grain $k_{SLS,v}$. Source: own image.

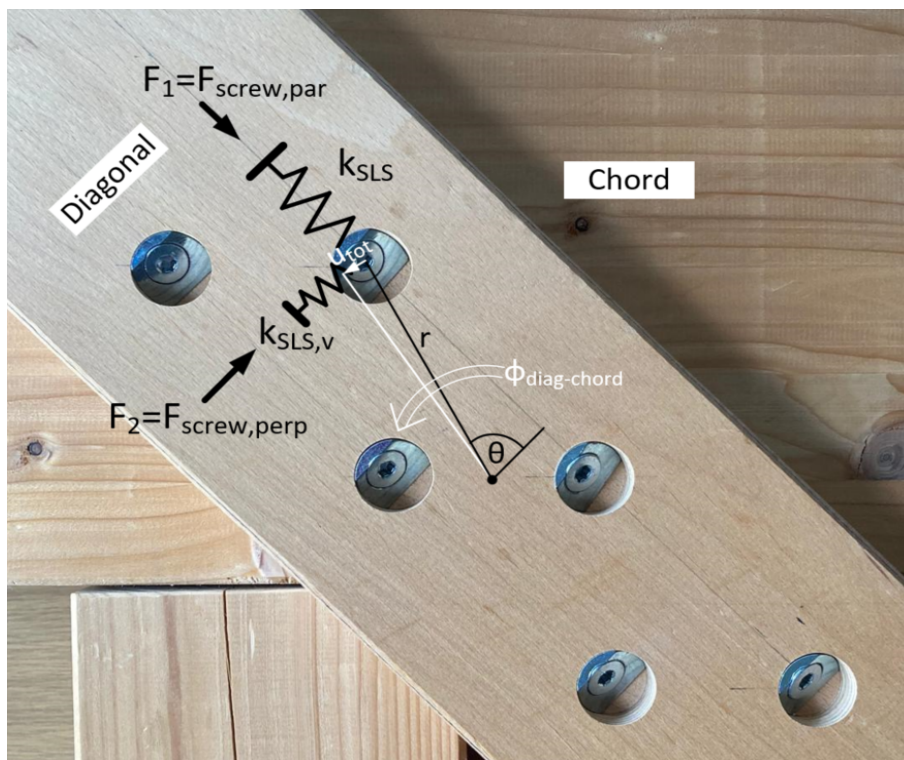


Figure 5.7: Schematic representation of truss connection subject to rotation $\phi_{diag-chord}$, with resulting screw forces perp. and par. to incl. direction of the screw $F_{screw,perp}$ and $F_{screw,par}$, respectively. Source: own image.

5.3.2. Eurocode 5: EN-1995-1-1 draft (2023)

In the pre-norm prEN-1995-1-1 [53] a method is proposed to calculate the lateral slip modulus for a dowel-type fastener K_{ser} as a function of the grain direction. According to this method, the slip modulus for fasteners loaded perpendicular to the grain should be reduced by 50 %, while the slip modulus remains unchanged for fasteners loaded parallel to the grain. For intermediate values, linear interpolation is proposed. See equation 5.23 for a mathematical representation.

$$K_{ser} = \frac{180 - \psi}{180} \cdot \frac{\rho_m^{1.5} d}{23} \quad [53, \text{sect. 11.3.7.2 (3)}] \quad (5.23)$$

In which:

- ψ : angle between the lateral loading direction of a dowel type fastener and grain direction [°]
- ρ_m : mean density [kg/m³]
- d : outer diameter of the fastener [mm]

5.3.3. Noguchi & Komatsu

It is stated by Noguchi & Komatsu [57] that the method for rotational stiffness derived in equation 5.11 does not take into account shear deformation. Noguchi & Komatsu [57] argue that shear deformation should be taken into account in the case of non-circular bolt patterns. Based on Castigliano's first theorem, Noguchi and Komatsu [57] propose equation 5.24.

$$k_r = \frac{4}{\frac{\sum_{i=1}^n \frac{x_i^2}{K_{si}}}{\left(\sum_{i=1}^n x_i^2\right)^2} + \frac{\sum_{i=1}^n \frac{y_i^2}{K_{si}}}{\left(\sum_{i=1}^n y_i^2\right)^2}} \quad (5.24)$$

In which:

- k_r : rotational stiffness of connection
- K_{si} : lateral stiffness of dowel i
- x_i distance in x-direction of dowel i to centre of rotation
- y_i distance in y-direction of dowel i to centre of rotation

In their derivation, Noguchi & Komatsu [57] present two different methods of modelling the connection. It is assumed that the connection can be modeled as a joint layer, as given in figure 5.8a. This joint layer is loaded in torsion. The earlier presented calculation method for rotational stiffness presented in section 5.3 assumes that the static torsion in the joint layer is transmitted according to pattern 5.8b (Coulomb's law), i.e. the stress distribution is proportional to the distance to the rotational centre [57]. Saint-Venant's theorem is adopted by Noguchi & Komatsu [57], however, the stresses in the x and y direction are assumed to be constant for constant x and y distances from the rotational center. The shear force distribution as given in figure 5.8c is finally proposed. This energy-based method provides an interesting alternative to the aforementioned method, which is based on the assumption that each individual dowel resembles a linear spring. Noguchi & Komatsu [57] state that the proposed method yields the same results as the spring method in the case of symmetrical bolt arrangements. For asymmetrical arrangements, [57] state that the linear spring method overestimates the rotational stiffness, and it was found by Noguchi & Komatsu [57] that the proposed method more closely resembles the results of their experimental tests.

The method proposed by Noguchi and Komatsu [57] in the form of equation 5.24 yields a division by zero in case of linear screw patterns, i.e. either $\sum_{i=1}^n x_i^2 = 0$ or $\sum_{i=1}^n y_i^2 = 0$. Equation 5.24 was plotted for ranges of sums of squared distances $\sum_{i=1}^n x_i^2$ and $\sum_{i=1}^n y_i^2$ in figure 5.9. Details of the plot are given in appendix D. Because a value of zero for either $\sum_{i=1}^n x_i^2$ or $\sum_{i=1}^n y_i^2$ yields a division by zero, a value of 0.001 is used instead as the lower bound. It is concluded that the method yields rotational stiffness values of nearly zero in the case of linear fastener patterns.

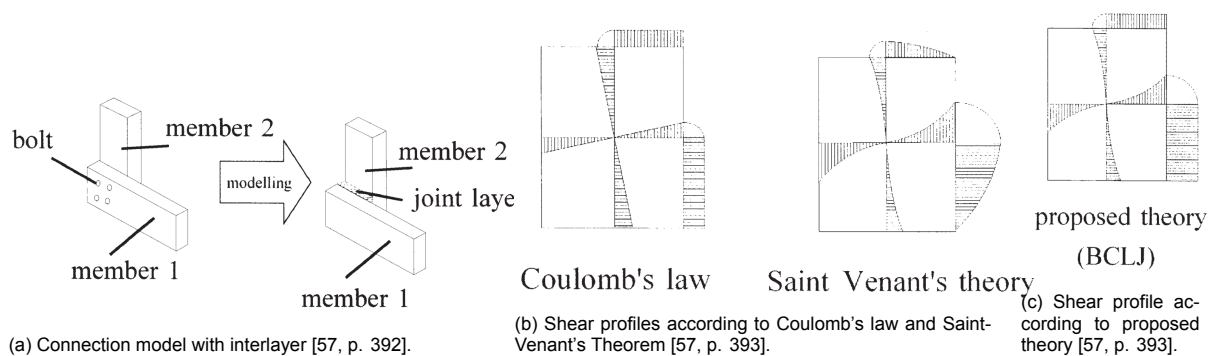


Figure 5.8

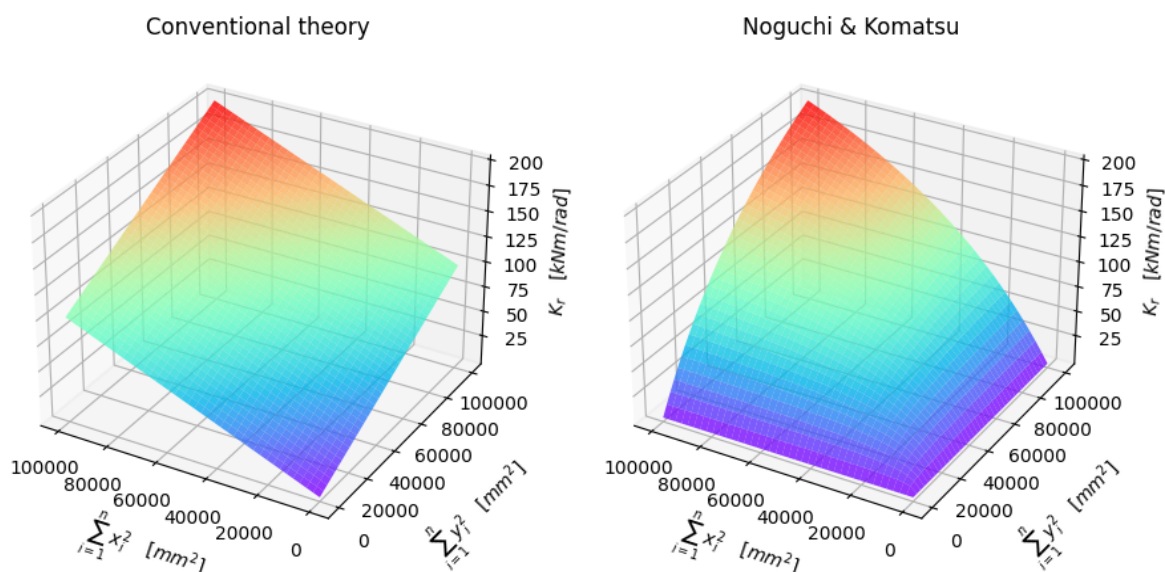


Figure 5.9: Rotational stiffness as a function of the sum of squared x distances and y distances, both for the conventional spring method and the method proposed by Noguchi & Komatsu. Details of the plot are given in appendix D. Source: own image.

5.3.4. Centre of rotation displacement

The aforementioned methods to determine the rotational stiffness both depend on the distance between each individual fastener and the geometrical centre of the connection. The implicit assumption is made that the geometrical centre is equal to the centre of rotation and that this centre point remains at the same location during the rotation.

Literature is ambiguous about whether and when this phenomenon occurs. A T-joint composed of a circularly arranged dowel pattern, loaded by both shear force and bending moment was studied by Bouchaïr et al. [16]. Tests with a finite element model and experiments were performed, and it was found that the centre of rotation remained at the same location under the loading conditions. Bader et al. [3] performed experimental tests of symmetrical dowel geometries loaded under pure bending moment, and it was found that the geometrical centre of the connection was also the rotational centre of the connection, i.e. no shift was found. In contrast to the aforementioned studies, higher individual dowel loads on one side of connections consisting of square geometries loaded by a bending moment and shear force were reported by Basterrechea-Arévalo et al. [5], indicating a shift of the centre of rotation [5, p. 11].

It is assumed that in case all fasteners have the same individual stiffness, and no additional kinematic

boundary conditions are introduced, no displacement in centre of rotation occurs. For these cases, therefore, the geometric centre of connections is assumed to be equal to the centre of rotation.

5.4. Conclusion

An analytical method to calculate the moment capacity of connections consisting of dowel-type connections is given in the literature, in which the individual dowel, the capacity of the reduced cross-section, and the increased shear force as a result of the moment should be checked. Regarding methods to quantify the rotational stiffness of connections with dowel-type fasteners, three distinct methods are identified:

- The spring model, given in equation 5.13, where the same lateral slip modulus K_{ser} as given in equation 3.18 is used for each dowel-type fastener.
- The spring model, where the individual lateral slip modulus K_{ser} of each dowel-type fastener is calculated as a function of the angle between the grain direction and loading direction as proposed in prEN-1995-1-1 [53, p. 188] and described in section 5.3.2. According to the analytical proof given in equations 5.14 to 5.21, it is possible to separate the lateral stiffness $k_{SLs,v}$ (taken as $0.5 \cdot K_{ser}$) and stiffness parallel to the inclination direction k_{SLs} , so that no interpolation for each individual screw is needed.
- The method proposed by Noguchi and Komatsu [57] as described by equation 5.24.

The two methods based on the spring model are considered viable methods for further analysis. As stated, the method proposed by Noguchi and Komatsu [57] yields unrealistically low values for rotational stiffness in the case of linear screw patterns. Therefore, the method is discarded and not used for further analysis. The original method based on the spring model is referred to as "EC", and the spring model method using the prEN-1995-1-1 reduction for stiffness under an angle to the grain is referred to as "0.5 EC".

6

Timber-to-timber friction

6.1. Introduction

In most of the described methods to assess the capacity and stiffness of individual inclined screw connections described in chapter 4, friction has already been taken into account. Besides the influence of friction on the individual screws, visual inspection after experiments conducted by Egner & Frese [24] suggested the hypothesis that friction also plays a role in the rotational behaviour of connections with inclined screws. Although further research is needed, it is expected that the influence of friction on the rotational stiffness of connections with inclined screws depends on the surface area, the coefficient of friction, tension stress, and the number of screws in the connection [25, p. 61].

6.2. Parameters influencing friction

An extensive literature study on timber-to-timber and timber-to-steel friction was carried out by Aurand and Blass [1]. Friction is typically given as the coefficient of friction (COF) μ , defined as the ratio of the friction force and the normal force. A special case is the static coefficient of friction, defined as the maximum friction force that is present before relative displacement between two specimens occurs. The influence of the following parameters on the coefficient of friction was studied by Aurand and Blass [1]:

- Contact pressure
- Sliding speed
- Timber density
- Moisture content
- Surface roughness
- Grain direction

The literature that was analysed by Aurand and Blass [1] reports contact pressures ranging between 0.0001 - 1 [N/mm²] for timber-to-timber friction. The relation between contact pressure and coefficient of friction is given in figure 6.1a. The logarithmic trend line is plotted, where first an increase of the coefficient of friction for larger values of contact pressure is identified, while later horizontal convergence is observed [1, p. 3]. The relation with sliding speed is given in figure 6.1b. Data from the literature studied by Aurand and Blass [1] reports sliding speeds in a range of 1 - 3300 [mm/min] for timber-to-timber friction. A similar relation as for contact pressure was found by Aurand and Blass [1, p. 5], with again increasing coefficients of friction for higher sliding speeds and later horizontal convergence. The relation between timber density and coefficient of friction is given in figure 6.1c. Aurand and Blass [1] report that no correlation was found between the density of the timber specimens and the coefficient of friction. The coefficient of friction was found to increase significantly as the moisture content of the specimens surpasses a value of 20 % [1, p. 5]. This effect was found for softwood, hardwood, and

engineered wood alike. Surface roughness is divided into three categories, being treated, planed, and rough-cut. Treated wood is further specified with the example of formwork panels. Surface roughness was found to have the largest influence on the coefficient of friction [1, p. 6]. Grain differentiation is divided into three categories by Aurand and Blass [1], namely parallel, perpendicular, and end grain. Parallel grain direction is defined by Aurand and Blass [1] as the case in which the grain directions of the two test specimens are oriented parallel to each other and to the line of exerted force. Perpendicular grain direction is defined as the case in which one of the two specimens is rotated 90 [°], and in the end grain orientation, both specimens are tested with the end grain facing toward each other [1, p. 6]. It was found that the grain direction is of negligible influence on the coefficient of friction, an exception being the end grain orientation. Aurand and Blass [1, p. 6] state that slightly higher values for the coefficient of friction are found for this case than for the parallel and perpendicular orientations.

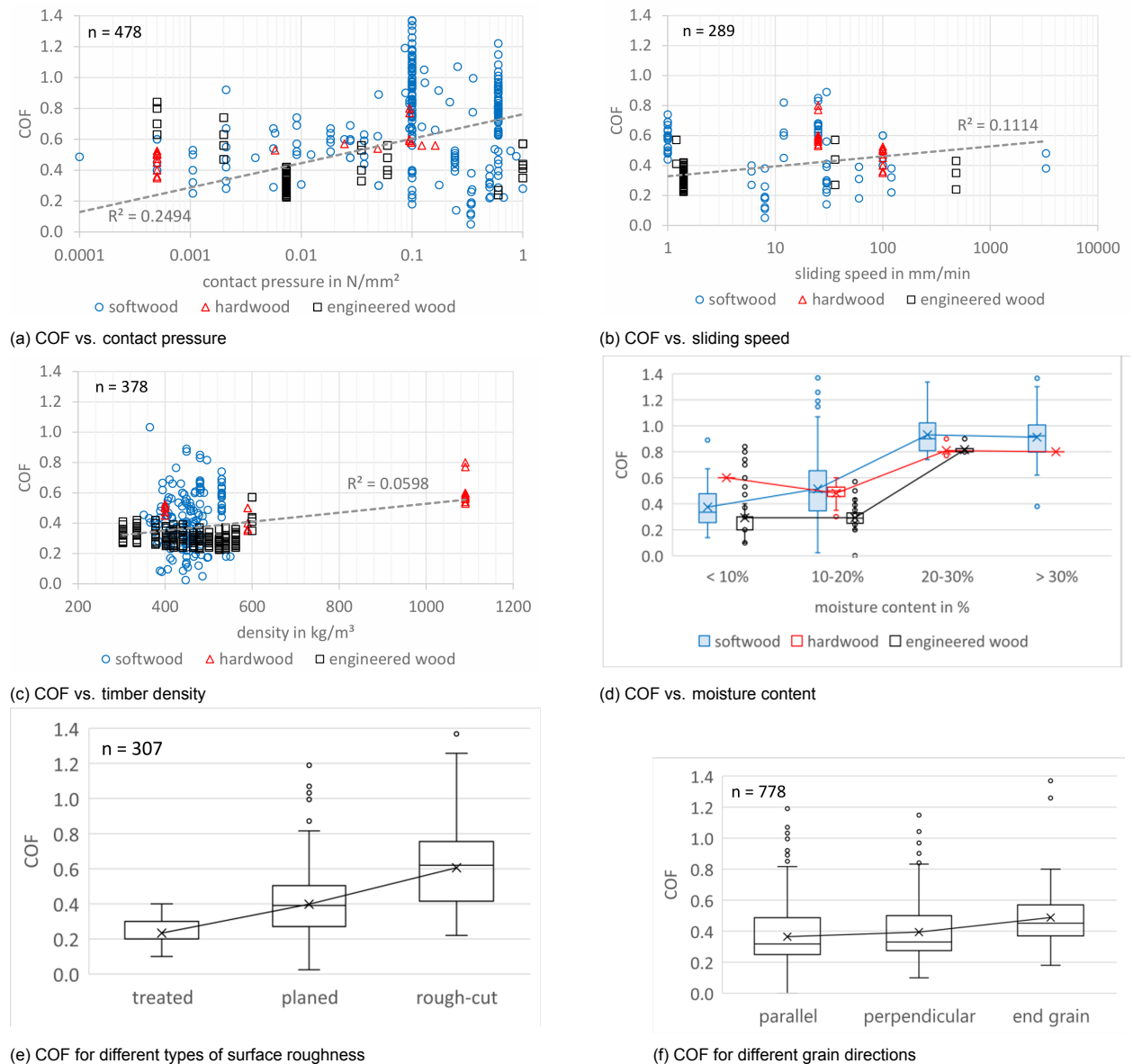


Figure 6.1: Parameters influencing the COF for timber-to-timber [1]

The main purpose of the study by Aurand and Blass [1] was to investigate different surface treatments for dovetail joist connectors, making use of inclined screws and densified veneer wood (DVW) as an alternative to steel, as shown on the right-hand side of figure 6.2. Fire safety is of utmost importance for connections in timber structures, and DVW could be an interesting material as it has beneficial

fire safety properties and a lower thermal conductivity than steel, conducting less heat to the timber elements [2]. To this end, multiple tests to find capacity and stiffness were carried out with different surface treatments of the DVW and screws inclined under 45° as shown on the left-hand side in figure 6.2. Among others, milled pyramid patterns of different depths were tested. It was found that deeper pyramid patterns yielded the highest load-bearing capacity as a result of higher friction, but also lower stiffness values. A possible explanation given by Aurand and Blass [1, p. 14] for this phenomenon is that flatter surfaces immediately experience full contact, whereas rougher surfaces first need some initial slip for interlocking to occur.

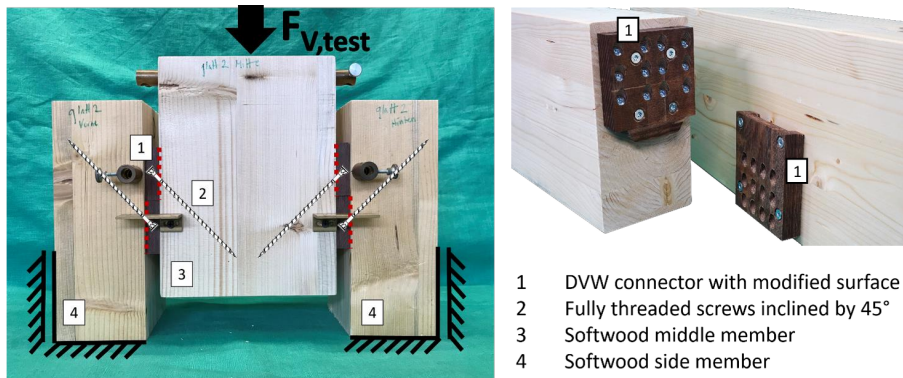


Figure 6.2: Dovetail connector as tested by Aurand and Blass [1]

6.3. Friction beech LVL and coniferous wood

As a part of the FaNaBu project, friction tests were carried out using the materials to be used in the FaNaBu truss; beech LVL and coniferous wood. Different surface milling treatments were tested for the beech LVL, while the coniferous specimens were left untreated [25, p. 18]. It is stated that because the beech LVL has a higher density and surface hardness, the milled surfaces of the beech LVL should be pressed into the coniferous wood so that interlocking occurs [25, p. 17]. The specimens were subjected to a contact pressure of $2.5 \text{ [N/mm}^2\text{]}$. For the specimens with untreated surfaces, an average value for the coefficient of friction was determined as 0.39 over ten tests [25, p. 20].

6.4. Conclusion

Surface roughness is concluded to have a high influence on the coefficient of friction. The coefficient of friction increases strongly after the moisture content surpasses a value of 20 %. A mean value for the coefficient of friction between beech LVL and coniferous wood in the context of the FaNaBu project was determined as 0.39.

Experimental investigations

7.1. Introduction

In order to test the rotational stiffness of connections with inclined screws, a test setup has been built, which is described in this chapter. Two series of tests have been carried out, with several differences between test series 1 and series 2. Test series 1 was originally described in the work of Eva Baldauf [4], and test series 2 in the work of Ronja Loreck [48]. Performing the tests was not part of this master's thesis, and therefore the information in this chapter is taken from the work of Eva Baldauf [4] and Ronja Loreck [48].

7.2. Test setup

The test setup is almost identical for both series and is given in figure 7.1. The only difference is the length of the lever arm, which is described later in this section. The test setup is designed to independently exert a normal (pulling) force and a rotation with therefrom resulting shear forces and bending moments, respectively, on a test specimen. The test specimen itself consists of an octagonal spruce glulam chord section which is attached to two beech laminated veneer lumber (LVL) side members. The octagonal chord section is placed inside a steel inner shell that fits inside an outer shell, with roller bearings at the interface of the two shells to enable them to rotate freely relative to one another. The rotational centre of the connection is therefore prescribed by the centre of both shells. The octagonal chord section is clamped between a V-shaped fork and the inner shell using threaded rods. The V-shaped fork in turn is connected to a lever arm which is controlled with a vertical cylinder, while the outer shell is rigidly connected to the base of the test setup. The distance between the centre of rotation and the vertical cylinder is 955 [mm] in test series 1 [4, p. 39], and 1000 [mm] in test series 2 [48, p. 30]. The side members of the test specimen are connected to a horizontal cylinder employing dowels. Via this horizontal cylinder, the side members can be subjected to a pulling force, while a rotation of these side members is prevented by a horizontal slider bearing. By exerting a vertical force on the lever arm with the vertical cylinder, a relative rotation between the chord section and both side members is established.

7.3. Test specimens

The exact testing procedure was slightly different for both test series. Therefore, they are described separately in the following sections.

7.3.1. Test series 1

In test series 1, the specimens consist of an octagonal chord section and two side members, which are connected with either two or four screws per shear plane. As each test specimen consists of two shear planes, the total amount of screws per test specimen amounts to either four or eight. The screws are inserted under an angle of 45° between the screw axis and the shear plane, and parallel to the longitudinal direction of the side members. The side members are arranged with their grain directions in the longitudinal direction so that the angle between the screw axis and the grain direction in the side

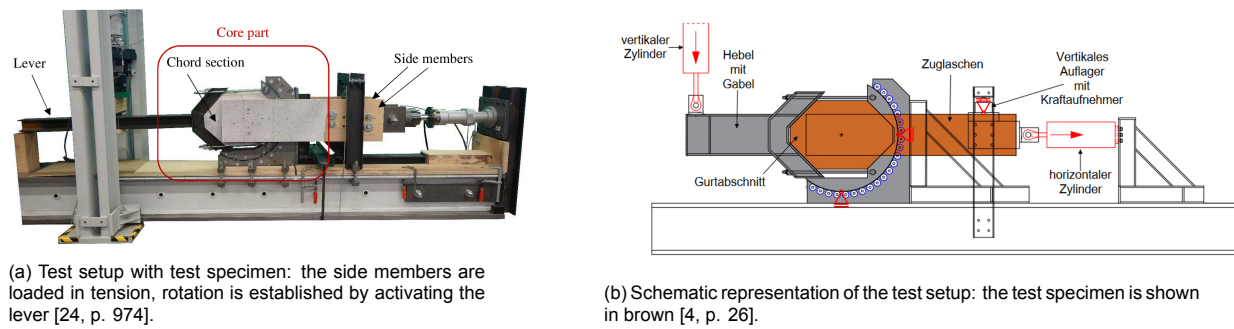


Figure 7.1

members is 45° [4, p. 26]. The chord section is arranged with the grain direction under an angle of 45° with respect to the side members and thus also with respect to the direction of the pulling cylinder, as given in figure 7.6a. As a consequence, the angle between the screw axis and chord grain direction is 60° [4, p. 26].

The chord section consists of spruce glued laminated timber (glulam), cut out of a spruce glulam beam of strength class GL24h. The side members consist of beech LVL of the type *BauBuche Typ S* produced by Pollmeier Massivholz GmbH & Co.KG. The side members were cut and pre-drilled by the firm Holzbau Bruno Kaiser GmbH with the help of a CNC-controlled carpentry machine [4, p. 22]. Two types of side members were produced (type A and type B, to be attached on either side of the chord section), each one with eight screw holes. The arrangement of the screw holes was chosen in such a fashion that the screws of both shear planes do not meet inside the glulam chord section. The geometry of the test specimens of type 1 is given in figure 7.2. The screws used for the connections are of the type *ASSY plus full-thread screws 8x240 mm* manufactured by Adolf Würth GmbH & Co. KG [4, p. 23]. According to the corresponding assessment document ETA-11/0190 [6], these screws should be pre-drilled with 6 [mm], which has been adopted in the tests. This pre-drilling was performed in two steps. First, a milling cutter with a diameter of 20 [mm] created an inclined edge under 45° so that the pre-drilling could be carried out on a perpendicular surface. After this, the holes with a diameter of 6 [mm] were drilled in the middle of the bevel [4, p. 23].

The exact dimensions of the parts of the specimens were measured after manufacturing of the individual timber parts [4, p. 24]. In combination with the weight of the parts, the density was calculated, and finally, the modulus of elasticity was decided based on vibration tests. The average density of the nine chord sections was $446 \text{ [kg/m}^3\text{]}$, with moisture contents between 11.5 and 12 [%] [4, p. 24]. For the eighteen side members, an average density of $812 \text{ [kg/m}^3\text{]}$ was calculated, which is slightly higher than the value of $800 \text{ [kg/m}^3\text{]}$ given by the manufacturer [4, p. 24]. The moduli of elasticity of the side members were found to lie between $16689 \text{ [N/mm}^2\text{]}$ and $18609 \text{ [N/mm}^2\text{]}$ [4, p. 24]. The average value is calculated as $17511 \text{ [N/mm}^2\text{]}$ and is again slightly higher than the value of $16800 \text{ [N/mm}^2\text{]}$ given by the manufacturer [4, p.24]. Due to the milling, the penetration length of the screws in the side members was reduced. To take this into account, the distances between the flat surfaces and the beginning of the screw holes were measured, as well as the distances between the screw exit point at the underside of the side members and the edges of the side members, and deviations of the planned dimensions were registered [4, p. 24]. The composition of the specimens was done based on measured density. Side members with roughly equivalent densities were assigned to the same chord section, to create test specimens that are as homogeneous as possible [4, p. 28].

7.3.2. Test series 2

In test series 2, the test specimens are built slightly differently. The octagonal chord section has the same dimensions as in test series 1, but the grain direction of the chord section is equal to that of the side members, as shown in figure 7.6a [48, p. 27]. This means that the grain direction of both the side members and the chord section is parallel to the longitudinal direction of the side members and thus also parallel to the pulling force exerted by the horizontal cylinder in the test setup. The chord

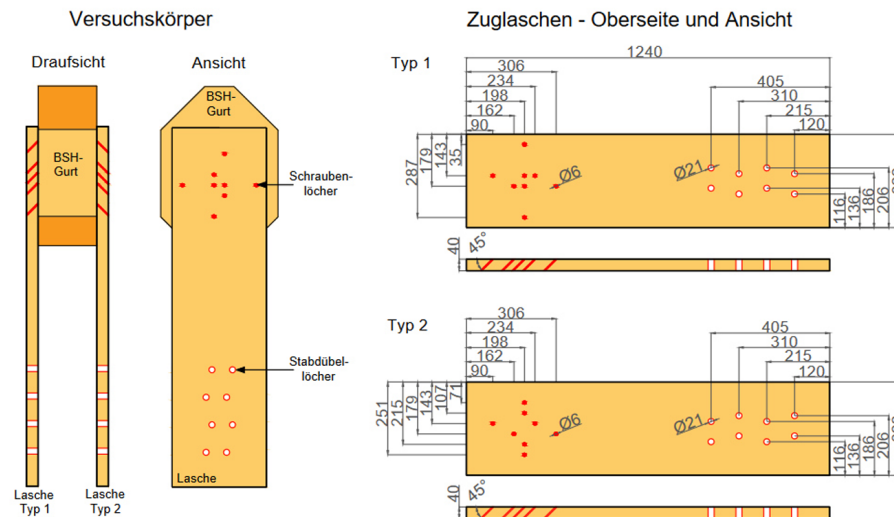
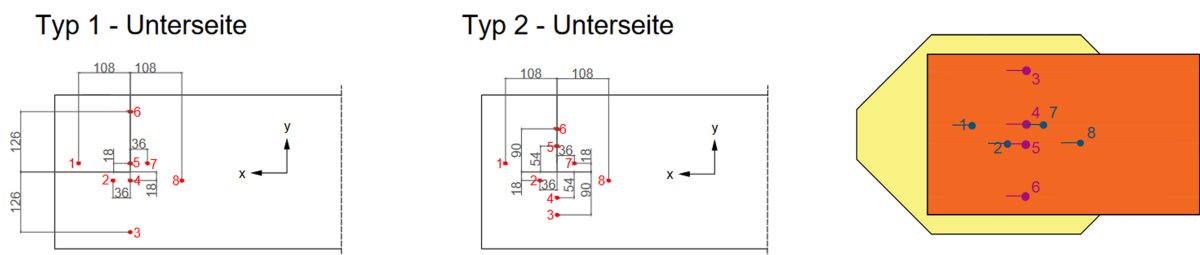


Figure 7.2: Test specimens of test series 1 [4, p. 23].



(a) Positions of the screw test series 1: the screw positions on either side are different so that the screws do not make contact inside the chord section [4, p. 29].

(b) Screw positions test series 1: the tails attached to the points indicate the part of the screw inside the timber [25, p. 54].

Figure 7.3

section and side members are connected with either two, four, or eight screws per shear plane [48, p. 32], which means a total of either four, eight, or sixteen screws per test specimen (as there are always two shear planes on either side of each test specimen). These screws are inserted under an angle of either 45 or 90 [°] between the screw axis and the shear plane [48, p. 28]. For this reason, each side member is pre-drilled with two screw patterns, both for 45 [°] and for 90 [°]. Inter screw distances are equal for both patterns. Test series 2 also features two additional screw positions compared to test series 1, namely position 9 and 10 [48, p. 32]. Also, test series 2 features some tests in which the friction in the shear planes is minimised. This is done by attaching sheets of polypropylene to the side and chord sections with adhesive tape and drilling oil. This combination was found to yield a coefficient of friction of 0.06 [48, p. 24]. Finally, because of practical reasons, the length of the side members is slightly longer (1250 [mm], [48, p. 27]) than in test series 1 (1240 [mm], [4, p. 22]), although this should not have any influence on the test results. Details of the specimens of test series 2 are given in figure 7.4. To generate specimens that are as homogeneous as possible, the two side members of each specimen are produced from the same LVL plate [48, p. 30].

The parts of the specimens consist of the same materials as in test series 1. In contrast to series 1 where only one type of screw type was featured, Loreck [48, p. 27] reports that for test series 2 the following 5 distinct screw types are used:

- ASSY plus fully threaded 4 CSMP 8x240 mm
- ASSY plus fully threaded 4 CSMP 8x200 mm
- ASSY plus fully threaded 4 CSMP 12x240 mm

- ASSY plus fully threaded 4 CSMP 12x200 mm
- ASSY plus partially threaded 4 CSMP 8x250 mm (170 mm)

The screws with a length of 240 [mm] are used for the 45-degree inclinations, and the screws with a length of 200 [mm] are used for the 90-degree inclinations [48, p. 28]. All screws are manufactured by Adolf Würth GmbH & Co. KG, and as in test series 1, pre-drilling is done as prescribed in the applicable ETA-11/0190 document [6]. This means the screws with a diameter of 8 [mm] are pre-drilled with holes of 6 [mm] diameter, and the screws with 12 [mm] diameter are pre-drilled with 8 [mm] holes [48, p. 28]. In contrast to test series 1, no inclined edge is milled before the pre-drilling is performed. The penetration length of each screw is checked by measuring the distances that the screws stick out of the side members after insertion [48, p. 30]. The screws of length 240 [mm] and diameter of 8 [mm] stick out 2 [cm]. Screws of length 240 [mm] and diameter 12 [mm] stick out 3 [cm]. Screws with length 200 [mm] and diameter 8 [mm] stick out 1 [cm], and screws with length 200 [mm] and diameter 12 [mm] stick out 1.5 [cm] [48, p. 27].

The density of the parts is determined in the same way as in test series 1. The average density of the 25 chord sections amounts to 449 [kg/m³], with a 5 %-quantile of 415 [kg/m³], which is higher than the characteristic density of GL24h of 380 [kg/m³] [48, p. 29]. The density of the beech LVL side members amounts to 819 [kg/m³], which is slightly higher than the value of 800 [kg/m³] given by manufacturer Pollmeier Massivholz GmbH & CO. KG [48, p. 29].

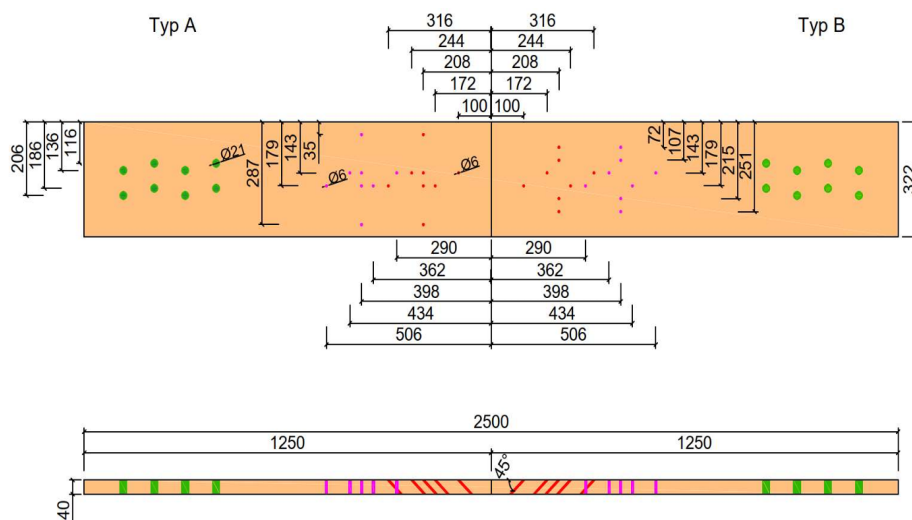


Figure 7.4: Side members of specimens for test series 2: Blue: pre-drilled holes for screws inserted under 90 [°], red: pre-drilled holes for screws inserted under 45 [°], green: pre-drilled holes for connection to horizontal cylinder [48, p. 28].

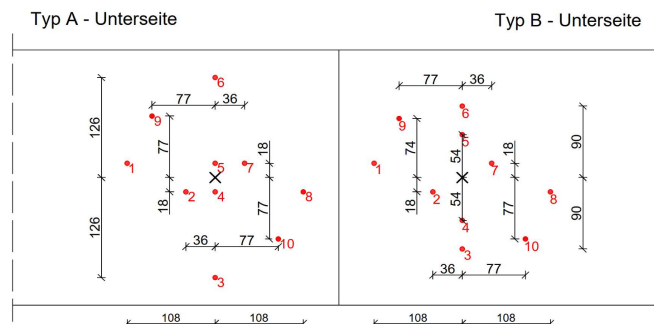


Figure 7.5: Positions of the screw in test series 2: positions are chosen so that screws do not touch inside chord section [48, p. 33].

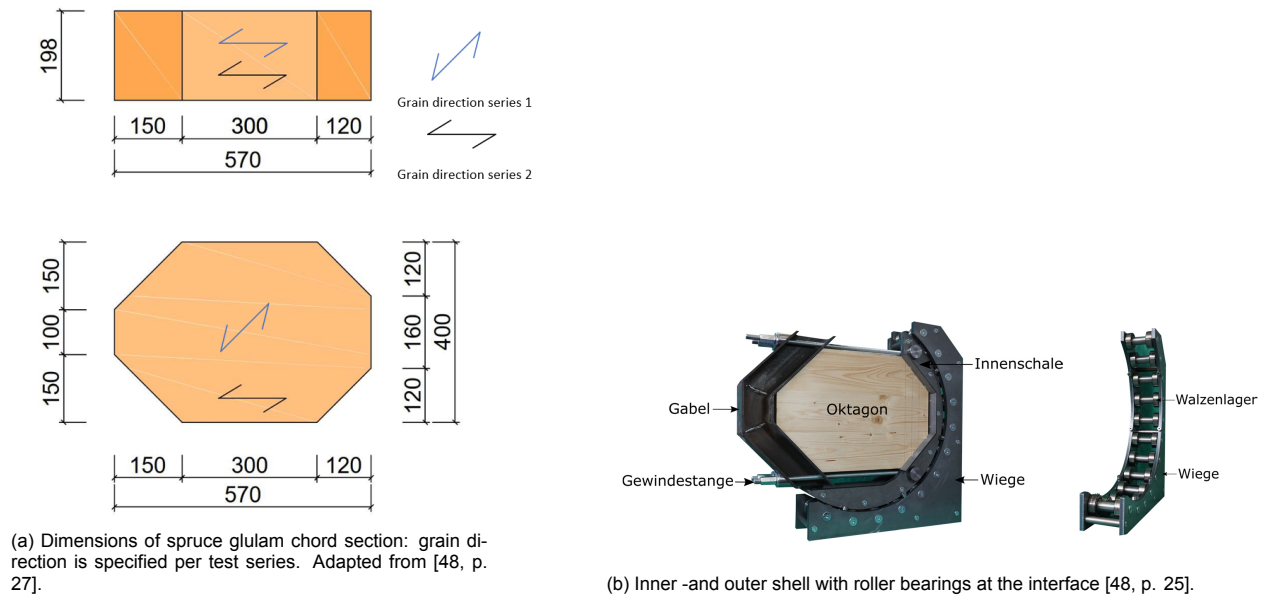


Figure 7.6

7.4. Testing procedure

The exact testing procedure was slightly different for both test series. Therefore, they are described separately below.

7.4.1. Test series 1

In test series 1, the screw combinations as given in table 7.1 were tested. These combinations are chosen so that the polar moments of inertia are equal for pairs of screw combinations. Combination 1+8 corresponds to combination 3+6, 2+7 corresponds to 4+5, and 1+2+7+8 corresponds to 3+4+5+6 [4, p. 28]. The application of the load as a result of the rotation on each screw is different among these combination pairs. Combinations 3+6, 4+5, and 3+4+5+6 are loaded in the direction parallel to the inclination direction as a result of the rotation. Combinations 1+8, 2+7, and 1+2+7+8 are loaded laterally by the force resulting from the rotation.

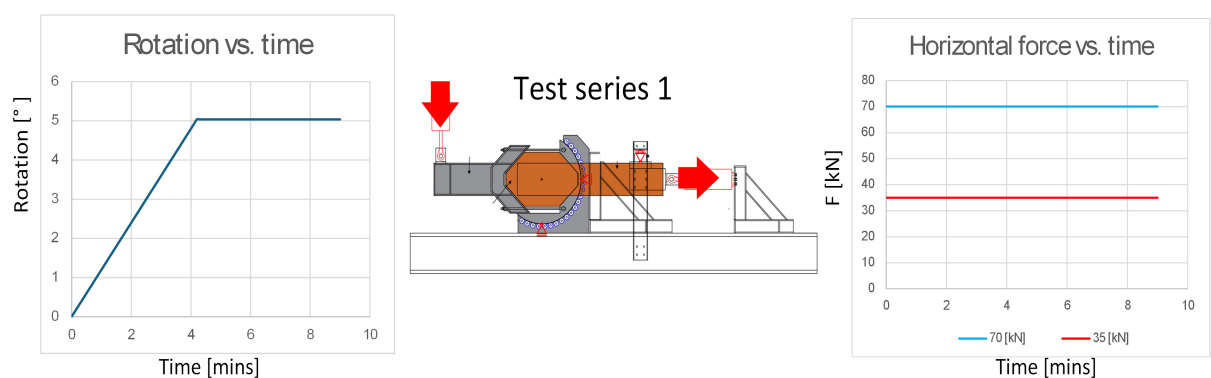


Figure 7.7: Rotation and horizontal force application in test series 1.

The testing procedure is initiated with the load-controlled horizontal cylinder applying a load of either 35 [kN] or 70 [kN]. The force of 35 [kN] is applied in case the connection consists of 4 screws, and 70 [kN] is applied in case the connection consists of 8 screws [4, p. 30]. This horizontal force resembles a service load and amounts to 40 % of the load-bearing capacity of the inclined screws [4, p. 30]. The

Screw combination	Sum of squared distances [mm ²]			Configuration 1	
	Type 1	Type 2	Total	d [mm] thread	α_s [°] frict.
1 + 8	23976	23976	47952	8 full	45 yes
3 + 6	31752	16200	47952	8 full	45 yes
2 + 7	3240	3240	6480	8 full	45 yes
4 + 5	648	5832	6480	8 full	45 yes
1 + 2 + 7 + 8	27216	27216	54432	8 full	45 yes
3 + 4 + 5 + 6	32400	22032	54432	8 full	45 yes

Table 7.1: Details of test series 1, adapted from [4, table 4-1].

load is kept constant during the testing procedure. The second step is the application of the vertical load on the lever arm so that a bending moment and consequently a rotation of the connection are initiated [4, p. 30]. The vertical cylinder is displacement-controlled with a displacement of 20 [mm/min] [25, p. 52]. With the length of the lever arm of 955 [mm] this corresponds to an angular velocity of 1.2 [° / min]. The load is phased out at rotations between 3° and 5° [4, p. 30].

7.4.2. Test series 2

The screw combinations that are tested in series 2 are given in table 7.2. The testing procedure is initiated with a load of 2 [kN] of the horizontal cylinder, irrespective of the test specimen [48, p. 36]. The vertical cylinder exerts a load of 0.1 [kNm] on the lever arm, which amounts to a moment of 0.1 [kNm] with a lever arm length of 100 [cm] [48, p. 36]. After this pre-loading phase, the load exerted by the load-controlled horizontal cylinder is increased up to a value of 35 [kN] in a period of 2 minutes. This amounts to $(35 - 2) \text{ [kN]} / 2 \text{ [min]} = 16.5 \text{ [kN/min]}$. After these 2 minutes, the horizontal load is kept constant until the end of the testing procedure. Simultaneously, the displacement-controlled cylinder increases the rotation with 0.1 [° / min], until a rotation of 0.8° is reached [48, p. 36]. After this point, the rotational speed is increased to 1 [° / min] [48, p. 36]. The vertical load is phased out after a rotation of approximately 5° is reached [48, p. 36].

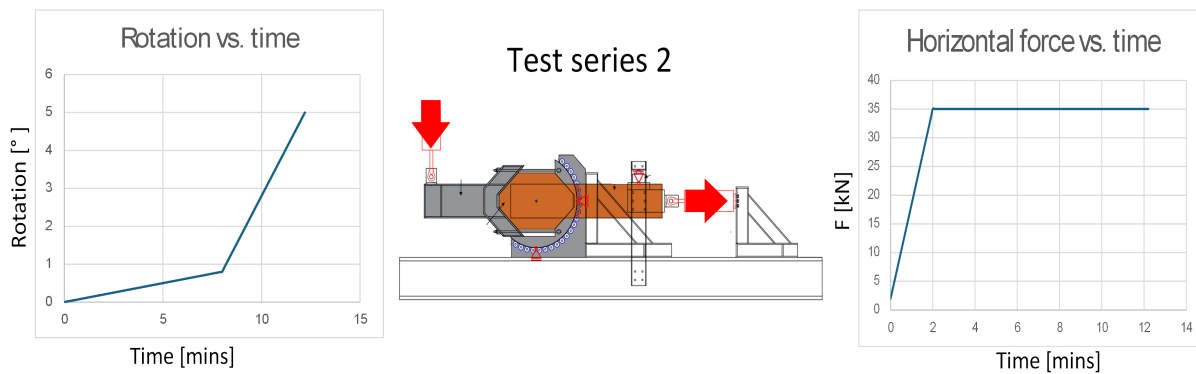


Figure 7.8: Rotation and horizontal force application in test series 2.

Screw combination				Configuration 1		Configuration 2		Configuration 3		Configuration 4		Configuration 5		Configuration 6	
	Sum of sqrd. dsts. [mm ²]			d [mm]	α_s [°]	d [mm]	α_s [°]	d [mm]	α_s [°]	d [mm]	α_s [°]	d [mm]	α_s [°]	d [mm]	α_s [°]
	Type 1	Type 2	Total	thread	frict.	thread	frict.	thread	frict.	thread	frict.	thread	frict.	thread	frict.
1 + 8	23976	23976	47952	8 full	45 yes	12 full	45 yes			8 full	45 no	8 full	90 yes	12 full	90 yes
3 + 6	31752	16200	47952	8 full	45 yes	12 full	45 yes			8 full	45 no	8 full	90 yes	12 full	90 yes
9 + 10	23963	23963	47926	8 full	45 yes										
2 + 7	3240	3240	6480	8 full	45 yes	12 full	45 yes			8 full	45 no	8 full	90 yes	12 full	90 yes
4 + 5	648	5832	6480	8 full	45 yes	12 full	45 yes			8 full	45 no	8 full	90 yes	12 full	90 yes
1 + 2 + 7 + 8	27216	27216	54432	8 full	45 yes							8 full	90 yes		
3 + 4 + 5 + 6	32400	22032	54432	8 full	45 yes			8 part.	45 yes			8 full	90 yes		
1 + 2 + 3 + 4 + 5 + 6 + 7 + 8	59616	49248	108864	8 full	45 yes							8 full	90 yes		

Table 7.2: Details of test series 2, adapted from [48, table 3-2].

7.5. Measuring technique and data processing

The relative deformations between the chord section and the side members of each test are measured by making use of the Q400 optical measuring system from LIMESS. Before performing the tests, the outer surfaces of the connection were painted white with black paint droplets so that a speckle pattern was created. Two cameras are aimed at the surface of the test setup at each side to capture the images. The images are analysed in the software programme ISTR4D. The exact calculation method for the rotation is slightly different for both test series and therefore described separately below.

7.5.1. Test series 1

In test series 1 a pulling force is exerted first, after which the rotation is initiated. Since the pulling force could, in theory, cause an accidental rotation, the below-described method is proposed to determine the rotation as a result of the intentional rotation only by Baldauf [4]. Two points are defined; point P_{LVL} is located in the centre of rotation on the LVL side member, and point P_{GL} is a point on the glulam chord section. The subscript 0 is used for the point in time after the pulling force and before the initiation of the imposed rotation, while the subscript t is used for a point in time after which the imposed rotation has been initiated. Using these definitions, the angle as a result of the pulling force $\Delta\alpha_0$ and the angle as a result of the imposed rotation $\Delta\alpha_t$ are calculated.

$$\Delta\alpha_0 = \tan^{-1} \left(\frac{y_{GL,0} - y_{LVL,0}}{x_{GL,0} - x_{LVL,0}} \right) \quad (7.1)$$

$$\Delta\alpha_t = \tan^{-1} \left(\frac{y_{GL,t} - y_{LVL,0}}{x_{GL,t} - x_{LVL,0}} \right) \quad (7.2)$$

$$\Delta\alpha = |\Delta\alpha_0 - \Delta\alpha_t| \quad (7.3)$$

In which:

- x_{GL} and y_{GL} : coordinates of point P_{GL} on the glulam chord section
- x_{LVL} and y_{LVL} : coordinates of point P_{LVL} on the LVL side member

It is important to note that the angle as a result of the pulling force can be either positive or negative. To take this into account, the absolute value is taken in equation 7.3. To illustrate, figure 7.9a shows both cases for positive and negative initial rotations. Because $\Delta\alpha$ is registered on each side of each test specimen, the average of both sides is taken to calculate the rotation of each specimen.

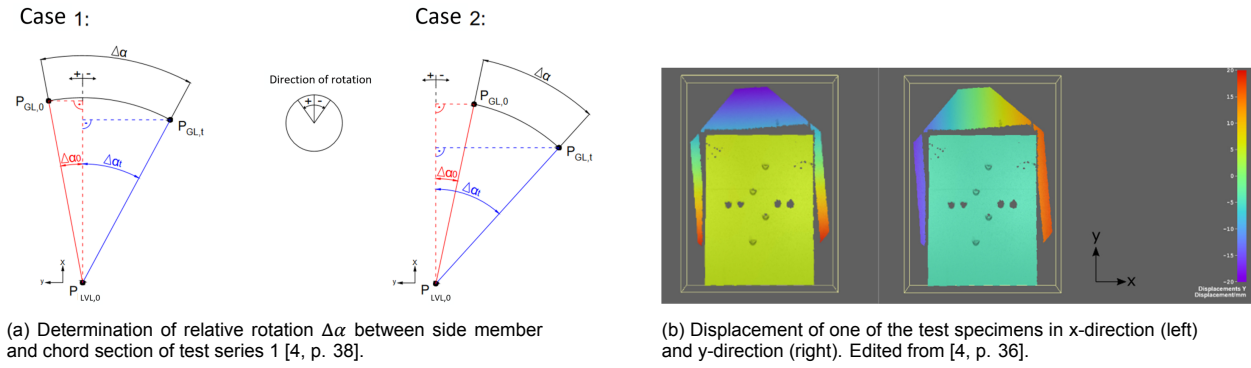


Figure 7.9

Finally, Baldauf [4, p. 38] proposes two values for the experimental rotational stiffness, which are given by equations 7.4 and 7.5 and based on EN 26891 [27].

$$K_{r,s} = \frac{0.4M_{max} - 0.1M_{max}}{\alpha_{0,4} - \alpha_{0,1}} \frac{180^\circ}{\pi} \quad (7.4)$$

$$K_{r,i} = \frac{0.4M_{max}}{\alpha_{0,4}} \frac{180^\circ}{\pi} \quad (7.5)$$

In which:

- $K_{r,s}$: modified experimental rotational stiffness (between 10 % and 40 % of max moment) [kNm/rad]
- $K_{r,i}$ initial experimental rotational stiffness (between 0 % and 40 % of max moment) [kNm/rad]
- M_{max} : maximum moment [kNm]
- $\alpha_{0,4}$ rotation at $0.4 \cdot M_{max}$ [°]
- $\alpha_{0,1}$ rotation at $0.1 \cdot M_{max}$ [°]

7.5.2. Test series 2

The calculation method for the relative rotation of the two timber elements is slightly different for test series 2 because the pulling force and rotation are executed simultaneously. In test series 2, the calculation of $\Delta\alpha_t$ is therefore slightly altered, as given in equation 7.6 and figure 7.6. The rest of the calculation remains the same as for test series 1.

$$\Delta\alpha_t = \tan^{-1} \left(\frac{y_{GL,t} - y_{LVL,t}}{x_{GL,t} - x_{LVL,t}} \right) \quad (7.6)$$

7.5.3. Test results

The results of the tests from series 1 are given in figure 7.11. In test series 1 a very stiff initial behaviour is observed in the moment-rotation plots. After this initial phase, the stiffness gradually decreases. A higher value for the maximum observed moment is found for connections in which the rotation causes loading in the inclination direction of the screws. Test series 2 in contrast shows very distinctive linear behaviour. After the first linear phase between rotations of 0° until 0.3 - 0.6°, a dent is observed, and a second linear phase with lower stiffness starts. Figure 7.12 only shows the results of configuration 1 from table 7.2 and the same screw configurations as in test series 1, so that an objective comparison is given between test series 1 and 2.

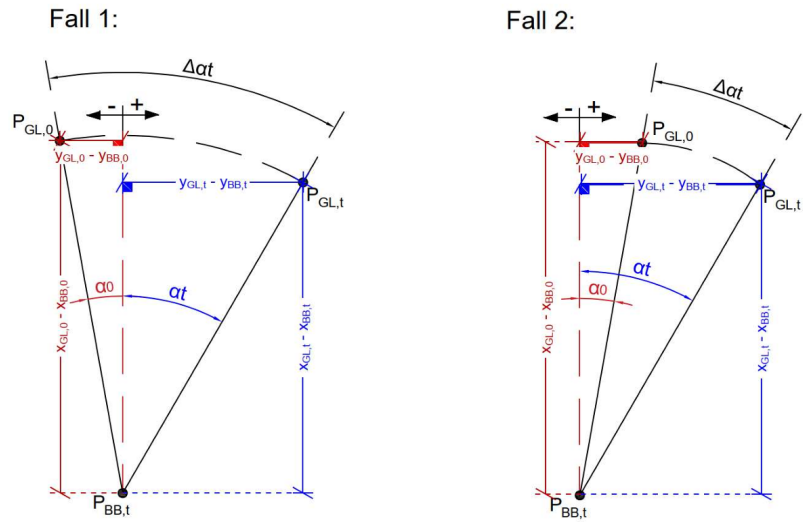


Figure 7.10: Determination of relative rotation $\Delta\alpha$ between side member and chord section for test series 2 [48, p. 44].

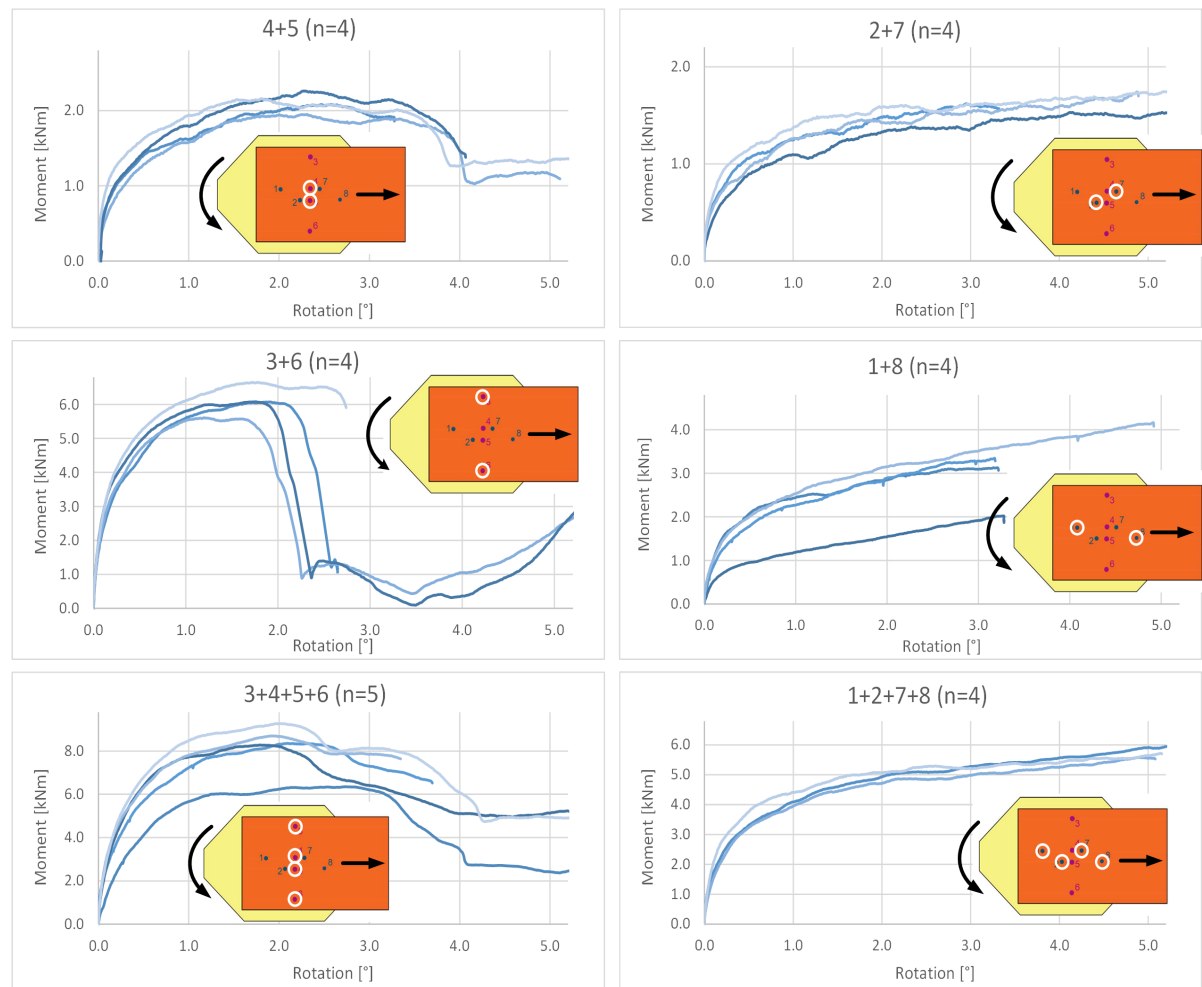


Figure 7.11: Moment vs. rotation plots from test series 1.

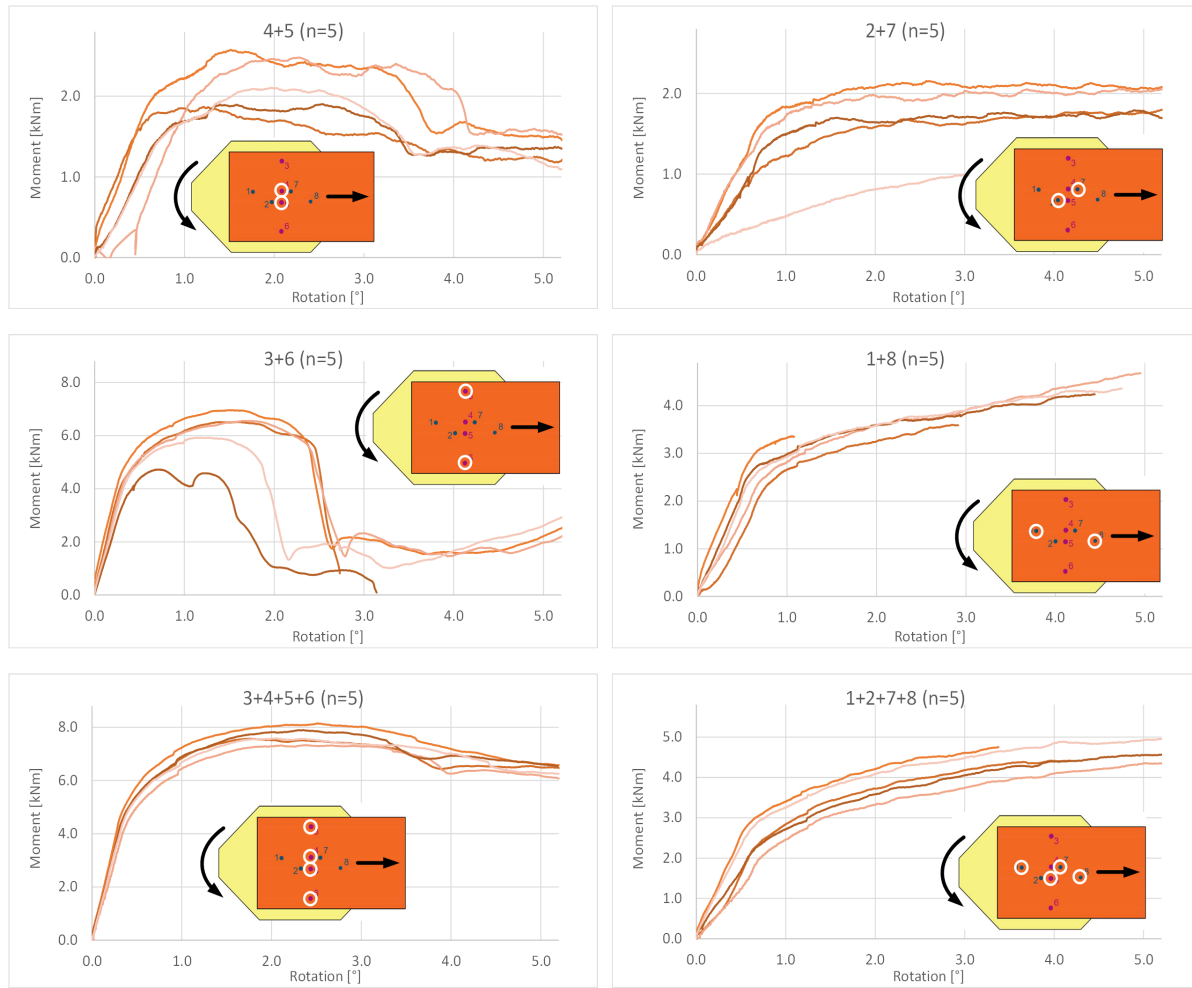
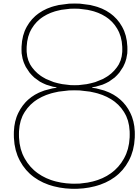


Figure 7.12: Moment vs. rotation plots from test series 2, configuration 1 (see table 7.2).



Calculation model

8.1. Introduction

In this section, a calculation model is proposed for the calculation of the rotational stiffness of timber-to-timber connections with inclined screws. To this end, the calculated stiffness values of different calculation methods are compared to the results of the rotational stiffness tests. After applying a correction for test series 1, good results are found and the best method is selected.

8.2. Testing of methods

The methods selected for further analysis in section 4.13 are used to calculate the theoretical rotational stiffness values of the tested specimens. For the stiffness values in the lateral direction, the "EC method" is used, as well as the "0.5 EC method", in which the stiffness for dowel-type fasteners is multiplied with a factor of 0.5 as the screw is loaded perpendicular to the grain. This makes a total of fourteen methods, which are listed in table 8.1.

In test series 1, the grain direction of the chord section makes an angle ϵ of 45° with the side members (see figure 7.6a), so that $\phi_1 = 0^\circ$ and $\phi_2 = 45^\circ$. The lateral stiffness $k_{SLs,v}$ in the chord section should therefore be calculated as $0.75 \cdot \rho_{mean}^{1.5} \cdot d/23$ according to the linear interpolation rule stated in prEN-1995-1-1 [53, p. 188]. Because prEN-1995-1-1 does not state a method to take this grain angle dependency into account in case two timber elements in the same connection have different load-to-grain angles and because the influence is assumed to be small, $0.5 \cdot \rho_{mean} \cdot d/23$ is used.

The coefficients of determination of the calculated stiffness values of each of the 14 methods are given in table 8.1 (columns "Test series 1 initial" and "Test series 2"). Good results are found for test series 2, especially for methods 7,8 and 14. For test series 1, results are rather poor, where most coefficients of determination are found to be negative. For test series 1, all results are included ($n=25$), and for test series 2 all test results with a screw axis-shear plane angle α_s of 45° are used ($n=66$), corresponding to configuration 1 to 4 in table 7.2. The tests with angles α_s of 90° are excluded from the analysis because the calculated stiffness values of methods 1,2,8 and 9 include the term $\cos(\alpha_s)$ and therefore can not be calculated for $\alpha_s = 90^\circ$. Additionally, the tests with $\alpha_s = 90^\circ$ do not qualify as inclined screws. The plotted values of the calculated stiffness values versus the experimental values $K_{r,s}$ are given in appendix A. The Python code used to calculate the rotational stiffness values for each method and compare them to the test data is given in appendix E.

8.3. Pre-load theory

The moment-rotation plots of test series 1 show distinctly different behaviour than those of series 2 (see figure 7.11 and 7.12). The moment-rotation plots of series 1 start very steeply, and a considerable moment is present before significant rotation occurs. The calculated stiffness values for test series 1 do not accurately predict the experimental stiffness values, as shown in table 8.1 (column "Test series 1 initial"). The hypothesis is formulated that a threshold value of the moment is needed before any

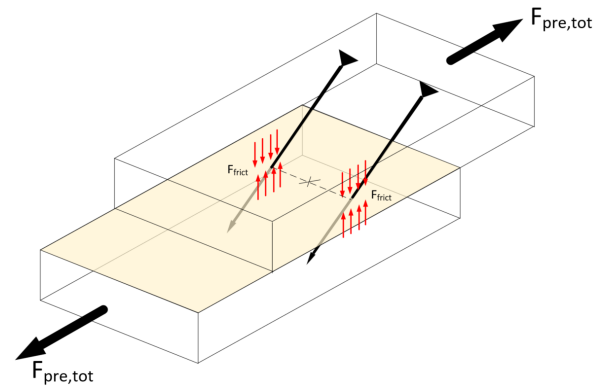
Method ID	Stiffness calculation axial direction k_{SLs}	r ² (n=25)		r ² (n=25)		r ² (n=66)	r ² (n=91)
		Lateral stiffness calculation $k_{SLs,v}$		Test series 1 initial	Test series 1 pre-load theory	Test series 2	Overall
		0.5 EC	EC				
1	Blass Steige	x		-0.923	0.675	0.800	0.766
2	Blass Steige friction	x		-0.436	0.730	0.791	0.774
3	Tomasi et al. (EC) single stiffness model	x		-0.600	0.764	0.757	0.759
4	Tomasi et al. (Blass Steige) single stiffness model	x		-0.072	-1.421	-2.287	-2.048
5	Tomasi et al. (EC) double stiffness model	x		-1.272	0.455	0.669	0.610
6	Tomasi et al. (Blass Steige) double stiffness model	x		-0.308	0.641	0.665	0.658
7	Santis Fragiaco	x		-0.943	0.664	0.818	0.776
8	Blass Steige		x	-0.716	0.664	0.822	0.779
9	Blass Steige friction		x	-0.233	0.710	0.771	0.754
10	Tomasi et al. (EC) single stiffness model		x	-0.395	0.747	0.737	0.740
11	Tomasi et al. (Blass Steige) single stiffness model		x	0.122	-1.464	-2.441	-2.171
12	Tomasi et al. (EC) double stiffness model		x	-1.063	0.449	0.713	0.640
13	Tomasi et al. (Blass Steige) double stiffness model		x	-0.106	0.618	0.629	0.626
14	Santis Fragiaco		x	-0.736	0.653	0.838	0.787

Table 8.1: Coefficients of determination for different calculation methods for the rotational stiffness.

rotation can occur in test series 1. This threshold value is believed to result from friction between the timber members at the shear plane, as a result of the pulling force that is present before the rotation is initiated, as shown in figure 8.1a). To quantify this moment, equation 8.1 is proposed.

$$M_{threshold} = \sum_{i=1}^n \sqrt{(x_i^2 + y_i^2)} \cdot \frac{F_{pre,tot}}{n} \cdot \tan(\alpha_s) \cdot \mu \quad (8.1)$$

The pre-load $F_{pre,tot}$ is divided by the number of screws present in the connection. The pre-load per screw is converted to the force perpendicular to the shear plane by taking the tangent of the angle α_s , and this force is multiplied by the coefficient of friction μ . Finally, this friction force is multiplied with the moment arm to arrive at the contribution of the individual screw to the total moment resulting from pre-load friction. For the experimental tests, a value for the coefficient of friction of 0.39 is used, as described in section 6.3.



(a) Frictional force due to normal force between the timber elements. Source: own image.

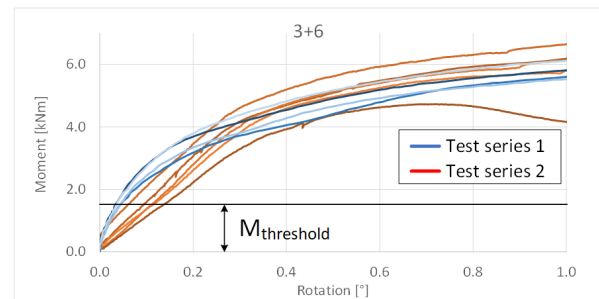
(b) $M_{threshold}$ value shown in moment-rotation plots of test series 1 and 2 for screw geometry 3+6. Source: own image.

Figure 8.1

Figure 8.1b shows the test data for screw geometry 3+6 both for test series 1 and test series 2. The value for $M_{threshold}$ is also given. The stiffness values for both test series are almost equal after the horizontal line indicating $M_{threshold}$ is surpassed. To take the pre-load effect into account, the theoretical values for $M_{threshold}$ calculated with equation 8.1 are subtracted from the experimental moment values of test series 1. In other words, the moment-rotation curves for test series 1 are all lowered with the value of $M_{threshold}$ applicable to the connection geometry. After this step, the modified

experimental rotational stiffness $K_{r,s}$ is calculated according to equation 7.4. The results obtained with these new experimental values for the rotational stiffness are given in table 8.1 under "Test series 1 pre-load theory". The coefficients of determination found using this method are significantly better than the initial values. The predicted stiffness values according to the 14 methods are plotted against the corrected experimental stiffness values in appendix A (last set of plots).

8.4. Spring model

To understand what happens in screw configurations that are exposed to an additional axial load as a result of the imposed rotation (configurations 3+6, 4+5, 3+4+5+6), they are compared to a model. The stiffness values of the screws loaded in the direction of inclination are modelled as linear elastic springs with stiffness k . The model therefore assumes that the springs have the same stiffness k both when initially elongated and when relaxed after initial elongation. Figure 8.2 schematically shows this model for a connection with two screws (combinations 3+6 and 4+5), both for test series 1 and test series 2. As mentioned before, in test series 1 the pulling force is exerted before the rotation is applied, and in series 2 both actions are applied simultaneously to the specimens.

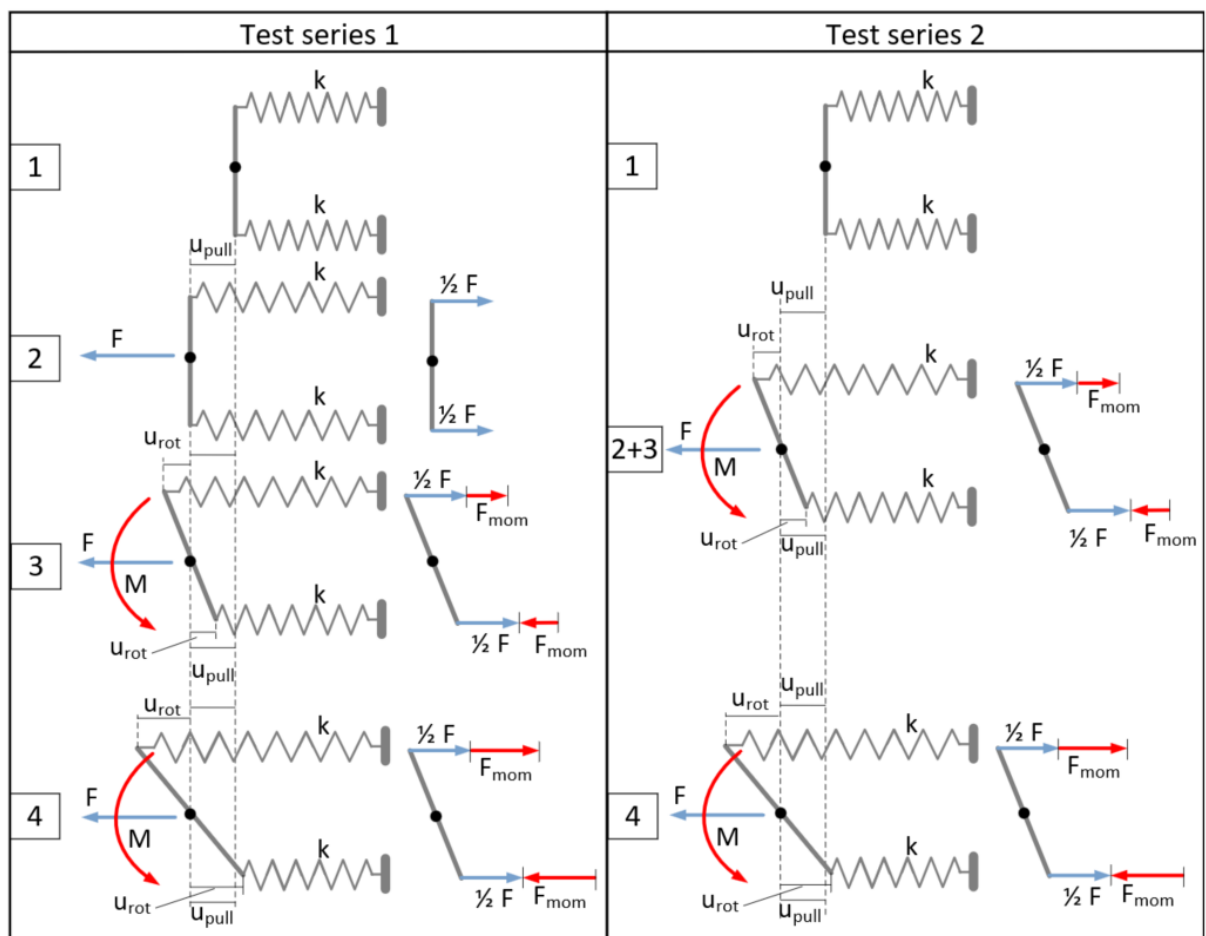


Figure 8.2: Model for connection geometries that experience additional load in inclination direction as a result of rotation, for both test series 1 and test series 2. Step 1: situation before any load is applied. Step 2+3: pulling force is applied and rotation is initiated. All screws are still in net tension (the rotational region where theoretically the rotational stiffness is calculated in the tests). Step 4: rotation is prolonged and the bottom screw experiences net compression. As soon as the screw experiences net compression, theoretically, the stiffness of that screw should be calculated according to the method for dowel-type fasteners loaded in shear, given by equation 3.18. Source: own image.

In the tests, the combined actions of pulling force and rotation (and corresponding moment M) cause a net pushing force in the bottom screw in case the force component as a result of the moment becomes larger than the force component as a result of the pulling force. In the model of figure 8.2 this

happens when $\frac{1}{2}F > F_{mom}$ (see step 4 in figure 8.2). As described by Tomasi et al. [22], the stiffness of inclined screws when loaded in compression should be calculated according to the standard EN-1995-1-1 equation for laterally loaded dowel type fasteners, as given by equation 3.18. This means that the stiffness of the inclined screw changes at the transition from net tension to net compression. The pulling force exerted with the horizontal cylinder in the tests is present to guarantee that all the screws are subjected to a net pulling force at the beginning of the testing procedure, where the rotational stiffness is calculated. The test is prolonged and the imposed rotation is increased so that after a certain amount of time (and corresponding rotation angle) the bottom screw experiences a pushing force.

Important to mention is the fact that in the tests, the centre of rotation is fixed. This is usually not the case in a connection, where the centre of rotation will always shift towards the stiffest spring. The stiffness of an inclined screw connection is likely higher in the case of relaxation after initial elongation than in the case of initial elongation, as given in figure 8.3a. Therefore, the model of test series 1 would theoretically change to figure 8.3b during the rotation phase, with a higher stiffness k_{relax} during the rotation for the bottom screw.

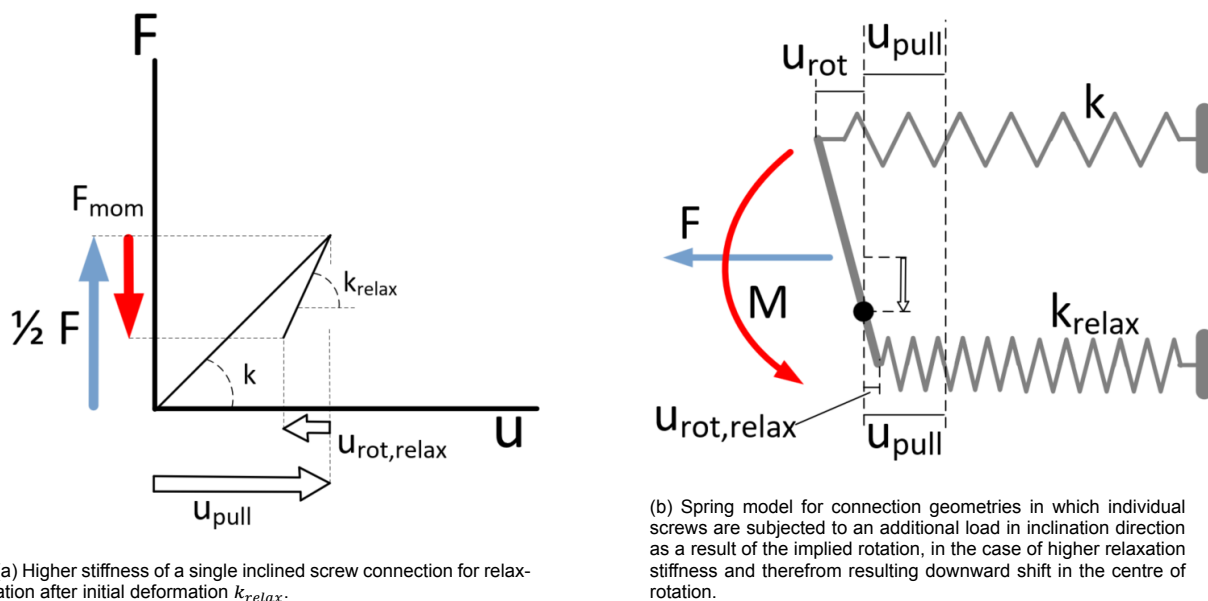


Figure 8.3: Source: own image.

Little is known about the stiffness of inclined screws during the relaxation phase. As this stiffness is not known, it is assumed that the stiffness is approximately equal for the case of initial elongation and the case of relaxation after initial elongation so that the model in figure 8.2 is assumed to be valid and used from now on.

8.5. Screws under compression

Under the assumption of linear elastic stiffness of the screw both under initial elongation and relaxation after initial elongation, it has been proven by Baldauf [4, p. 47] that each screw in combination 3+6 for test series 1 stays in tension until a rotation of 0.4° , so that indeed the stiffness of the connection according to equation 7.4 is calculated in the "tension only" range in which all screws experience a net tensile force. It is assumed that this is the case for the other connection geometries in test series 1 as well. For test series 2, it was checked whether the bottom screw is in tension in the first part of the test, as was planned. For screw geometries 3+6, 4+5 and 3+4+5+6 this check is performed. Making use of the experimental test data, the theoretical contribution from the moment and the pulling force per screw are summed to this end, as described in more detail in appendix C. In this procedure, V11

(3+6), V8 (4+5) and V28 (3+4+5+6) were checked, as their values for $K_{r,s}$ lie closest to the average $K_{r,s}$ values of the tests for their geometry. Results are given in figure 8.4. In geometries (3+6) and (4+5), a small compression force is found for small rotations (up to appr. 0.3°), after which the compression force increases significantly. In geometry (3+4+5+6) the compression force is larger, probably because the pulling force per screw is much lower, and so the compression force as a result of the rotation is not compensated enough. Therefore, according to this information, it would not be justified to use the stiffness for an inclined screw connection under tensile force, and instead the EN-1995-1-1 formula should be used, as given by equation 3.18.

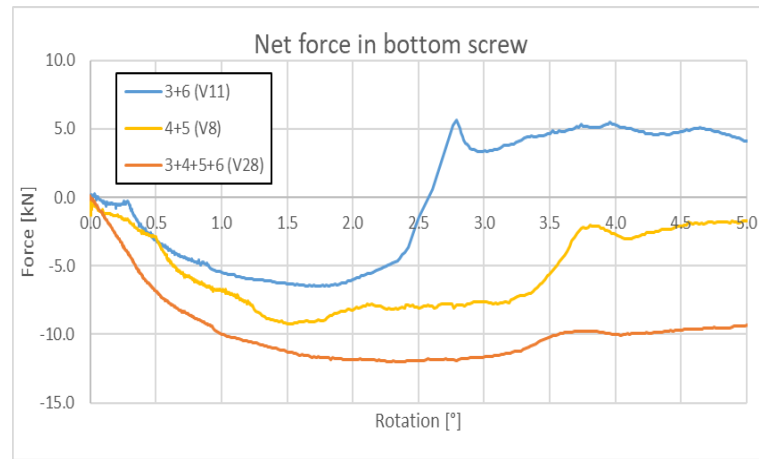


Figure 8.4: Net force in the bottom screw vs. rotation in tests V11, V8 and V28. Tension positive, compression negative. Source: own image.

It would be very complicated to use different formulas per screw after a positive check for compression. Also, it is not valid to simply use the EN-1995-1-1 stiffness given by equation 3.18 for the bottom screw in case it is found to be under net compressive force. In case the bottom screw experiences a net compressive force, one part of the force as a result of the moment is a function of the screw stiffness under tension, and the other part is a function of the stiffness under compression. This is shown in figure 8.5 of screw configuration 3+6, where the forces F_{N3} and F_{N6} are the screw forces as a result of the normal force N , and the forces F_{M3} and F_{M6} are the forces as a result of the exerted moment M . For the bottom screw (screw 6), $F_{M6,c} = F_{M6} - F_{N6}$ is the net force exerted on the screw. This net force is a compressive force so that the EN-1995-1-1 stiffness should be used. However, simply using the EN-1995-1-1 stiffness for screw 6 in the equation for rotational stiffness is not correct, as it assumes that for the entire force F_{M6} the stiffness under net compressive force can be used, which is not the case (the part $F_{M6,t}$ is a function of the stiffness for inclined screw under tension, as are F_{N3} , F_{M3} and F_{N6}). Equation 8.2 gives the proof that the moments are indeed not equal, using the screw displacement as a result of rotation u_{rot} and the screw displacement as a result of the pulling force u_{pull} , as given in figure 8.2 (specifically, step 4 of test series 2 in figure 8.3). The forces used in equation 8.2 are given in figure 8.5. Because of these complexities and because it is assumed that the influence of the effect is small, the assumption is made that all screws stay under tension during the tests.

$$\begin{aligned}
 M_{tot} &= (F_{N3} + F_{M3}) \cdot r + F_{M6,c} \cdot r \\
 &= (u_{pull} \cdot k_{SLS} + u_{rot} \cdot k_{SLS}) \cdot r + (u_{rot} - u_{pull}) \cdot k_{EC} \cdot r \\
 &\neq u_{rot} \cdot k_{SLS} \cdot r + u_{rot} \cdot k_{EC} \cdot r
 \end{aligned} \tag{8.2}$$

8.6. Conclusion

It is concluded that the correction of the experimental stiffness values referred to as the pre-load theory drastically improves the results for the fourteen methods in test series 1. Based on all results after the correction referred to as pre-load theory, it is concluded that several methods show good results

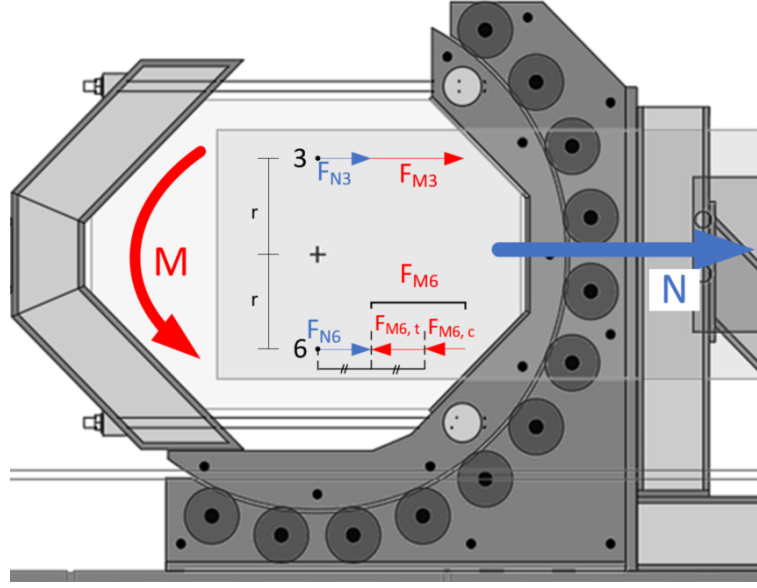


Figure 8.5: Forces per screw for geometry 3+6 in test series 2 in case the bottom screw experiences a net compressive force. The moment is a function of the stiffness of inclined screws k_{SLs} and the EN-1995-1-1 stiffness for dowel-type fasteners loaded in shear, as given by equation 3.18. Adapted from [25, p. 51].

compared to the experimental test data. Methods 1, 2, 3, 7, 8 and 14 all show very good similarity with the results, with only minimal differences in coefficient of determination. With regards to the lateral stiffness calculation, no conclusion can be drawn on whether the "0.5 EC method" or the "EC method" is to be preferred. Some methods show better results for the "0.5 EC method" and others for the "EC method". Method 14 is selected as this method yields the highest coefficient of determination, as given in the plot in figure 8.6a. The calculation method is given in equations 8.3 to 8.5b. The plot given in figure 8.6b gives the rotational stiffness values in case K_{ser} (see equation 3.18) is used for both the stiffness parallel to the inclination direction k_{SLs} and the stiffness perpendicular to the inclination direction $k_{SLs,v}$.

With regards to the experimental test programme, it is concluded that in test series 2, a compressive force is present in the bottom screw for geometries 3+6, 4+5 and 3+4+5+6, so that it is not completely legitimate to calculate the stiffness of this bottom screw as if it is loaded in tension. As discussed in section 8.5, it is not possible to analytically correct the rotational stiffness calculation for this phenomenon. The influence of this effect is deemed small, but it should be mentioned that the calculated rotational stiffness values are slightly overestimated by not taking this effect into account.

$$k_r = \sum_{i=1}^n k_{SLs,i} \cdot y_i^2 + \sum_{i=1}^n k_{SLs,v,i} \cdot x_i^2 \quad (8.3)$$

$$k_{SLs,v,i} = \frac{1}{23} \cdot \sqrt{\rho_1 \cdot \rho_2}^{1.5} \cdot d \quad (8.4)$$

$$k_{SLs,i} = zz \cdot (\rho_1^{ww} \cdot l_1^{xx} + \rho_2^{ww} \cdot l_2^{xx}) \cdot d^{0.76} \quad \alpha_s \geq 60^\circ \quad * \quad (8.5a)$$

$$k_{SLs,i} = \frac{zz \cdot d^{yy}}{\frac{1}{\rho_1^{ww} \cdot l_1^{xx}} + \frac{1}{\rho_2^{ww} \cdot l_2^{xx}}} \quad \alpha_s < 60^\circ \quad * \quad (8.5b)$$

α_s (°)	ww	xx	yy	zz
15	1.14	0.86	0.47	0.095
30	1.09	0.77	0.58	0.23
45	1.07	0.68	0.65	0.29
60	1.07	0.51	0.76	0.31
75	1.04	0.056	1.11	0.18
90	1.04	0.056	1.11	0.18

Table 8.2: Interpolation factors.

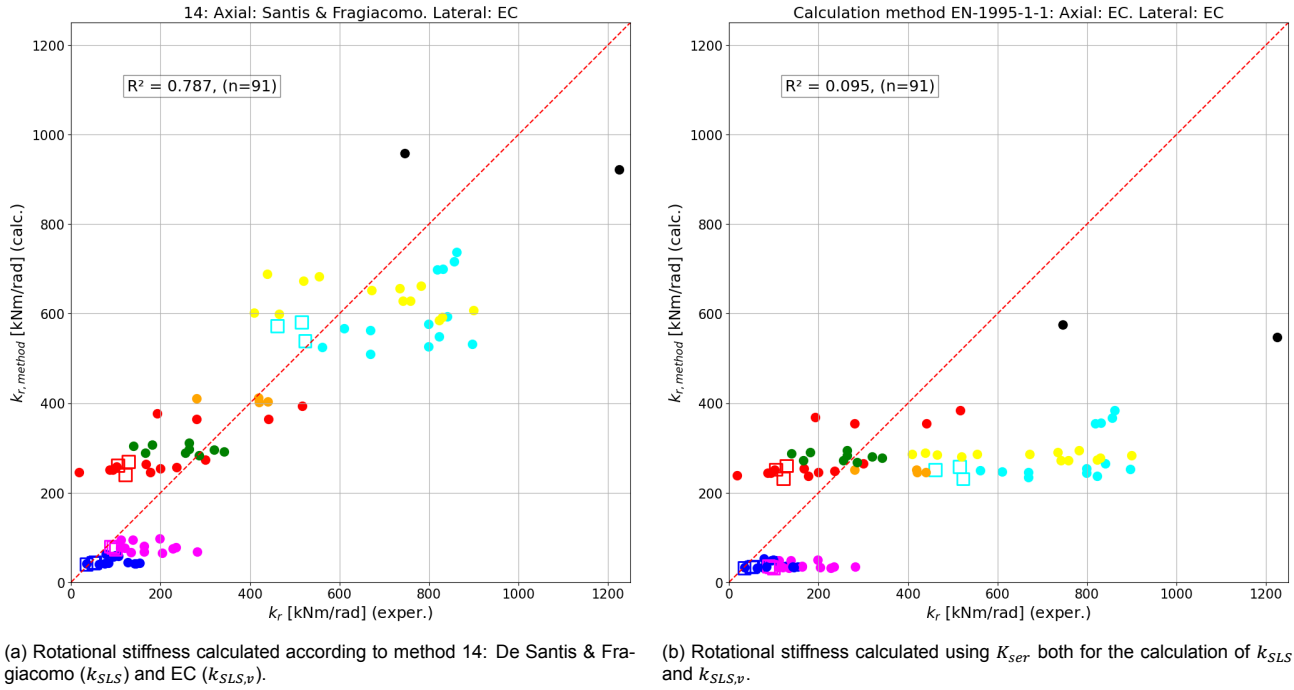


Figure 8.6: Experimentally found stiffness values vs. calculated stiffness values of all tests (series 1 and 2), after adjusting test series 1 using the pre-load theory. Method 14 and the calculation utilising K_{ser} given in EN-1995-1-1 are shown. Tests without friction are indicated with open squares. Legend is given in appendix A. Source: own image.

In which:

- k_r : rotational stiffness of the connection [Nmm/rad]
- $k_{SLS,v,i}$: stiffness of inclined screw i in lateral direction [N/mm]
- $k_{SLS,i}$: stiffness of inclined screw i in direction of inclination [N/mm]
- x_i, y_i : horizontal resp. vertical distance from centre of rotation to screw i [mm]
- d : outer diameter of the screw [mm]
- ρ_1, ρ_2 : density of timber element 1 resp. 2 [kg/m³]
- l_1, l_2 : penetration length of the screw in timber element 1 resp. 2 [mm]
- ww, xx, yy, zz : interpolation factors, see table 8.2.

* The method is experimentally verified only for $\alpha_s = 45^\circ$

9

Truss model

9.1. Introduction

In chapter 8, a method was presented that accurately describes the experimentally obtained rotational stiffness values of the connections with inclined screws. This chapter focuses on the application of these connections in truss structures, making use of prototype versions of the FaNaBu truss concept. Specifically, this chapter focuses on the influence of the rotational stiffness of the chord-diagonal connections on the serviceability and ultimate limit state behaviour of the FaNaBu truss.

9.2. Grasshopper model

Grasshopper is a visual programming language, used in combination with Rhinoceros. Grasshopper allows the use of embedded tools that add more functionalities to the programme. One of these embedded tools is Karamba3D, which allows users to perform structural analysis using finite element analysis (FEA). A parametric model of the FaNaBu truss was built in Grasshopper to study the influence of rotational and translational connection stiffness on different truss geometries.

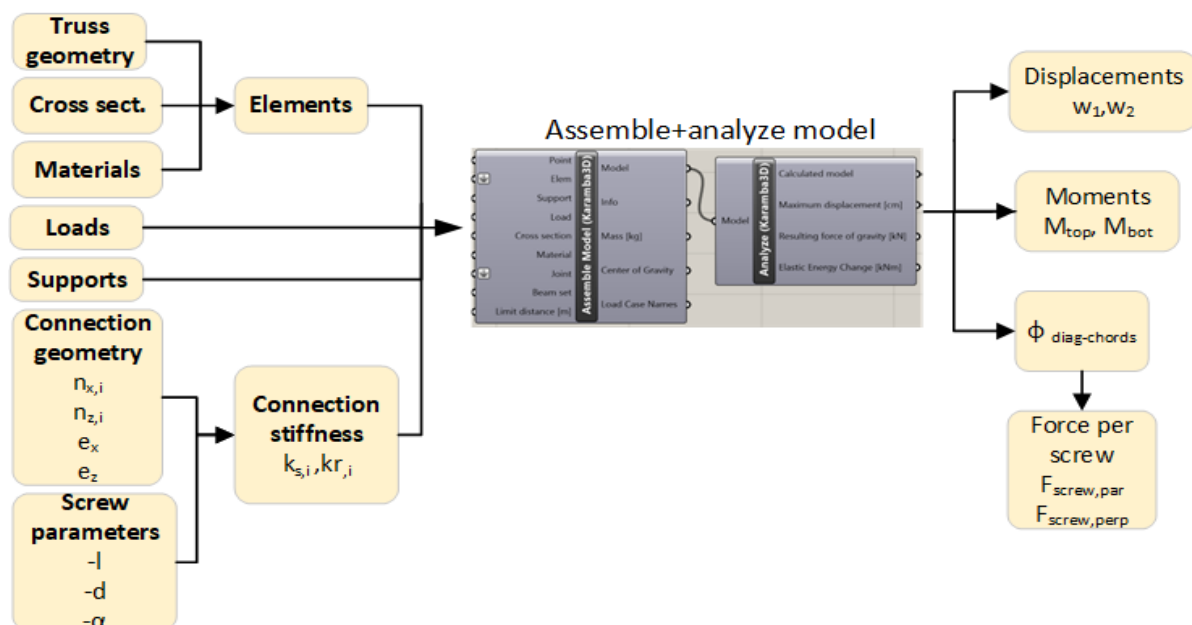


Figure 9.1: Schematic representation of the Grasshopper model. Source: own image.

A block schematic overview of the model is given in figure 9.1. Relevant parameters for the structural calculation programme (geometry, cross sections, materials, loads and support conditions) are pro-

vided to the "Assemble" and "Analyze" components of Grasshopper. These components also require the user to provide stiffness information of the connections. In order to provide this data, an algorithm is programmed within the Grasshopper environment in which connection geometry and individual screw parameters can be inserted. With this information, the translational and rotational stiffness for the chord-diagonal connection j per shear plane $k_{s,j}$ and $k_{r,j}$ respectively, are calculated.

The geometry of the FaNaBu truss is relatively simple. In the Grasshopper model, the double diagonals on either side of the chord sections are modelled as single cross sections, with a double depth compared to that of the real structure. The truss is loaded with point loads located on each node of the top chord, excluding the two outer nodes. The truss is simply supported, with lateral supports at each node to prevent lateral torsion buckling. The posts and chords are modelled as GL24h which is available in the material library of Grasshopper. The diagonals are given custom material properties of GL75 laminated veneer lumber, taken from the Pollmeier declaration of performance [58].

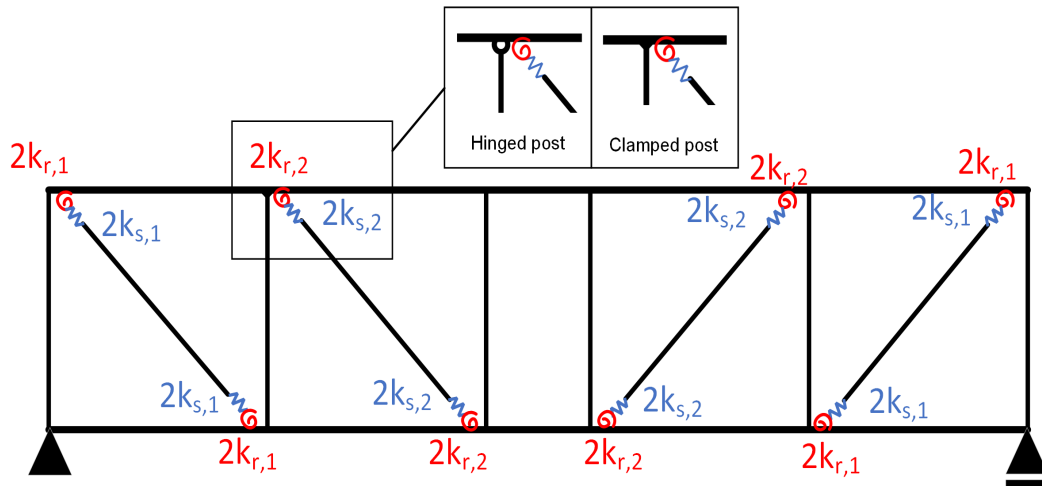


Figure 9.2: Definitions in the truss model, in this case with $j=2$ distinct chord-diagonal connections. Above: chord-post connection as a clamped connection. The hinged post case and clamped post case are shown. The stiffness values per shear plane $k_{s,j}$ and $k_{r,j}$ are multiplied with a factor 2 as double diagonals on either side of the chord are used in the FaNaBu truss.

The truss has two types of connections, which are the chord-diagonal connections and the chord-post connections. Besides the chord-diagonal connections, the chord-post connections are assumed to have a significant influence on the structural behaviour of the truss. The chord-post connections remain outside of the scope of this research project. In the FaNaBu project, compressive tests of the vertical chord-post connection showed very high values of stiffness [25, p. 41]. Therefore, their translational stiffness is assumed to be infinite. For their rotational stiffness, both the case of perfect hinges and clamped connections are studied, see figure 9.2. As stated, a script was written in the Grasshopper model that automatically calculates the translational and rotational stiffness of the chord-diagonal connections $k_{s,j}$ and $k_{r,j}$. The screws of the connections are modelled as fully threaded screws so that the connection is fully defined when screw length, screw diameter, angle of insertion and distances between the screws are known. The contour of the geometry of the connection is programmed as a parallelogram with the upper and lower edges always parallel to the chords of the undeformed truss, and the side edges parallel to the diagonals, as indicated in figure 9.3. In this way, the following parameters of the connection can be set in the model:

- n_x : number of screws in x direction [-] (see figure 9.3)
- n_z : number of screws in z direction [-] (see figure 9.3)
- e_x : distance between screws in x direction [mm] (see figure 9.3)
- e_z : distance between screws in z direction [mm] (see figure 9.3)
- α_s : angle between screw axis and shear plane [°]

- d : screw outer diameter [mm]
- l : screw length [mm]

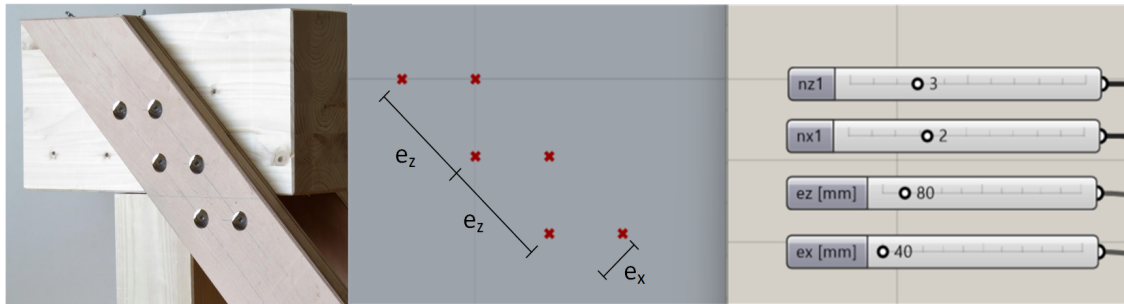


Figure 9.3: Left: connection detail of truss. Centre: model in Rhino with distances. Right: Grasshopper parametric sliders to adjust the connection.

With the connection fully defined, the values for $k_{s,j}$ and $k_{r,j}$, are calculated and communicated to the structural model. The translational stiffness per shear plane $k_{s,j}$ is calculated using the method of De Santis et al. [62], (see equation 8.5b), while the rotational stiffness is calculated using the method found in chapter 8 (see equation 8.3).

From the calculated model, the displacements w_1 and w_2 , moments in the chord-diagonal connections M_{top} and M_{bot} and corresponding relative rotations $\phi_{diag-chords}$ are extracted. With these rotations, the theoretical forces parallel and perpendicular to the inclination direction of the screws can be calculated, according to equation 5.22 derived in section 5.3.1.

9.3. Small-scale prototype

A small-scale prototype of a FaNaBu truss was both tested in the laboratory and analysed in the finite element programme ANSYS by Steige & Frese [66]. In this study, the influence of the rotational stiffness between diagonals and chords is not taken into account, so only a translational stiffness was effective. Partially threaded screws were used. The dimensions of the small-scale prototype are given in figure 9.4 and in the table shown in figure 9.5.

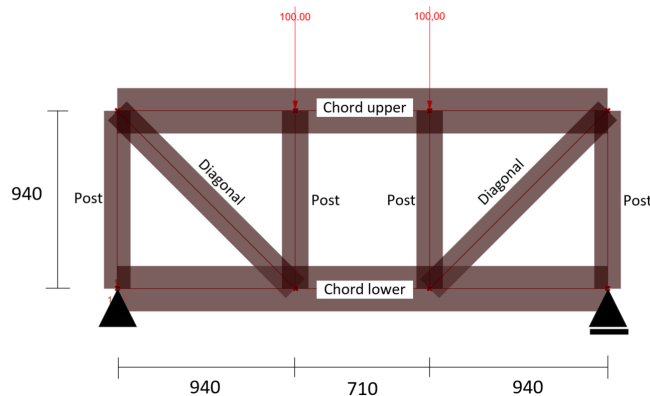


Figure 9.4: Small-scale truss model as built in Grasshopper, dimensions in [mm].

	Material	Cross section
Upper/lower chords	GL24h	240x140 [mm]
Posts	GL24h	240x140 [mm]
Diagonals	LVL GL75	2x140x40 [mm]

Figure 9.5: Dimensions small truss prototype.

To mitigate the effect of compression forces perpendicular to the grain in the chords, beech LVL plates are applied in the contact area between the posts and the chords in the prototype truss [66]. The truss is loaded in four-point bending as shown in figure 9.4 with two point loads of each 100 [kN] in magnitude. This load is equal to a service load of approximately 40 % of the load-bearing capacity of the truss [66, p. 288]. The deformation of the lower chord (w_1) and the relative deformation of the posts (w_2) were

measured in the experiment, and a sensitivity analysis was carried out in the ANSYS model, in which the translational stiffness was increased from 10 to 190 [kN/mm] per shear plane, see figure 9.7b. The definitions of displacements w_1 and w_2 are illustrated in figure 9.6.

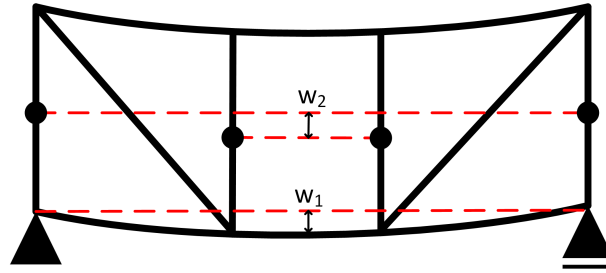
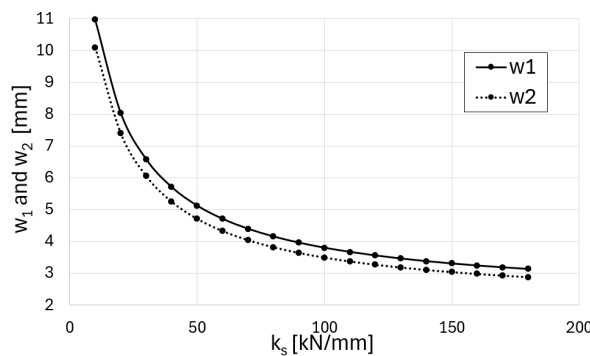
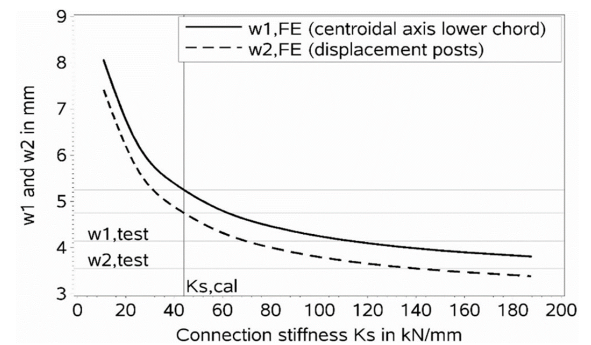


Figure 9.6: Deformations of the lower chord (w_1) and relative deformation of the centres of the posts (w_2).



(a) Sensitivity analysis in the Grasshopper model with $k_r=0$. The hinged post case is shown.



(b) Sensitivity analysis in ANSYS, with $k_r=0$ [66, p. 289]

Figure 9.7

9.3.1. Serviceability limit state

The truss was built in the Grasshopper model (see figure 9.4), and the same sensitivity analysis has been carried out as described by Steige & Frese [66], which is given in figure 9.7a. The displacements w_1 and w_2 show relatively good similarity, however, the Grasshopper model shows larger deformations for small values for k_s and smaller deformations for large values of k_s compared to the ANSYS model presented by Steige & Frese. Reasons for this could include the fact that the ANSYS model models the connections between the chords and posts more realistically. This includes:

- The posts in the ANSYS model connect to the bottom surface of the top chord and the top surface of the bottom chord. This is a difference from the Grasshopper model, in which the connections between elements are always modelled as a single node so that displacements in the chords as a result of compression perpendicular to the grain are not taken into account. This modelling inaccuracy also means that in the Grasshopper model, the posts are slightly longer than in the ANSYS model (amounting to 240 [mm]), so they experience slightly larger axial deformation.
- In the ANSYS model the LVL plates between chords and posts are modelled, whereas in the Grasshopper model, they are omitted. These LVL plates, loaded perpendicular to the grain, have an influence on the relative displacements between the top and bottom chord that is not taken into account in the Grasshopper model.
- In the ANSYS model, the moduli of elasticity in the longitudinal direction of the chords, posts and diagonals were obtained from dynamic measurements [66, p. 288], whereas in the Grasshopper model, tabulated values are used.

- In the ANSYS model, the chord sections in which screws are present were assigned higher moduli of elasticity [66, p. 288], whereas in the Grasshopper model, the chords are assigned equal moduli of elasticity at each location.

Despite the slightly different values for the deformations that were obtained from the Grasshopper sensitivity analysis, it is concluded that the Grasshopper model gives realistic results for the deformations w_1 and w_2 . The model is therefore used to conduct a sensitivity analysis in which the influence of the rotational stiffness k_r on the displacement w_1 is studied, see figure 9.8. The translational stiffness k_s was calculated based on 6 fully threaded 8x240 [mm] screws, yielding a value of $k_s = 70455$ [kN/m]. Different multiplications of this value were considered. It was found that for all cases, the influence of rotational stiffness on the deformation is negligible. This was found both for the case of clamped and hinged connections, where the clamped case yields slightly smaller deflection values.

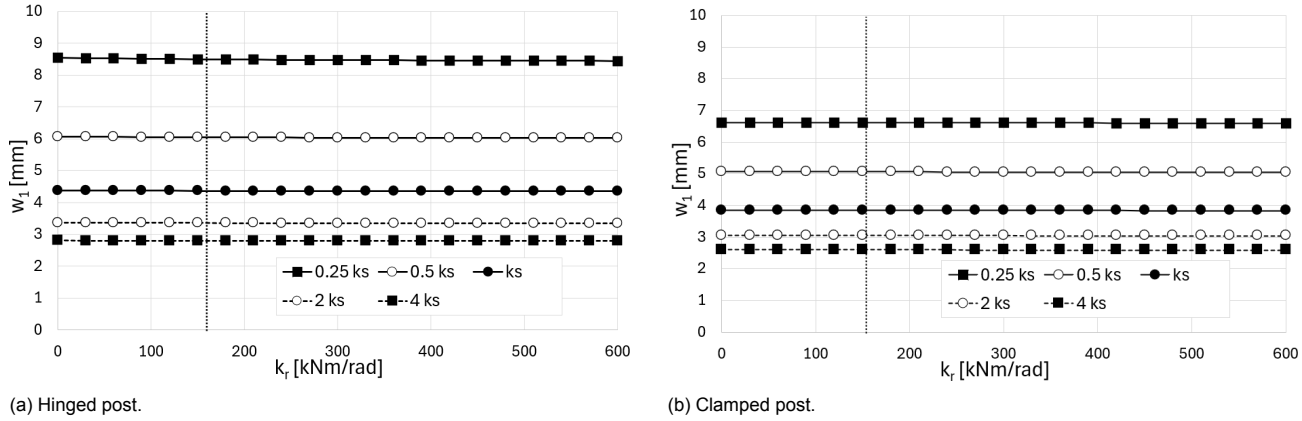


Figure 9.8: Sensitivity analysis small-scale truss for the serviceability limit state. $k_s = 70455$ [kN/m], hinged post case and clamped post case are shown. The vertical dotted line indicates the calculated rotational stiffness of the connection (see table 9.1).

9.3.2. Ultimate limit state

In the small truss experiment, Frese & Steige [66] used partially threaded screws for the connections. However, the experimental testing programme described in chapter 7 consists almost exclusively of fully threaded screws and the calculation model described in chapter 8 therefore is also based on fully threaded screws. For this reason, fully threaded screws are assumed in the Grasshopper model for the connections between the diagonals and chords. The type of screw that is selected for the connections is the ASSY plus fully threaded 4 CSMP 8x240 mm. It is stated by Frese & Steige that a force of 100 [kN] per node is equal to approximately 40 % of the load-bearing capacity [66, p.288]. Although this truss is constructed with partially threaded screws, and thus also the load-bearing capacity is calculated based on partially threaded screws, it is assumed that 250 [kN] can be used as an estimate for the load-bearing capacity for an identical truss with fully threaded screws.

The values for distances e_x and e_z are taken equal to the minimum distances between inclined screws given in EN-1995-1-1, see table 3.1. These depend on the screw diameter, so that for a screw with diameter of 8 [mm] inserted under 45° , $e_x = \sqrt{2} \cdot a_1 = \sqrt{2} \cdot 7 \cdot 8 \approx 80$ [mm] and $e_z = a_2 = 5 \cdot 8 = 40$ [mm]. In reality, the screws on either side of the chord sections must be inserted at a different place, so that crossing screws do not touch inside the chords. This has been simplified in the Grasshopper model so that the connections are modelled identically on either side of the chords. The results relevant to the ultimate limit state case from the structural model are given in table 9.1.

A sensitivity analysis for the ultimate limit state case is performed, in which the influence of the rotational stiffness per shear plane k_r on the moment values in the chord-diagonal connections are studied, both at the top and bottom chord. The analysis is given in figure 9.9. For this analysis, both the case of a hinged chord-post connection and a clamped chord-post connection are included. It is found that the

n_z	n_x	k_s [kN/m] (per shear plane)	k_r [kNm/rad] (per shear plane)	M_{top} [kNm] (per shear plane)	M_{bot} [kNm] (per shear plane)	$F_{screw,par,max}$ [kN]	$F_{screw,perp,max}$ [kN]
6	2	70455.3	164.1	0.65	0.05	0.93	1.92

Table 9.1: Calculated stiffnesses k_s and k_r , Moments and maximum forces per screw from the Grasshopper model for the small-scale prototype.

connection at the top chord experiences a larger moment than the connection at the bottom chord, both in the hinged post case and in the clamped post case. The reason for this is that the relative rotation between the chord and diagonal becomes larger moving away from the midspan of the truss. Since the truss has falling diagonals, the top connection of each diagonal is positioned further away from the midspan. Furthermore, it is found that the moment values are larger in the hinged post case, as no moment can be taken up by the posts in this case. An exception to this last statement is observed in the bottom chord for very low rotational stiffness values. A reason for this odd behaviour could be that in the small-scale prototype, the members are subjected to relatively high values of bending moment and shear force due to the large ratio of truss height and truss span, causing some odd behaviour.

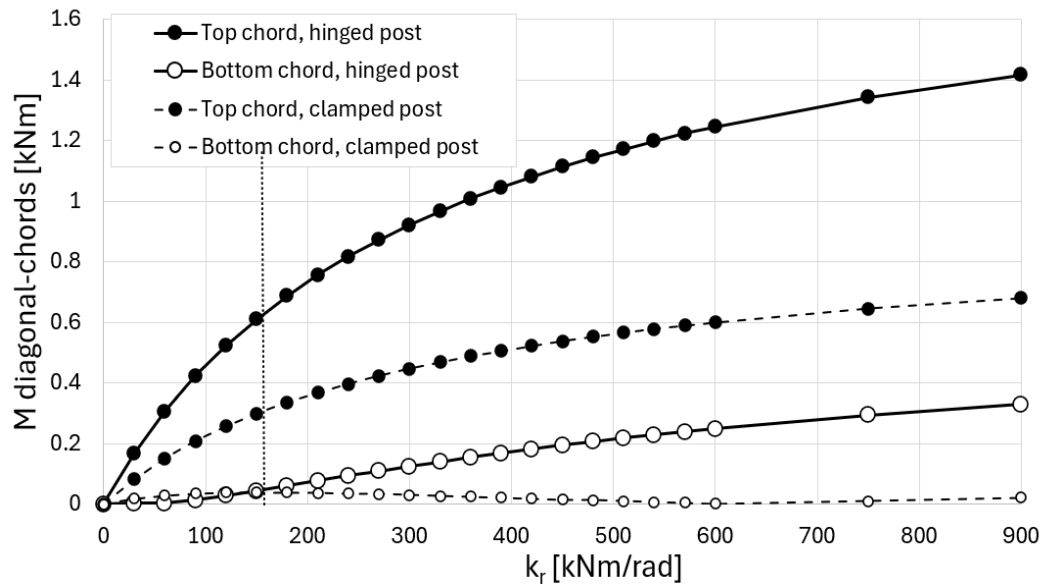


Figure 9.9: Sensitivity analysis small-scale truss for the ultimate limit state, with $k_s = 70455$ [kN/m]. The vertical dotted line indicates the calculated rotational stiffness of the connection (see table 9.1).

The screw force perpendicular to the inclination direction of the screw $F_{screw,perp,max}$ causes a compression force perpendicular to the grain in the diagonal. Using equations 8.3.1 and 8.3.2 in EN-1995-1-1 [55, p. 80], the characteristic embedment strength of the LVL perpendicular to the grain $f_{h,90,k}$ and the embedment strength of the GL24h $f_{h,45,k}$ can be calculated. It is concluded that the diagonals and chords have enough capacity against compression perpendicular to the grain, as given in appendix F.

From the calculated unity check for compression perpendicular to the grain in the diagonals, it is concluded that compression perpendicular to the grain has a negligible influence. The maximum force parallel to the direction of inclination of the screw as a result of the moment in the connections is found to be equal to 0.93 [kN]. As this force works in the same direction as the tension force on the screw as a result of the tension force in the diagonal, the capacity of the screw group is lower than in case no

moments in the connection are considered.

9.4. Large-scale prototype

A large-scale prototype has also been tested in the laboratory, as described by Egner & Frese [25, p. 63]. The dimensions and material properties of this truss are more complicated compared to the small truss. Firstly, the upper and lower chords consist of a composite cross-section of GL24h and LVL [25]. The reasons to apply composite chord cross sections are larger capacity for compression, tension and especially bending moment. Also, the capacity of the chords for compression perpendicular to the grain is increased in this way, which is especially relevant for the connections between the posts and chords [25]. Secondly, the posts in the centre have a smaller cross-section than the posts nearer to the supports, as is also the case for the diagonals. The number of screws that are used per chord-diagonal connection also decreases towards the centre of the truss, as the normal force per diagonal decreases towards the midspan. Finally, the two posts on the outer sides of the truss directly connect to the supports, so that compression perpendicular to the grain as a result of the support reaction in the chords is prevented at this point. Figure 9.10 shows the geometry of the FaNaBu truss.

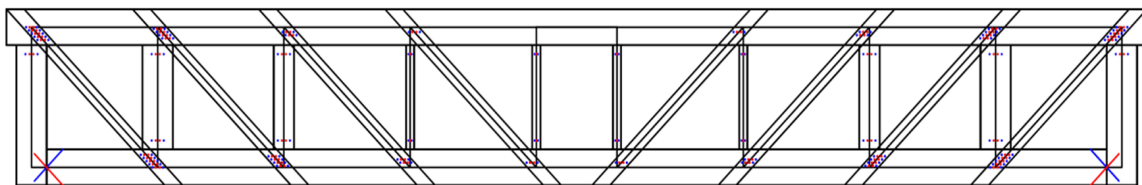


Figure 9.10: Geometry of the large FaNaBu truss prototype [25, p. 64].

A more simplified version of the large truss that was tested experimentally is modelled in Grasshopper, see figure 9.11. The upper and lower chords are modelled as homogeneous cross-sections of GL24h. The posts are all given equal dimensions, as well as the diagonals. Finally, the outer posts are not modelled connecting directly to the supports, and instead, the chords are therefore continuous beams in the Grasshopper model. An overview of the dimensions used for the model is given in table 9.2.

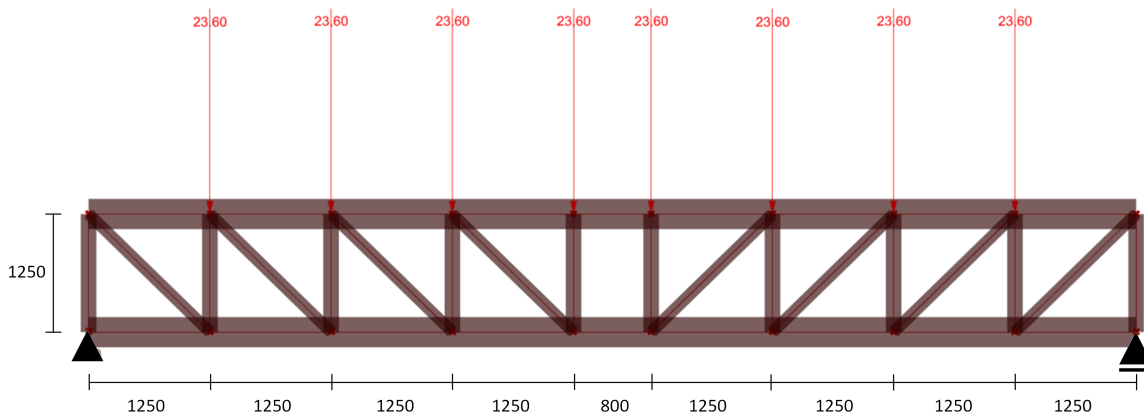


Figure 9.11: Dimensions and loading for the large truss prototype as built in Grasshopper.

The deformations in the large-scale prototype as built and tested by Egner and Frese [25, p. 69] were compared with the deformations found in the model. The connection geometries (see table 9.4) as built in the prototype were used in the Grasshopper model for this analysis. The results are given in table 9.3.

	Material	Cross section
Upper/lower chords	GL24h	320x160 [mm]
Posts	GL24h	160x160 [mm]
Diagonals	LVL GL75	2x125x80 [mm]

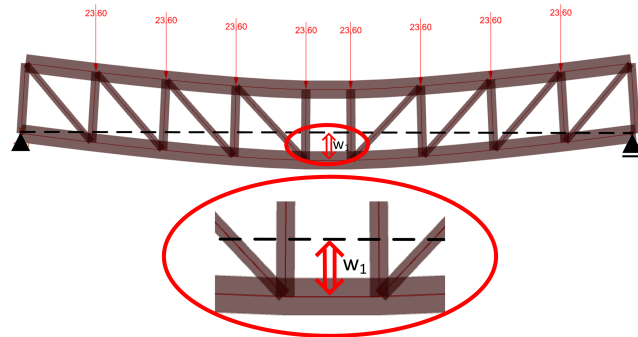
Table 9.2: Dimensions large truss prototype as modelled in Grasshopper.

Total load [kN]	Load per node [kN]	w_1 tests [mm]	w_1 GH model [mm]
472	59.0	52.3	41.4
189	23.6	22.1	17.0

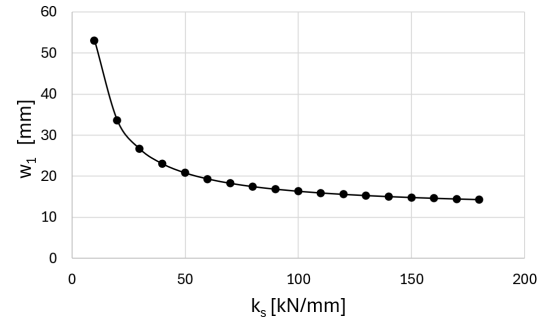
Table 9.3: Deflections at midspan found in tests of the large-scale truss and deflections found with the Grasshopper model

9.4.1. Serviceability limit state

The experimentally tested truss has a characteristic load capacity of 472 [kN] [25, p. 69]. This load is distributed over the 8 connections between the posts and upper chord so that a load of 59 [kN] per connection is present in the ultimate limit state. A service load is taken as 40 % of this load (23.6 [kN]). With this load in place, a sensitivity analysis is performed in the Grasshopper model, in which the deflection at the midspan of the bottom chord is measured with a rotational stiffness $k_r = 0$ in place at each connection. The results are given in figure 9.12b. Only w_1 is plotted, as it was found that the two values are very similar and their lines would overlap in the figure.



(a) Deformation of the lower chord (w_1) in the large truss.



(b) Sensitivity analysis in Grasshopper of large truss, $k_r=0$, hinged post case.

Figure 9.12

The influence of the rotational stiffness on the deformation behaviour was also studied, as shown in the sensitivity analysis given in figure 9.13. In this analysis, each chord-diagonal connection in the truss is modelled with equal stiffness properties. The connection geometry of connection 1, which is the connection closest to the supports, is taken as the base case (see table 9.4 for the calculated values of k_s and k_r). Different multiplications of the translational stiffness k_s of connection 1 are analysed. As was the case for the small-scale prototype, rotational stiffness k_r has a negligible influence on the deformation w_1 of the structure both in the clamped post case and in the hinged post case.

9.4.2. Ultimate limit state

The amount of screws used per connection in the experimentally tested FaNaBu truss decreases towards the midspan. The screws used are fully threaded screws with a length of 280 [mm] and a diameter of 8 [mm]. The distances between the screws were not taken from EN-1995-1-1, but from ETA-11/0190 [6]. The minimum screw spacing parallel to the grain a_1 in this document is given as $5 \cdot d$, so that $e_z = 5 \cdot \sqrt{2} \cdot d = 57[mm]$ is used in the Grasshopper model. Because adjacent screw pairs should not touch each other inside the chord, the minimum edge distance $a_{2,CG}$ of $3 \cdot d$ was used on one side of the chord in the construction of the FaNaBu truss. In this way, enough space is left for the screws on the adjacent side of the chord to fit between these screw locations. In the Grasshopper model, it is assumed that the connections have identical geometries on either side of the chord so that $e_x = 125 - 3 \cdot 8 - 3 \cdot 8 = 77[mm]$ is used in the Grasshopper model.

Again a sensitivity analysis is carried out for the ultimate limit state case, as given in figure 9.14. The analysis is carried out with equal rotational and translational stiffness properties in each chord-diagonal connection. The translational stiffness of all chord-diagonal connections is kept constant and is calcu-

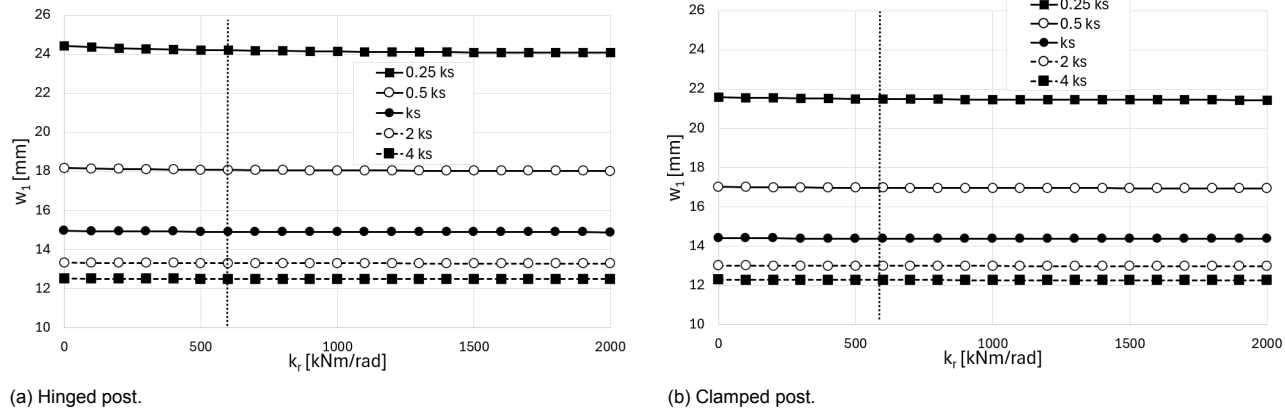


Figure 9.13: Sensitivity analysis large-scale truss for the serviceability limit state. $k_s = 140946$ [kN/m], hinged post case and clamped post case are shown. The vertical dotted line indicates the calculated rotational stiffness of the connection (see table 9.4).

lated according to the geometry of connection 1 (nearest to the supports). For reference, the vertical dotted line indicates the calculated rotational stiffness of connection 1. As was the case for the small truss, the moment is found to be larger at the top chord than at the bottom chord. Again the case in which the posts are hinged yields higher moment values in the connection than the clamped case.

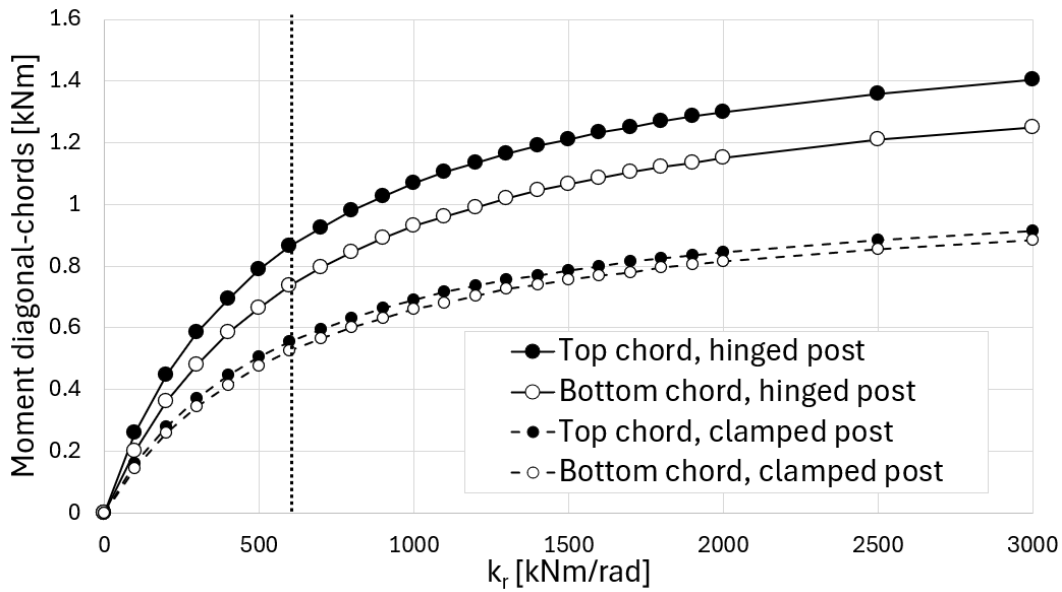


Figure 9.14: Sensitivity analysis large-scale truss for the ultimate limit state for connection 1 (nearest to the supports), with $k_s = 140946$ [kN/m]. The vertical dotted line indicates the calculated rotational stiffness of the connection (see table 9.4).

The amount of screws per shear plane in the FaNaBu truss is 2x5, 2x4, 2x2 and 2x1, as seen from the supports towards the midspan. Using the Grasshopper model, again the moments in the connections and forces on the screws are calculated, as given in table 9.4. The check for compression perpendicular to the grain is performed in appendix F.

It is concluded that for the large truss, compression perpendicular to the grain in the diagonal has negligible influence, with a unity check of 0.05 for the most heavily loaded screw. As a result of the moment in the connection, individual screws receive an additional load in the direction of the tensile force in the diagonal. The maximum additional tensile force per screw $F_{screw,par,max}$ is given in table 9.4. The tensile force per diagonal is divided by the number of screws and given in table 9.5. It was

Connection	n_z	n_x	k_s [kN/m] (per shear plane)	k_r [kNm/rad] (per shear plane)	M_{top} [kNm] (per shear plane)	M_{bot} [kNm] (per shear plane)	$F_{screw,par,max}$ [kN]	$F_{screw,perp,max}$ [kN]
1	5	2	140946.0	596.3	0.88	0.80	0.8	1.09
2	4	2	112756.8	382.4	0.74	0.56	1.04	1.16
3	2	2	56378.4	128.1	0.32	0.15	1.33	0.80
4	1	2	28189.2	56.2	0.16	0.04	1.48	0.51

Table 9.4: Calculated stiffnesses k_s and k_r , Moments and maximum forces per screw from the Grasshopper model for the large-scale prototype.

Connection	$F_{screw,par,max}$ [kN]	$\frac{F_{diag}}{n_{screws}}$ [kN]	mult. factor [-]
1	0.801	16.2	1.05
2	1.04	15.8	1.07
3	1.33	19.2	1.07
4	1.48	15.0	1.10

Table 9.5: Multiplication factor of the force per screw in the inclination direction as a result of the moment in the connections

found that the connections receive an additional load as a result of the moment of 5 to 10 % of the individual screw force as a result of the tensile force in the diagonal. Higher percentages were found for connections towards the midspan. Although the moments in these connections are lower, fewer screws per connection are applied as the tensile force in the diagonals decreases towards mid-span.

9.5. Screw forces as a result of moment in the connections

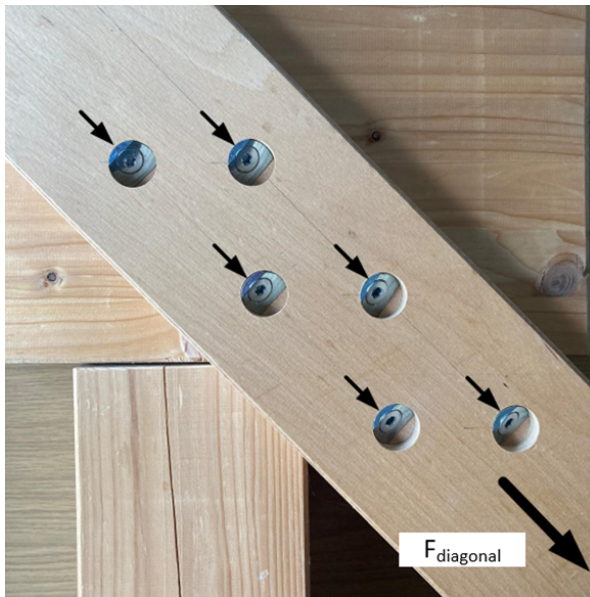
The forces per screw are calculated according to the equations derived in section 5.3.1. These equations are repeated below, given by equations 9.1.

$$\begin{aligned} F_{screw,par,i} &= k_{SLS} \cdot \cos(\theta_i) \cdot \phi_{diag-chord} \cdot r_i \\ F_{screw,perp,i} &= k_{SLS,v} \cdot \sin(\theta_i) \cdot \phi_{diag-chord} \cdot r_i \end{aligned} \quad (9.1)$$

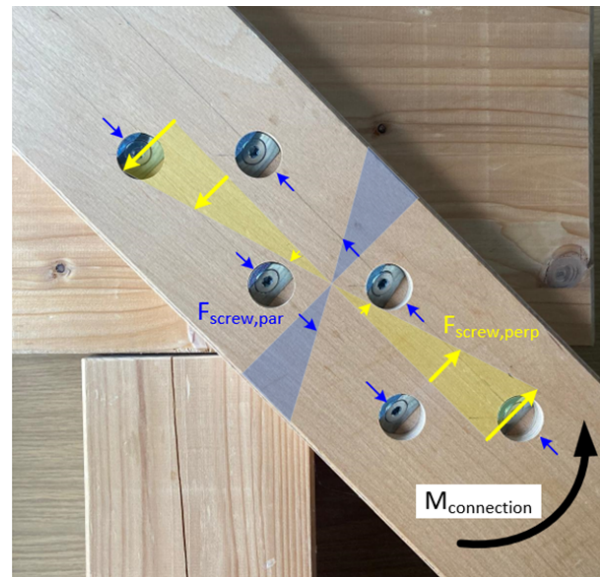
In which:

- $F_{screw,par,i}$: force parallel to the inclination direction of screw i
- $F_{screw,perp,i}$: force perpendicular to the inclination direction of screw i
- r_i : distance between screw i and centre of rotation
- θ_i : angle between line r_i and the line perpendicular to the inclination direction of the screw
- $\phi_{diag-chord}$: relative rotation between the timber elements

According to the derivation, the forces per screw increase linearly with increasing distances from the centre of rotation. The forces are given in figure 9.15. The individual screws receive a load in the inclination direction as a result of the tensile force that is present in the diagonal, indicated by the black arrows in figure 9.15a. The derived equations describe the load perpendicular to the inclination direction $F_{screw,perp}$ and parallel to the inclination direction $F_{screw,par}$, indicated in yellow and blue, respectively, in figure 9.15b. The loads as a result of both the tensile force and the moment in the connection are summed, so that the screws on the left side of the connections receive an additional load in the inclination direction as a result of the moment in the connection. The forces on the screws on the right side of the connection become smaller in magnitude, as the forces work in opposite directions.



(a) Forces per screw as a result of the tensile force in the diagonal.



(b) Forces per screw parallel and perpendicular to the inclination direction of the screw as a result of the moment in the connection.

Figure 9.15

9.6. Conclusion

A parametric model of the FaNaBu truss is built in Rhinoceros Grasshopper. Using this model, the influence of the rotational stiffness of the chord-diagonal connections on the midspan deflection and the connection moments in two prototypes of the truss was analysed. It is concluded that the rotational stiffness does not influence the deflection at midspan. For larger values of rotational stiffness, the moments in the connections increase, reaching a horizontal tangent for very large values of rotational stiffness. The forces per screw are analysed, and it is found that individual screws in the large-scale FaNaBu prototype experience a 5 to 10 % increase in load in the main loading direction as a result of the connection moments. The developed Grasshopper model can be used in the preliminary design of FaNaBu truss girders to quantify the additional connection moments and screw forces as a result of rotational connection stiffness.

10

Connection details

10.1. Diagonal-chord connection in trusses

In the FaNaBu truss, the connections between the chords and diagonals are constructed with inclined screws. This results in a complex geometry, in which detailing is important. The screws on either side of the connection should cross one another inside the chord section. In case the screws would not cross, a net pulling force would develop in the chord. This is a force perpendicular to the grain, which could result in the splitting of the timber in the chord section. The minimum overlap of the screws is specified in prEN-1995-1-1 [53] and amounts to $4 \cdot d$. Direct contact of the screws inside the chord should however be prevented, as this can damage the screw thread, and drastically reduces the withdrawal capacity of the screws in the chord section.

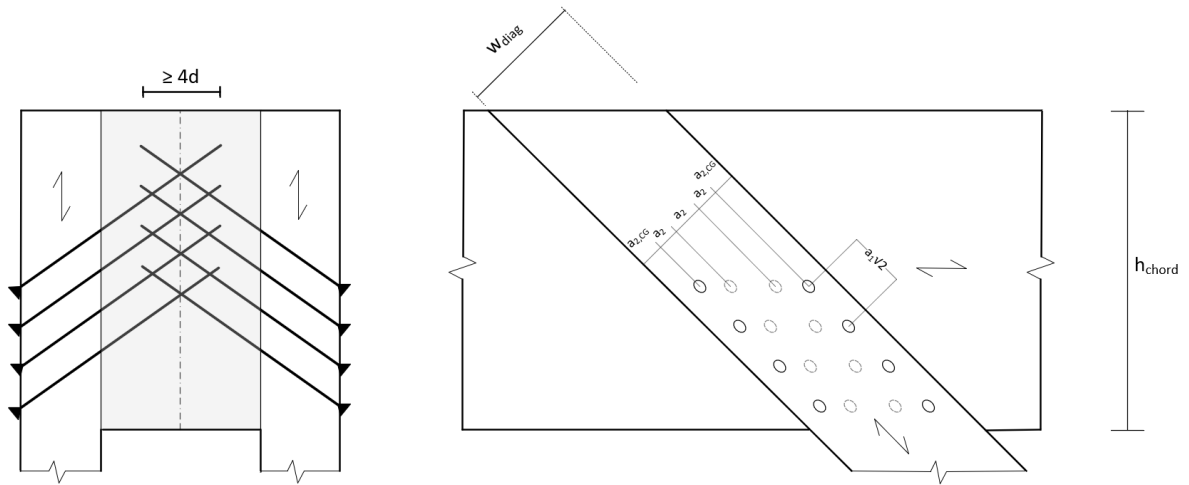


Figure 10.1: Chord-diagonal connection in the FaNaBu truss.

To prevent brittle failure mechanisms, the minimum end and edge distances must be respected, as well as minimum spacings between screws. These minimum distances do put certain restrictions on the minimum sizes of the chords and diagonals, see equations 10.1 and 10.2 which specify the minimum height of the chord and minimum width of the diagonal, respectively.

$$h_{chord,min} = \begin{cases} \sin(\epsilon) \cdot ((n_z - 1) \cdot \frac{a_1}{\sin(\alpha)} + l_2 \cdot \cos(\alpha) + a_{1,CG} - \frac{1}{2} \cdot l_2 \cdot \cos(\alpha)) & \text{if } a_{1,CG} > \frac{1}{2} \cdot l_2 \cdot \cos(\alpha) \\ \sin(\epsilon) \cdot ((n_z - 1) \cdot \frac{a_1}{\sin(\alpha)} + l_2 \cdot \cos(\alpha)) & \text{if } a_{1,CG} \leq \frac{1}{2} \cdot l_2 \cdot \cos(\alpha) \end{cases} \quad (10.1)$$

$$w_{diag,min} = (n_{x,tot} - 1) \cdot a_2 + 2 \cdot a_{2,CG} \quad (10.2)$$

In which:

- $h_{chord,min}$: minimum height of the chord section [mm]
- $w_{diag,min}$: minimum height of the diagonal [mm]
- a_1 : minimum spacing in plane parallel to the longitudinal direction of the diagonal [mm]
- ϵ : Angle between chord section and diagonal [°]
- n_z : number of screws in a row in a plane parallel to the longitudinal direction of diagonal [-]
- α : angle of insertion of individual screw [°]
- l_2 : insertion length in chord section of individual screw [mm]
- $a_{1,CG}$: minimum end distance of the centre of gravity of the threaded part of the screw in the chord section [mm]
- $n_{x,tot}$: number of screw rows in a plane perpendicular to the longitudinal direction of the diagonal, for the total connection (screws from either side of the chord section) [-]

Because of the geometrical restrictions formulated by equations 10.1 and 10.2, it is recommended to shape the entire connection as a parallelogram as shown in figure 10.1, because this minimises both the height of the chord and width of the diagonal. In case a wider connection is chosen, the minimum width of the diagonals increases, whereas a higher connection increases the minimum height of the chords. As found in chapter 9, screws that experience a high lateral load as a result of a moment in connections do not pose a problem in the ultimate limit state, as unity checks for stress perpendicular to the grain remain small. However, screws that experience high loads in the inclination direction as a result of a moment in connections impose an additional load as a result of the moment in the same direction as the normal force in the diagonal. Therefore, individual screws experience a larger force in this direction. Based on this phenomenon, it is advisable to use long, narrow connections (so that n_z is larger than n_y) to minimise the magnitude of $F_{screw,par}$. To guarantee that moments in the connections are kept to a minimum, it is recommended to use the minimum spacings given by EN-1995-1-1, or of the European Technical Assessment document of the specific product, if applicable.

The top chord of the truss experiences a compression force, while the bottom chord on the contrary is loaded in tension. The diagonals that are loaded in tension introduce the compressive and tensile forces in the top and bottom chords, respectively. To maximise the normal force capacity of the chords both in tension and compression, it is important that the normal forces are introduced without eccentricities so that bending moments in the chords are prevented as much as possible and normal loads are introduced as close to the centre of the cross-sections as possible. Therefore, the z-coordinate of the geometric centre of the connections on either side of the chords should coincide with the z-coordinate of the central axis of the chords.

For the screws that are applied in the connection, either fully-threaded or partially-threaded screws can be used. The partially threaded screws, of which the threaded length corresponds with the anchorage length in the chords, should be combined with angled washers. The partially threaded screws find their application in combination with diagonals with a smaller thickness, as the limited threaded length in the diagonal would fail to provide sufficient withdrawal capacity. In case the diagonal has a larger thickness, fully threaded screws can be used as the threaded length in the diagonals can reach a higher withdrawal capacity [25, p. 49].

10.2. Chord connection

Due to restrictions on manufacturing and transport, long elements are often composed of multiple elements in large-span timber structures. This forces engineers to design robust connections for this purpose. Examples include beams or the chords of long-span trusses. In the first case, large values of bending moment are to be expected. In an ideal truss structure, only normal forces are found in the chords, although moderate values of bending moment are to be expected. Inclined screws could be

used to connect the two chord members in a truss with the help of two side members, as shown in figure 10.2.

Although the magnitudes of bending moments in truss chords are generally limited, it is desirable to have large rotational stiffness in the connections to guarantee the continuity of the chords. The rotational stiffness tests have shown that the greatest rotational stiffness is found for geometries in which the screws are loaded parallel to their inclination direction with a large distance to the centre of rotation (geometries 3+6 and 3+4+5+6). Therefore, it is recommended to connect the side members and the chords with horizontal rows of screws, with a large vertical distance separating these rows.

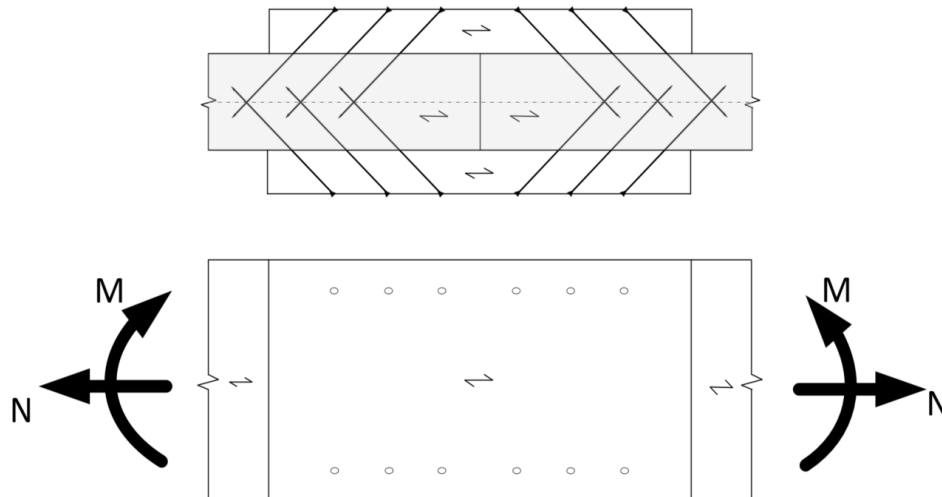


Figure 10.2: Chord connection under tensile force and bending moment as seen in cross-section (top) and from the side (bottom).

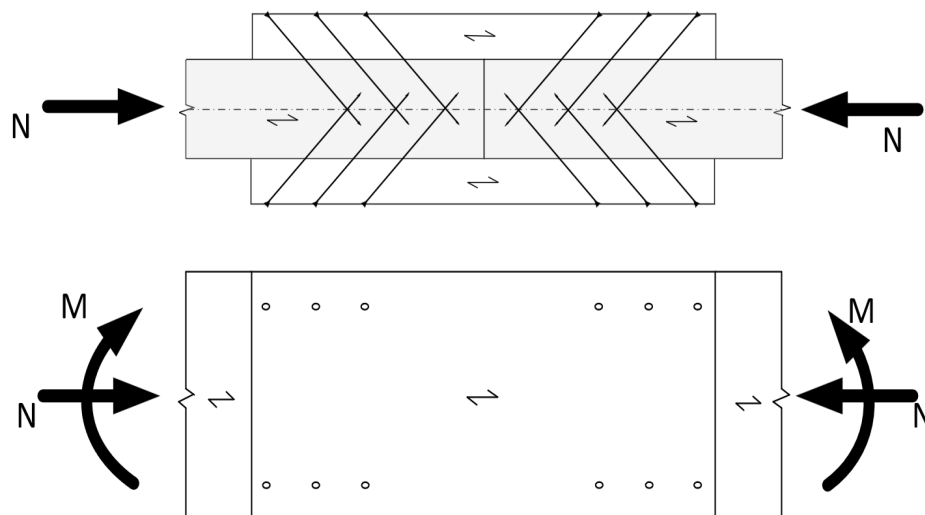


Figure 10.3: Chord connection under compressive force and bending moment as seen in cross-section (top) and from the side (bottom).

In such connection types, the inclination direction of the screw should be the same as the axial load direction of the connection (either tensile or compressive force). In the tensile connection, a tensile force and bending moment can cause a displacement of the centre of rotation, in case the chord sections make contact. The screws are then still loaded in the correct direction. In the compressive connection, a combination of compressive force and bending moment would result in the screws being loaded in the opposite direction in case the chord sections make contact and the bending moment contribution

per screw is larger than the contribution of compressive force. Therefore, the connection type seems less suitable for compressive connections in which large values of bending moment are expected.

10.3. Beam-column joint

Finally, a possible application of axially loaded screws in a connection under both normal force and bending moment is a beam-column connection. Beam-column joints are often used to connect the columns and beams in hall structures, where the connection is subjected to high values of bending moment. Inclined screws could be used for these kind of structures. A concept is proposed as given in figure 10.4, where the beam and column are in direct contact with one another to transfer shear force in the beam to the column, where it is taken up as normal force. The beam and column are connected with two side members, one on either side of the connection. The side members are loaded in tension and are connected to the beam and column with inclined screws. The moment is taken up by a couple, existing of the compressive normal force between column and beam, and the tensile force taken up by one pair of side members. Shear dowels are used to transfer any possible shear forces in the joint. A point worth mentioning is that in this proposed connection, the beam is loaded perpendicular to the grain. Especially in case a large bending moment is applied to the connection, the compressive force could concentrate on a small area in the joint because the centre of rotation shifts. It should be checked whether the beam has enough capacity for compression perpendicular to the grain for this combination of bending moment and normal force from the column.

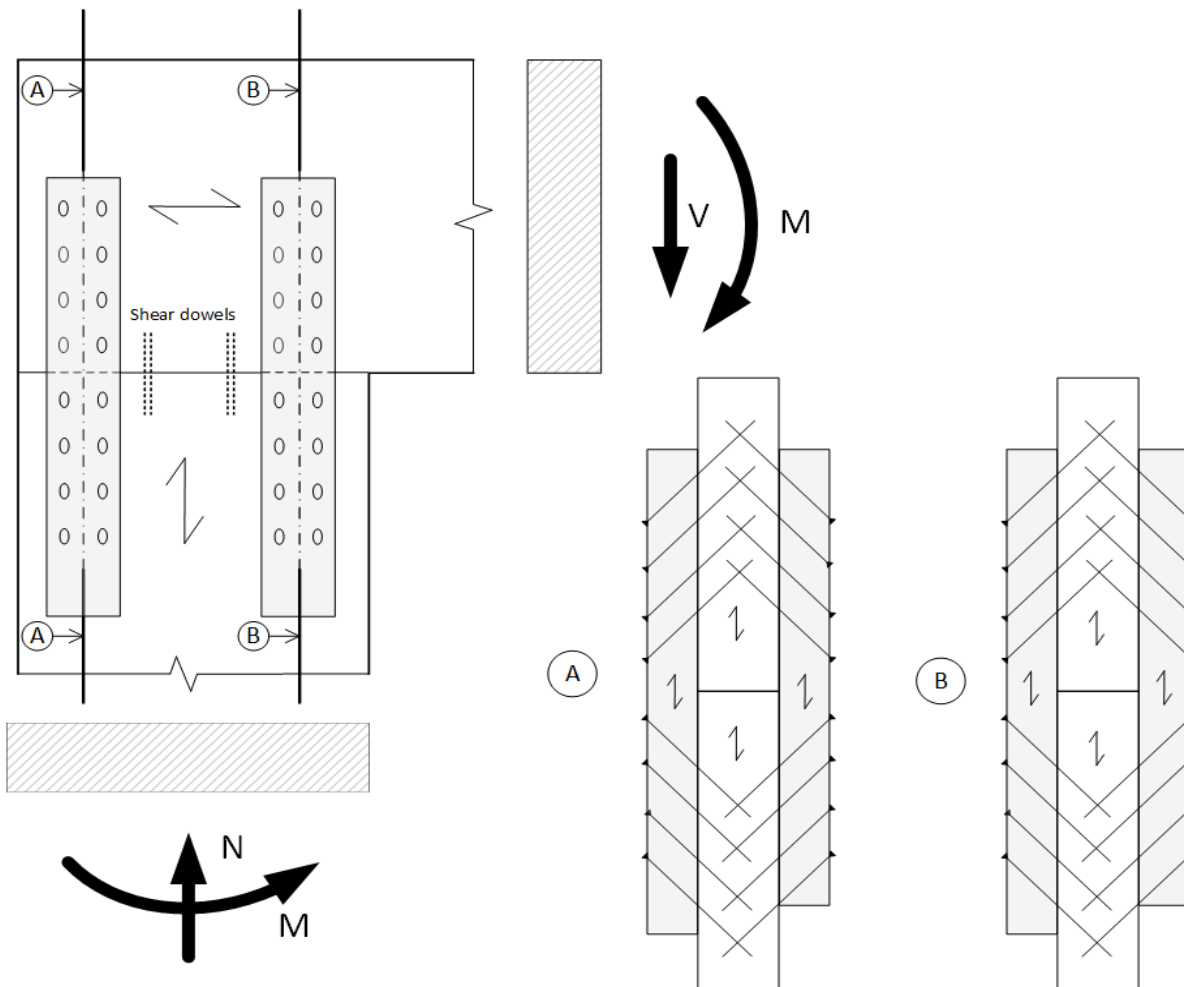


Figure 10.4: Proposed beam-column joint utilising inclined screws.

It should be noted that in this connection type, the bending moment is taken up by the screws only being loaded in their inclination direction. This is done because large values of bending moment are

expected in these kind of connections, and thus the screws should be loaded in the direction in which they have the largest load-bearing capacity. The calculation method for rotational stiffness proposed in chapter 8 is therefore not applicable to these connections.

Conclusion and discussion

This section answers the main research question that was formulated in the introduction of the thesis. Also, the sub-questions are answered. The section ends with a discussion of the results.

11.1. Conclusion

11.1.1. Main research question

The main research question of the thesis is formulated as follows:

How can the rotational stiffness of timber-to-timber connections with inclined screws be quantified?

To answer the main research question, a total of fourteen methods to calculate the rotational stiffness of connections with inclined screws have been selected for analysis. These methods are compared to the rotational stiffness data from experimental tests carried out as a part of the FaNaBu project before the start of this MSc thesis project. The experimental tests consist of two test series. It is found that the results of test series 2 show good similarity with multiple of the fourteen selected calculation methods, where method 14 is identified as the best method, resulting in a coefficient of determination of 0.84. For test series 1, this is not the case, and the calculated stiffness values of all methods show very poor similarity to test results with a coefficient of determination of only 0.12 for the best-performing method.

The sequence of the load application is found to be different for the two test series. A correction of the experimental test results for the friction between the timber elements as a result of the specific sequence of the load application in test series 1 yields a considerable improvement for all but two calculation methods. After this correction, referred to as the pre-load theory, the calculated stiffness values of method 14 show the best similarity with the experimental test results, yielding a coefficient of determination of 0.79 for all results of both test series. This method utilises the method by De Santis & Fragiacomio for stiffness in inclination direction k_{SLs} , and the current EN-1995-1-1 equation for the stiffness of dowel-type fasteners for the lateral stiffness $k_{SLs,v}$. It should be noted that these results are based on tests under an angle α_s of 45° only.

11.1.2. Sub-questions

The sub-questions are answered separately in the following section.

What are current calculation methods for the stiffness and capacity of connections with inclined screws, and how do these compare?

In the current version of EN-1995-1-1, the load-bearing capacity of inclined screws is checked for the combination of axial load and shear force. In contrast to the load-bearing capacity, a calculation approach for the stiffness of inclined screws is not given in EN-1995-1-1. Therefore, an extensive literature study is carried out to identify different proposed methods to calculate the stiffness. Most of these methods propose a model in which the screw stiffness in both timber elements is taken into account,

the so-called double stiffness model. Tomasi et al. [67] propose also a single stiffness model, in which the stiffness of the screw in only timber member 1 (the member of the head side of the screw) is taken into account, and the stiffness of the screw in member 2 (the member of the screw tip side) is assumed to be infinite. The methods proposed by Tomasi et al. [67], Jockwer et al. [38] and prEN-1995-1-1 [53] are found to be very similar. The methods proposed by Kevarinmäki [44] and Girhammar et al. [33] depend on parameters that are to be experimentally determined, and are therefore not used in the comparison with the rotational stiffness tests. Seven methods are concluded to be suitable for further analysis and are used in the methods that are compared to the rotational stiffness tests. These methods are given in table 4.2.

What are current calculation methods for the rotational stiffness and moment capacity of connections with dowel-type fasteners and how do these compare?

The moment capacity of connections with dowel-type fasteners depends on the capacity of the individual dowels and the capacity of the reduced cross-section of the connected elements. An additional shear force is introduced as a result of the moment decomposition of the individual dowels.

Three methods are identified to calculate the rotational stiffness of a connection with dowel-type fasteners. The first is the linear spring method, which models each fastener as a linear spring and utilises the displacement method to relate the moment in the connection to the displacements of the individual fasteners as a result of the relative rotation of the connected timber members. Inclined screws have a larger stiffness in the direction of their inclination than in the direction perpendicular to their inclination direction. These stiffness values, denoted as k_{SLS} and $k_{SLS,v}$, respectively, can be used separately in the linear spring method, as an analytical derivation performed in the thesis demonstrates. A second method is identified, using an extension of the lateral stiffness calculation of dowel-type fasteners given in prEN-1995-1-1 [53]. A third method is found in literature, in which Noguchi & Komatsu [57] present an alternative to the linear spring method. Further investigations of the method show that it results in unrealistically low values for rotational stiffness in the case of screw patterns in a single row. The first two methods are very similar and are based on a spring model. They differ only in their calculation for $k_{SLS,v}$. Both are used in the comparison with the rotational stiffness tests.

Which parameters are of influence for the (rotational) stiffness of connections with axially loaded screws?

The method obtained for the rotational stiffness (method 14) takes into account the penetrated length of the screw in each of the two timber elements (regardless of the threaded length), the outer screw diameter, the density of the two timber elements and the angle between the screw axis and the shear plane. The influence of friction is somewhat ambiguous, as the method that shows the best similarity with the test results does not include a parameter for friction. In the rotational stiffness tests, a total of twelve tests are performed with a friction-reducing interlayer between the timber elements, that seem to show lower rotational stiffness values than the average of their connection geometry. This would suggest that lower values for the coefficient of friction would result in lower rotational stiffness values.

What is the influence of the rotational stiffness of connections on the serviceability and ultimate limit state behaviour of structures in which the connections are applied?

A software model of the FaNaBu truss is built in the parametric software package Rhinoceros Grasshopper. Two previously experimentally tested versions of the FaNaBu truss are analysed, in which first the serviceability limit state behaviour is studied. The deformation at midspan shows an exponential decrease for increasing translational stiffness k_s . The deformation at midspan approaches a certain value even for very high stiffness values, which is the result of timber deformation only.

A sensitivity analysis is carried out in which the influence of the rotational stiffness of the connections on the deflection at midspan is investigated for both trusses. It is found that the rotational stiffness does not influence the midspan deflection of both versions of the truss. A second analysis is carried out in which the influence of rotational stiffness of the chord-diagonal connections on the moments in these connections is investigated. The connection moment shows higher values for increasing rotational stiff-

ness, and it approaches a horizontal tangent for large values of rotational stiffness. Relatively large reductions of the moment can be attained for rotational stiffness reductions in the lower stiffness ranges.

The theoretical forces on the individual screws in the connections are determined using an analytically derived equation, which is incorporated in the Grasshopper model. In this way, the force parallel and perpendicular to the inclination direction of the screw as a result of the moment in the connections $F_{screw,par}$ and $F_{screw,perp}$, respectively, are quantified. The magnitude of the perpendicular force is found to be very small compared to the embedment capacity of the timber. The force parallel to the inclination direction of the screw $F_{screw,par}$ works in the same direction as the tensile force in the diagonal. For the large truss prototype, the additional load amounts to 5 to 10 % of the load per screw as a result of the tensile force in the diagonal. The structural model that is developed can be used in the preliminary design of the FaNaBu truss to quantify the moments in the connections and the forces per screw.

What would be other possible applications of connections with inclined screws, and is the developed method for rotational stiffness applicable to these connections?

The inclined screw connection in the FaNaBu truss has a complex geometry, and the connection geometry governs the size of the chords and diagonals of the truss. Other than in trusses, the connection type can find an application in connections of multiple chord sections of long-span trusses, as an alternative to dowel connections. The rotational stiffness calculation as proposed in this thesis is valid under the condition that the chord sections do not make contact as a result of the rotation. In that case, the location of the centre of rotation would change and the method is not valid anymore. A concept for a beam-column connection is proposed in which high values of bending moment are to be resisted by the connection. For high values of bending moment, the connection as applied in the FaNaBu truss is not suitable since the inclined screws would be loaded in the opposite direction (compression instead of tension). Therefore, the compressive forces are planned to be taken up by compression of the beam and column element, and the tensile forces with inclined screws. The proposed method for rotational stiffness is not valid for this connection concept because of the aforementioned shift of the centre of rotation.

11.2. Discussion

In the thesis, an extensive literature study was carried out, in which calculation methods for the stiffness of inclined screws were identified and discussed, as well as rotational stiffness methods for connections with dowel-type fasteners. These methods were combined to obtain methods for the calculation of the rotational stiffness of connections with inclined screws. A parametric software model was developed of the FaNaBu truss, in which these connections are applied. Using this model, the influence of the rotational stiffness of these connections on the serviceability and ultimate limit state was analysed, as well as the individual screw forces.

11.2.1. Calculation method for rotational stiffness

It is noted that the experimentally determined rotational stiffness values show a relatively large spread, for which the exact reason is not known. The complexity of the connection type makes it difficult to fully simulate the behaviour of the connections in structures, examples include the fixation of the centre of rotation or the loading sequence and magnitudes of applied rotation and pulling force. Finally, the influence of long-term loading effects, varying moisture content or cyclic loads are not taken into account in the tests, and could have a relevant influence on the rotational stiffness values of the connections.

Regarding the rotational stiffness methods, very small differences in coefficient of determination are found between the EC method and 0.5 EC method, with some methods giving better results for either the EC method or the 0.5 EC method. In the plots of all 91 tests, the difference between the EC method and 0.5 EC method is observed for screw geometries 1+2+7+8 (green dots) and 1+8 (red dots), as in these geometries the screws are loaded in the lateral direction as a result of the rotation. Visual inspection of the plots for all results suggests a slight overestimation of calculated stiffness for these geometries in the EC method and a better fit for the 0.5 EC method. No clear conclusions can be drawn

as to whether the single stiffness or double stiffness model should be used, as methods incorporating either one of them yield good results. This also applies to the EC method and the 0.5 EC method. Methods 1, 2, 3, 7, 8, 9, 10 and 14 all give coefficients of determination larger than 0.7, indicating the small differences between the calculation methods.

11.2.2. Structural model

The structural modelling is carried out for only two previously built prototypes of the FaNaBu truss. The validation of the Grasshopper model is performed based on the midspan displacement of experimentally tested prototypes. It is found that the grasshopper model gives valid results. The values of the moment in the connections and forces per screw are not validated through models or tests. With regards to the calculation of the forces per screw, it can be argued whether the assumption of an equal distribution of the moment and forces on the connection over the individual screws is justified, given the fact that the first and last fasteners in connections subjected to pulling force theoretically take the highest loads. The trusses are only analysed for the load case of equally distributed point loads facing downwards.

Recommendations

12.1. Recommendations for connection design

With regards to the design of the connections with inclined screws in timber trusses, it is recommended to design connections that are long and narrow, i.e. a large number of n_z and a small number of n_x screws. Because in long connections the screws are almost exclusively loaded in the direction perpendicular to the inclination direction as a result of rotation, the rotational stiffness of the connection is low. A small value for rotational stiffness means that the moments in the connections are kept to a minimum. Plenty of capacity for screw loads perpendicular to the inclination direction is found for the analysed FaNaBu prototype trusses, whereas loading in the inclination direction of the screws would increase screw loads in the main loading direction.

Specifically for the application in trusses, a software model is built in Grasshopper. It is recommended to design the connections in the truss based on the axial capacity for the first iteration. The truss geometry including the connections can be inserted in the model. The model automatically calculates the theoretical forces parallel and perpendicular to the inclination direction of the screw, using the calculated rotational connection stiffness values and the occurring rotations in the connections. In this second iteration, the capacity of the individual screws should be checked, in which the additional load as a result of the moments in the connections is taken into account. In case the capacity is not met, individual screws should be added to the connection or other screws should be used.

Inclined screws are a means of connecting timber elements under tensile loads. It is recommended to use connections with inclined screws subjected to axial load and bending moment only under the condition that all the screws remain loaded in tension (i.e. the axial load is large enough to compensate for the compression load as a result of the moment and thus keep each individual screw under tensile load). The research discussed in this thesis focuses only on a very specific case, namely a connection with multiple inclined screws in which all screws are inclined in the same direction. In case connections are subjected to larger values of bending moment, it is recommended to take up the moment via a couple generated as a result of compression of the timber elements and tension of inclined screws, as in the beam-column joint in chapter 10.

12.2. Recommendations for future research

It is recommended to perform the rotational stiffness tests according to the method used in test series 2, in which the connections are subjected to pulling force and rotation simultaneously. However, it is recommended to increase the tensile load according to the number of screws in the connection, so that the large compressive force in the bottom screw in geometry (3+4+5+6) is prevented. Also, it could be interesting to execute the rotation at a slower rate at the beginning of the tests, so that all the screws in all the tests experience a net pulling force at the beginning of the tests.

It would be interesting to perform tests for connections consisting of larger numbers of screws, in different geometries. The hypothesis that longer, narrow connections yield smaller moments in connections

could be proved in this way. Also, a wider range of timber species could be tested, as well as different screw sizes and inclination angles. Although technically challenging, future research could focus on the development of a test setup in which the centre of rotation is not fixed, to investigate whether a shift occurs. Finally, future research could focus on the influence of time-dependent behaviour and influences of the moisture content.

An interesting direction for future research would be to develop a reduction factor for inclined screw connections that can be used in the ultimate limit state directly. The connection type subjected to the experimental test programme is suited for transferring axial loads primarily, and the bending moments are a secondary effect specific to their application in trusses. Considering this relatively narrow application of the proposed rotational stiffness calculation method, it would be more logical to focus directly on an empirically determined reduction factor for the load-bearing capacity of connections under the combination of axial tensile load and secondary bending moments, similar to the research carried out by Schilling [65] described in section 2.5.

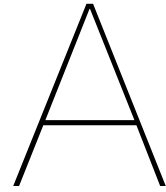
Bibliography

- [1] Simon Aurand and Hans Joachim Blass. "Connections with inclined screws and increased shear plane friction". In: *The International Network on Timber Engineering Research (INTER)* 54 (2021).
- [2] Simon Aurand and Hans Joachim Blass. "Verbinder aus Kunstharzpressholz – Versuche mit ersten Prototypen für Traglasten bis 500 kN". In: *Bautechnik* 98 (S1 2021), pp. 40–50. DOI: 10.5445/IR/1000129082.
- [3] Thomas K. Bader et al. "Dowel deformations in multi-dowel LVL connections under moment loading". In: *Wood Material Science & Engineering* 10.3 (2015), pp. 216–231. DOI: <http://dx.doi.org/10.1080/17480272.2015.1070372>.
- [4] Eva Baldauf. "Untersuchungen zur Rotationssteifigkeit von Anschlüssen mit geneigt eingebrachten Schrauben in Fachwerkkonstruktionen (unpublished)". MA thesis. Karlsruher Institut für Technologie, 2022.
- [5] M. Basterrechea-Arévalo et al. "Modelling of moment transmitting beam-to-column timber connections accounting for frictional transmission". In: *Engineering Structures* 247 (2021). DOI: <https://doi.org/10.1016/j.engstruct.2021.113122>.
- [6] Deutsches Institut für Bautechnik. *European Technical Assessment ETA-11/0190 of 23 July 2018*. Tech. rep. Deutsches Institut für Bautechnik, 2018.
- [7] Ireneusz Betjka. "Verstärkung von Bauteilen aus Holz mit Vollgewindeschrauben". PhD thesis. Fakultät für Bauingenieur-, Geo- und Umweltwissenschaften der Universität Fridericiana zu Karlsruhe, 2005.
- [8] H. J. Blass, A. Bienhaus, and V. Krämer. "Effective Bending Capacity of Dowel-Type Fasteners". In: *Proceedings from meeting thirty-three of the international council for building research studies and documentation, CIB, Working Commission W18– Timber Structures* (2000), pp. 139–150.
- [9] Hans Joachim Blass, Ireneusz Betjka, and Thomas Uibel. *Tragfähigkeit von Verbindungen mit selbstbohrenden Holzschraube mit Vollgewinde*. Vol. Band 4. Karlsruher Berichte zum Ingenieurholzbau. Straße am Forum 2, D-76131 Karlsruhe: Universitätsverlag Karlsruhe c/o Universitätsbibliothek, 2006. ISBN: 3-86644-034-0.
- [10] Hans Joachim Blass and Ireneusz Betjka. "Joints with inclined screws". In: *Proceedings from meeting thirty-five of the international council for building research studies and documentation, CIB, Working Commission W18– Timber Structure* (2002), pp. 141–154.
- [11] Hans Joachim Blass and Ireneusz Betjka. "Screws with continuous threads in timber connections". In: *Proceedings PRO 22: International RILEM Symposium on Joints in Timber Structures* (2001), pp. 193–201.
- [12] Hans Joachim Blass and Markus Enders-Comberg. *Fachwerkträger für den industriellen Holzbau*. Vol. Band 22. Karlsruher Berichte zum Ingenieurholzbau. Straße am Forum 2, D-76131 Karlsruhe: KIT Scientific Publishing, 2012. ISBN: 978-3-86644-854-4.
- [13] Hans Joachim Blass and Carmen Sandhaas. *Timber Engineering - principles for design*. KIT Scientific Publishing, 2017. ISBN: 978-3-7315-0673-7. DOI: 10.5445/KSP/1000069616.
- [14] Hans Joachim Blass and Yvonne Steige. *Steifigkeit axial beanspruchter vollgewindeschrauben*. Vol. Band 34. Karlsruher Berichte zum Ingenieurholzbau. Straße am Forum 2, D-76131 Karlsruhe: KIT Scientific Publishing, 2018. ISBN: 978-3-7315-0826-7. DOI: 10.5445/KSP/1000085040.
- [15] Hans Joachim Blass et al. *E DIN 1052*. Tech. rep. DIN-Normenausschuss Bauwesen (NABau), 2000.
- [16] A. Bouchaïr, P. Racher, and J. F. Bocquet. "Analysis of dowelled timber to timber moment-resisting joints". In: *Materials and Structures* 40 (2007), pp. 1127–1141. DOI: 10.1617/s11527-006-9210-0.

- [17] Pollmeier Massivholz GmbH & Co.KG. *Kapitel 08 - Fachwerktr ager*. Pollmeier Massivholz GmbH & Co.KG.
- [18] Calvin O. Cramer. "Load Distribution in Multiple-Bolt Tension Joints". In: *Journal of the Structural Division* 94.ST5 (May 1968), pp. 1101–1118.
- [19] Roberto Crocetti. "Large-Span Timber Structures". In: *Proceedings of the World Congress on Civil, Structural, and Environmental Engineering (CSEE'16)* (2016). DOI: 10.11159/icseem16.124.
- [20] Carl Culmann. *Die graphische Statik*. Z rich: Meyer & Zeller, 1866. DOI: <https://doi.org/10.3931/e-rara-20052>.
- [21] Deutsches Institut f r Bautechnik. *Allgemeine baufsichtliche Zulassung, SFS Befestiger WT-S-6,5, WT-T-6,5, WT-T-8,2, WR-T-9,0 und WR-T-13 als Holzverbindungsmitel. Z-9.1 472*. Tech. rep. Deutsches Institut f r Bautechnik, 2011.
- [22] Deutsches Institut f r Bautechnik. *Allgemeine baufsichtliche Zulassung, SFS Befestiger WT-T-6,5, WT-T-8,2, WT-R-8,9 als Holzverbindungsmitel. Z-9.1 472*. Tech. rep. Deutsches Institut f r Bautechnik, 2006.
- [23] Pierre Dubas. *Einf hrung in die Norm SIA 164 (1981) Holzbau - Autographie zum Fortbildungskurs f r Bauingenieure*. Z rich: Lehrstuhl f r Baustatik und Stahlbau ETH Z rich, 1981. URL: https://issuu.com/lignum/docs/ibk_dl64_1981.
- [24] Sebastian Egner and Matthias Frese. "Rotational stiffness of timber-to-timber connections with self-tapping axially loaded screws". In: *Proceedings ICEM20 20th International Conference on Experimental Mechanics* (2023).
- [25] Sebastian Egner and Matthias Frese. *Schlussbericht zum Verbundvorhaben Fachwerktr ger aus Nadel- und Buchenholz*. Tech. rep. Karlsruher Institut f r Technologie (KIT), 2023.
- [26] J rgen Ehlbeck and Hartmut Werner. "Softwood and Hardwood Embedding Strength for Dowel-type Fasteners - Background of the formulae in EUROCODE 5, draft April 1992". In: *Proceedings from meeting twenty-five of the international council for building research studies and documentation, CIB, Working Commission W18– Timber Structures* (1992), pp. 555–568.
- [27] European Committee for Standardization (CEN). *Timber structures - Joints made with mechanical fasteners - General principles for the determination of strength and deformation characteristics (ISO 6891:1983)*. Standard. European Committee for Standardization, Jan. 1991.
- [28] European Committee for Standardization (CEN). *Timber structures - Test methods - Determination of embedment strength and foundation values for dowel type fasteners*. Standard. European Committee for Standardization, Jan. 2007.
- [29] European Committee for Standardization (CEN). *Timber structures - Test methods - Determination of the yield moment of dowel type fasteners*. Standard. European Committee for Standardization, Apr. 2009.
- [30] European Committee for Standardization (CEN). *ENV 1995-1-1:Design of timber structures. Part 1-1: General rules and rules for buildings*. Standard. European Committee for Standardization, Dec. 1993.
- [31] E. Gehri et al. "Entwurf und Bemessung von Schnittholz-Konstruktionen mit neuzeitlichen Verbindungen. Fortbildungskurs XI der SAH". In: Zurich: Schweizerische Arbeitsgemeinschaft f r Holzforschung, Nov. 8, 1979.
- [32] Ernst Gehri. "Betrachtungen zum Tragverhalten von Bolzenverbindungen im Holzbau". In: *Schweizer Ingenieur und Architekt* 98.51-52 (Dec. 1980).
- [33] Ulf Arne Girhammar, Nicolas Jacquier, and Bo K llsner. "Stiffness model for inclined screws in shear-tension mode in timber-to-timber joints". In: *Engineering Structures* 136 (2017), pp. 580–595.
- [34] R.L. Hankinson. "Investigation of crushing strength of spruce at varying angles of grain". In: *Air Force Information Circular* 3.259 (1929).
- [35] H. Hartmann. "Structural behaviour and reliability of timber trusses with dowelled steel-to-timber connections". In: *Bauingenieur* 90 (2015).

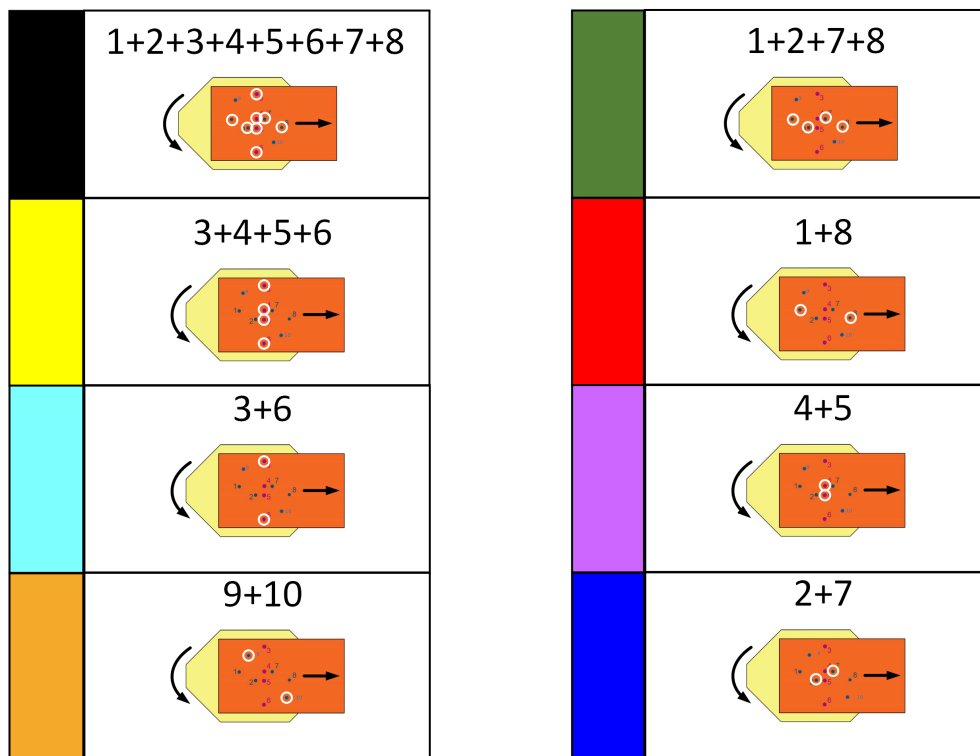
- [36] Bodo Heimeshoff. *Berechnung von Rahmenecken mit Dübelanschluss (Dübelkreis)*. Arbeitsgemeinschaft Holz e.V., Nov. 1979.
- [37] B.O. Hilson. "Joints with dowel-type fasteners - Theory". In: Centrum Hout, 1995. Chap. lecture C3. URL: <https://e-step.net/c-joints-2> (visited on 05/15/2024).
- [38] Robert Jockwer, Andrea Frangi, and René Steiger. "Design model for inclined screws under varying load to grain angles". In: *The International Network on Timber Engineering Research (INTER)* 47 (2014), pp. 141–155.
- [39] Robert Jockwer and André Jorissen. "Stiffness and deformation of connections with dowel-type fasteners". In: *Design of Connections in Timber Structures - A state-of-the-art report by COST Action FP1402 / WG3* (2018), pp. 95–126.
- [40] Marek Johanides et al. "Analysis of Rotational Stiffness of the Timber Frame Connection". In: *Sustainability* 13.156 (2021). DOI: <https://dx.doi.org/10.3390/su13010156>.
- [41] K.W. Johansen. "Theory of Timber Connections". In: *International Association of Bridge and Structural Engineering* 9 (1949), pp. 249–262. DOI: <https://doi.org/10.5169/seals-9703>.
- [42] André Jorissen. "Double Shear Timber Connections with Dowel Type Fasteners". PhD thesis. Delft University of Technology, 1998.
- [43] André Jorissen and Hans Joachim Blass. "The fastener yield strength in bending". In: *Proceedings from meeting thirty-one of the international council for building research studies and documentation, CIB, Working Commission W18— Timber Structures* (1998), pp. 264–272.
- [44] Ari Kevarinmäki. "Joints with inclined screws". In: *The International Network on Timber Engineering Research (INTER)* 35 (2002), pp. 127–140.
- [45] Peter Kobel, Andrea Frangi, and René Steiger. "Dowel-type connections in LVL made of beech wood". In: *The International Network on Timber Engineering Research (INTER)* 47 (Sept. 2014), pp. 105–115.
- [46] Gustav Kullander and Alexander Sandström. *Combined loading of angles screws in timber connections*. 2023.
- [47] G. Lantos. "Load Distribution in a Row of Fasteners subjected to Lateral load". In: *Wood Science* 1.3 (Jan. 1969), pp. 129–136.
- [48] Ronja Loreck. "Untersuchungen zur Rotationssteifigkeit von Anschlüssen mit Schrauben in Fachwerkträgern (unpublished)". MA thesis. Karlsruher Institut für Technologie, 2023.
- [49] Mike Mellaard. *Stiffness Modelling of Large Timber Connections in Stability Trusses*. 2023.
- [50] Nico Meyer and Hans Joachim Blass. "Fachwerkträger aus Buchenfurnierschichtholz". In: *Bautechnik* 94 (11 Sept. 2017), pp. 751–759. DOI: <https://doi.org/10.1002/bate.201700071>.
- [51] K. Möhler. "Spannungen und Durchbiegungen parallelgurtiger Fachwerkträger aus Holz". In: *Bauen mit Holz* 4 (1966), pp. 155–161.
- [52] Koninklijk Nederlands Normalisatie-instituut. *National Annex to NEN-EN 1990+A1:2006+A1:2006/C2:2019 Eurocode: Basis of structural design*. Standard. Koninklijk Nederlands Normalisatie-instituut, Nov. 2019.
- [53] European Committee for Standardization (CEN). *Eurocode 5: Design of timber structures – Part 1-1:2023 (Draft) General - Common rules and rules for buildings*. Standard. European Committee for Standardization, Sept. 2023.
- [54] Swedish Wood. *Design of timber structures - Structural aspects of timber construction - Volume 1*. Standard. www.swedishwood.com, Apr. 2022.
- [55] European Committee for Standardization (CEN). *Eurocode 5: Design of timber structures – Part 1-1: General - Common rules and rules for buildings*. Standard. European Committee for Standardization, Nov. 2011.
- [56] Swedish Wood. *Design of timber structures - Rules and formulas according to Eurocode 5 - Volume 2*. Standard. www.swedishwood.com, Apr. 2022.

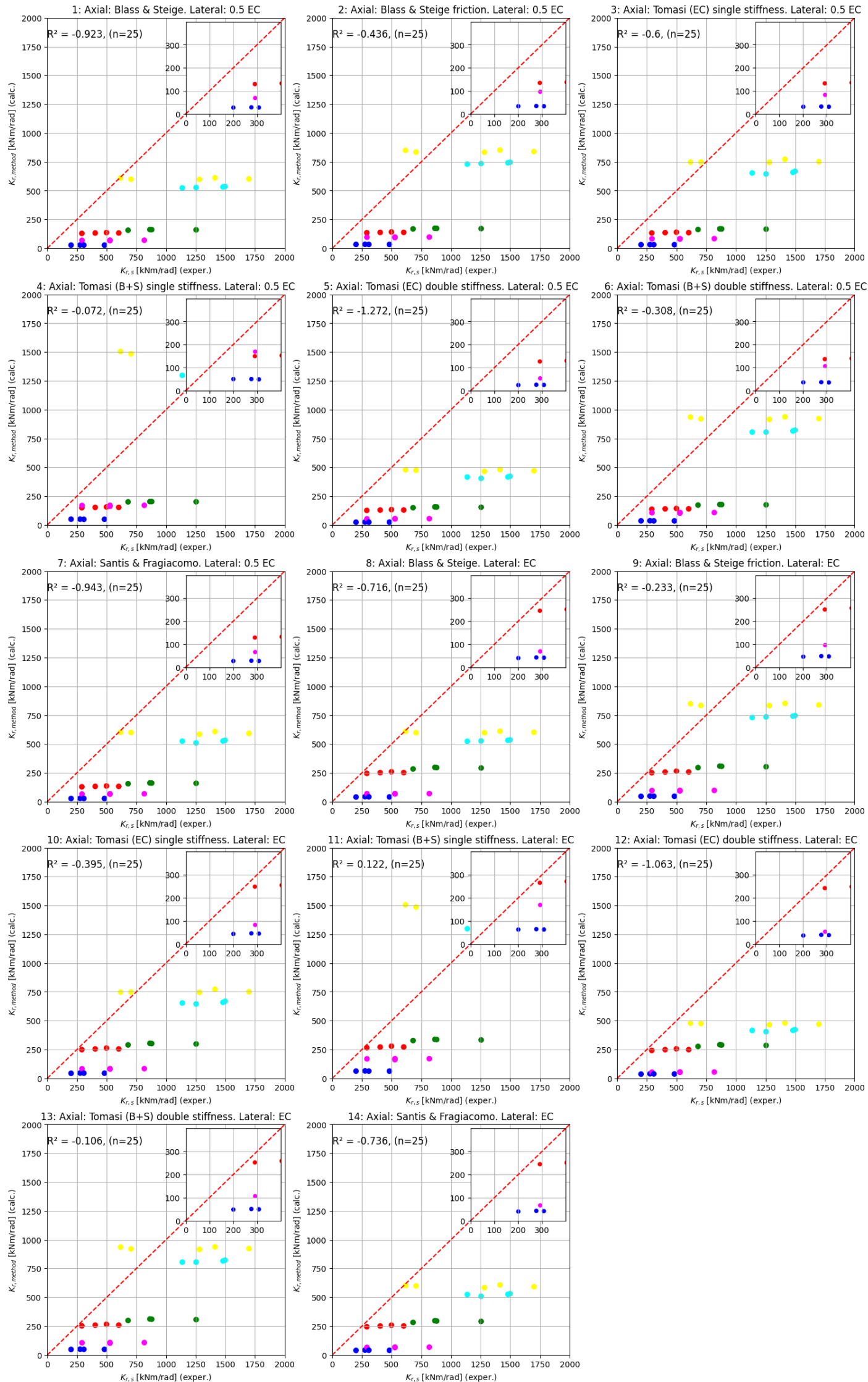
- [57] Masahiro Noguchi and Kohei Komatsu. "A new method for estimating stiffness and strength in bolted timber-to timber joints and its verification by experiments (II): bolted cross-lapped beam to column joints". In: *The Japan Wood Research Society* 50 (2004), pp. 391–399. DOI: 10.1007/s10086-003-0606-y.
- [58] Pollmeier. *Beam BauBuche GL75 - Declaration of Performance (Ref. Nr. PM-019-2022)*. Tech. rep. Austrian Institute of Construction Engineering (Österreichisches Institut für Bautechnik), 2022. URL: <https://www.pollmeier.com/product/beam-baubuche-gl75/#gref>.
- [59] United Nations Environment Programme. *Building Materials and the Climate: Constructing a New Future*. Tech. rep. United Nations Environment Programme, 2023.
- [60] P. Racher. "Moment Resisting Connections". In: Centrum Hout, 1995. Chap. lecture C16. URL: <https://e-step.net/c-joints-2> (visited on 05/02/2024).
- [61] Carmen Sandhaas. "MECHANICAL BEHAVIOUR OF TIMBER JOINTS WITH SLOTTED-IN STEEL PLATES". PhD thesis. Delft University of Technology, 2012.
- [62] Yuri de Santis and Massimo Fragiocomo. "Slip modulus formulas for timber-to-timber inclined screw connections Comparison with other simplified models". In: *The International Network on Timber Engineering Research (INTER)* 54 (2021), pp. 131–145.
- [63] C. Scheer and B. Golze. "Berechnung von Fachwerkkonstruktionen unter Berücksichtigung des durchlaufenden Ober- und Untergurts". In: *Bauen mit Holz* 7 (1981).
- [64] Stephan Schilling. "Structural behaviour and reliability of timber trusses with dowelled steel-to-timber connections". PhD thesis. ETH Zurich, 2022.
- [65] Stephan Schilling et al. "Design of timber trusses with dowelled steel-to-timber connections". In: *The International Network on Timber Engineering Research (INTER)* 55 (Aug. 2022), pp. 285–299. DOI: <https://doi.org/10.3929/ethz-b-000649518>.
- [66] Yvonne Steige and Matthias Frese. "Study on a newly developed diagonal connection for hybrid timber trusses made of spruce glulam and beech laminated veneer lumber". In: *Wood Material Science and Engineering* 14.5 (2019), pp. 280–290. ISSN: 1748-0272 (Print) 1748-0280 (Online). DOI: 10.1080/17480272.2019.1626908.
- [67] Roberto Tomasi, Alessandro Crosatti, and Maurizio Piazza. "Theoretical and experimental analysis of timber-to-timber joints connected with inclined screws". In: *Construction and Building Materials* 24.9 (2010), pp. 1560–1571. ISSN: 09500618. DOI: 10.1016/j.conbuildmat.2010.03.007.
- [68] Peter de Vries. "Collegedictaat CT2052 Deel Houtconstructies". In: Feb. 2012. URL: <https://www.webedu.nl/bestellen/tudelft/?action=order&og=1728> (visited on 04/30/2024).

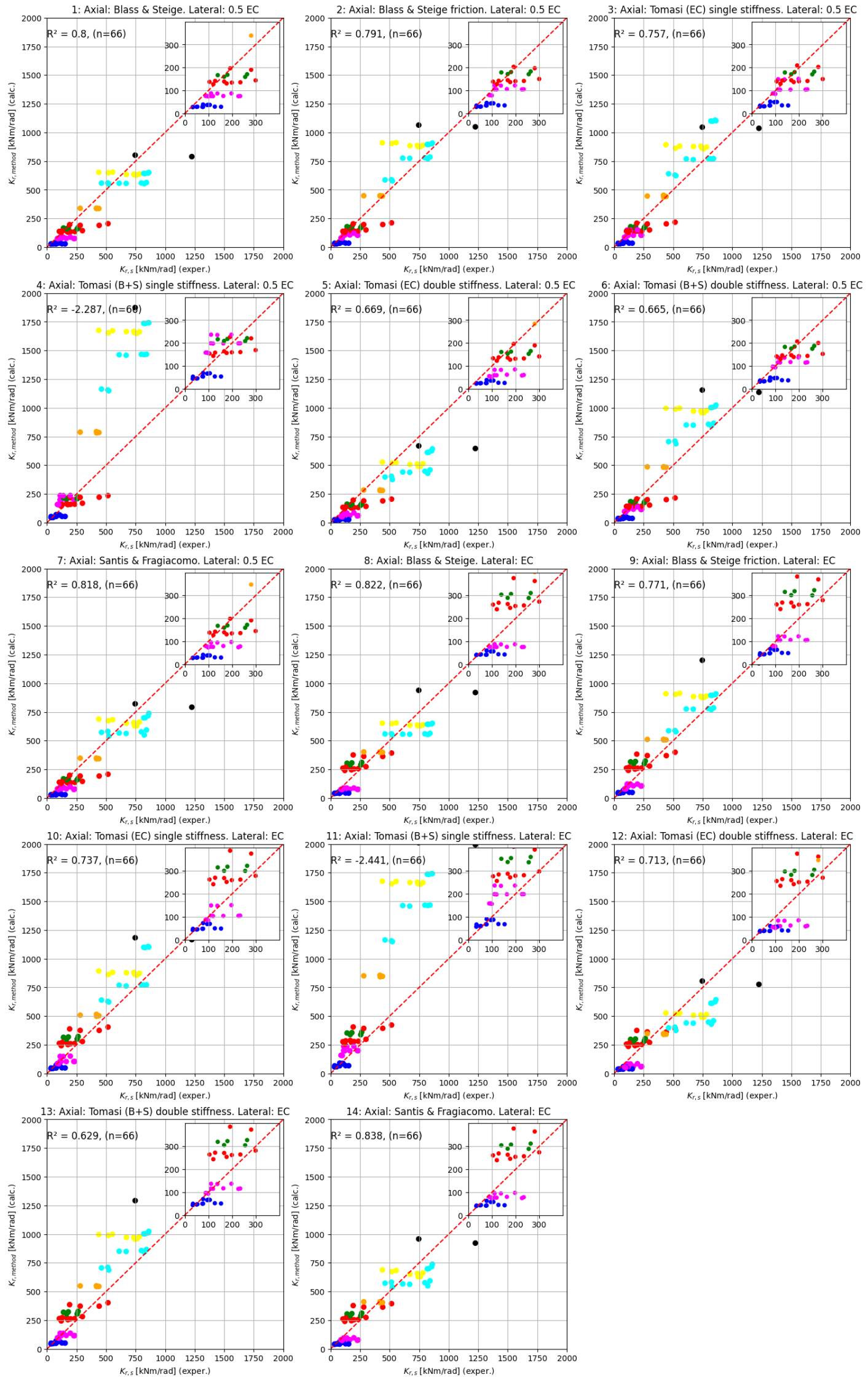


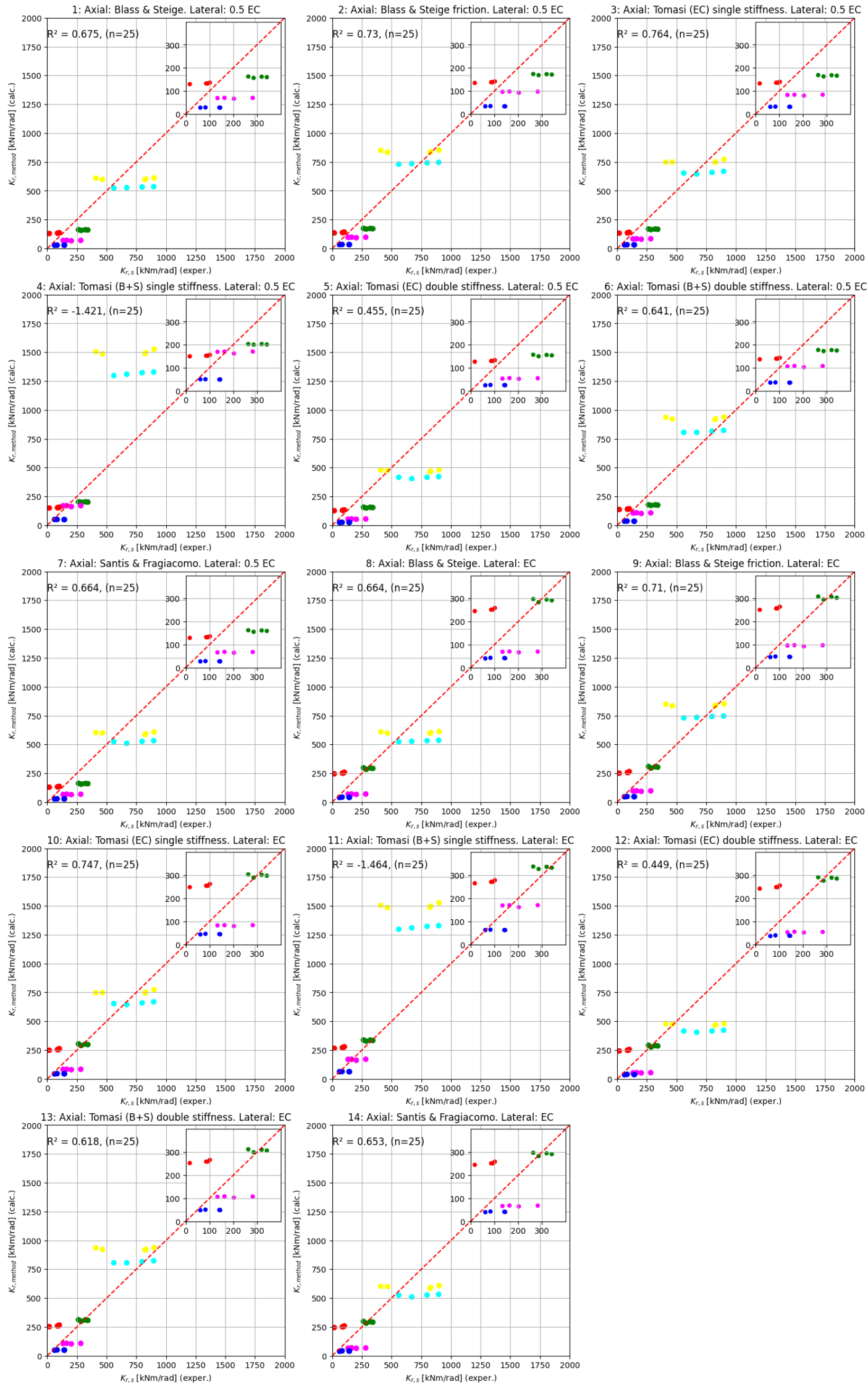
Method plots

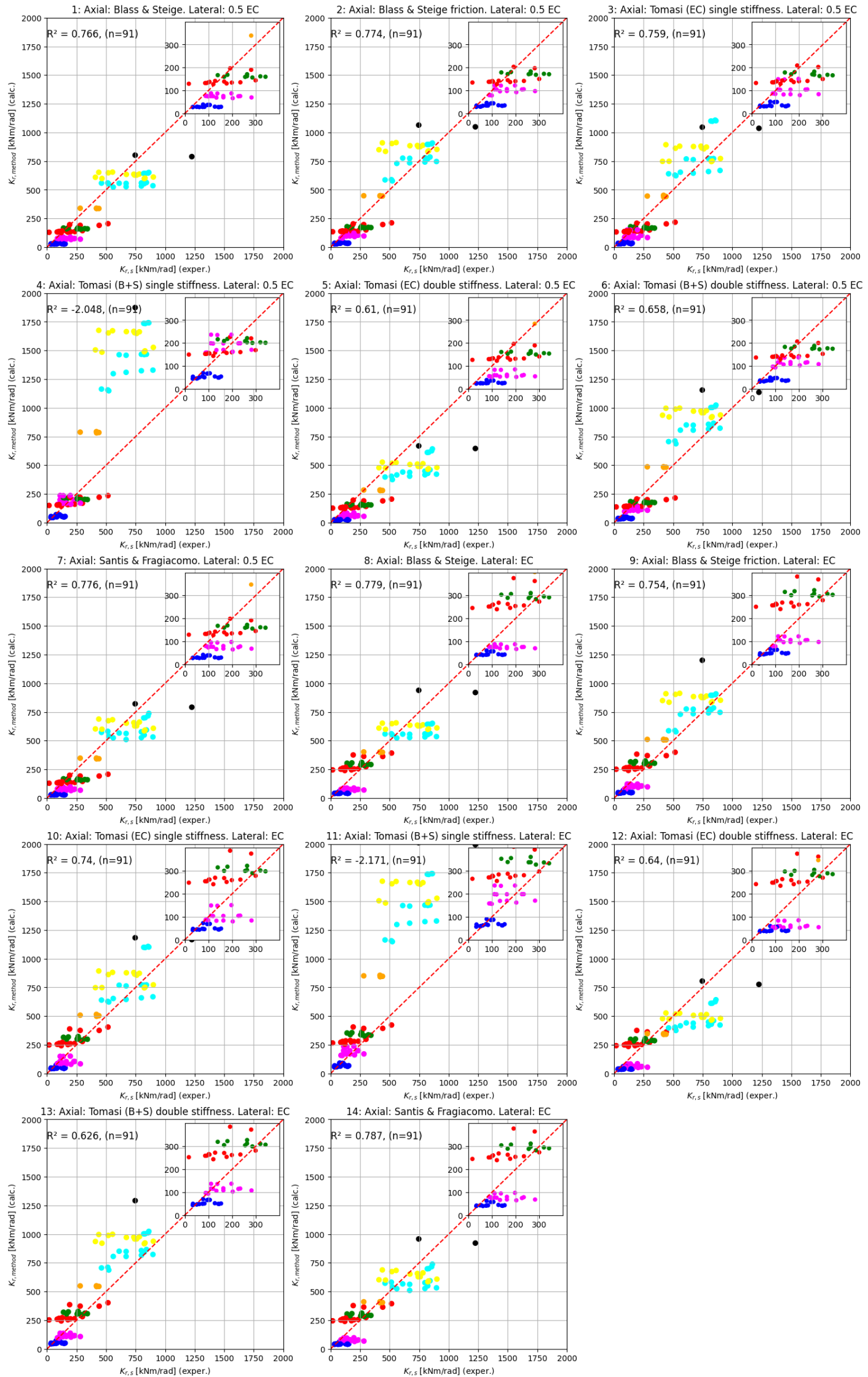
Plots of test series 1, test series 2 and test series 1 after experimental results are adjusted.





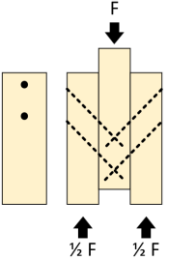
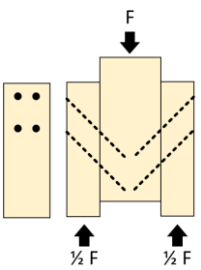
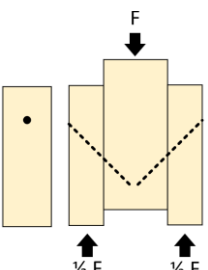
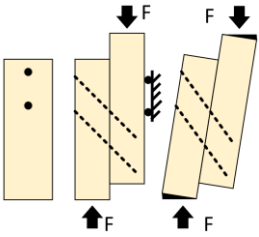


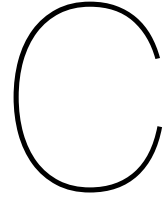




B

Details of performed tests found in
literature

	Double stiffness model (DSM) / single stiffness model (SSM)	Total number of tests performed [-]	Tested angles screw axis-shear plane α_s [°]	Setup of tests
Kevarinmäki	DSM	145 total, 40 for shear-tension	45°	double shear plane compression, 2x2 screws 
Tomasi et al.	DSM / SSM	64 total, 32 for shear-tension	45°, 60°, 75°, 90°	double shear plane compression, 2x2 and 2x4 screws (double row of screws) 
Jockwer et al.	DSM	57 total, 29 for shear-tension	45°, 60°, 90°	double shear plane compression, 2x1 screws 
Blass & Steige	DSM	85 for shear-tension	45°	single shear plane compression, 1x2 screws, perpendicular and diagonal set-up 



Compression screws

To calculate the net force in the bottom screw for screw combinations 3+6 and 4+5, the contributions from the pulling normal force and moment as a result of the rotation are summed (see equation C.1). The total normal force applied on the test specimen N is divided by 4, as there are two shear planes with two screws each. The moment contribution F_M is calculated by dividing the total moment applied to the test specimen M by four times the moment arm r . The moment arm r is calculated as the average of the planned distance in y-direction from the screw to the rotation center of both shear planes.

$$F_{screw} = \frac{N}{4} - F_M \quad (C.1)$$

In which:

- N : Total normal force applied to the test specimen [kN]
- F_M : force contribution from moment M [kNm]. $F_M = \frac{M}{4 \cdot r}$
- $r = \frac{126+90}{2} = 108$ [mm] (see figure 7.5 for distances)
- $r = \frac{54+18}{2} = 36$ [mm] (see figure 7.5 for distances)

The net force in the bottom screw for screw combination 3+4+5+6 is calculated in a similar way, as given by equation C.2. In this case, the total normal force N is divided by 8 as there are two shear planes with 4 screws each. The derivation of the contribution from the moment is given in equations C.3 and C.4.

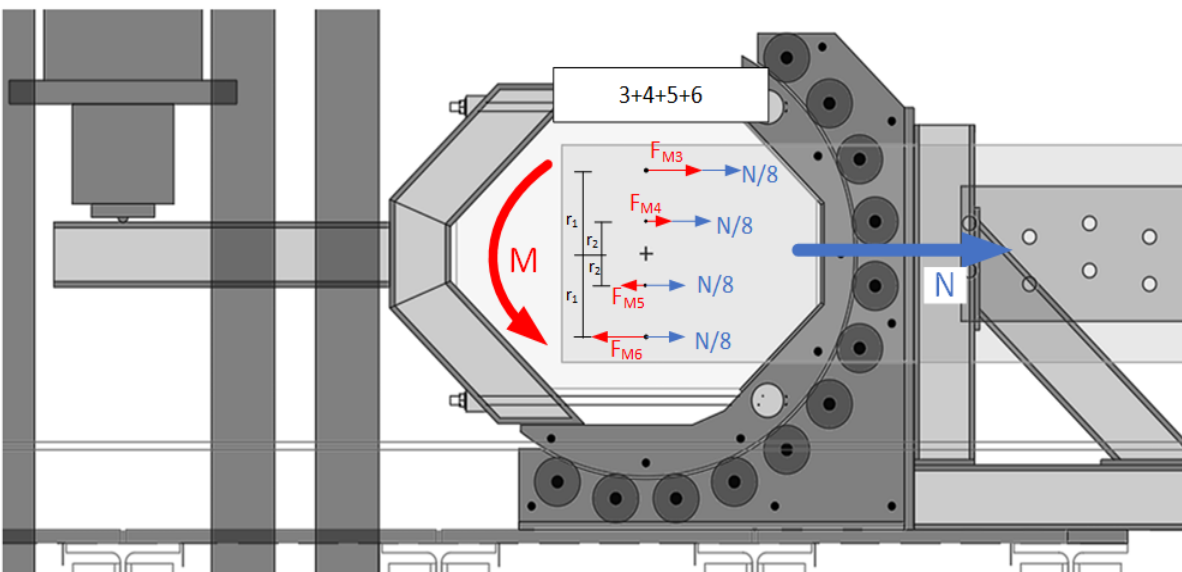
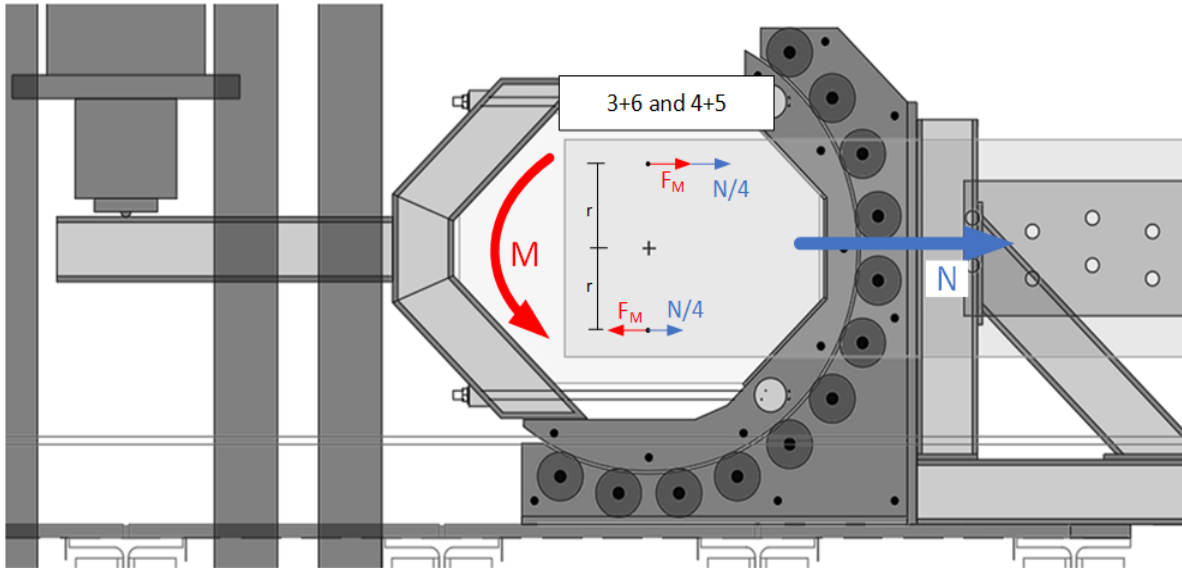
$$F_{screw} = \frac{N}{8} - F_{M6} \quad (C.2)$$

In which:

- N : Total normal force applied to the test specimen [kN]
- F_{M6} : force contribution from moment M [kNm]. $F_{M6} = \frac{M}{4 \cdot (r_1 + \frac{r_2}{r_1} \cdot r_2)}$ (see equations C.3 and C.4)
- $r_1 = \frac{126+90}{2} = 108$ [mm] (see figure 7.5 for distances)
- $r_2 = \frac{54+18}{2} = 36$ [mm] (see figure 7.5 for distances)

$$\left. \begin{aligned} M &= (F_{M3} \cdot r_1 + F_{M4} \cdot r_2 + F_{M5} \cdot r_2 + F_{M6} \cdot r_1) \cdot 2 \\ F_{M3} &= F_{M6} \\ F_{M4} &= F_{M5} \end{aligned} \right\} \Rightarrow M = 4 \cdot (F_{M6} \cdot r_1 + F_{M5} \cdot r_2) \quad (C.3)$$

$$\left. \begin{aligned} M &= 4 \cdot (F_{M6} \cdot r_1 + F_{M5} \cdot r_2) \\ F_{M5} &= \frac{r_2}{r_1} \cdot F_{M6} \end{aligned} \right\} \Rightarrow M = 4 \cdot (F_{M6} \cdot r_1 + F_{M6} \cdot \frac{r_2}{r_1} \cdot r_2) \Rightarrow F_{M6} = \frac{M}{4 \cdot (r_1 + \frac{r_2}{r_1} \cdot r_2)} \quad (C.4)$$



D

Python code plot Noguchi & Komatsu

```
In [3]: import numpy as np
import matplotlib.pyplot as plt
from mpl_toolkits.mplot3d import Axes3D
```

```
In [4]: def function1(Ksi1, Ksi2, xsquared, ysquared):
return (Ksi1 * xsquared + Ksi2 * ysquared) / 1000

def function2(Ksi1, Ksi2, xsquared, ysquared):
return (4 / (((xsquared / Ksi1) / (xsquared ** 2)) + ((ysquared / Ksi2) / (ysquared ** 2))))

x = np.linspace(0.001, 100000, 40)
y = np.linspace(0.001, 100000, 40)

X, Y = np.meshgrid(x, y)
Z1 = function1(1,1,X,Y)
Z2 = function2(1,1,X,Y)

fig, ((ax1, ax2)) = plt.subplots(1, 2, figsize=(11, 5), subplot_kw={'projection': '3d'})

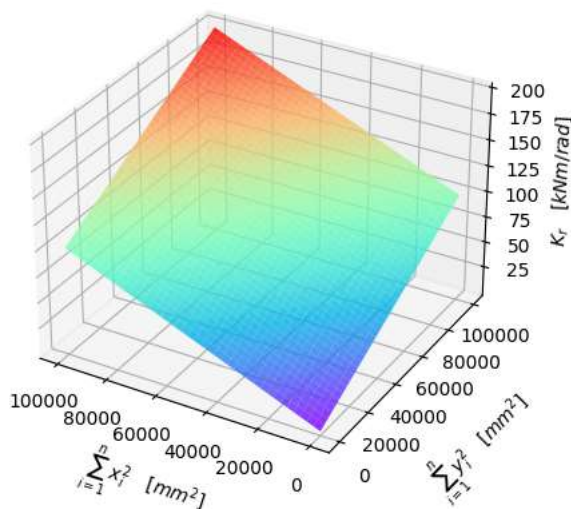
surf1 = ax1.plot_surface(X, Y, Z1, cmap = 'rainbow', alpha=0.8)
ax1.set_title('Conventional theory')
ax1.set_xlabel('$\sum_{i=1}^n x_i^2 \text{ \quad [mm}^2\text{]}$', labelpad=10)
ax1.set_ylabel('$\sum_{i=1}^n y_i^2 \text{ \quad [mm}^2\text{]}$', labelpad=15)
ax1.set_zlabel('$K_r \text{ \quad [kNm/rad]}$')
ax1.invert_xaxis()

surf2 = ax2.plot_surface(X, Y, Z2, cmap = 'rainbow', alpha=0.8)
ax2.set_title('Noguchi & Komatsu')
ax2.set_xlabel('$\sum_{i=1}^n x_i^2 \text{ \quad [mm}^2\text{]}$', labelpad=10)
ax2.set_ylabel('$\sum_{i=1}^n y_i^2 \text{ \quad [mm}^2\text{]}$', labelpad=15)
ax2.set_zlabel('$K_r \text{ \quad [kNm/rad]}$')
ax2.invert_xaxis()

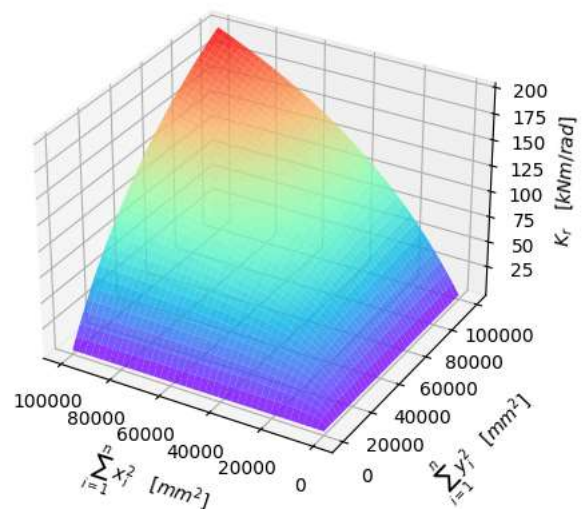
plt.subplots_adjust(wspace=0.1, hspace=0.2)

plt.show();
```

Conventional theory



Noguchi & Komatsu



E

Python code methods

```
In [1]: import numpy as np
import math
import matplotlib.pyplot as plt
import pandas as pd
from pandas import read_excel
!pip install openpyxl
from sklearn.metrics import r2_score
from mpl_toolkits.axes_grid1.inset_locator import inset_axes;
```

C:\Users\Pieter Zeelenberg\Anaconda3\lib\site-packages\numpy_distributor_init.py:32: UserWarning: loaded more than 1 DLL from .libs:
C:\Users\Pieter Zeelenberg\Anaconda3\lib\site-packages\numpy\.libs\libopenblas.GK7GX5KEQ4F6UY03P26ULGBQYHGQ07J4.gfortran-win_amd64.dll
C:\Users\Pieter Zeelenberg\Anaconda3\lib\site-packages\numpy\.libs\libopenblas.XWYDX2IKJW2NMTWSFYNGFUWKQU3LYTCZ.gfortran-win_amd64.dll
stacklevel=1)
Requirement already satisfied: openpyxl in c:\users\pieter zeelenberg\anaconda3\lib\site-packages (3.0.10)
Requirement already satisfied: et_xmlfile in c:\users\pieter zeelenberg\anaconda3\lib\site-packages (from openpyxl) (1.1.0)

```
In [2]: # Load the DataFrame from the Excel file
# Assuming the headers are on the first two rows
df = pd.read_excel('Ergebnisse zusammengestellt_Überarbeitung Pieter - all results.xlsx',
    sheet_name = 'Geometrie', header=[5, 6], index_col = 0)

# Flattening the multi-level columns
df.columns = ['_'.join(map(str, col)).strip() for col in df.columns.values]
df.fillna(0, inplace=True)

df.set_index('Versuchs-Nr. _Unnamed: 1_level_1', inplace=True)

df = df.rename(columns={'Bemerkung _Unnamed: 2_level_1': 'Remark',
    'Prüf-körper _Unnamed: 3_level_1': 'Test Specimen',
    'Laschen_A': 'Latch A', 'Laschen_B': 'Latch B', 'Gurt_M': 'strap M', 'Ø [mm]_8': 'd=8',
    'Ø [mm]_12': 'd=12', 'Neigung_45°': 'Angle=45', 'Neigung_90°': 'Angle=90',
    'Mittlere Dichte_[mm]': 'd', 'Mittlere Dichte_[ ° ]': 'Screw-in angle α',
    'Mittlere Dichte_Seite 1': 'Mittlere_Dichte_Seite_1',
    'Mittlere Dichte_Seite 2': 'Mittlere_Dichte_Seite_2',
    'Mittlere Dichte_-]': 'coefficient_of_friction'})

test_series_2 = df.iloc[:69,:]
test_series_1 = df.iloc[103:130,:]
df = pd.concat([test_series_2, test_series_1])

# # to take out results without friction, uncomment below:
# test_series_21 = df.iloc[:49,:]
# test_series_22 = df.iloc[61:69,:]
# test_series_1 = df.iloc[103:130,:]
# df = pd.concat([test_series_21, test_series_22, test_series_1])
```

```
In [3]: # Loading the rotational stiffness measurements, which are located in the tab Übersicht in the excel file
df2 = pd.read_excel('Ergebnisse zusammengestellt_Überarbeitung Pieter - all results.xlsx',
    sheet_name = 'Übersicht', header=[5, 6])

df2.fillna(0, inplace=True)
df2.set_index(df2.iloc[:,1], inplace=True)

test_series_2 = df2.iloc[:69,:]
test_series_1 = df2.iloc[103:130,:]
df2 = pd.concat([test_series_2, test_series_1])

# # to take out results without friction, uncomment below:
# test_series_21 = df2.iloc[:49,:]
# test_series_22 = df2.iloc[61:69,:]
# test_series_1 = df2.iloc[103:130,:]
# df2 = pd.concat([test_series_21, test_series_22, test_series_1])
```

```
In [4]: class Tomasi:
    def __init__(self, rho1, rhom, rho2, d_outer, L_ef1, L_ef2, alpha, mu, modeltype):
        self.rho_mean1 = np.sqrt(rho1 * rhom)
        self.rho_mean2 = np.sqrt(rho2 * rhom)
        self.rho_typA = rho1
        self.rho_typB = rho2
        self.rho_gurt = rhom
        self.d_outer = d_outer
        self.L_ef1 = L_ef1
        self.L_ef2 = L_ef2
        self.alpha = alpha
        self.mu = mu
        self.modeltype = modeltype
```

```

def screwstiffnessax_EC5newgen(self, rho_inner, rho_outer, row):
    if self.L_ef1 == 0 or self.L_ef2 == 0:
        return 0
    K_serax1 = 160 * (rho_outer / 420) ** 0.85 * self.d_outer ** 0.9 * self.L_ef1 ** 0.6
    K_serax2 = 160 * (rho_inner / 420) ** 0.85 * self.d_outer ** 0.9 * self.L_ef2 ** 0.6
    K_lat = np.sqrt(rho_inner * rho_outer) ** 1.5 * self.d_outer * (1 / 23)
    K_par = 1 / ((1 / K_serax1) + (1 / K_serax2))
    K_serdouble = (K_lat * np.cos(np.deg2rad(self.alpha)) * (np.cos(np.deg2rad(self.alpha))
        - self.mu * np.sin(np.deg2rad(self.alpha))) + K_par * np.sin(np.deg2rad(self.alpha))
        * (np.sin(np.deg2rad(self.alpha)) + self.mu * np.cos(np.deg2rad(self.alpha))))
    K_sersingle = (K_lat * np.cos(np.deg2rad(self.alpha)) * (np.cos(np.deg2rad(self.alpha))
        - self.mu * np.sin(np.deg2rad(self.alpha))) + np.min([K_serax1, K_serax2])
        * np.sin(np.deg2rad(self.alpha)) * (np.sin(np.deg2rad(self.alpha)) + self.mu
        * np.cos(np.deg2rad(self.alpha))))
    if self.modeltype == 'single':
        return K_sersingle
    elif self.modeltype == 'double':
        return K_serdouble

def screwstiffnessax_BS(self, rho_inner, rho_outer, row):
    if self.L_ef1 == 0 or self.L_ef2 == 0:
        return 0
    K_serax1 = 0.48 * self.d_outer ** 0.4 * self.L_ef1 ** 0.4 * rho_outer ** 0.3 * 1000
    K_serax2 = 0.48 * self.d_outer ** 0.4 * self.L_ef2 ** 0.4 * rho_inner ** 0.3 * 1000
    K_lat = np.sqrt(rho_inner * rho_outer) ** 1.5 * self.d_outer * (1 / 23)
    K_par = 1 / ((1 / K_serax1) + (1 / K_serax2))
    K_serdouble = (K_lat * np.cos(np.deg2rad(self.alpha)) * (np.cos(np.deg2rad(self.alpha))
        - self.mu * np.sin(np.deg2rad(self.alpha))) + K_par * np.sin(np.deg2rad(self.alpha))
        * (np.sin(np.deg2rad(self.alpha)) + self.mu * np.cos(np.deg2rad(self.alpha))))
    K_sersingle = (K_lat * np.cos(np.deg2rad(self.alpha)) * (np.cos(np.deg2rad(self.alpha))
        - self.mu * np.sin(np.deg2rad(self.alpha))) + np.min([K_serax1, K_serax2])
        * np.sin(np.deg2rad(self.alpha)) * (np.sin(np.deg2rad(self.alpha)) + self.mu
        * np.cos(np.deg2rad(self.alpha))))
    if self.modeltype == 'single':
        return K_sersingle
    elif self.modeltype == 'double':
        return K_serdouble

def screwstiffnessEC(self, rho):
    EC = (1 / 23) * self.d_outer * rho ** 1.5
    return 0.5 * EC

def rotstiff_05EC_EC5newgen(self, row):
    rotstiffnesslistseite1 = []
    for i in range(10):
        self.L_ef1 = row.iloc[128 + i]
        self.L_ef2 = row.iloc[138 + i]
        ydist = row.iloc[74 + i]
        xdist = row.iloc[64 + i]
        rotstiffnesslistseite1.append(self.screwstiffnessax_EC5newgen(self.rho_gurt, self.rho_typA, row)
            * ydist ** 2 + self.screwstiffnessEC(self.rho_mean1) * xdist ** 2)
    rotstiffnesslistseite2 = []
    for i in range(10):
        self.L_ef1 = row.iloc[148 + i]
        self.L_ef2 = row.iloc[158 + i]
        ydist = row.iloc[96 + i]
        xdist = row.iloc[86 + i]
        rotstiffnesslistseite2.append(self.screwstiffnessax_EC5newgen(self.rho_gurt, self.rho_typB, row)
            * ydist ** 2 + self.screwstiffnessEC(self.rho_mean2) * xdist ** 2)
    return np.sum(np.add(rotstiffnesslistseite1, rotstiffnesslistseite2))

def rotstiff_EC_EC5newgen(self, row):
    rotstiffnesslistseite1 = []
    for i in range(10):
        self.L_ef1 = row.iloc[128 + i]
        self.L_ef2 = row.iloc[138 + i]
        ydist = row.iloc[74 + i]
        xdist = row.iloc[64 + i]
        rotstiffnesslistseite1.append(self.screwstiffnessax_EC5newgen(self.rho_gurt, self.rho_typA, row)
            * ydist ** 2 + 2 * self.screwstiffnessEC(self.rho_mean1) * xdist ** 2)
    rotstiffnesslistseite2 = []
    for i in range(10):
        self.L_ef1 = row.iloc[148 + i]
        self.L_ef2 = row.iloc[158 + i]
        ydist = row.iloc[96 + i]
        xdist = row.iloc[86 + i]
        rotstiffnesslistseite2.append(self.screwstiffnessax_EC5newgen(self.rho_gurt, self.rho_typB, row)
            * ydist ** 2 + 2 * self.screwstiffnessEC(self.rho_mean2) * xdist ** 2)
    return np.sum(np.add(rotstiffnesslistseite1, rotstiffnesslistseite2))

def rotstiff_05EC_BS(self, row):
    rotstiffnesslistseite1 = []

```

```

for i in range(10):
    self.L_ef1 = row.iloc[128 + i]
    self.L_ef2 = row.iloc[138 + i]
    ydist = row.iloc[74 + i]
    xdist = row.iloc[64 + i]
    rotstiffnesslistseite1.append(self.screwstiffnessax_BS(self.rho_gurt, self.rho_typA, row)
        * ydist ** 2 + self.screwstiffnessEC(self.rho_mean1) * xdist ** 2)
rotstiffnesslistseite2 = []
for i in range(10):
    self.L_ef1 = row.iloc[148 + i]
    self.L_ef2 = row.iloc[158 + i]
    ydist = row.iloc[96 + i]
    xdist = row.iloc[86 + i]
    rotstiffnesslistseite2.append(self.screwstiffnessax_BS(self.rho_gurt, self.rho_typB, row)
        * ydist ** 2 + self.screwstiffnessEC(self.rho_mean2) * xdist ** 2)
return np.sum(np.add(rotstiffnesslistseite1, rotstiffnesslistseite2))

def rotstiff_EC_BS(self, row):
    rotstiffnesslistseite1 = []
    for i in range(10):
        self.L_ef1 = row.iloc[128 + i]
        self.L_ef2 = row.iloc[138 + i]
        ydist = row.iloc[74 + i]
        xdist = row.iloc[64 + i]
        rotstiffnesslistseite1.append(self.screwstiffnessax_BS(self.rho_gurt, self.rho_typA, row) * ydist ** 2
            + 2 * self.screwstiffnessEC(self.rho_mean1) * xdist ** 2)
    rotstiffnesslistseite2 = []
    for i in range(10):
        self.L_ef1 = row.iloc[148 + i]
        self.L_ef2 = row.iloc[158 + i]
        ydist = row.iloc[96 + i]
        xdist = row.iloc[86 + i]
        rotstiffnesslistseite2.append(self.screwstiffnessax_BS(self.rho_gurt, self.rho_typB, row) * ydist ** 2
            + 2 * self.screwstiffnessEC(self.rho_mean2) * xdist ** 2)
    return np.sum(np.add(rotstiffnesslistseite1, rotstiffnesslistseite2))

df['kr_tomasi_and_0.5EC_EC5newgen_single'] = df.apply(lambda x: Tomasi(x['Rohdichten [kg/m³]_Typ A'],
    x['Rohdichten [kg/m³]_Gurt'], x['Rohdichten [kg/m³]_Typ B'], x['d'],
    0, 0, 90 - x['Screw-in angle α'], x['coefficient_of_friction'],
    'single').rotstiff_05EC_EC5newgen(x), axis=1)
df['kr_tomasi_and_0.5EC_BS_single'] = df.apply(lambda x: Tomasi(x['Rohdichten [kg/m³]_Typ A'],
    x['Rohdichten [kg/m³]_Gurt'], x['Rohdichten [kg/m³]_Typ B'], x['d'],
    0, 0, 90 - x['Screw-in angle α'], x['coefficient_of_friction'],
    'single').rotstiff_05EC_BS(x), axis=1)
df['kr_tomasi_and_0.5EC_EC5newgen_double'] = df.apply(lambda x: Tomasi(x['Rohdichten [kg/m³]_Typ A'],
    x['Rohdichten [kg/m³]_Gurt'], x['Rohdichten [kg/m³]_Typ B'], x['d'],
    0, 0, 90 - x['Screw-in angle α'], x['coefficient_of_friction'],
    'double').rotstiff_05EC_EC5newgen(x), axis=1)
df['kr_tomasi_and_0.5EC_BS_double'] = df.apply(lambda x: Tomasi(x['Rohdichten [kg/m³]_Typ A'],
    x['Rohdichten [kg/m³]_Gurt'], x['Rohdichten [kg/m³]_Typ B'], x['d'],
    0, 0, 90 - x['Screw-in angle α'], x['coefficient_of_friction'],
    'double').rotstiff_05EC_BS(x), axis=1)
df['kr_tomasi_and_EC_EC5newgen_single'] = df.apply(lambda x: Tomasi(x['Rohdichten [kg/m³]_Typ A'],
    x['Rohdichten [kg/m³]_Gurt'], x['Rohdichten [kg/m³]_Typ B'], x['d'],
    0, 0, 90 - x['Screw-in angle α'], x['coefficient_of_friction'],
    'single').rotstiff_EC_EC5newgen(x), axis=1)
df['kr_tomasi_and_EC_BS_single'] = df.apply(lambda x: Tomasi(x['Rohdichten [kg/m³]_Typ A'],
    x['Rohdichten [kg/m³]_Gurt'], x['Rohdichten [kg/m³]_Typ B'], x['d'],
    0, 0, 90 - x['Screw-in angle α'], x['coefficient_of_friction'],
    'single').rotstiff_EC_BS(x), axis=1)
df['kr_tomasi_and_EC_EC5newgen_double'] = df.apply(lambda x: Tomasi(x['Rohdichten [kg/m³]_Typ A'],
    x['Rohdichten [kg/m³]_Gurt'], x['Rohdichten [kg/m³]_Typ B'], x['d'],
    0, 0, 90 - x['Screw-in angle α'], x['coefficient_of_friction'],
    'double').rotstiff_EC_EC5newgen(x), axis=1)
df['kr_tomasi_and_EC_BS_double'] = df.apply(lambda x: Tomasi(x['Rohdichten [kg/m³]_Typ A'],
    x['Rohdichten [kg/m³]_Gurt'], x['Rohdichten [kg/m³]_Typ B'], x['d'],
    0, 0, 90 - x['Screw-in angle α'], x['coefficient_of_friction'],
    'double').rotstiff_EC_BS(x), axis=1)

```

```

In [5]: class Blasssteige:
    def __init__(self, alpha, d_outer, L_ef1, L_ef2, rho1, rhom, rho2, mu):
        self.alpha = alpha
        self.d_outer = d_outer
        self.L_ef1 = L_ef1
        self.L_ef2 = L_ef2
        self.alpha = alpha
        self.rho1 = rho1
        self.rhom = rhom
        self.rho2 = rho2
        self.mu = mu

```

```

def screwstiffnessax(self, rho_outer, rho_m):
    if self.L_ef1 == 0 or self.L_ef2 == 0:
        return 0
    else:
        k_ax1 = 0.48 * self.d_outer ** 0.4 * self.L_ef1 ** 0.4 * rho_outer ** 0.3 * 1000
        k_ax2 = 0.48 * self.d_outer ** 0.4 * self.L_ef2 ** 0.4 * rho_m ** 0.3 * 1000
        k = (np.cos(np.deg2rad(self.alpha)) ** 2) / ((1 / k_ax1) + (1 / k_ax2))
        return k

def screwstiffnessEC(self, rho):
    EC = (1 / 23) * self.d_outer * rho ** 1.5
    return 0.5 * EC

def rotstiff_05EC(self, row):
    rotstiffnesslistseite1 = []
    for i in range(10):
        self.L_ef1 = row.iloc[128 + i]
        self.L_ef2 = row.iloc[138 + i]
        ydist = row.iloc[74 + i]
        xdist = row.iloc[64 + i]
        rotstiffnesslistseite1.append(self.screwstiffnessax(self.rho1, self.rhom) * ydist ** 2
                                     + self.screwstiffnessEC(np.sqrt(self.rho1 * self.rhom)) * xdist ** 2)
    rotstiffnesslistseite2 = []
    for i in range(10):
        self.L_ef1 = row.iloc[148 + i]
        self.L_ef2 = row.iloc[158 + i]
        ydist = row.iloc[96 + i]
        xdist = row.iloc[86 + i]
        rotstiffnesslistseite2.append(self.screwstiffnessax(self.rho2, self.rhom) * ydist ** 2
                                     + self.screwstiffnessEC(np.sqrt(self.rho2 * self.rhom)) * xdist ** 2)
    return np.sum(np.add(rotstiffnesslistseite1, rotstiffnesslistseite2))

def rotstiff_EC(self, row):
    rotstiffnesslistseite1 = []
    for i in range(10):
        self.L_ef1 = row.iloc[128 + i]
        self.L_ef2 = row.iloc[138 + i]
        ydist = row.iloc[74 + i]
        xdist = row.iloc[64 + i]
        rotstiffnesslistseite1.append(self.screwstiffnessax(self.rho1, self.rhom) * ydist ** 2
                                     + 2 * self.screwstiffnessEC(np.sqrt(self.rho1 * self.rhom)) * xdist ** 2)
    rotstiffnesslistseite2 = []
    for i in range(10):
        self.L_ef1 = row.iloc[148 + i]
        self.L_ef2 = row.iloc[158 + i]
        ydist = row.iloc[96 + i]
        xdist = row.iloc[86 + i]
        rotstiffnesslistseite2.append(self.screwstiffnessax(self.rho2, self.rhom) * ydist ** 2
                                     + 2 * self.screwstiffnessEC(np.sqrt(self.rho2 * self.rhom)) * xdist ** 2)
    return np.sum(np.add(rotstiffnesslistseite1, rotstiffnesslistseite2))

# Add a new column to the DataFrame. L_ef1 and L_ef2 are inserted as 0 because they are
# overwritten in rotstiff method.

df['kr_blasssteige_and_05EC'] = df.apply(lambda x: Blasssteige(x['Screw-in angle α'], x['d'], 0, 0,
                                                             x['Rohdichten [kg/m³]_Typ A'], x['Rohdichten [kg/m³]_Gurt'],
                                                             x['Rohdichten [kg/m³]_Typ B'], 0.25).rotstiff_05EC(x), axis=1)

df['kr_blasssteige_and_EC'] = df.apply(lambda x: Blasssteige(x['Screw-in angle α'], x['d'], 0, 0,
                                                             x['Rohdichten [kg/m³]_Typ A'], x['Rohdichten [kg/m³]_Gurt'],
                                                             x['Rohdichten [kg/m³]_Typ B'], 0.25).rotstiff_EC(x), axis=1)

```

In [6]:

```

class Blasssteigewithfriction:
    def __init__(self, alpha, mu, d_outer, L_ef1, L_ef2, rho1, rhom, rho2):
        self.alpha = alpha
        self.mu = mu
        self.d_outer = d_outer
        self.L_ef1 = L_ef1
        self.L_ef2 = L_ef2
        self.alpha = alpha
        self.rho1 = rho1
        self.rhom = rhom
        self.rho2 = rho2

    def screwstiffnessax(self, rho_outer, rho_m, row):
        # prevent division by zero in final return
        if self.L_ef1 == 0 or self.L_ef2 == 0:
            return 0
        k_ax1 = 0.48 * self.d_outer ** 0.4 * self.L_ef1 ** 0.4 * rho_outer ** 0.3 * 1000
        k_ax2 = 0.48 * self.d_outer ** 0.4 * self.L_ef2 ** 0.4 * rho_m ** 0.3 * 1000
        k = (((1 + self.mu * np.tan(np.deg2rad(self.alpha)))) * np.cos(np.deg2rad(self.alpha)) ** 2)
            / ((1 / k_ax1) + (1 / k_ax2)))

```

```

return k

def screwstiffnessEC(self, rho):
    EC = (1 / 23) * self.d_outer * rho ** 1.5
    return 0.5 * EC

def rotstiff_05EC(self, row):
    rotstiffnesslistseite1 = []
    for i in range(10):
        self.L_ef1 = row.iloc[128 + i]
        self.L_ef2 = row.iloc[138 + i]
        ydist = row.iloc[74 + i]
        xdist = row.iloc[64 + i]
        rotstiffnesslistseite1.append(self.screwstiffnessax(self.rho1, self.rhom, row) * ydist ** 2
                                     + self.screwstiffnessEC(np.sqrt(self.rho1 * self.rhom)) * xdist ** 2 )
    rotstiffnesslistseite2 = []
    for i in range(10):
        self.L_ef1 = row.iloc[148 + i]
        self.L_ef2 = row.iloc[158 + i]
        ydist = row.iloc[96 + i]
        xdist = row.iloc[86 + i]
        rotstiffnesslistseite2.append(self.screwstiffnessax(self.rho2, self.rhom, row) * ydist ** 2
                                     + self.screwstiffnessEC(np.sqrt(self.rho2 * self.rhom)) * xdist ** 2 )
    return np.sum(np.add(rotstiffnesslistseite1, rotstiffnesslistseite2))

def rotstiff_EC(self, row):
    rotstiffnesslistseite1 = []
    for i in range(10):
        self.L_ef1 = row.iloc[128 + i]
        self.L_ef2 = row.iloc[138 + i]
        ydist = row.iloc[74 + i]
        xdist = row.iloc[64 + i]
        rotstiffnesslistseite1.append(self.screwstiffnessax(self.rho1, self.rhom, row) * ydist ** 2
                                     + 2 * self.screwstiffnessEC(np.sqrt(self.rho1 * self.rhom)) * xdist ** 2 )
    rotstiffnesslistseite2 = []
    for i in range(10):
        self.L_ef1 = row.iloc[148 + i]
        self.L_ef2 = row.iloc[158 + i]
        ydist = row.iloc[96 + i]
        xdist = row.iloc[86 + i]
        rotstiffnesslistseite2.append(self.screwstiffnessax(self.rho2, self.rhom, row) * ydist ** 2
                                     + 2 * self.screwstiffnessEC(np.sqrt(self.rho2 * self.rhom)) * xdist ** 2 )
    return np.sum(np.add(rotstiffnesslistseite1, rotstiffnesslistseite2))

df['kr_blasssteigewithfriction_and_EC'] = df.apply(lambda x: Blasssteigewithfriction(x['Screw-in angle  $\alpha$ '],
                                          x['coefficient_of_friction'], x['d'], 0, 0,
                                          x['Rohdichten [kg/m3']_Typ A'],
                                          x['Rohdichten [kg/m3']_Gurt'],
                                          x['Rohdichten [kg/m3']_Typ B']).rotstiff_EC(x), axis=1)

df['kr_blasssteigewithfriction_and_05EC'] = df.apply(lambda x: Blasssteigewithfriction(x['Screw-in angle  $\alpha$ '],
                                          x['coefficient_of_friction'], x['d'], 0, 0,
                                          x['Rohdichten [kg/m3']_Typ A'],
                                          x['Rohdichten [kg/m3']_Gurt'],
                                          x['Rohdichten [kg/m3']_Typ B']).rotstiff_05EC(x), axis=1)

```

```

In [7]: class santisfragiacomo:
    def __init__(self, rho1, rho2, rhom, L_ef1, L_ef2, d_outer, theta):
        self.rho1 = rho1
        self.rho2 = rho2
        self.rhom = rhom
        self.L_ef1 = L_ef1
        self.L_ef2 = L_ef2
        self.d_outer = d_outer
        self.theta = theta

    def interpolate(self):
        if 0 <= self.theta <= 15:
            return 1.04, 0.056, 1.11, 0.18
        elif 15 < self.theta <= 30:
            aa = np.interp(self.theta, [15, 30], [1.04, 1.07])
            bb = np.interp(self.theta, [15, 30], [0.056, 0.51])
            cc = np.interp(self.theta, [15, 30], [1.11, 0.76])
            dd = np.interp(self.theta, [15, 30], [0.18, 0.31])
            return aa, bb, cc, dd
        elif 30 < self.theta <= 45:
            aa = np.interp(self.theta, [30, 45], [1.07, 1.07])
            bb = np.interp(self.theta, [30, 45], [0.51, 0.68])
            cc = np.interp(self.theta, [30, 45], [0.76, 0.65])
            dd = np.interp(self.theta, [30, 45], [0.31, 0.29])
            return aa, bb, cc, dd

```

```

        elif 45 < self.theta <= 60:
            aa = np.interp(self.theta, [45, 60], [1.07, 1.09])
            bb = np.interp(self.theta, [45, 60], [0.68, 0.77])
            cc = np.interp(self.theta, [45, 60], [0.65, 0.58])
            dd = np.interp(self.theta, [45, 60], [0.29, 0.23])
            return aa, bb, cc, dd
        elif 60 < self.theta <= 75:
            aa = np.interp(self.theta, [60, 75], [1.09, 1.14])
            bb = np.interp(self.theta, [60, 75], [0.77, 0.68])
            cc = np.interp(self.theta, [60, 75], [0.58, 0.47])
            dd = np.interp(self.theta, [60, 75], [0.23, 0.095])
            return aa, bb, cc, dd
        else:
            raise ValueError("theta value is out of range (0 <= theta <= 75)")

def screwstiffnessax(self, rho_1, rho_2):
    if self.L_ef1 == 0 or self.L_ef2 == 0:
        return 0
    aa, bb, cc, dd = self.interpolate()
    if self.theta < 15:
        k_serint = dd * (rho_1 ** aa * self.L_ef1 ** bb + rho_2 ** aa * self.L_ef2 ** bb) * self.d_outer ** cc
    elif 15 <= self.theta < 30:
        aa_15, bb_15, cc_15, dd_15 = self.interpolate(15)
        aa_30, bb_30, cc_30, dd_30 = self.interpolate(30)
        kserint15 = (dd_15 * (rho_1 ** aa_15 * self.L_ef1 ** bb_15
            + rho_2 ** aa_15 * self.L_ef2 ** bb_15) * self.d_outer ** cc_15)
        kserint30 = ((dd_30 * self.d_outer ** cc_30) / ((1 / (rho_1 ** aa_30 * self.L_ef1 ** bb_30))
            + (1 / (rho_2 ** aa_30 * self.L_ef2 ** bb_30))))
        k_serint = np.interp(self.theta, [15, 30], [kserint15, kserint30])
    else:
        k_serint = ((dd * self.d_outer ** cc) / ((1 / (rho_1 ** aa * self.L_ef1 ** bb))
            + (1 / (rho_2 ** aa * self.L_ef2 ** bb))))
    return k_serint

def screwstiffnessEC(self, rho_1, rho_2):
    EC = (1 / 23) * self.d_outer * np.sqrt(rho_1 * rho_2) ** 1.5
    return 0.5 * EC

def rotstiff_05EC(self, row):
    rotstiffnesslistseite1 = []
    for i in range(10):
        self.L_ef1 = row.iloc[128 + i]
        self.L_ef2 = row.iloc[138 + i]
        ydist = row.iloc[74 + i]
        xdist = row.iloc[64 + i]
        rotstiffnesslistseite1.append(self.screwstiffnessax(self.rho1, self.rhom)
            * ydist ** 2 + self.screwstiffnessEC(self.rho1, self.rhom) * xdist ** 2)
    rotstiffnesslistseite2 = []
    for i in range(10):
        self.L_ef1 = row.iloc[148 + i]
        self.L_ef2 = row.iloc[158 + i]
        ydist = row.iloc[96 + i]
        xdist = row.iloc[86 + i]
        rotstiffnesslistseite2.append(self.screwstiffnessax(self.rho2, self.rhom)
            * ydist ** 2 + self.screwstiffnessEC(self.rho2, self.rhom) * xdist ** 2)
    return np.sum(np.add(rotstiffnesslistseite1, rotstiffnesslistseite2))

def rotstiff_EC(self, row):
    rotstiffnesslistseite1 = []
    for i in range(10):
        self.L_ef1 = row.iloc[128 + i]
        self.L_ef2 = row.iloc[138 + i]
        ydist = row.iloc[74 + i]
        xdist = row.iloc[64 + i]
        rotstiffnesslistseite1.append(self.screwstiffnessax(self.rho1, self.rhom)
            * ydist ** 2 + 2 * self.screwstiffnessEC(self.rho1, self.rhom) * xdist ** 2)
    rotstiffnesslistseite2 = []
    for i in range(10):
        self.L_ef1 = row.iloc[148 + i]
        self.L_ef2 = row.iloc[158 + i]
        ydist = row.iloc[96 + i]
        xdist = row.iloc[86 + i]
        rotstiffnesslistseite2.append(self.screwstiffnessax(self.rho2, self.rhom)
            * ydist ** 2 + 2 * self.screwstiffnessEC(self.rho2, self.rhom) * xdist ** 2)
    return np.sum(np.add(rotstiffnesslistseite1, rotstiffnesslistseite2))

df['kr_santisfragiaco_and_EC'] = df.apply(lambda x: santisfragiaco(
    x['Rohdichten [kg/m³]_Typ A'],
    x['Rohdichten [kg/m³]_Typ B'],
    x['Rohdichten [kg/m³]_Gurt'],
    0, 0, x['d'], 90 - x['Screw-in angle α']
), rotstiff_EC(x), axis=1)

```

```
df['kr_santisfragiaco_and_05EC'] = df.apply(lambda x: santisfragiaco(
    x['Rohdichten [kg/m³]_Typ A'],
    x['Rohdichten [kg/m³]_Typ B'],
    x['Rohdichten [kg/m³]_Gurt'],
    0, 0, x['d'], 90 - x['Screw-in angle α']
), rotstiff_05EC(x), axis=1)
```

```
In [8]: rows_to_drop = df2[df2.iloc[:, -9] == 0].index

# Drop these rows without measured values from df and df2
df2.drop(index=rows_to_drop, inplace=True)
df.drop(index=rows_to_drop, inplace=True)
```

```
In [9]: # Rather Long method to categorize the screw configuration types, in order to plot them in separate colors

df['category1'] = np.where((df['Schraubenbild_1']== 'x') & (df['Schraubenbild_2']== 0) &
    (df['Schraubenbild_3']== 0) & (df['Schraubenbild_4']== 0) & (df['Schraubenbild_5']== 0) &
    (df['Schraubenbild_6']== 0) & (df['Schraubenbild_7']== 0) & (df['Schraubenbild_8']== 'x'), 1, 0)
df['category2'] = np.where((df['Schraubenbild_1']== 0) & (df['Schraubenbild_2']== 'x') &
    (df['Schraubenbild_3']== 0) & (df['Schraubenbild_4']== 0) & (df['Schraubenbild_5']== 0) &
    (df['Schraubenbild_6']== 0) & (df['Schraubenbild_7']== 'x') & (df['Schraubenbild_8']== 0), 2, 0)
df['category3'] = np.where((df['Schraubenbild_1']== 'x') & (df['Schraubenbild_2']== 'x') &
    (df['Schraubenbild_3']== 0) & (df['Schraubenbild_4']== 0) & (df['Schraubenbild_5']== 0) &
    (df['Schraubenbild_6']== 0) & (df['Schraubenbild_7']== 'x') & (df['Schraubenbild_8']== 'x'), 3, 0)
df['category4'] = np.where((df['Schraubenbild_1']== 0) & (df['Schraubenbild_2']== 0) &
    (df['Schraubenbild_3']== 'x') & (df['Schraubenbild_4']== 0) & (df['Schraubenbild_5']== 0) &
    (df['Schraubenbild_6']== 'x') & (df['Schraubenbild_7']== 0) & (df['Schraubenbild_8']== 0), 4, 0)
df['category5'] = np.where((df['Schraubenbild_1']== 0) & (df['Schraubenbild_2']== 0) &
    (df['Schraubenbild_3']== 0) & (df['Schraubenbild_4']== 'x') & (df['Schraubenbild_5']== 'x') &
    (df['Schraubenbild_6']== 0) & (df['Schraubenbild_7']== 0) & (df['Schraubenbild_8']== 0), 5, 0)
df['category6'] = np.where((df['Schraubenbild_1']== 0) & (df['Schraubenbild_2']== 0) &
    (df['Schraubenbild_3']== 'x') & (df['Schraubenbild_4']== 'x') & (df['Schraubenbild_5']== 'x') &
    (df['Schraubenbild_6']== 'x') & (df['Schraubenbild_7']== 0) & (df['Schraubenbild_8']== 0), 6, 0)
df['category7'] = np.where((df['Schraubenbild_1']== 'x') & (df['Schraubenbild_2']== 'x') &
    (df['Schraubenbild_3']== 'x') & (df['Schraubenbild_4']== 'x') & (df['Schraubenbild_5']== 'x') &
    (df['Schraubenbild_6']== 'x') & (df['Schraubenbild_7']== 'x') & (df['Schraubenbild_8']== 'x'), 7, 0)
df['category8'] = np.where((df['Schraubenbild_1']== 0) & (df['Schraubenbild_2']== 0) &
    (df['Schraubenbild_3']== 0) & (df['Schraubenbild_4']== 0) & (df['Schraubenbild_5']== 0) &
    (df['Schraubenbild_6']== 0) & (df['Schraubenbild_7']== 0) & (df['Schraubenbild_8']== 0) &
    (df['Schraubenbild_9']== 'x') & (df['Schraubenbild_10']== 'x'), 8, 0)
df['category9'] = np.where((df['Schraubenbild_1']== 'x') & (df['Schraubenbild_2']== 0) &
    (df['Schraubenbild_3']== 0) & (df['Schraubenbild_4']== 0) & (df['Schraubenbild_5']== 0) &
    (df['Schraubenbild_6']== 0) & (df['Schraubenbild_7']== 0) & (df['Schraubenbild_8']== 0) &
    (df['Schraubenbild_9']== 0) & (df['Schraubenbild_10']== 0), 9, 0)

df['category'] = (df['category1'] + df['category2'] + df['category3'] + df['category4'] + df['category5'] +
    df['category6'] + df['category7'] + df['category8'] + df['category9'])
```

```
In [10]: # Map categories to colors
colors = {1: 'red', 2: 'blue', 3: 'green', 4: 'cyan', 5: 'magenta', 6: 'yellow',
    7: 'black', 8: 'orange', 9: 'yellow'}
df['color'] = df['category'].map(colors)
```

```
In [11]: # Prepare data
x_data = df2['modifizierter Verschiebungs-modul Kr,s']
colors = df['color']

# Define figure and axes
fig, axs = plt.subplots(5, 3, figsize=(18, 30))

# List of y-data and titles
y_data = [
    df['kr_blassesteige_and_05EC'] / 1000000,
    df['kr_blassesteigewithfriction_and_05EC'] / 1000000,
    df['kr_tomasi_and_0.5EC_EC5newgen_single'] / 1000000,
    df['kr_tomasi_and_0.5EC_BS_single'] / 1000000,
    df['kr_tomasi_and_0.5EC_EC5newgen_double'] / 1000000,
    df['kr_tomasi_and_0.5EC_BS_double'] / 1000000,
    df['kr_santisfragiaco_and_05EC'] / 1000000,
    df['kr_blassesteige_and_EC'] / 1000000,
    df['kr_blassesteigewithfriction_and_EC'] / 1000000,
    df['kr_tomasi_and_EC_EC5newgen_single'] / 1000000,
    df['kr_tomasi_and_EC_BS_single'] / 1000000,
    df['kr_tomasi_and_EC_EC5newgen_double'] / 1000000,
    df['kr_tomasi_and_EC_BS_double'] / 1000000,
    df['kr_santisfragiaco_and_EC'] / 1000000
]
titles = [
    '1: Axial: Blass & Steige. Lateral: 0.5 EC',
    '2: Axial: Blass & Steige friction. Lateral: 0.5 EC',
```

```

'3: Axial: Tomasi (EC) single stiffness. Lateral: 0.5 EC',
'4: Axial: Tomasi (B+S) single stiffness. Lateral: 0.5 EC',
'5: Axial: Tomasi (EC) double stiffness. Lateral: 0.5 EC',
'6: Axial: Tomasi (B+S) double stiffness. Lateral: 0.5 EC',
'7: Axial: Santis & Fragiaco. Lateral: 0.5 EC',
'8: Axial: Blass & Steige. Lateral: EC',
'9: Axial: Blass & Steige friction. Lateral: EC',
'10: Axial: Tomasi (EC) single stiffness. Lateral: EC',
'11: Axial: Tomasi (B+S) single stiffness. Lateral: EC',
'12: Axial: Tomasi (EC) double stiffness. Lateral: EC',
'13: Axial: Tomasi (B+S) double stiffness. Lateral: EC',
'14: Axial: Santis & Fragiaco. Lateral: EC'
]

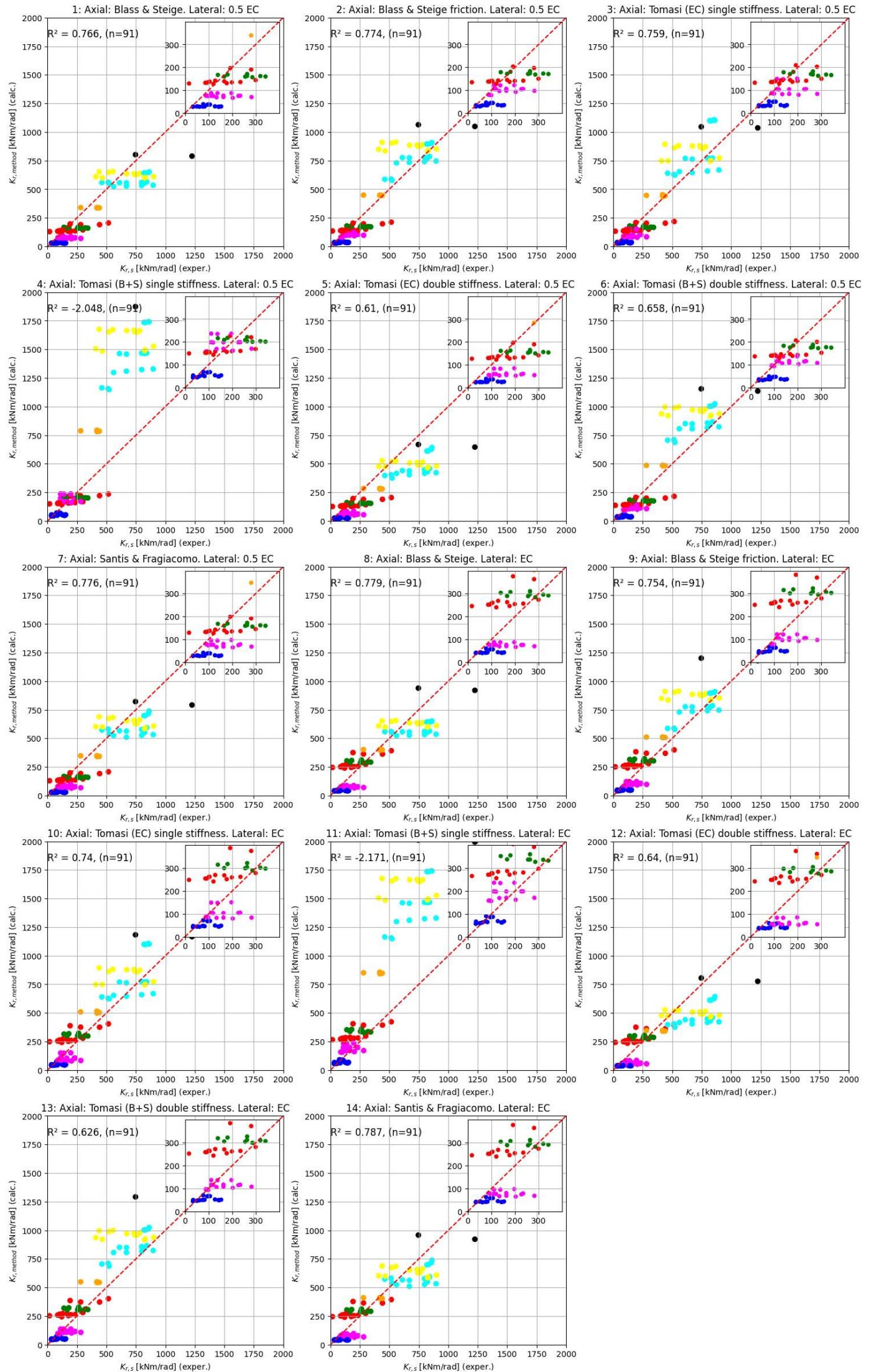
# Plotting
for ax, y, title in zip(axes.flatten(), y_data, titles):
    ax.scatter(x_data, y, c=colors)
    ax.plot(np.linspace(0, 2000, 2001), np.linspace(0, 2000, 2001), 'r--')
    ax.set_ylim(0, 2000)
    ax.set_xlim(0, 2000)
    ax.set_title(title)
    ax.set_xlabel('$K_{r,s}$ [kNm/rad] (exper.)')
    ax.set_ylabel('$K_{r,method}$ [kNm/rad] (calc.)')
    ax.text(0, 1900, f'R² = {np.round(r2_score(df2["modifizierter Verschiebungs-modul Kr,s"], y), 3)}, (n={len(x_data)})',
           fontsize=12, verticalalignment='top')
    ax.grid(True)

# Create inset of zoomed-in lower left part
ax_inset = inset_axes(ax, width="40%", height="40%", loc='upper right')
ax_inset.scatter(x_data, y, c=colors, s=20)
ax_inset.plot(np.linspace(0, 400, 401), np.linspace(0, 400, 401), 'r--')
ax_inset.set_xlim(0, 400)
ax_inset.set_ylim(0, 400)
ax_inset.set_xticks([0, 100, 200, 300])
ax_inset.set_yticks([0, 100, 200, 300])
ax_inset.grid(True)

# Remove the last empty subplot
fig.delaxes(axes[-1, -1])

plt.show();

```



In [12]:

```
# Data extraction
x_data = df2['modifizierter Verschiebungs-modul Kr,s']
y_data = df['kr_santisfragiaco_and_EC'] / 1000000
colors = df['color']

# # Handle potential NaNs
# mask = x_data.notna() & y_data.notna()
# x_data = x_data[mask]
# y_data = y_data[mask]
# colors = colors[mask]

# Define criterion for plotting
cross_condition = df['coefficient_of_friction'] > 0.052

# Define figure and axes with constrained layout
fig, ax = plt.subplots(figsize=(10, 10), constrained_layout=True)

# Plotting for method 14
for i in range(len(x_data)):
    if cross_condition.iloc[i]:
        ax.scatter(x_data.iloc[i], y_data.iloc[i], c=colors.iloc[i], s=100)
    else:
        ax.scatter(x_data.iloc[i], y_data.iloc[i], facecolors='none', edgecolors=colors.iloc[i],
                    linewidth=2, marker='s', s=200)

# Reference Line
ax.plot(np.linspace(0, 1250, 1251), np.linspace(0, 1250, 1251), 'r--')
ax.set_ylim(0, 1250)
ax.set_xlim(0, 1250)
ax.set_title('Method 14: Axial: Santis & Fragiaco. Lateral: EC', fontsize=18)
ax.set_xlabel('$k_{r}$ [kNm/rad] (exper.)', fontsize=18)
ax.set_ylabel('$k_{r,method}$ [kNm/rad] (calc.)', fontsize=18)
ax.grid(True)

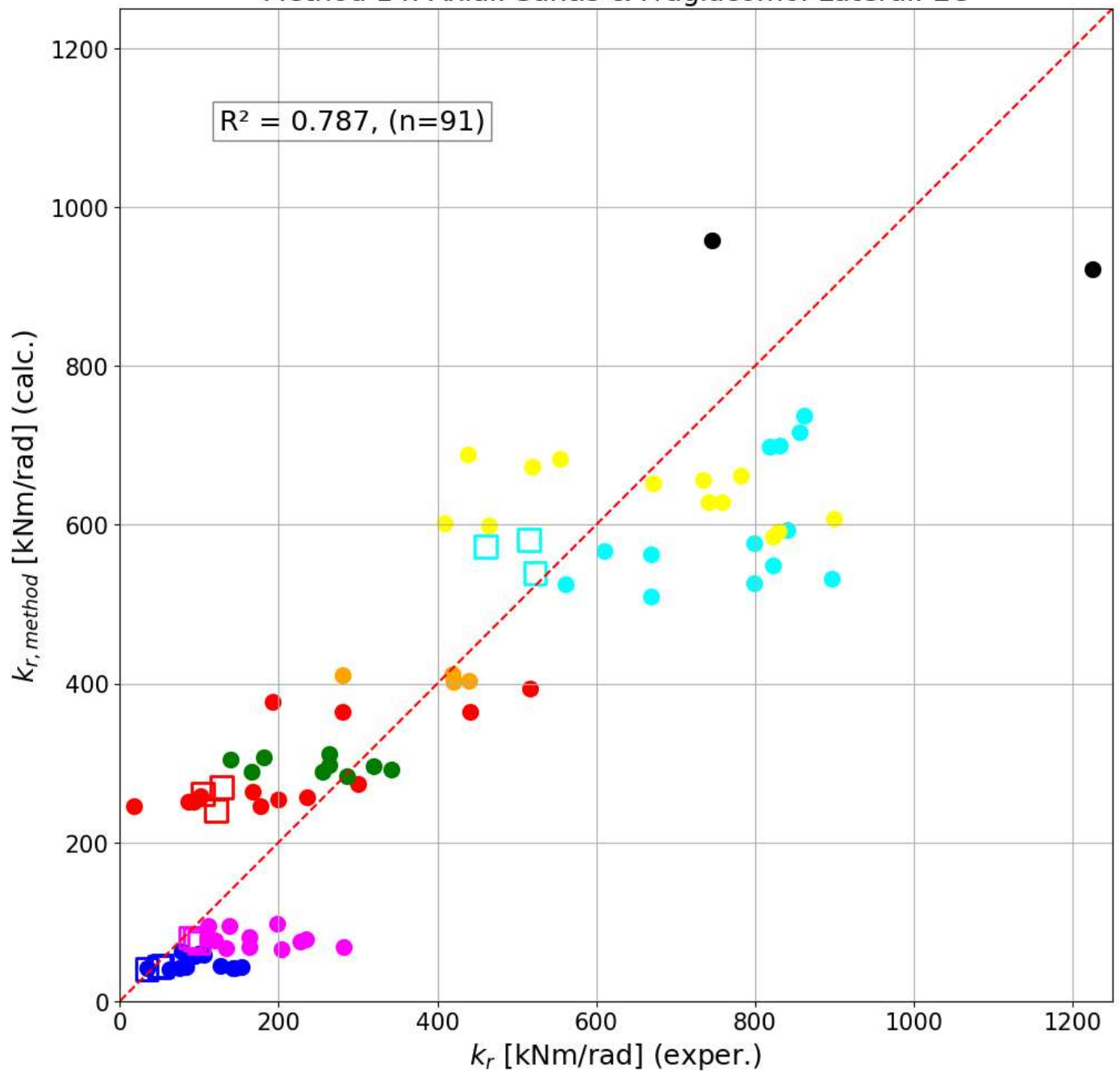
# Increase the font size of the tick labels
ax.tick_params(axis='both', labelsize=15)

# Set aspect ratio to equal for a square plot
ax.set_aspect('equal', adjustable='box')

# Calculate and display R² value
r_squared = np.round(r2_score(x_data, y_data), 3)
ax.text(0.1, 0.9, f'R² = {r_squared}, (n={len(x_data)})', transform=ax.transAxes,
        fontsize=18, verticalalignment='top', bbox=dict(facecolor='white', alpha=0.5))

# Show the plot
plt.show()
```

Method 14: Axial: Santis & Fragiacommo. Lateral: EC



```
In [13]: class EC:
def __init__(self, alpha, d_outer, L_ef1, L_ef2, rho1, rhom, rho2):
    self.alpha = alpha
    self.d_outer = d_outer
    self.L_ef1 = L_ef1
    self.L_ef2 = L_ef2
    self.alpha = alpha
    self.rho1 = rho1
    self.rhom = rhom
    self.rho2 = rho2

def screwstiffnessax(self, rho_outer, rho_m):
    if self.L_ef1 == 0 or self.L_ef2 == 0:
        return 0
    else:
        k = (1 / 23) * self.d_outer * (np.sqrt(rho_outer * rho_m)) ** 1.5
        return k

def screwstiffnessEC(self, rho):
    EC = (1 / 23) * self.d_outer * rho ** 1.5
    return 0.5 * EC

def rotstiff_EC(self, row):
    rotstiffnesslistseite1 = []
    for i in range(10):
        self.L_ef1 = row.iloc[128 + i]
        self.L_ef2 = row.iloc[138 + i]
        ydist = row.iloc[74 + i]
        xdist = row.iloc[64 + i]
        rotstiffnesslistseite1.append(self.screwstiffnessax(self.rho1, self.rhom) * ydist ** 2
```

```

        + 2 * self.screwstiffnessEC(np.sqrt(self.rho1 * self.rhom)) * xdist ** 2)
    rotstiffnesslistseite2 = []
    for i in range(10):
        self.L_ef1 = row.iloc[148 + i]
        self.L_ef2 = row.iloc[158 + i]
        ydist = row.iloc[96 + i]
        xdist = row.iloc[86 + i]
        rotstiffnesslistseite2.append(self.screwstiffnessax(self.rho2, self.rhom) * ydist ** 2
                                     + 2 * self.screwstiffnessEC(np.sqrt(self.rho2 * self.rhom)) * xdist ** 2)
    return np.sum(np.add(rotstiffnesslistseite1, rotstiffnesslistseite2))

# Add a new column to the DataFrame. L_ef1 and L_ef2 are inserted as 0 because they are
# overwritten in rotstiff method.

df['kr_EC_and_EC'] = df.apply(lambda x: EC(x['Screw-in angle  $\alpha$ '], x['d'], 0, 0,
                                           x['Rohdichten [kg/m3]-Typ A'], x['Rohdichten [kg/m3]-Gurt'],
                                           x['Rohdichten [kg/m3]-Typ B'])).rotstiff_EC(x), axis=1)

```

```

In [14]: # Data extraction
x_data = df2['modifizierter Verschiebungs-modul Kr,s']
y_data = df['kr_EC_and_EC'] / 1000000
colors = df['color']

# # Handle potential NaNs
# mask = x_data.notna() & y_data.notna()
# x_data = x_data[mask]
# y_data = y_data[mask]
# colors = colors[mask]

# Define criterion for plotting
cross_condition = df['coefficient_of_friction'] > 0.052

# Define figure and axes with constrained layout
fig, ax = plt.subplots(figsize=(10, 10), constrained_layout=True)

# Plotting for method 14
for i in range(len(x_data)):
    if cross_condition.iloc[i]:
        ax.scatter(x_data.iloc[i], y_data.iloc[i], c=colors.iloc[i], s=100)
    else:
        ax.scatter(x_data.iloc[i], y_data.iloc[i], facecolors='none', edgecolors=colors.iloc[i],
                  linewidth=2, marker='s', s=200)

# Reference line
ax.plot(np.linspace(0, 1250, 1251), np.linspace(0, 1250, 1251), 'r--')
ax.set_ylim(0, 1250)
ax.set_xlim(0, 1250)
ax.set_title('14: Axial: EC. Lateral: EC', fontsize=18)
ax.set_xlabel('$k_{r,s}$ [kNm/rad] (exper.)', fontsize=18)
ax.set_ylabel('$k_{r,method}$ [kNm/rad] (calc.)', fontsize=18)
ax.grid(True)

# Increase the font size of the tick labels
ax.tick_params(axis='both', labelsize=15)

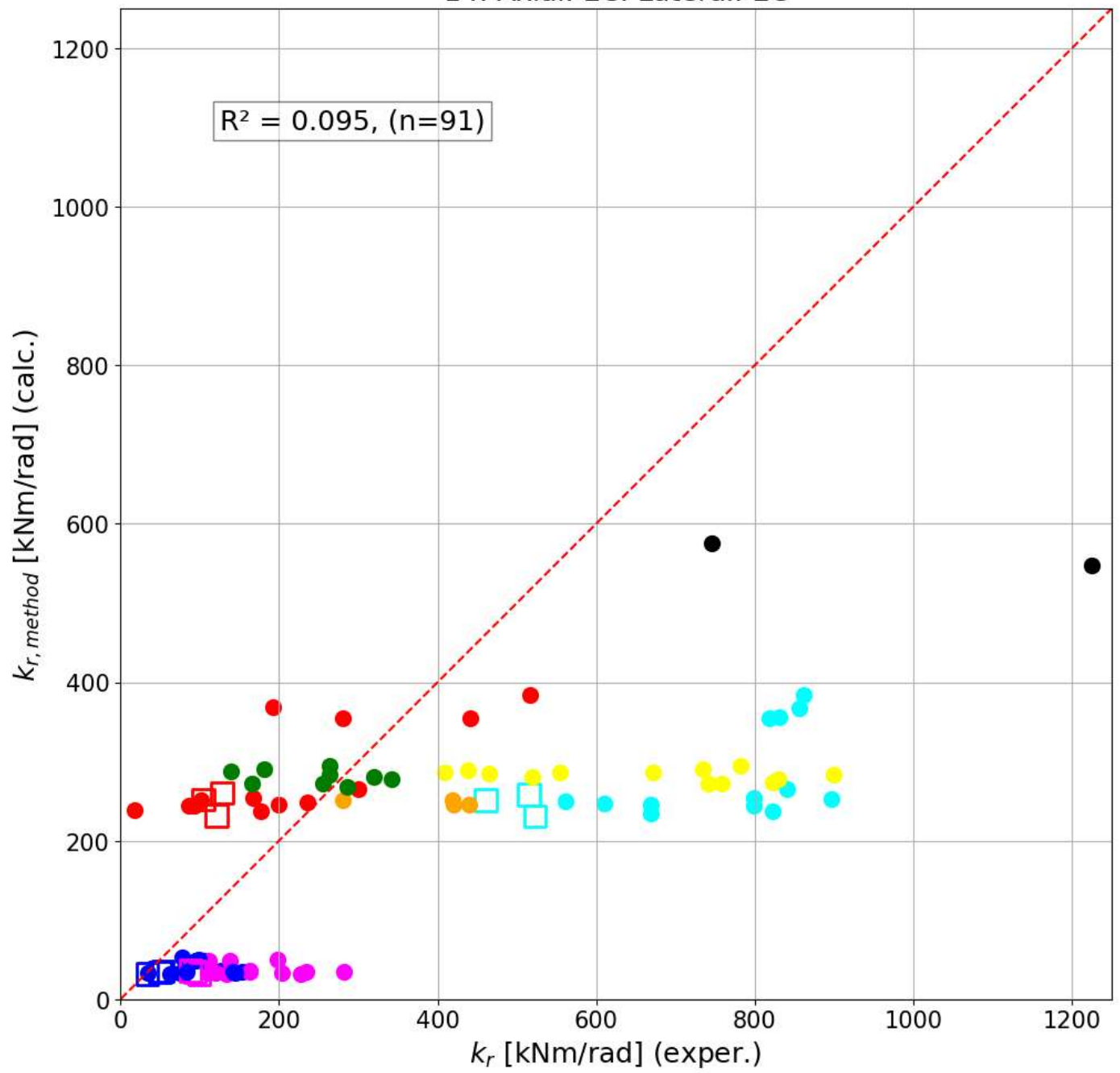
# Set aspect ratio to equal for a square plot
ax.set_aspect('equal', adjustable='box')

# Calculate and display R2 value
r_squared = np.round(r2_score(x_data, y_data), 3)
ax.text(0.1, 0.9, f'R2 = {r_squared}, (n={len(x_data)})', transform=ax.transAxes,
       fontsize=18, verticalalignment='top', bbox=dict(facecolor='white', alpha=0.5))

# Show the plot
plt.show()

```

14: Axial: EC. Lateral: EC



In [15]:

Embedment capacity truss prototypes

The embedment capacity for the force perpendicular to the inclination direction $F_{screw,perp}$ (see figure F.1) is checked both for the LVL and the GL24h according to EN-1995-1-1 [55] equations 8.31 and 8.32. The embedment capacities of the chord and diagonal can be used to check all failure modes of the EYM, due to time constraints only embedment capacity is checked here. Assumptions: $k_{mod} = 0.9$, $\gamma_M = 1.3$.

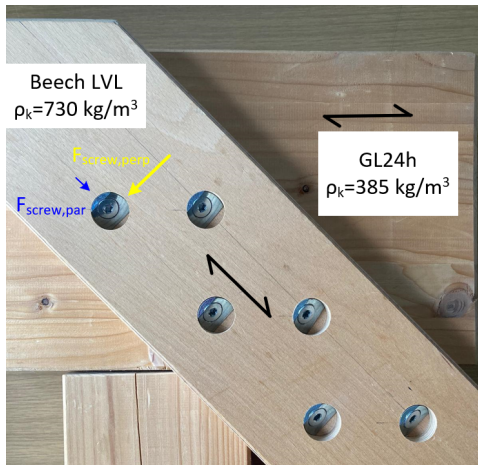


Figure F.1: Screw loaded by force perpendicular to the inclination direction $F_{screw,perp}$ (in yellow).

$$f_{h,0,k} = 0.082 \cdot (1 - 0.01 \cdot d) \cdot \rho_k \quad (F.1)$$

$$f_{h,\alpha,k} = \frac{f_{h,0,k}}{k_{90} \cdot \sin^2(\alpha) + \cos^2(\alpha)} \quad (F.2)$$

$$UC = \frac{\sigma_{screw,perp,max}}{f_{h,\alpha,k}} = \frac{\left(\frac{F_{screw,perp,max}}{l_i \cdot d} \right)}{\left(\frac{f_{h,\alpha,k} \cdot k_{mod}}{\gamma_M} \right)} \quad (F.3)$$

In which:

- $f_{h,0,k}$: characteristic embedment strength parallel to grain direction [N/mm²]
- $f_{h,\alpha,k}$: characteristic embedment strength under an angle α to grain direction [N/mm²]
- d : screw diameter [mm]
- l_i : length of screw in timber element i
- ρ_k : characteristic timber density [kg/m³]
- $k_{90} = \begin{cases} 1.35 + 0.015 \cdot d & \text{for coniferous wood (such as spruce GL24h)} \\ 1.3 + 0.015 \cdot d & \text{LVL} \end{cases}$
- α : angle between load and grain direction = $\begin{cases} 90^\circ & \text{for the LVL diagonal} \\ 45^\circ & \text{for the GL24h chord} \end{cases}$

small prototype

	ρ_k [kg/m ³]	k_{90} [-]	angle to grain α [°]
LVL	730	1.42	90
GL24h	385	1.47	45

d [mm]	8
l [mm]	240
l_1 [mm]	56.57
l_2 [mm]	223.43
$F_{\text{screw,perp,max}}$ [N]	1920

k_{mod}	0.9
γ_M	1.3

	LVL
$f_{h,0,k}$ [N/mm ²]	55.07
$f_{h,90,k}$ [N/mm ²]	38.78
$f_{h,90,d}$ [N/mm ²]	26.85
UC [-]	0.16

	GL24h
$f_{h,0,k}$ [N/mm ²]	29.04
$f_{h,45,k}$ [N/mm ²]	23.52
$f_{h,45,d}$ [N/mm ²]	16.28
UC [-]	0.07

large prototype

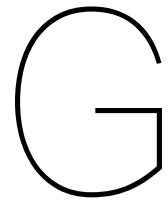
	ρ_k [kg/m ³]	k_{90} [-]	angle to grain α [°]
LVL	730	1.42	90
GL24h	385	1.47	45

d [mm]	8
l [mm]	280
l_1 [mm]	113.14
l_2 [mm]	166.86
$F_{\text{screw,perp,max}}$ [N]	1160

k_{mod}	0.9
γ_M	1.3

	LVL
$f_{h,0,k}$ [N/mm ²]	55.07
$f_{h,90,k}$ [N/mm ²]	38.78
$f_{h,90,d}$ [N/mm ²]	26.85
UC [-]	0.05

	GL24h
$f_{h,0,k}$ [N/mm ²]	29.04
$f_{h,45,k}$ [N/mm ²]	23.52
$f_{h,45,d}$ [N/mm ²]	16.28
UC [-]	0.05



Rotational stiffness values tests

The experimental values from the rotational stiffness tests are given in the table below. The tests with angle α_s of 90 [°] are not used in the thesis, but are given for completeness. The table also gives the stiffness values after the correction according to the pre-load theory, and the calculated stiffness values according to method fourteen.

Test Nr.	α_s [°]	Screw type	Screw geometry										Initial experimental rotational stiffness $K_{r,i}$ [kNm/rad]	Modified experimental rotational stiffness $K_{r,s}$ [kNm/rad]	$K_{r,s}$ after pre-load theory [kNm/rad]	Calculated rotational stiffness method 14 [kNm/rad]
Test series 1			1	2	3	4	5	6	7	8	9	10				
1	45°	VGS 8x240	x							x			683	602	93	252
2	45°	VGS 8x240		x						x						
3	45°	VGS 8x240			x	x	x	x					725	617	410	602
4	45°	VGS 8x240	x							x			497	404	86	252
5	45°	VGS 8x240		x						x			368	276	83	43
6	45°	VGS 8x240			x	x	x	x					836	706	465	600
7	45°	VGS 8x240			x				x				1411	1137	561	525
8	45°	VGS 8x240				x	x						678	528	163	69
9	45°	VGS 8x240	x	x					x	x			1136	865	263	297
10	45°	VGS 8x240	x							x			333	291	17	245
11	45°	VGS 8x240		x						x			265	201	62	40
12	45°	VGS 8x240			x	x	x	x					1591	1282	823	585
13	45°	VGS 8x240			x				x				1554	1254	670	510
14	45°	VGS 8x240				x	x						376	293	134	66
15	45°	VGS 8x240	x	x						x	x		852	681	286	283
16	45°	VGS 8x240	x								x		624	499	102	259
17	45°	VGS 8x240		x						x			410	308	142	42
18	45°	VGS 8x240			x	x	x	x					2069	1699	829	592
19	45°	VGS 8x240			x				x				1921	1498	897	532
20	45°	VGS 8x240				x	x						480	528	203	65
21	45°	VGS 8x240	x	x						x	x		1074	880	320	295
22	45°	VGS 8x240			x				x				1835	1480	799	527
23	45°	VGS 8x240				x	x						1034	817	282	68
24	45°	VGS 8x240	x	x						x	x		1501	1254	342	292
25	45°	VGS 8x240	x								x					
26	45°	VGS 8x240		x						x			640	482	145	41
27	45°	VGS 8x240			x	x	x	x					1717	1413	900	608
Test series 2																
V1	45°	VGS 8x240			x				x				902	823		550
V2	45°	VGS 8x240				x	x						291	227		75
V3	45°	VGS 8x240	x								x		140	177		246
V4	45°	VGS 8x240		x						x			92	75		42
V5	45°	VGS 8x240	x								x		366	300		274
V6	45°	VGS 8x240		x						x			138	127		45
V7	45°	VGS 8x240			x				x				1086	842		594
V8	45°	VGS 8x240				x	x						197	163		80

V9	45°	VGS 8x240	x						x		183	167		263
V10	45°	VGS 8x240		x					x		145	153		43
V11	45°	VGS 8x240			x			x			799	799		577
V12	45°	VGS 8x240				x	x				70	234		78
V13	45°	VGS 8x240	x						x		256	235		257
V14	45°	VGS 8x240		x					x		86	77		43
V15	45°	VGS 8x240			x			x			640	611		566
V16	45°	VGS 8x240				x	x				112	110		77
V17	45°	VGS 8x240	x						x		217	199		254
V18	45°	VGS 8x240		x					x		45	35		42
V19	45°	VGS 8x240			x			x			743	670		563
V20	45°	VGS 8x240				x	x				109	119		76
V21	45°	VGS 8x240	x	x					x	x	164	166		290
V22	45°	VGS 8x240			x	x	x	x			824	759		629
V23	45°	VGS 8x240	x	x					x	x	310	264		312
V24	45°	VGS 8x240			x	x	x	x			860	782		662
V25	45°	VGS 8x240	x	x					x	x	143	140		304
V26	45°	VGS 8x240			x	x	x	x			671	672		652
V27	45°	VGS 8x240	x	x					x	x	200	181		308
V28	45°	VGS 8x240			x	x	x	x			782	735		657
V29	45°	VGS 8x240	x	x					x	x	282	256		289
V30	45°	VGS 8x240			x	x	x	x			761	742		628
V31	45°	VGS 8x240	x	x	x	x	x	x	x	x				
V32	45°	VGS 8x240	x	x	x	x	x	x	x	x	903	746		958
V33	45°	VGS 8x240	x	x	x	x	x	x	x	x	1571	1226		922
V34	45°	VGS 12x240	x						x		650	516		394
V35	45°	VGS 12x240		x					x		80	77		62
V36	45°	VGS 12x240			x			x			696	862		738
V37	45°	VGS 12x240				x	x							
V38	45°	VGS 12x240	x						x		294	442		364
V39	45°	VGS 12x240		x					x		118	106		58
V40	45°	VGS 12x240			x			x			796	819		698
V41	45°	VGS 12x240				x	x				125	111		95
V42	45°	VGS 12x240	x						x		343	281		365
V43	45°	VGS 12x240		x					x		99	95		58
V44	45°	VGS 12x240			x			x			979	831		700
V45	45°	VGS 12x240				x	x				163	138		95
V46	45°	VGS 12x240	x						x		198	192		378
V47	45°	VGS 12x240		x					x		105	99		59
V48	45°	VGS 12x240			x			x			938	856		716
V49	45°	VGS 12x240				x	x				225	197		97
V50*	45°	VGS 8x240	x						x		130	105		261
V51*	45°	VGS 8x240		x					x		44	50		43
V52*	45°	VGS 8x240			x			x			488	461		572
V53*	45°	VGS 8x240				x	x				89	94		78
V54*	45°	VGS 8x240	x						x		129	128		269
V55*	45°	VGS 8x240		x					x		41	53		44
V56*	45°	VGS 8x240			x			x			418	515		581

V57*	45°	VGS 8x240				X	X						68	88		80
V58*	45°	VGS 8x240	X							X			124	121		240
V59*	45°	VGS 8x240		X						X			39	34		40
V60*	45°	VGS 8x240			X				X				527	523		539
V61*	45°	VGS 8x240				X	X						106	99		73
V62	45°	TGS 8x250			X	X	X	X					572	438		688
V63	45°	VGS 8x240									X	X	374	418		411
V64	45°	TGS 8x250			X	X	X	X								
V65	45°	VGS 8x240									X	X	280	281		410
V66	45°	TGS 8x250			X	X	X	X					705	555		684
V67	45°	VGS 8x240									X	X	432	439		404
V68	45°	TGS 8x250			X	X	X	X					650	519		674
V69	45°	VGS 8x240									X	X	404	420		403
V70	90°	VGS 12x200	X							X			34	26		
V71	90°	VGS 12x200			X				X				9	7		
V72	90°	VGS 12x200		X						X						
V73	90°	VGS 12x200				X	X									
V74	90°	VGS 12x200	X							X			68	54		
V75	90°	VGS 12x200		X						X						
V76	90°	VGS 12x200			X				X				55	52		
V77	90°	VGS 12x200				X	X						1	11		
V78	90°	VGS 12x200	X							X			41	54		
V79	90°	VGS 12x200		X						X						
V80	90°	VGS 12x200			X				X				13			
V81	90°	VGS 12x200				X	X									
V82	90°	VGS 8x200	X	X	X	X	X	X	X	X	X		221	181		
V83	90°	VGS 8x200	X	X	X	X	X	X	X	X	X		224	183		
V84	90°	VGS 8x200	X	X	X	X	X	X	X	X	X		226	190		
V85	90°	VGS 8x200	X	X						X	X		89	80		
V86	90°	VGS 8x200			X	X	X	X					66			
V87	90°	VGS 8x200	X	X						X	X		18	14		
V88	90°	VGS 8x200			X	X	X	X								
V89	90°	VGS 8x200	X	X						X	X		78	58		
V90	90°	VGS 8x200			X	X	X	X					138	134		
V91	90°	VGS 8x200		X						X						
V92	90°	VGS 8x200				X	X						4	10		
V93	90°	VGS 8x200	X								X		7			
V94	90°	VGS 8x200			X				X				13	32		
V95	90°	VGS 8x200		X						X			5			
V96	90°	VGS 8x200				X	X						3			
V97	90°	VGS 8x200	X								X		10	9		
V98	90°	VGS 8x200			X				X				11	9		
V99	90°	VGS 8x200		X						X			9	31		
V100	90°	VGS 8x200				X	X									
V101	90°	VGS 8x200	X							X			34	41		
V102	90°	VGS 8x200			X				X				10	12		

* Test performed with friction-reducing interlayer

Rotational stiffness value could not be calculated from the test